Correlating Functional Near-Infrared Spectroscopy with Underlying Brain Regions for Adult and Infant Populations by Theoretical Light Propagation Analysis

July 2021

CAI, Lin

A Thesis for the Degree of Ph.D. in Engineering

Correlating Functional Near-Infrared Spectroscopy with Underlying Brain Regions for Adult and Infant Populations by Theoretical Light Propagation Analysis

July 2021

Graduate School of Science and Technology

Keio University

CAI, Lin

Abstract

Functional near-infrared spectroscopy (fNIRS) is a noninvasive neuroimaging modality that assesses neural activity by measuring changes in oxygenated and deoxygenated hemoglobin after positioning single/multiple source-detector (SD) pairs over the human scalp. In the past few decades, fNIRS has widely been used to investigate the function of the adult brain and developing brain in the field of cognitive neuroscience. The fast growth of fNIRS studies is due to the several advantages that fNIRS is highly portable and has a relatively robust tolerance for body movements, which is suitable for different experimental settings and various populations including neonates, children, and adults. However, it remains a challenge for fNIRS to target specific brain regions of interest by the positioning of SD pairs on the scalp. Since fNIRS data does not provide any anatomical information on the cerebral cortex, it is extremely important to establish a scalp-cortex correlation (SCC) between the scalp location of the SD pair and brain regions for measuring brain functions. Given that the near-infrared light is strongly scattered in head tissues, the objective of this thesis is to establish the precise optics-based SCC using the light propagation analysis based on the diffusion equation for the adult and infant populations.

Chapter 1 describes the purpose and background of this thesis.

Chapter 2 validates that the diffusion approximation is a highly efficient and robust light propagation analysis methodology, which can be used to obtain the precise optics-based SCC, by comparing optics-based SCC results obtained by the finite element method and Monte Carlo method that is viewed as the gold standard method.

Chapter 3 proposes a sensitivity-based matching (SBM) method to establish the optics-based SCC for 45 subject-specific adult head models. Furthermore, when the SCC was computed, the performance of the SBM method was compared with that of three conventional geometrical matching methods ignoring the effect of light scattering. The results demonstrate that the light scattering and individual anatomical differences in the head affect the SCC, which further indicates that the SBM method is compulsory to obtain the precise SCC.

Chapter 4 aims to establish optics-based SCC for 0-, 1-, 2-year-old infants using the SBM method, and to determine the optimal SD distance for this age period, during which the most dynamic growth in head structures and remarkable cognitive changes occur.

Chapter 5 summarizes the main findings of this thesis and presents conclusions with future works.

Content

List of Figures

List of Tables

List of Abbreviations

0-yo	0-year-old
1-yo	1-year-old
2-yo	2-year-old
3D	three-dimensional
3D-SPGR	3-dimensional spoiled gradient echo
AAL	automated anatomical labeling
ASSET	array spatial sensitivity encoding technique
BRIGHT	Brain Imaging for Global Health
CBF	cerebral blood flow
CSF	cerebrospinal fluid
DOT	diffuse optical tomography
DPF	differential path length factor
EEG	electroencephalography
FA	flip angle
FAST	FMRIB's Automated Segmentation Tool
FEM	finite element method
FIESTA	fast imaging employing steady-state acquisition
fMRI	functional magnetic resonance imaging
fNIRS	functional near-infrared spectroscopy
FS-PDW	fat-saturated proton density weighted
GM	geometrical matching
HbO	oxygenated-hemoglobin
HbR	deoxygenated-hemoglobin
MCM	Monte Carlo method
MEG	magnetoencephalography
MLCBR	most likely corresponding brain region
MNI	Montreal Neurological Institute
MRI	magnetic resonance imaging
N_{CBR}	number of corresponding brain regions
NEX	number of excitation
OD	optical density
PMDF	photon measurement density function
PPL	partial optical pathlength

RBFT	radial basis functional transform
SBM	sensitivity-based matching
SCC	scalp-cortex correlation
SD	source-detector
SSP	spatial sensitivity profile
T1W	T1-weighted
TE	echo time
TI	inversion time
TR	repetition time
WTS	Wald-type statistic

Chapter 1

1 Introduction

1.1 Noninvasive neuroimaging techniques

In the cognitive neuroscience field, there are mainly four noninvasive neuroimaging techniques, such as electroencephalography (EEG), magnetoencephalography (MEG), functional magnetic resonance imaging (fMRI), and functional near-infrared spectroscopy (fNIRS), that have been widely utilized to investigate the function of the human brain. These techniques are classified into two general categories according to measured brain activity. EEG and MEG provide a direct measurement of neural activity by recording the electromagnetic signals emitted by the brain, while fMRI and fNIRS provide indirect hemodynamic indicators of neuronal activity (Baillet, 2017; Buzsáki et al., 2012; Logothetis, 2008; Pinti et al., 2020). EEG has an excellent temporal resolution which is in the millisecond range. The main limitation of EEG is its poor spatial resolution due to no unique solution for the spatial location of the neural activity (Luck, 2014; Teplan, 2002). Similar to EEG, MEG also provides high temporal resolution on the order of milliseconds (Singh, 2014). Moreover, MEG signal sources can be localized with millimeter precision (Papadelis et al., 2009). On the contrary, fMRI provides a reasonably

good spatial resolution (~1 mm) but a very poor temporal resolution (~1 s). Notoriously, both fMRI and MEG require a participant to keep still, even fMRI requires the participant to lay in a supine position, which is hard for some special populations, such as infants or children with attention deficit hyperactivity disorder (Faro & Mohamed, 2006). Like fMRI, fNIRS is also a noninvasive functional neuroimaging technique based on neurovascular coupling that reflects the tight temporal and regional relationship between local neural activity and cerebral blood flow (Phillips et al., 2016). Importantly, fNIRS can simultaneously measure concentration changes of oxygenated-hemoglobin (HbO) and deoxygenated-hemoglobin (HbR) at the level of the cortical microcirculation blood vessels (Boas et al., 2014; Pinti et al., 2020; Quaresima & Ferrari, 2019b). The major advantages of fNIRS include (a) a balanced temporal-spatial resolution, (b) the use of low-cost, silent, and portable instrumentation, (c) the measurement of changes in both HbO and HbR, delineating a more complete picture of the hemodynamic response, and (d) the tolerability to movement during the fNIRS measurements. Due to these advantages of fNIRS, it has been widely used as an important neuroimaging tool to monitor functional brain activity in a variety of populations (e.g., behaving infants) and experimental settings (e.g., person-to-person social interactions) during the past decades (Lloyd-Fox et al., 2010; Quaresima & Ferrari, 2019a; Vanderwert & Nelson, 2014). From the perspective

of portability and cost, EEG and NIRS are movable from a laboratory to another, while fMRI and MEG are fixed at the structure of the building. Furthermore, MEG and fMRI suffer from the high cost of the recording instrumentation, while EEG and fNIRS have low cost. The pros and cons of 4 types of noninvasive neuroimaging techniques are listed in Table 1.1 according to five criteria: (1) temporal resolution, (2) spatial resolution, (3) tolerance to motion, (4) cost, and (5) portability.

Table 1. 1 List of noninvasive neuroimaging techniques and their major features.

Neuroimaging techniques	Temporal resolution	Spatial resolution	Tolerance to motion	Portability	Cost
EEG	High	Low	High	Moderate	Low
MEG	High	Relatively high	Very low	Low	High
fMRI	Low	High	Very low	Low	High
fNIRS	Moderate	Moderate	High	High	Low

1.2 Brain functional measurement using fNIRS

In the actual fNIRS measurement, a source-detector (SD) pair consisting of a source and a detector, which illuminates and receives near-infrared light, respectively, is fixed to the scalp as shown in Fig. 1.1. Most biological tissues have low absorption characteristics in the near-infrared spectral window (650–950 nm, namely ‘optical window’), such as water, hemoglobin, and collagen (Fig. 1.2). Consequently, the light can travel through

several different types of head tissues, such as the scalp, skull, and cerebrospinal fluid (CSF), both before and after passing through the brain (Jobsis, 1977). Since HbO and HbR are the dominant absorbers and have different optical absorption characteristics in the spectral range of the 'optical window', the attenuation of near-infrared light in the wavelength range 650–950 nm monitored by the detector is well suited to determine changes in HbO and HbR. Specifically, when a brain area is active, the metabolic demand for oxygen and glucose increases, leading to an oversupply in regional cerebral blood flow (CBF) through a mechanism called neurovascular coupling. Consequently, the oversupply in regional CBF produces an increase in HbO and a slight decrease in HbR (Kumar et al., 2017). On the other hand, the near-infrared light is also strongly scattered when it passes through the head tissues. Since scattering in head tissues is 100 times more frequent than absorption, the light travels considerably in tissues farther than the physical length between the source and the detector, following a banana-shaped path. Changes in the concentration of HbO and HbR in the brain result in attenuation in detected light intensity (Pinti et al., 2020).

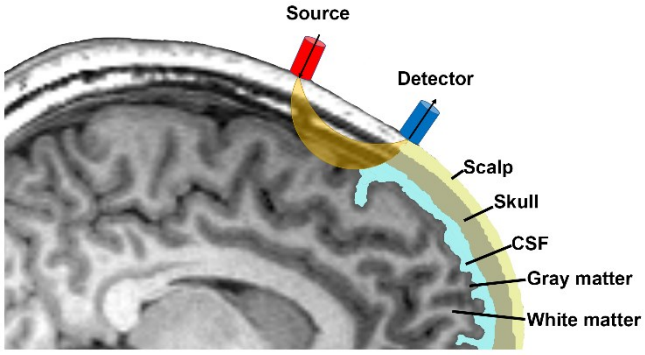

Figure 1. 1 Schematic representation of the near-infrared light traveling through the head tissues (e.g., scalp, skull, CSF, gray matter, and white matter) in the form of a banana-shaped path. A pair of source and detector attached to the scalp emits and receives light at a distance (usually 30 mm for adults).

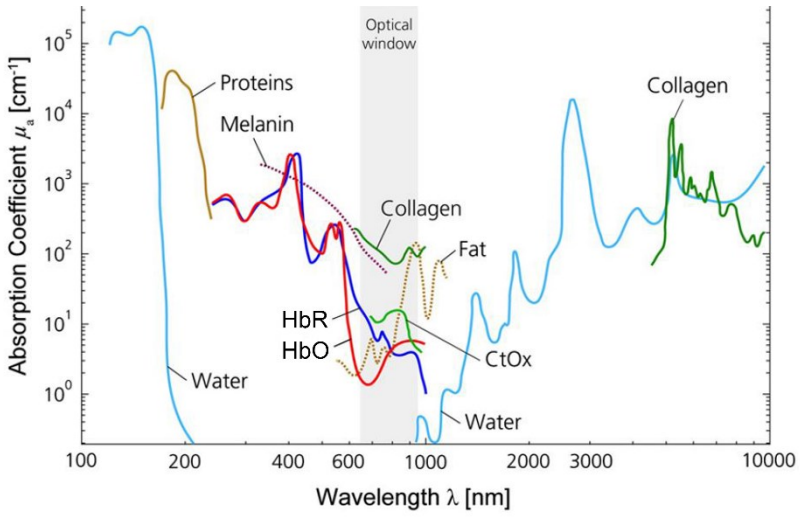

Figure 1. 2 Absorption spectra (natural logarithm base) for different chromophores present in human tissue. Shown are the spectra for HbO, HbR, proteins, water, collagen, fat, and cytochrome oxidase (CtOx) in the region from 100 nm to 10,000 nm. The spectra are given with respect to the specific concentration in mM. This figure was adapted from Scholkmann et al., 2014.

1.2.1 Optical properties of head tissues

To understand how near-infrared light propagates in the human head, the optical properties of head tissues should be clarified. In addition to the refractive index of light, the optical properties mainly including the absorption and scattering parameters have been used to characterize different head tissues. The absorption and scattering characteristics of head tissues are described by absorption coefficient μ_a and scattering coefficient μ_s, both of which are dependent on the wavelength of light and tissue types.

The absorption coefficient μ_a is defined as the probability of photon being absorbed per unit of length. The absorption coefficient of one tissue type is determined by all absorbing substances (chromophores), which can be expressed as the sum of the products of each concentration chromophore, c (unit, [M]), and its molar extinction coefficient, ε (unit, [M^{-1} mm^{-1}]),

$$\mu_a(\lambda) = \Sigma_i \varepsilon_i(\lambda) c_i, \quad (1)$$

where the index i indicates all chromophores (for instance, HbO, HbR, myoglobin, cytochrome oxidase) in one tissue type.

The scattering coefficient, μ_s, is defined as the probability of a photon being scattered per unit of length, which is determined by the refractive index of the two media and the size of the scattering particle, and the wavelength of light.

In every scattering event, the angular distribution of the scattered photon relative to the incident photon is described by a scattering phase function, p (Fig. 1.3). The phase scattering function can be expressed as a function of the scalar product of the unit vectors in the initial and final directions, which is equal to the cosine of the scattering angle θ.

$$p(\boldsymbol{s}, \boldsymbol{s}') = p(cos(\theta)) \quad (2)$$

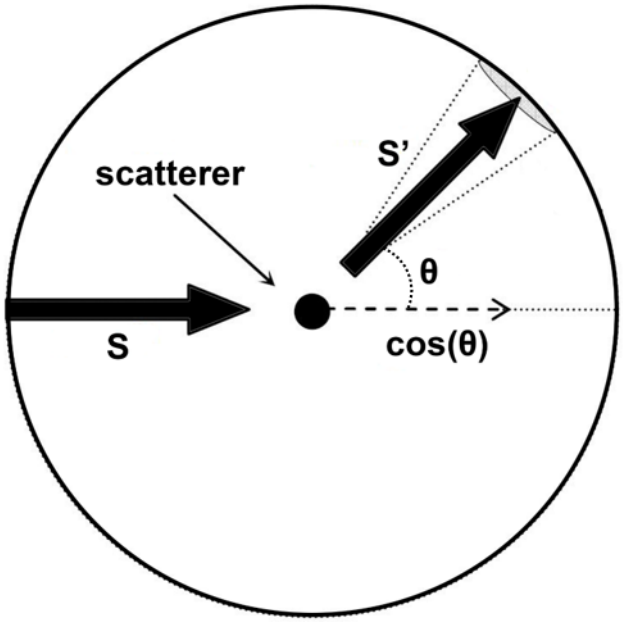

Figure 1. 3 Scattering phase function. The incident photon travels in the s direction and the scattered photon exits in the s′ direction.

The anisotropy factor, g, is the average value of the cosine of the phase scattering function and measures the anisotropy of scattering. If the scattering is isotropic, then g = 0. If the scattering is entirely forward, then g = 1, and the highly backward scattering

results in the value of g approaches -1. Notably, g is in the range from 0.69 to 0.99 in biological tissue, revealing strongly forward scattering (Cheong et al., 1990). Additionally, in the diffusion theory of light propagation in random media, the characteristic scattering of tissue is often expressed by the reduced scattering coefficient (μ_s'),

$$\mu_s' = \mu_s(1 - g), \tag{3}$$

which represents the effective equivalent number of isotropic scatters per unit of length.

Based on an exhaustive review (Jacques, 2013), it is easy to infer that different head tissues have different absorption and scattering coefficients, because of composition in one tissue type is distinguished from that of another. More importantly, maturation of various head tissues with age affects the optical properties of head tissues. The comparison between infants and adults can provide some important evidence. For example, relative to the adult brain, the myelination of the infant brain including gray matter and white matter is far from complete (Dubois et al., 2014; Timmler & Simons, 2019). Because myelinated cells give rise to an appreciable amount of extra light scattering than non-myelinated cells, the scattering coefficient of the infant brain is considerably smaller than that of the adult brain (Van der Zee, 1993). According to a prior study (Van der Zee et al., 1993), it can be deduced that the absorption coefficients of gray matter and white matter of full-term neonates are slightly larger than those of adults in

the spectral range of the 'optical window'. Furthermore, the skull is still in the process of ossification from birth to 2 years (Delye et al., 2015; Gallo et al., 2012). Particularly, the absorption and scattering coefficients of the fontanel that is a type of non-ossified cartilage are slightly larger than those of the adult skull (Dehaes et al., 2013).

1.2.2 Modified Beer-Lambert law

The difference between the incident and detected light intensity levels is described by the modified Beer-Lamber law (Cope et al., 1988; Delpy et al., 1988; Maki et al., 1995). The law describes the loss of light intensity in tissue (optical density *OD*, unitless) for wavelength λ and measurement time t as a function of the chromophore molar concentrations (c, units [M]), molar absorption coefficients (α, [M^{-1} mm^{-1}], natural-logarithm based, different from the molar extinction coefficient (ε) by a scaling factor equal to ln(10)), differential pathlength factor (*DPF*, unitless), SD distance (d, [mm]) and G (unitless):

$$OD(t,\lambda) = -\ln\left(\frac{I(t,\lambda)}{I_0(t,\lambda)}\right) = \sum_i \alpha_i(\lambda) c_i(t) DPF(\lambda) d + G(\lambda), \quad (4)$$

where the index i indicates all investigated chromophores (i.e., HbO and HbR). I_0 and I indicate the incident light intensity and detected light intensity, respectively. The additive term G is an unknown geometry dependent factor. Given that the change in scattering is small compared to the change in absorption, G can be assumed to be constant during the

measurement period. Therefore, this term can be canceled out when determining the change in optical density ($\Delta OD(\Delta t,\lambda) = OD(t_1,\lambda) - OD(t_0,\lambda)$) for a time point t_1 against to an initial time point t_0. In addition, the intensity of incident light I_0 can also be assumed to be constant, then $\Delta OD(\Delta t,\lambda)$ can be rewritten as the following equation:

$$\Delta OD(\Delta t, \lambda) = -\ln\left(\frac{I(t_1,\lambda)}{I(t_0,\lambda)}\right) = \sum_i \alpha_i(\lambda)\Delta c_i DPF(\lambda)d, \quad (5)$$

where $\Delta c_i = c_i(t_1) - c_i(t_0)$ is the temporal change in chromophore molar concentration. Because the two forms of hemoglobin have different absorption spectra, it is possible to measure the relative concentration of HbO and HbR using measurements at two wavelengths (λ_1, λ_2). Furthermore, the values for α and DPF can be found in the literature. Finally, the resulting system of equations are used to obtain the concentration change of HbO and HbR:

$$\begin{bmatrix}\Delta[HbO]\\ \Delta[HbR]\end{bmatrix} = (d)^{-1}\begin{bmatrix}\alpha_{HbO,\lambda 1} & \alpha_{HbR,\lambda 1}\\ \alpha_{HbO,\lambda 2} & \alpha_{HbR,\lambda 2}\end{bmatrix}^{-1}\begin{bmatrix}\Delta OD(\Delta t,\lambda 1)/DPF(\lambda 1)\\ \Delta OD(\Delta t,\lambda 2)/DPF(\lambda 2)\end{bmatrix}. \quad (6)$$

1.2.3 Partial optical pathlength and spatial sensitivity profile

Since the term DPF in Equation (5) is a unitless scalar that adjusts for scattering, the mean optical pathlength through head tissues is approximated by the product of the SD distance and a wavelength dependent DPF. Thus, Equation (5) can be expressed as follows,

$$\Delta OD = \Delta\mu_a\langle L\rangle. \quad (7)$$

where the change in absorption coefficient in the tissue $\Delta\mu_a$ (unit [mm^{-1}]) and $\langle L \rangle$ (unit [mm]) is mean optical pathlength in the tissue. The mean optical pathlength in the tissue between the source and the detector can be directly measured by time- or phase-resolved experiments.

Given that the concentration changes in HbO and HbR occur only in the brain and not in other superficial head tissues, Equation (5) is not strictly applicable for brain function measurements. Assuming that the head comprises several homogeneous tissues, a partial optical pathlength (PPL) is defined as the mean optical pathlength that the detected light travels in each tissue region. If the head is segmented into M regions, the change in optical density can then be described by the sum of the product of the partial optical path lengths $\langle L_i \rangle$ and the corresponding absorption coefficient change ($\Delta\mu_{ai}$) in each region *i* (Hiraoka et al., 1993; Okada & Delpy, 2003a):

$$\Delta OD = \sum_{i=1}^{M} \Delta\mu_{ai} \langle L_i \rangle. \quad (8)$$

The PPL in the region *i* can be defined as a partial derivative of the measured optical density versus the absorption coefficient μ_{ai} in the region *i* (Koyama et al., 2005):

$$\langle L_i \rangle = \frac{\partial OD}{\partial \mu_{ai}}. \quad (9)$$

The PPL in a given brain region indicates the sensitivity of fNIRS signal to concentration changes in hemoglobin evoked by the activation in that brain region. Although the mean

optical pathlength of the head can be measured by time- or phase-resolved experiments, the PPL cannot be directly measured by experiment.

The spatial sensitivity profile (SSP) is a more rigorous parameter representing the spatial distribution of tissue volume that contributes to the fNIRS signal. The SSP at position **r**, SSP(**r**), can be defined as the distribution of the PPL in small voxels $\langle L_{voxel}(\boldsymbol{r})\rangle$ at position **r** in the head. The PPL within a voxel approximates a partial derivative of the measured optical density versus absorption coefficient in the voxel (Okada & Delpy, 2003a).

$$SSP(\boldsymbol{r}) = \langle L_{voxel}(\boldsymbol{r})\rangle \approx \frac{\partial OD}{\partial \mu_{a\,voxel}(\boldsymbol{r})} \tag{10}$$

1.2.4 Problem of spatial localization of fNIRS

Although fNIRS can quantitatively measure regional hemodynamic change caused by a local change in brain activation state relative to a rest state, it is difficult to localize the exact spatial origin of the hemodynamic response within the brain because fNIRS measurements are from the surface of scalp. It is well known that the structure of the human brain is the substrate of brain function, it is necessary to establish the scalp-cortex correlation (SCC) between the scalp surface positions where SD pairs are placed and the underlying brain regions for fNIRS, which only provides functional information. Once the SCC is available, fNIRS data will be interpreted from an anatomical perspective,

which makes it possible to compare fNIRS findings with those derived from other neuroimaging modalities.

1.3 Traditional scalp-cortex correlation (SCC) matching methods

To address the problem of spatial localization of fNIRS signal, most fNIRS studies have been adopted a point-to-point geometrical manner to link fNIRS measurement data and underlying brain regions. In the following subsections, some representative geometrical matching methods calculating the SCC are listed.

1.3.1 Geometrical matching method using fNIRS-MRI coregistration

A common geometrical matching method is to attach MRI-visible markers (e.g., Vitamin E tablets) to the SD pairs or measurement channel positions (i.e., the middle point of an SD pair) on the scalp, and then obtain their positions through scanning a subject with fNIRS probes in an MRI scanner. Subsequently, the most probable cortical region corresponding to each channel is identified by projecting each marker position to the cortical surface (Cai et al., 2018; Cai et al., 2019; Chen et al., 2017; Kovelman et al., 2009). This method is usually realized in one or some of subjects, which may ignore the individual anatomical variabilities. Scanning every subject wearing fNIRS probes, especially young children, is costly and labor intensive.

When only structural MRI images of a subject and relative locations of fNIRS

probes on subject's head surface are available, a 3D digitizer can be used to localize the brain regions that SD pairs interrogate. Specifically, the positions of SD pairs are firstly measured by the 3D digitizer, together with the positions of several scalp landmarks (e.g., the bilateral preauricular points, nasion, and inion) in a real-world coordinate system. Only by identifying these scalp landmarks in the structural MRI images of the human head as anchor points, the positions of SD pairs obtained by the 3D digitizer can be transformed onto the MRI images. Finally, the brain region corresponding to each SD pair is identified (Tsuzuki & Dan, 2014). Nevertheless, the 3D digitizer is easily affected by the highly conductive material in the participant's surroundings and a slight head motion during the measurement, which usually results in distorted digitization points. Thus, for the infant population, some research groups utilized head circumference measurements and photographs of the infants wearing the fNIRS probe to identify locations of SD pairs on the MRI images of the infant heads. And then brain regions and their probability on an age-appropriate infant template corresponding to SD pairs were obtained by the balloon-inflation algorithm (Emberson et al., 2017; Lloyd-Fox et al., 2014). Moreover, some recent studies developed a photo-based photogrammetry optode registration method (Hu et al., 2020) or a video-based method (Jaffe-Dax et al., 2020) for estimating the positions of SD pairs on head surface to overcome the weakness of the 3D digitizer.

1.3.2 Geometrical matching method using a group of subjects' structural MRI

Acquiring structural MRI images of every subject participating an fNIRS experiment undermines the advantages of fNIRS technique and imposes unnecessary burden on subjects. Thus, instead of scanning the subjects' own structural MRI images, several pioneer researchers utilized structural MRI images stored in a reference database to establish the SCC between the electrode placement system and brain regions. The most widely adopted the electrode placement system, e.g., the international 10-20/10-10 system (see Fig. 1.4), defines fiducial points on the scalp according to anatomical landmarks on the head surface (Jasper, 1958; Klem et al., 1999; Nuwer, 2018). By using a group of subjects' MRI images, several studies have demonstrated that there is a reasonable positional correlation between the fiducial points and the anatomical structure of the cerebral cortex for both adults (Blume et al., 1974; Homan et al., 1987; Koessler et al., 2009; Okamoto et al., 2004) and infants (Kabdebon et al., 2014; Tsuzuki et al., 2017).

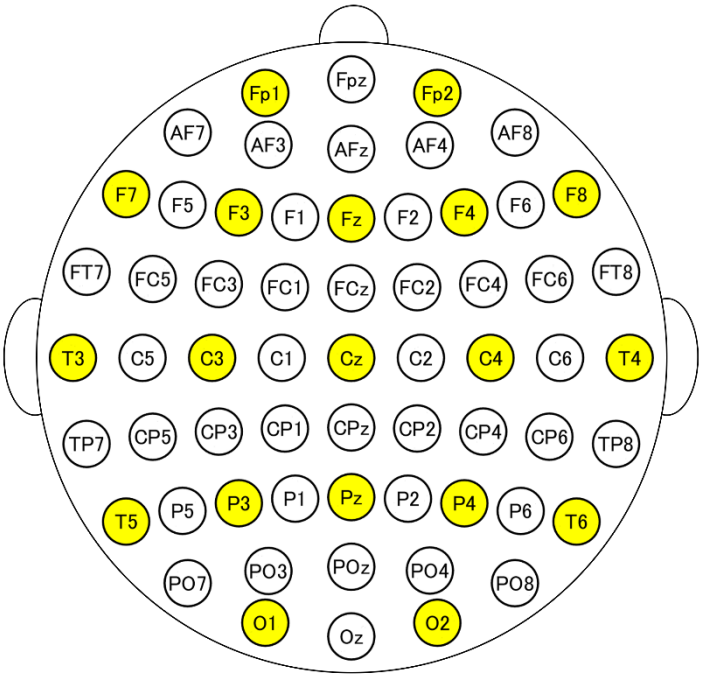

Figure 1. 4 International 10–10 system including 61 fiducial points, of which 10–20 fiducial points are filled with yellow color.

1.3.3 Geometrical matching method without subject own structural MRI

The probabilistic registration method (Singh et al., 2005) developed by Dan's group is the most popular geometrical matching method, which has been cited for 495 times until June of 2021. This method utilizes 17 subjects' MRI provided in a reference database (Okamoto et al., 2004) instead of a subject's own MRI. Specifically, they firstly obtained the coordinates of fNIRS measurement channels and some scalp landmarks using the 3D digitizer in the real-word coordinate system. Then, they applied the affine transformation to obtain the 17 MNI (Montreal Neurological Institute) coordinates for each channel via

scalp landmarks due to considering 17 different adult heads. These MNI coordinates on the scalp surface were further projected onto the cortical surface by the balloon-inflation algorithm (Okamoto & Dan, 2005). Finally, they used 17 cortical surface points to compute the cortical surface centroid and estimate the corresponding brain regions.

Similarly, another research group proposed a transcranial brain atlas (Xiao et al., 2018) and a functional transcranial brain atlas (Jiang et al., 2020) to directly target the brain regions of interest with the aid of a 3D digitizer. Nevertheless, the point on the scalp was also geometrically projected onto the cortical surface of the subject by the balloon-inflation algorithm (Okamoto and Dan, 2005), during the process of constructing these brain atlases.

1.3.4 Geometrical matching method with stand-alone fNIRS data

However, the methods described above require the careful measurement of scalp positions of SD pairs. This limits the application of these methods in some clinical situations or the infant population. The virtual registration method was developed to make it possible for spatially localizing fNIRS signal without structural MRIs of the subjects and a 3D-digitizer (Tsuzuki et al., 2007). Specifically, a holder deformation algorithm was constructed for some fixed-shaped probe holders. Then, Tsuzuki et al. simulated the registration of virtual holders on synthetic heads and brains generated by randomly

combining one subject's MRI images from reference database with head sizes and shapes. For each synthetic head and brain, the holder deformation algorithm was applied to estimate the cortical surface points and converted them to MNI coordinates. After repeating 1000 times for above procedure, the mean MNI coordinates and the standard deviation were estimated. Moreover, the modified version of virtual registration method has also been employed to estimate the underlying cortical regions corresponding to multiple SD pairs in infant studies by linearly reducing the size of the adult or infant average MRI templates (Hakuno et al., 2020; Minagawa et al., 2017; Uchida-Ota et al., 2019; Watanabe et al., 2013).

To sum up, all the above methods were proposed based on the simplified assumption that the absorption change occurs at the cortical projection point below the midpoint between the SD pair.

1.4 Computer modeling of light propagation in head model

Since near-infrared light is strongly scattered in head tissues, an SD pair of fNIRS usually interrogates broad areas, not a single point in the cerebral cortex. To establish a precise SCC, adequate modeling of photon transport in the head consisting of various types of tissues with different optical properties must be conducted using computer simulation. There are two types of computer simulation methods of light propagation,

statistical and deterministic methods. The Monte Carlo method (MCM) is an example of the former, which is based on simulating the radiative transfer equation by tracing a large number of photons. The MCM is one of the most reliable methods for analyzing light propagation in various biological tissues, particularly, the low-scattering CSF layer. Nevertheless, its drawback is that require enormous computation time to keep statistical errors within a reasonable limit. On the other hand, a diffusion equation that approximates the radiative transport equation has frequently been used to simulate light propagation through biological tissues. The finite element method (FEM), as one of the deterministic methods, has been used to solve the diffusion equation. The FEM not only deals with the complex geometry of a heterogeneous medium, but also has the advantage of fast computation time. However, the diffusion theory is not valid in the low-scattering medium. More descriptions of the two types of computer simulation methods can be found in Chapter 2.

1.4.1 Slab model

To assess the effect of superficial tissues on light propagation in the brain, the slab head model that simplifies the geometry of the tissue structure has always been constructed. The slab model comprises five types of tissue layers that are parallel to each other (for an illustration, Fig. 1.5).

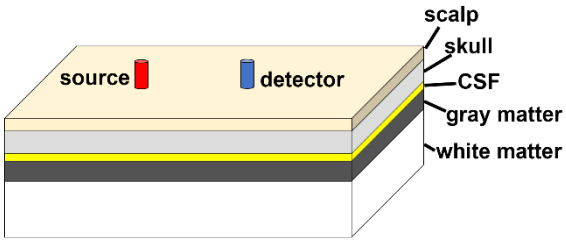

Figure 1. 5 The slab model consists of five types of tissues.

A simulation study using the slab model has suggested that the heterogeneity of the head tissues, especially the non-scattering CSF that surrounds the brain, has a strong influence on light propagation in the brain (Okada et al., 1997). Specifically, Okada et al. (1997) compared light propagation results from models with and without a CSF layer and found that both the PPL and the SSP of the models with a CSF layer are quite different from those without the CSF layer. Given that the CSF layer is not a non-scattering layer, but a low scattering media that is full of arachnoid trabeculae, Okada and Delpy (2003a) adopted the MCM to investigate the effect of low scattering in the CSF layer on light propagation by constructing an adult slab model with discrete scatterers distributed within the CSF layer. They found that the low scattering CSF layer strongly affects the PPL, even that the sensitivity of fNIRS signal is improved by the low-scattering CSF layer (Okada & Delpy, 2003a). More importantly, the thickness of the skull and CSF varies due to individual differences and different positions in the same individual. Thus, a previous

study (Okada & Delpy, 2003b) also used the MCM to examine systematically the effect of the thickness of skull and CSF layer on light propagation in an adult slab model. They reported that, when the SD distance is 30 mm, the PPL in the brain decreases as the skull thickness increases. Besides, results from the SSP, which indicates the volume of tissue interrogated by an SD pair, show a deeper penetration from the head surface in the model with a thicker skull. However, the PPL in the brain scarcely depends on the CSF thickness, whereas the SSP becomes much broader when the CSF thickness increases.

1.4.2 Realistic model

Though an early simulation study using a layered slab with slots mimicking the sulci demonstrates the geometry of the sulci has little influence on the SSP for SD distances of 30 or 40 mm (Okada et al., 1997). However, it is difficult to use the slab model to precisely simulate the photon transport in the real brain structures, because the slab model does not consider the sophisticated geometry of anatomical structures. To address the role of the complex anatomical geometry in light propagation, a three-dimensional (3D) realistic head model with five types of tissues based upon MRI scans is always constructed (Fig. 1.6). The realistic head model consists of a large number of elements, each of which is specified by its optical properties.

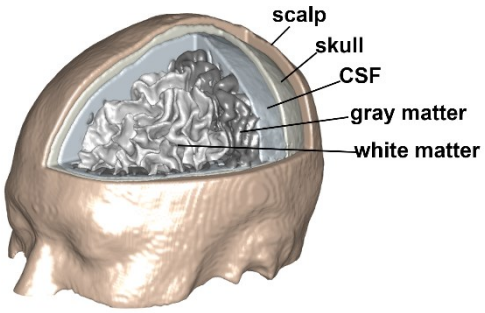

Figure 1. 6 Illustration of the 3D realistic head model

A seminal study (Fukui et al., 2003) using two-dimensional realistic adult and neonatal head models demonstrates that a low scattering CSF layer strongly affects the light propagation in the adult head, rather than the neonatal head. In addition, they found intensely sensitive region is constrained within the gray matter in both adult and neonatal models, whereas the SSP in the neonatal model penetrates the white matter. Subsequently, a series of simulation studies using 3D realistic head models further reveal that light propagation is influenced by the anatomical geometry of the head, or the thickness of superficial layers (Chuang et al., 2013; Dehaes et al., 2011b; Li et al., 2011; Mansouri et al., 2010; Strangman et al., 2013; Strangman et al., 2014). For example, Li et al. (2011) reported that the larger sulcus width results in that the banana shape of the SSP changes to the tropical fish shape which is due to that some fNIRS signals are from the surface of the white matter (Li et al., 2011). Strangman et al. (2014) investigated the effect of scalp and skull on photon transport in the standard head template, revealing that the fNIRS

sensitivity varies significantly due to the measurement positions. Furthermore, the thicker the thickness of the scalp and skull, the smaller the sensitivity to the brain (Strangman et al., 2014). In particular, by constructing subject-specific adult head models, Nakamura et al. demonstrated that variability of the PPL in the brain is very high between subjects and between fiducial points, and that PPL was strongly associated with the depth of the brain surface (Nakamura et al., 2016). These studies described above indirectly reveal that the establishment of precise SCC should be based on the 3D realistic head models mimicking the real head geometry, simultaneously taking account effects of superficial layers.

1.5 Individual difference and early development of head tissue

1.5.1 Individual difference of head tissue structure

Sharma et al investigated the thickness of scalp from 85 subjects aged from 9 months to 17 years. They reported that children younger than 7 years display little variability in the scalp thickness, while subjects who are older than 7 years have slightly increased thickness with age (Sharma et al., 2020). A similar study also demonstrates significant changes in the scalp thickness occur before adulthood. These findings suggest the scalp thickness changes little between each adult individual. However, individual variations in the human skull thickness have been found by different techniques. For instance, Ruan and Prasad reported the thicknesses of the frontal bone of seven adult

human cadaver skulls ranges from 5.05 to 8.13 mm using ultrasonic technology (Ruan & Prasad, 2001). Similarly, some computed tomography studies also demonstrate that there is a substantial individual difference regarding the skull thickness in adults (De Boer et al., 2016; Lillie et al., 2016). Furthermore, structural MRI studies provide evidence of individual differences in terms of the adult brain anatomy (Fleming et al., 2010; Kanai & Rees, 2011), particularly, differences in hemispheric asymmetry of gray matter volumes of Heschl's gyrus caused by gender (Knaus et al., 2006).

1.5.2 Early development of head tissue

Comparing with the individual variability in the anatomical structure of head tissues, the early development of head tissues during the first two years of life is more drastic. First, the brain volume of neonates is only half that of the adult brain, growing quickly to about 90% adult brain volume at the end of the second year (Shi et al., 2011). Second, the scalp thickness increases from 1 to 9 months while decreases from 9 months to 2 years (Young, 1959). Of note, the skull thickness increases significantly from birth to the first year of life and remains a gradual increase until 2 years (Delye et al., 2015; Li et al., 2015). Moreover, the skull thickness is not uniformly distributed among the skull during the early developmental stages (Li et al., 2015). Third, to support the remarkable behavioral and cognitive development, the cortical gray matter volume increases substantially, with

the different growth rates in different cortices from birth to 2 years, in particular, during the first year of life (Gilmore et al., 2012; Wang et al., 2019a). Similarly, the cortical surface and gyrification also display a nonlinear rapid development (Li et al., 2013; Li et al., 2014).

1.6 Source-detector distance

In addition to the heterogeneous structures and optical properties of the head caused by individual differences and the normal development of humans, the SD distance must have a significant influence on the fNIRS sensitivity to brain tissues. Several previous adult studies reveal that the SSP is confined to the extra-cerebral superficial tissues when the SD distance is shorter than 20 mm, while it shifts towards the brain tissue for longer SD distances (Mansouri et al., 2010; Wang et al., 2019b). As the SD distance increases, the PPL in brain tissue increases, and the SSP extends broader (Okada et al., 1997; Strangman et al., 2013; Strangman et al., 2014; Wang et al., 2019b). Importantly, most studies have suggested that the optimal SD distance should be narrowed down to 30–35 mm for the adult population (Chuang et al., 2013; Li et al., 2011; Strangman et al., 2013).

However, only a few studies examined the effect of the SD distance on the fNIRS sensitivity to infant brain tissue. For example, Fukui et al. found that the sensitivity to gray matter and white matter of neonates proportionally increases as the SD distance

increases, whereas that to gray matter is almost constant beyond 30 mm of the SD distance. More importantly, they reported that the sensitivity extends to the deeper region (i.e., white matter) of the brain for the SD pair with a large separation of 40 and 50 mm, which is quite different from adult results (Fukui et al., 2003). Additionally, by actual fNIRS measurement, Taga et al. systematically assessed the effect of the SD distance on hemodynamic responses when 3-month-old infants were presented with auditory stimuli. They declared that the highest sensitivity could be obtained for 3-month-olds when the SD distance is 20 mm by considering the signal-to-noise ratio (Taga et al., 2007).

1.7 Motivation and outline

These threads of evidence from subject-specific and age-related characteristics of head tissues, as well as the influence of heterogeneity of head tissues on light propagation, enlightened me to consider the light scattering in adults and infants when calculating the SCC between SD pairs on the scalp surface and underlying brain regions. Moreover, to date, little is known about how individual differences in the anatomical structure in adults and age-related structural changes during the first 2 years affect the optics-based SCC. I believe that the establishment of precise optics-based SCC is beneficial to investigate the brain function in the adult population during some specific tasks or the functional development in the infant population. Therefore, in this thesis, to address the inaccuracy

of traditional spatial localization methods that adopted point-to-point geometrical correspondence between scalp and cortex, I analyzed the light propagation in 5-layered subject-specific adult head models and age-appropriate infant head models. In addition, I examined the role of inter-individual structural variability in the adult SCC, and how age and SD distance affected the infant SCC.

Chapter 2 discusses that the light propagation analysis methodology used in this thesis is sufficient to guarantee the robustness of the optics-based SCC results for adult and infant populations.

Chapter 3 discusses the feasibility and superiority of the proposed sensitivity-based matching (SBM) method, by comparing it with three other geometrical matching (GM) methods when the SCC was calculated based on the subject-specific adult head models.

Chapter 4 discusses the optics-based SCC for 0-, 1-, and 2-year-old (yo) infants and the effect of age and SD distance on the infant SCC. The optimal SD distance is recommended for future infant fNIRS studies.

Chapter 5 summarizes the current work and main conclusion in this thesis. A potential future work is also presented.

Chapter 2

2 Methodological Verification of Light Propagation Analysis

2.1 Radiative transfer equation

A precise description of photon transport in tissue is provided by the radiative transport equation (Arridge, 1999). The radiation transport equation is given as follows,

$$\frac{1}{c}\frac{\partial I(r,t,\hat{s})}{\partial t} + \hat{s}\nabla I(r,t,\hat{s}) = -(\mu_a + \mu_s)I(r,t,\hat{s}) + \mu_s \int_{4\pi} p(\hat{s},\hat{s}')\, I(r,t,\hat{s}')d\hat{s}' + q(r,t,\hat{s}), \quad (11)$$

where c is the speed of light in the medium, $I(r,t,\hat{s})$ is the radiance at position r and time t, propagating in the direction $\hat{s}$. The phase function $p(\hat{s},\hat{s}')$ is the probability of scattering from direction $\hat{s}$ to $\hat{s}'$. $q(r,t,\hat{s})$ is the light power injected per unit volume at position r in the direction $\hat{s}$ and at time t. This equation is restricted to interactions between light particles themselves and is derived by considering changes in energy flow due to incoming, outgoing, absorbed, and emitted photons within an infinitesimal volume in the medium (energy balance). The left two terms in this equation indicate the difference between the number of photons entering the volume and leaving it per unit time. The term $-(\mu_a + \mu_s)I(r,t,\hat{s})$ represents the attenuation given to light due to absorption and

scattering. The term $\mu_s \int_{4\pi} p(\hat{s}, \hat{s}')\, I(r, t, \hat{s}') d\hat{s}'$ represents the increase in the light due to scattering from all directions to final direction $\hat{s}$.

2.2 Diffusion approximation to the radiative transfer equation

2.2.1 Diffusion equation and finite element method (FEM)

The diffusion equation is the simplest approximation of the radiative transfer equation. The diffusion equation is valid only when $\mu_s \gg \mu_a$ and $1/\mu_s'$ is much smaller than the SD distance (Capart et al., 2021). Since the finite element method (FEM) can numerically solve partial differential equations such as the diffusion equation, it has been widely employed to analyze photon transport in heterogeneous head models with a sophisticated geometry (Arridge et al., 1993; Kawaguchi et al., 2007). The current thesis aims to establish the optics-based SCC between all SD pairs on 10-10 fiducial points and underlying brain regions for subject-specific adult head models and 3 age-appropriate infant head models. A large number of subjects and fiducial points require plenty of computation time and cost, thus the FEM was adopted to simulate the light propagation, instead of the Monte Carlo method (MCM) that is extremely time-consuming. More importantly, key results derived from the FEM were compared with those from the MCM to validate the practical feasibility and reliability of the diffusion approximation to light propagation when calculating of the optics-based SCC. Specifically, the FEM involves

dividing a region of interest into a finite number of volume or area elements. The boundary of one element consists of discrete points called nodes. Surface domains are subdivided into triangles while volumes are subdivided into tetrahedral shapes. Each element is assigned with optical properties (μ_a and μ_s') according to the tissue type which it belongs to. In this thesis, the time-independent diffusion equation was used as follows:

$$-\nabla \cdot k(r)\nabla\Phi(r) + \mu_a(r)\Phi(r) = q_0(r), \tag{12}$$

where $\Phi(r)$ is the photon density at position r, $q_0(r)$ is the continuous wave isotropic light source, $\mu_a(r)$ is the absorption coefficient, and $k(r)$ is the diffusion coefficient defined as

$$k(r) = \frac{1}{3[\mu_a(r)+\mu_s'(r)]} \tag{13}$$

where $\mu_s'(r)$ is the reduced scattering coefficient. An isotropic source located at the distance $1/\mu_s'(r)$ below the surface of the head model is used to approximate the collimated light source. The outgoing flux, $I_{out}(\xi)$, which denotes the intensity of the detected light at position ξ on the boundary, can be obtained from the solution $\Phi(\xi)$ as follows:

$$I_{out}(\xi) = -k(\xi)\hat{n} \cdot \nabla\Phi(\xi), \tag{14}$$

where $\hat{n}$ is the outward normal at position ξ. The PPL can be calculated by the following equation:

$$\langle L_i \rangle = \Delta OD(\xi) \,/\, \Delta\mu_{ai} = \ ln(I_{out0}(\xi)/I_{out1}(\xi))/\Delta\mu_{ai}, \quad (15)$$

$\Delta OD(\xi)$ denotes the change in optical density caused by an ~1% absorption change $\Delta\mu_{ai}$ in a particular region *i*. $I_{out0}(\xi)$ and $I_{out1}(\xi)$ are the intensity of the detected light at position ξ in the rest and activated periods, respectively. Furthermore, the SSP can be further calculated by the photon measurement density function (PMDF). The PMDF $J(\xi, \zeta, r)$ is obtained based on the following equation:

$$J(\xi, \zeta, r) = \Phi(r)\Phi_{adj}(r), \quad (16)$$

where $\Phi(r)$ is the photon density at position r due to an isotropic light source at position ζ and $\Phi_{adj}(r)$ is the photon density at position r due to a hypothetical light source at detector position ξ.

2.2.2 Calculation of optics-based SCC using FEM

An adult subject was selected to illustrate the procedure of calculating the optics-based SCC using the FEM (Fig. 2.1). First, the structural MRI images from the adult subject (Fig. 2.1a) were segmented to a realistic adult head model comprising 5 types of head tissues, i.e., scalp, skull, CSF, gray matter and white matter (Fig. 2.1b). Second, the head model was converted to the mesh model that consisted of a finite number of tetrahedron elements (Fig. 2.1c). Third, the two orientational SD pairs were set on the scalp surface of the mesh model according to the 10-10 system (Fig. 2.1d). Fourth, the

light propagation was analyzed after the adult's optical properties were assigned to each mesh element, which has specific values of absorption and scattering coefficients according to tissue type it belongs to (Fig. 2.1e). Fifth, the brain of the chosen subject was parcellated into 116 brain regions (the abbreviations of brain regions are summarized in Table 2.1) according to the AAL atlas (Fig. 2.1f). Finally, the optics-based SCC was computed by the normalized PPL ($L_{norm,M}$) which was defined in section 2.4.6. Notably, the pipeline for the infant population is similar to that for the adult population. The different points are that three age-appropriate structural MRI images of 0-yo, 1-yo, and 2-yo infants were used to construct infant head models. Moreover, two orientational SD pairs with the five different SD distances (SD distances =10, 15, 20, 25, 30 mm) were set on 10-10 fiducial points.

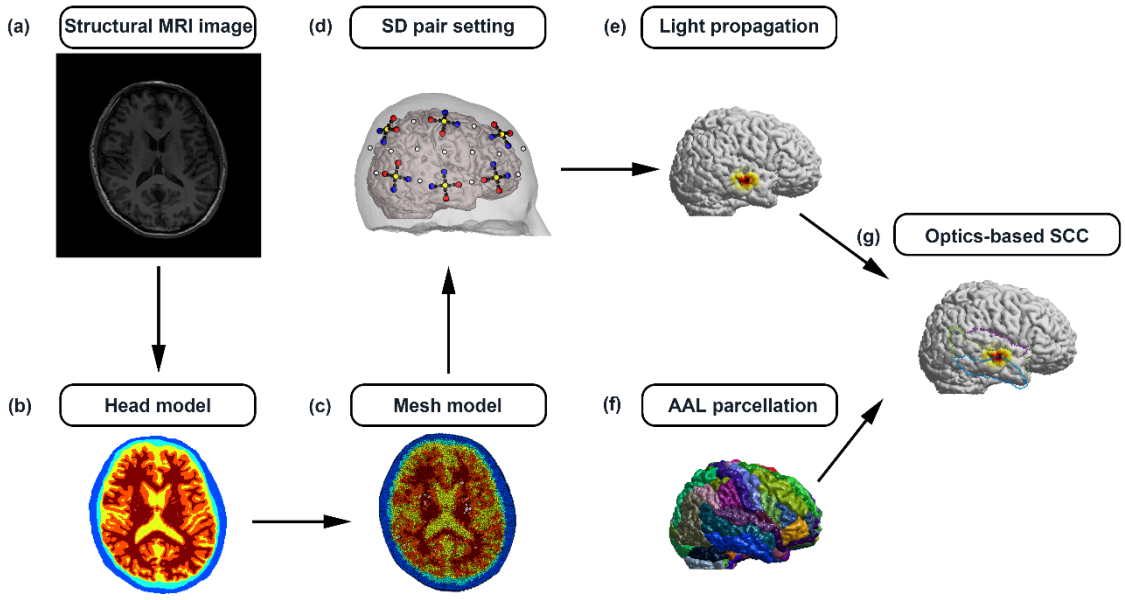

Figure 2. 1 Pipeline of calculating the optics-based SCC using the FEM. (a) Structural MRI images are used to create a 5-layered adult head model. (b) The MRI images are first segmented into 5 tissue types, namely, scalp, skull, CSF, gray matter, and white matter. (c) A FEM mesh model is created using the iso2mesh toolbox. (d) The SD pairs with circumferential and vertical orientations are set at every fiducial point of the international 10-10 system. (e) A spatial sensitivity profile is calculated using the Nirfast light modeling software. (f) The brain is parcellated into 116 brain regions according to the AAL atlas. (g) The optics-based SCC is calculated by using results from (e) and (f).

Table 2. 1 AAL brain regions.

Index	AAL region	Abbreviation	Index	AAL region	Abbreviation
1	Precentral_L	PreCG-L	59	Parietal_Sup_L	SPG-L
2	Precentral_R	PreCG-R	60	Parietal_Sup_R	SPG-R
3	Frontal_Sup_L	SFGdor-L	61	Parietal_Inf_L	IPL-L
4	Frontal_Sup_R	SFGdor-R	62	Parietal_Inf_R	IPL-R
5	Frontal_Sup_Orb_L	ORBsup-L	63	SupraMarginal_L	SMG-L
6	Frontal_Sup_Orb_R	ORBsup-R	64	SupraMarginal_R	SMG-R
7	Frontal_Mid_L	MFG-L	65	Angular_L	ANG-L
8	Frontal_Mid_R	MFG-R	66	Angular_R	ANG-R
9	Frontal_Mid_Orb_L	ORBmid-L	67	Precuneus_L	PCUN-L
10	Frontal_Mid_Orb_R	ORBmid-R	68	Precuneus_R	PCUN-R
11	Frontal_Inf_Oper_L	IFGoperc-L	69	Paracentral_Lobule_L	PCL-L
12	Frontal_Inf_Oper_R	IFGoperc-R	70	Paracentral_Lobule_R	PCL-R
13	Frontal_Inf_Tri_L	IFGtriang-L	71	Caudate_L	CAU-L
14	Frontal_Inf_Tri_R	IFGtriang-R	72	Caudate_R	CAU-R
15	Frontal_Inf_Orb_L	ORBinf-L	73	Putamen_L	PUT-L
16	Frontal_Inf_Orb_R	ORBinf-R	74	Putamen_R	PUT-R
17	Rolandic_Oper_L	ROL-L	75	Pallidum_L	PAL-L
18	Rolandic_Oper_R	ROL-R	76	Pallidum_R	PAL-R
19	Supp_Motor_Area_L	SMA-L	77	Thalamus_L	THA-L
20	Supp_Motor_Area_R	SMA-R	78	Thalamus_R	THA-R
21	Olfactory_L	OLF-L	79	Heschl_L	HES-L
22	Olfactory_R	OLF-R	80	Heschl_R	HES-R
23	Frontal_Sup_Medial_L	SFGmed-L	81	Temporal_Sup_L	STG-L
24	Frontal_Sup_Medial_R	SFGmed-R	82	Temporal_Sup_R	STG-R
25	Frontal_Med_Orb_L	ORBmed-L	83	Temporal_Pole_Sup_L	TPOsup-L
26	Frontal_Med_Orb_R	ORBmed-R	84	Temporal_Pole_Sup_R	TPOsup-R
27	Rectus_L	REC-L	85	Temporal_Mid_L	MTG-L
28	Rectus_R	REC-R	86	Temporal_Mid_R	MTG-R
29	Insula_L	INS-L	87	Temporal_Pole_Mid_L	TPOmid-L

Table 2. 1 AAL brain regions (Continued).

Index	AAL region	Abbreviation	Index	AAL region	Abbreviation
30	Insula_R	INS-R	88	Temporal_Pole_Mid_R	TPOmid-R
31	Cingulum_Ant_L	ACG-L	89	Temporal_Inf_L	ITG-L
32	Cingulum_Ant_R	ACG-R	90	Temporal_Inf_R	ITG-R
33	Cingulum_Mid_L	MCG-L	91	Cerebelum_Crus1_L	CERCRU1-L
34	Cingulum_Mid_R	MCG-R	92	Cerebelum_Crus1_R	CERCRU1-R
35	Cingulum_Post_L	PCG-L	93	Cerebelum_Crus2_L	CERCRU2-L
36	Cingulum_Post_R	PCG-R	94	Cerebelum_Crus2_R	CERCRU2-R
37	Hippocampus_L	HIP-L	95	Cerebelum_3_L	CER3-L
38	Hippocampus_R	HIP-R	96	Cerebelum_3_R	CER3-R
39	ParaHippocampal_L	PHG-L	97	Cerebelum_4_5_L	CER4_5-L
40	ParaHippocampal_R	PHG-R	98	Cerebelum_4_5_R	CER4_5-R
41	Amygdala_L	AMYG-L	99	Cerebelum_6_L	CER6-L
42	Amygdala_R	AMYG-R	100	Cerebelum_6_R	CER6-R
43	Calcarine_L	CAL-L	101	Cerebelum_7b_L	CER7b-L
44	Calcarine_R	CAL-R	102	Cerebelum_7b_R	CER7b-R
45	Cuneus_L	CUN-L	103	Cerebelum_8_L	CER8-L
46	Cuneus_R	CUN-R	104	Cerebelum_8_R	CER8-R
47	Lingual_L	LING-L	105	Cerebelum_9_L	CER9-L
48	Lingual_R	LING-R	106	Cerebelum_9_R	CER9-R
49	Occipital_Sup_L	SOG-L	107	Cerebelum_10_L	CER10-L
50	Occipital_Sup_R	SOG-R	108	Cerebelum_10_R	CER10-R
51	Occipital_Mid_L	MOG-L	109	Vermis_1_2	VER1_2
52	Occipital_Mid_R	MOG-R	110	Vermis_3	VER3
53	Occipital_Inf_L	IOG-L	111	Vermis_4_5	VER4_5
54	Occipital_Inf_R	IOG-R	112	Vermis_6	VER6
55	Fusiform_L	FFG-L	113	Vermis_7	VER7
56	Fusiform_R	FFG-R	114	Vermis_8	VER8
57	Postcentral_L	PoCG-L	115	Vermis_9	VER9
58	Postcentral_R	PoCG-R	116	Vermis_10	VER10

2.3 Monte Carlo method (MCM)

2.3.1 Principle of MCM

The MCM is a stochastic method that has been used to describe light propagation in turbid media with complicated structures. Since MCM can theoretically solve the radiative transport equation with any desired accuracy (Flock et al., 1989), it has been viewed as the gold standard method to model light propagation in biological tissues and to validate other less rigorous methods such as the diffusion approximation to the radiative transport equation. The MCM can predict light propagation in head tissues by tracing random walk steps of many photon packets. The transport of each photon packet is determined by the absorption coefficient, scattering coefficient, scattering phase function, reflex index, and random numbers. At the beginning of a photon packet entering the head model, it has a survival weight, which is related to light intensity. The step size will be sampled randomly based on the optical properties of the head model. When the photon packet hits a boundary, its transmission and reflection will be calculated by Snell's law and Fresnel's law. Next, the photon packet migrates in the head model step by step until it exits the tissue model or is completely absorbed. Consequently, the cumulative distribution of all photon paths obtained from all launched photon packets can estimate accurately the true light propagation. More details about the principle of the MCM could

be found in a review (Zhu & Liu, 2013) and some books (Jacques & Wang, 1995; Kalos & Whitlock, 2009).

2.3.2 Calculation of optics-based SCC using MCM

The diffusion equation cannot rigorously model light propagation in low-level scattering CSF layer and at short SD distances, so the MCM was used to verify results obtained by the FEM. A previously described variance reduction technique (Hiraoka et al., 1993; Oki et al., 2009) was employed to simulate photon transport in the adult and infant head models. Unlike the FEM using the mesh model, the MCM can directly use the voxel-based 5-layered head model to analyze light propagation. Therefore, the pipeline of calculating the optics-based SCC using the MCM is different from that for the FEM only in steps c and e in Fig. 2.1. Specifically, the scattering coefficient of each voxel $\mu_s(\boldsymbol{r})$ in the head model was calculated from the reduced scattering coefficient μ_s' and the scattering anisotropy factor g.

$$\mu_s(\boldsymbol{r}) = \mu_s'(\boldsymbol{r})/(1-g). \tag{17}$$

The propagation of each photon packet in the head model is co-determined with the scattering coefficient, scattering phase function, and random numbers. The Henyey-Greenstein function is used to calculate the scattering phase function and the scattering anisotropy factor is set as 0.9, due to light being highly forward scattering in biological

tissue. Each photon packet has a survival weight which represents the number of photons successively propagating without absorption. The weight W corresponding to the number of photons absorbed in a voxel at a point $\boldsymbol{r}$ was calculated as

$$W = W_j\left[1 - \exp\left(-\mu_a(\boldsymbol{r})l_j\right)\right] = \Phi(\boldsymbol{r})\mu_a(\boldsymbol{r}), \quad (18)$$

Where W_j is the survival weight at the incident point on the voxel, l_j is the path length in the voxel and $\Phi(\boldsymbol{r})$ is the photon density. The weight corresponding to the number of photons absorbed in each voxel is accumulated for all the photon packets (a hundred million photon packets are traced for each SD pair) to calculate the distribution of the photon density. When the photon packet reaches the detector, the survival weight at the exit point and optical pathlength in each voxel are recorded to calculate the PPL in each AAL brain region. In addition, the SSP is calculated from Equation (16).

2.4 Light propagation analysis of subject-specific adult head models

2.4.1 Acquisition of MRI images

Forty-five healthy Japanese adults (23 males; age range, 21–58 years; mean = 37.7 years; SD = 11.5) were recruited to participate in this study after providing written informed consent. All MRI data are from a previous study (Kurihara et al., 2015), which was approved by the Ethics and Radiation Safety Committees of the National Institute of Radiological Sciences, Chiba, Japan. The collection and use of current data were also

approved by the research ethics committee of the Faculty of Science and Technology, Keio University.

For each adult subject, T1-weighted (T1W), fat-saturated proton density weighted (FS-PDW) and fast imaging employing steady-state acquisition (FIESTA) images were acquired under a 3.0-T clinical MR system (SignaHDx 3.0; GE Healthcare, Milwaukee, WI, USA). The detailed scan parameters of the three contrast variant images are as follows: a) T1W, 3-dimensional spoiled gradient echo (3D-SPGR) with inversion pulse and array spatial sensitivity encoding technique (ASSET), repetition time (TR) / echo time (TE) / inversion time (TI) = 6.8/1.9/450 ms, flip angle (FA) = 12 degree, matrix = 256 × 256, number of excitation (NEX) = 1; b) FS-PDW, 3D-SPGR with ASSET and tailored radiofrequency pulse for FS, TR/TE = 13.8/1.9 ms, FA = 6 degree, matrix = 256 × 256, NEX = 1; c) FIESTA, TR/TE = 13.8/1.9, FA = 45 degree, matrix = 256 × 256, NEX = 1. ASSET factor of 2 was applied to all sequences using ASSET. The field of view and slice thickness of all the images are 26.0 cm and 1.0 mm, respectively. All the image data were anonymized before the segmentation process.

2.4.2 Construction of subject-specific adult head models

The analysis pipeline for constructing the head model is based on the previous work (Kurihara et al., 2015). Firstly, the air/scalp, scalp/skull, and skull/CSF boundaries were

extracted from the FS-PDW images, due to a low signal intensity at the skull and high signal intensity at the scalp and CSF in the FS-PDW images (Keller et al., 1987). Since the CSF has a higher signal intensity than the gray matter in the FIESTA image, the CSF/brain boundaries could be easily extracted using the FIESTA image (Schmitz et al., 2003). The brain tissues extracted from the FIESTA image were further segmented into gray matter and white matter using the T1W image by the FMRIB's Automated Segmentation Tool (FAST) (Zhang et al., 2001). The extra-cerebral regions were segmented by binarization and morphological operations. The 3D view (Fig. 2.2a) and different slice views (Figs. 2.2b-d) of a 5-layered subject-specific head model (Subject ID: 25) with the complex anatomical structure are shown.

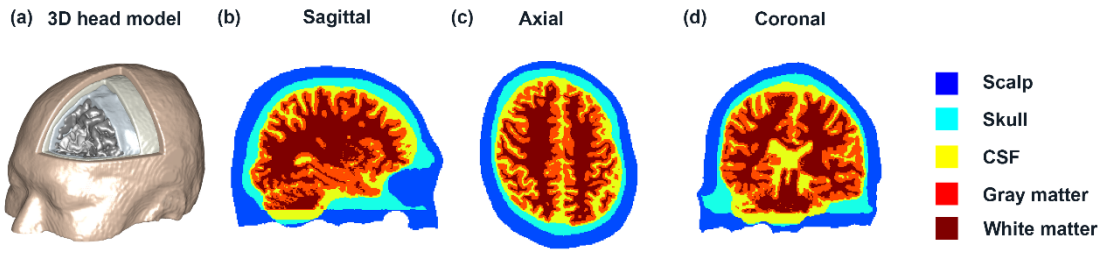

Figure 2. 2 The 5-layered subject-specific adult head model. MR images are segmented into the scalp, skull, CSF, gray matter, and white matter (a) 3D segmented geometry of the head model for one representative subject. (b-d) The segmented images for different slice views from the same subject.

2.4.3 Subject-specific brain parcellation

To compute the optics-based SCC at the individual level, it is necessary to parcellate the brain into different multiple non-overlapping brain regions for every subject. Because it is time-consuming to parcellate each individual brain by manual delineation, a semi-automatic pipeline was used to parcellate the brain of 45 subjects according to an unpublished master's thesis (Tsuyuki, 2016). Herein, the AAL atlas that parcellates a human brain according to the macro-anatomical structure (Tzourio-Mazoyer et al., 2002) was transferred onto the brain of each individual subject (Fig. 2.3). Given that the AAL atlas is generated using a single subject brain (Colin27) in MNI space, the ICBM-152 brain template defined in the MNI coordinates was selected as a reference brain to parcellate the individual brain. The ICBM-152 has been demonstrated to be the best template for the description of scalp positions and their correlation to MNI coordinates of the underlying cerebral structures by combining both high spatial resolution and signal-to-noise while avoiding the "single brain" criticism subject to the vagaries of any single brain (Cutini et al., 2011; Huang et al., 2016). Since the AAL atlas is based on gyri and sulci, the 17 major sulci as landmarks were first extracted from both the individual brains (Fig. 2.3a) and the ICBM-152 brain template (Fig. 2.3b). Here, the 17 sulci are longitudinal fissure, bilateral central sulcus, bilateral pre-central sulcus, bilateral post-

central sulcus, bilateral superior frontal sulcus, bilateral inferior frontal sulcus, bilateral sylvian fissure, bilateral superior temporal sulcus, and bilateral intraparietal sulcus. Next, the brain template with 17 sulci was transformed to align with the individual brain with 17 sulci by SPM DARTEL (Fig. 2.3c) (Ashburner, 2007). However, the sulci of the transformed brain template misaligned slightly with those of the individual brain. Hence, a radial basis functional transform (RBFT) algorithm (Pighin et al., 2006) was applied to further reshape the transformed brain template to align with the individual brain (Fig. 3.2d), by using sulcal positions as anchor points. Consequently, the AAL brain regions on the brain template (Fig. 2.3e) were transferred onto the structure of the individual brain (Fig. 2.3f). The combination of DARTEL with a transformation based on the shape of the sulci improved the consistency and accuracy of the alignment performance (Auzias et al., 2011). Finally, 116 brain regions on the AAL atlas (Table 2.1) were transferred from the brain template to the individual brain using transformation functions obtained by SPM DARTEL and RBFT. The above pipeline was repeated for the brain structures of the 45 subjects. Using the 45 subject-specific adult head models, the effect of inter-subject anatomical variability on the optics-based SCC can be analyzed.

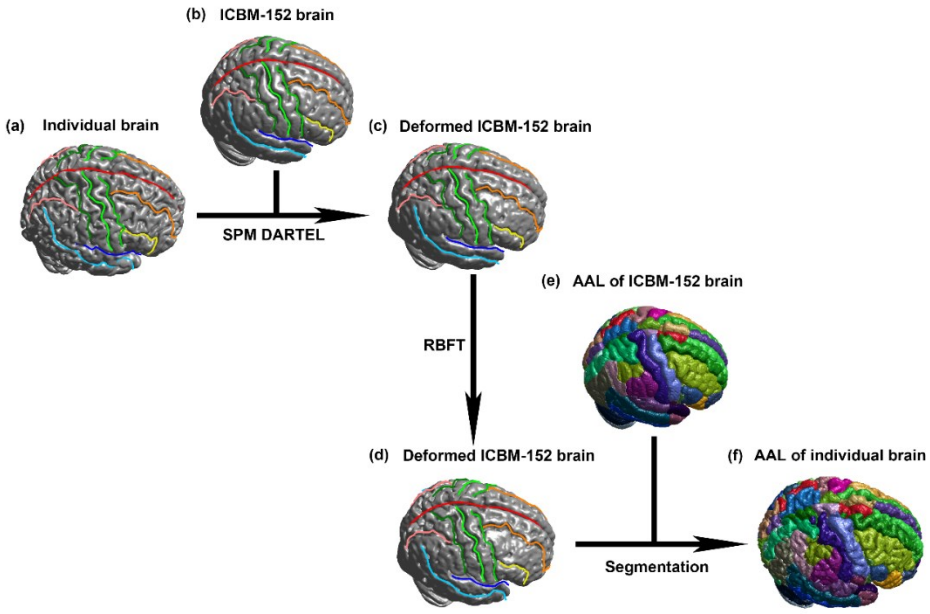

Figure 2. 3 Parcellation of subject-specific brain according to the AAL atlas. The 17 major sulci were identified on the structures of each brain of the 45 individual subjects (a) and the ICBM-152 brain template (b). The brain structure and sulci of a representative subject are shown in (a). The sulcal positions were used to accurately transform the ICBM-152 brain template into each individual brain. The AAL regions on the ICBM-152 brain template (e) were transferred to the individual brain (f) by applying the transformation functions, SPM DARTEL (c) and RBFT (d), based on the brain structure and sulcal positions. The AAL regions of the representative subject are shown in (f).

2.4.4 Quality evaluation for subject-specific mesh models

Before calculating the optics-based SCC using the SBM method, the 45 subject-specific mesh models must be created, and their mesh quality should be evaluated. Specifically, the volumetric tetrahedral mesh for each segmented 3D head model was generated by the iso2mesh toolbox (Fang & Boas, 2009). The number of nodes, faces, elements for each adult mesh model was calculated. Importantly, I also computed the Joe-

Lie quality index (Liu & Joe, 1994), q_{vol}, for every tetrahedron for each adult mesh model using the following equation:

$$q_{vol} = \frac{12 \times (3 \times vol)^{\frac{2}{3}}}{\sum_{0 \le i \le j \le 3} l_{i,j}^2}, \tag{19}$$

where *vol* is the tetrahedral volume and $l_{i,j}$ are the lengths of the edges of the tetrahedron. This metric is equal to 1 for equilateral tetrahedra and tends to 0 for degenerated tetrahedra. The higher q_{vol} values, the higher quality of the mesh. Table 2.2 displays that the total number (N) of nodes, faces and elements, as well as the mean q_{vol} (across all tetrahedrons) with its standard deviation. I found that the number of nodes, faces and elements are similar across all 45 subjects. The mean values of q_{vol} for each adult mesh model are higher than 0.75, suggesting that all meshes achieve a relatively high quality. These results demonstrate that most elements are close to equilateral and no elements are completely degenerated, guaranteeing the good quality of every mesh model to conduct the light propagation analysis.

Table 2. 2 For every adult subject, the properties of the volumetric mesh (number of nodes, faces, elements and the Joe–Liu quality index) are reported.

Subject ID	N nodes	N faces	N elements	Mean q_{vol} ± std
Subject01	332991	925690	2005948	0.773±0.134
Subject02	330857	850000	1991795	0.776±0.134
Subject03	386378	1009160	2329062	0.778±0.133
Subject04	334604	895734	2015049	0.773±0.135
Subject05	388305	936544	2330277	0.787±0.128
Subject06	371523	961654	2232227	0.781±0.131
Subject07	355387	984476	2135847	0.774±0.133
Subject08	333277	908792	2002244	0.777±0.132
Subject09	366811	944664	2213374	0.775±0.134
Subject10	363199	915658	2178862	0.786±0.128
Subject11	360929	875696	2163869	0.787±0.128
Subject12	356372	891198	2138734	0.787±0.128
Subject13	372426	920336	2233957	0.784±0.130
Subject14	361424	865688	2169531	0.786±0.129
Subject15	363768	1010758	2191933	0.775±0.133
Subject16	296421	807884	1769325	0.775±0.133
Subject17	309954	836066	1862887	0.775±0.133
Subject18	315278	820802	1898395	0.783±0.130
Subject19	336344	865314	2016804	0.785±0.129
Subject20	348943	862112	2093070	0.783±0.130
Subject21	398675	1003148	2387859	0.786±0.128
Subject22	339352	889640	2036276	0.783±0.129
Subject23	393873	959498	2360304	0.780±0.132
Subject24	403026	1099570	2425408	0.781±0.129
Subject25	374194	944756	2248983	0.778±0.133
Subject26	360396	919986	2160958	0.789±0.125
Subject27	352911	904244	2124045	0.778±0.133
Subject28	302518	801842	1811217	0.775±0.133
Subject29	338059	887572	2019250	0.785±0.128
Subject30	323506	881344	1939768	0.777±0.132

Table 2. 2 For every adult subject, the properties of the volumetric mesh (number of nodes, faces, elements and the Joe–Liu quality index) are reported (Continued).

Subject ID	N nodes	N faces	N elements	Mean q_{vol} ± std
Subject31	343869	877844	2063402	0.783±0.130
Subject32	344962	897156	2071738	0.778±0.133
Subject33	413630	1051778	2477568	0.786±0.128
Subject34	390706	1013650	2346196	0.783±0.129
Subject35	412180	1056160	2476876	0.774±0.135
Subject36	355873	952976	2132844	0.778±0.132
Subject37	342496	941882	2056445	0.771±0.135
Subject38	375994	986258	2257930	0.783±0.129
Subject39	340017	858814	2043639	0.782±0.131
Subject40	409317	977686	2461934	0.782±0.131
Subject41	374825	1041746	2245562	0.782±0.129
Subject42	436207	1075322	2618778	0.790±0.126
Subject43	415434	981524	2492235	0.791±0.126
Subject44	309896	848302	1861158	0.772±0.135
Subject45	387816	1050852	2326165	0.781±0.129

2.4.5 Arrangement of SD pairs at 10-10 fiducial points

Numerous researchers in the fNIRS community have adopted the 10-10 or 10-20 system to position their SD pairs to detect targeted brain regions (Anderson et al., 2017; Jiang et al., 2015; Minagawa-Kawai et al., 2007; Moriguchi & Hiraki, 2009). As such, the optics-based SCC at the fiducial points of the 10-10 system was analyzed. Specifically, the coordinates of anatomical landmarks corresponding to the inion, nasion, and left and right periauricular points were firstly identified manually in each subject-specific head model. Then all of 61 fiducial points on the scalp of the head model according to the 10-

10 system (Jurcak et al., 2007; Nuwer, 2018) were set. To examine whether the orientation of the SD pair affects the optics-based SCC, two SD pairs were placed in a circumferential and vertical orientation at each fiducial point. The distance between the source and detector was set as 30 mm because the SD distance of 30 mm has been identified as the optimal SD spacing for adult fNIRS studies (Strangman et al., 2013), and the midpoint of SD pairs was set on the fiducial points. The positions of SD pairs as rendered in a head model with different views are shown in Fig. 2.4.

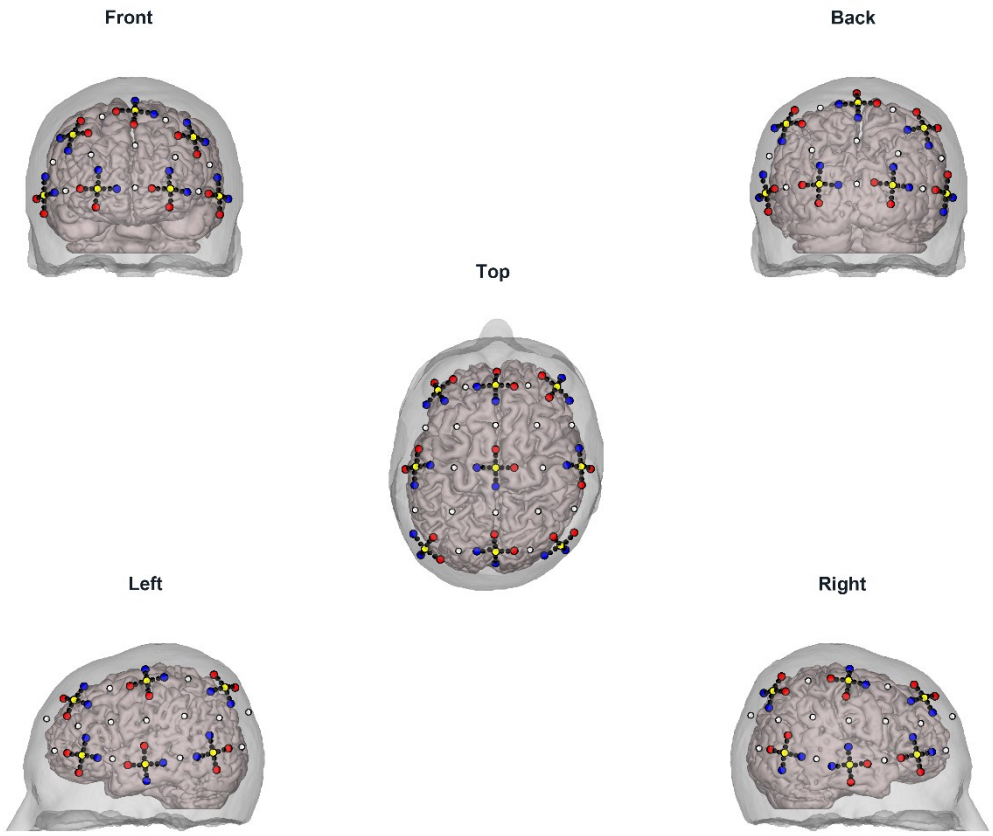

Figure 2. 4 The arrangement of SD pairs according to the 10–10 system. Two orientational SD pairs set at 10–20 fiducial points (yellow dots) superposed on the surface of one subject's scalp for different views. The sources and detectors are indicated by red and blue circles, respectively. Black dotted lines are used for displaying circumferential and vertical probe pairs. Note that SD pairs are also attached on the 10–10 fiducial points (white dots), but are not shown to avoid complications.

2.4.6 Calculation of optics-based SCC

The light propagation in the head models was calculated by Nirfast, a finite element-based package that uses a diffusion approximation for modeling photon transport in tissue (Dehghani et al., 2009; Jermyn et al., 2013). Optical properties (i.e., the absorption

coefficient μ_a, scattering coefficient μ_s, anisotropy factor g, and refractive index n) in every tissue layer of adult head models were specified from the reported data for each type of tissue, i.e., scalp (Torricelli et al., 2001); skull (Bevilacqua et al., 1999; Firbank, 1994); CSF (Hale & Querry, 1973; Okada & Delpy, 2003a); gray matter and white matter (Bevilacqua et al., 1999; Gebhart et al., 2006) at an 800-nm wavelength as shown in Table 2.3. Notably, the reduced scattering coefficient μ_s' should be used in analyzing light propagation using the diffusion equation, where $\mu_s' = \mu_s(1- g)$.

Table 2. 3 Adult optical properties of tissue types for light propagation analysis.

	μ_a (mm^{-1})	μ_s (mm^{-1})	g	n
Scalp	0.016	13.5	0.9	1.4
Skull	0.01	9.8	0.9	1.4
CSF	0.004	3	0.9	1.4
Gray matter	0.019	8.6	0.9	1.4
White matter	0.011	41.6	0.9	1.4

The SBM was defined as a methodology to analyze the SCC based on a light propagation analysis. Based on the results obtained from a light propagation analysis using the FEM or MCM, the PMDF was calculated at each node of the mesh model for FEM, while the PMDF was calculated at each voxel of the head model. Under the conditions in the light propagation analysis of this study, the PMDF has the same spatial

distribution as the SSP (Oki et al., 2009). Since the SSP can be considered the PPL in a small volume, the sum of the SSP in a brain region is equivalent to the PPL of the same region. In other words, the sum of PMDF in a brain region is linearly related to the PPL within the same region. Given that each node (or voxel) in the head model is labeled as a specific AAL brain region, the normalized PPL ($L_{norm,M}$) in a given brain region M was defined using the following equation to quantify the optics-based SCC:

$$L_M = \frac{l_M}{\sum_{j=1}^{N} l_j} \tag{20}$$

where l_M and l_j is the sum of PMDF of all nodes (or voxels) within the brain regions M and j, respectively. N is the number of brain regions within the whole brain tissue. As PMDF is a probability density function (Arridge & Schweiger, 1995), the $L_{norm,M}$ is regarded as the probability that the fNIRS signal is affected by the brain activation of the region M. The $L_{norm,M}$ was calculated for circumferential and vertical SD pairs at every fiducial point for all 45 subjects. Note that the 45 subject-specific individual head models with unique individual brain parcellation were used to obtain the $L_{norm,M}$.

2.5 Light propagation analysis of age-appropriate infant head models

2.5.1 Infant head structure and AAL atlas

The anatomical head structure of the infants at 0-, 1- and 2 years of age and the corresponding brain atlas used in this study were obtained from publicly available data

(Shi et al., 2011). The use of data from open-access database was approved by the research ethics committee of the Faculty of Science and Technology, Keio University. In the present study, age-appropriate average structural images acquired with a 3T magnetic resonance imaging (MRI) scanner were used. A set of longitudinal images of 95 healthy infants (56 males and 39 females, gestational age at birth: 37.9 ± 1.8 (mean ± standard deviation) weeks) were scanned three times when their postmenstrual age was 41.5 ± 1.7, 94.2 ± 3.4, and 146.2 ± 4.9 weeks, respectively. Judging from the difference of subtracting gestational age from postmenstrual age, the population used in this study could be divided into 3 age groups concentrating around 0, 1 and 2 years of age. All participants in the dataset had normal fetal ultrasound during pregnancy and were free of congenital anomalies, metabolic disease, and focal lesions after birth. T2-weighted images were obtained with a voxel size of 1.25 × 1.25 × 1.95 mm^3 for 0-yo and T1-weighted images were obtained with a voxel size of 1 × 1 × 1 mm^3 for 1-yo and 2-yo. The tissue probability maps of GM, WM, and CSF that exhibit similar geometry to the structural images were also used for the head tissue segmentation.

To obtain the optics-based SCC between the fiducial points and brain regions, the AAL atlas was chosen to parcellate the infant's brain. The AAL atlas is widely used in cognitive neuroscience. In addition, remarkably, it parcellates a human brain into multiple

non-overlapping regions according to the identification of main sulci, which are already clearly visible from birth and preserved throughout normal brain development (Kabdebon et al., 2014). The AAL atlas with 90 brain regions excluding cerebellum (see brain regions from 1-90 in Table 2.1) in the infant space was used, which maintains the consistency of the AAL map propagation from the adult Colin 27 brain to the infant images using indirect fusion approach and a feature-based groupwise registration algorithm (Shi et al., 2011). Infant atlases from 0-, 1-, and 2-yo were built using infant MRI segmentation and groupwise registration methods. The atlases are publicly available on the NITRC website (https://www.nitrc.org/projects/pediatricatlas).

2.5.2 Construction of age-appropriate infant head models

An age-appropriate template of the head can be used to substitute the subject-specific head anatomy to localize the macro-anatomical structure when individual infant MRIs are not available (Emberson et al., 2017; Lloyd-Fox et al., 2014). Hence, three age-appropriate head models were constructed by segmenting the tissues of average MRI images from 0-, 1-, and 2-yo infants for further light propagation analysis. Specifically, a semiautomatic approach was used to segment the MRI images into air and five types of head tissues with different optical properties. First, the head masks, that is, the air/scalp boundaries, were extracted from the average T2-weighted images for 0-yo, and T1-

weighted images for 1- and 2-yo using a simple thresholding method. Second, the tissue probability maps of CSF, gray matter, and white matter were converted to binary intracranial regions in each image. It was difficult to identify the scalp/skull and skull/CSF boundaries in the average MRI images because of the thin structures of the scalp and skull and blurring caused by the averaging of slightly misaligned multi-subject images. Thus, morphological operations were applied to extract the scalp/skull and skull/CSF boundaries based on the representative thickness of the scalp (3.5, 4.0, and 4.0 mm for 0-, 1-, and 2-yo, respectively) and skull (2.2, 3.0, and 3.8 mm for 0-, 1-, and 2-yo, respectively), as described in the literature (Li et al., 2015; Young, 1959). Finally, 5-layered head models of 0-, 1-, and 2-yo infants were created by integrating the above intracranial regions and boundaries of superficial tissues. Contradictions in the integration process were manually and/or automatically corrected. The age-appropriate 5-layered infant models for the three age groups are shown in Fig. 2.5.

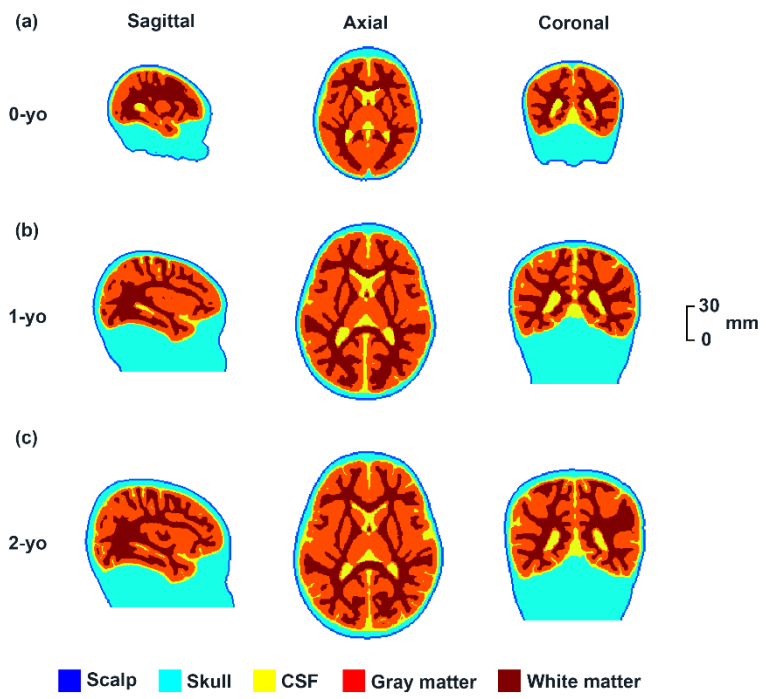

Figure 2. 5 Age-appropriate 5-layered infant head models for 0-yo (a), 1-yo (b), and 2-yo (c) infants, which comprise the scalp, skull, CSF, gray matter, and white matter. The first, second, and third columns show the sagittal, axial, and coronal views of the infant head models, respectively.

2.5.3 Quality evaluation for age-appropriate infant mesh models

Before analyzing the light propagation, the quality of infant mesh models should also be assessed, since infants have very thin superficial layers. Therefore, the number of nodes, faces, elements and the Joe-Lie quality index for each infant mesh model were computed for each infant mesh model. The first three rows in Table 2.4 displays that the total number (N) of nodes, faces and elements. The fourth row in Table 2.4 shows the mean q_{vol} (across all tetrahedrons) with its standard deviation. The number of nodes, faces

and elements increases from 0 year to 2 years. The mean values of q_{vol} for each age group are higher than 0.75, suggesting that all meshes achieve a relatively high quality. In addition, 76.9%, 80.5% and 79.2% of all meshes have q_{vol} values higher than 0.7 for 0-yo, 1-yo, and 2-yo infants, respectively. The lowest q_{vol} value observed in any of the meshes is 0.11. These results demonstrate that every infant mesh model has a good quality to conduct the light propagation analysis.

Table 2. 4 For every age, the properties of the volumetric mesh (number of nodes, faces, elements and the Joe–Liu quality index) are reported.

	0-yo	1-yo	2-yo
N nodes	101056	212418	243541
N faces	293208	519898	555656
N elements	594241	1260896	1451619
Mean q_{vol} ± std	0.784 ± 0.131	0.799 ± 0.123	0.793 ± 0.127

2.5.4 Arrangement of SD pairs at 10-10 fiducial points

The international 10-10 system positions (Jurcak et al., 2007; Nuwer, 2018) were virtually set on the age-appropriate head models of 0-, 1-, and 2-yo using custom analysis scripts written in MATLAB (Mathworks, Natick, MA). First, I manually identified the four anatomical landmarks, including the inion, nasion, and left and right periauricular points on the scalp surface of the infant head models. Then, 61 fiducial points of the 10-10 system were automatically assigned to the scalp of the head model of every age, as depicted in Fig. 2.6.

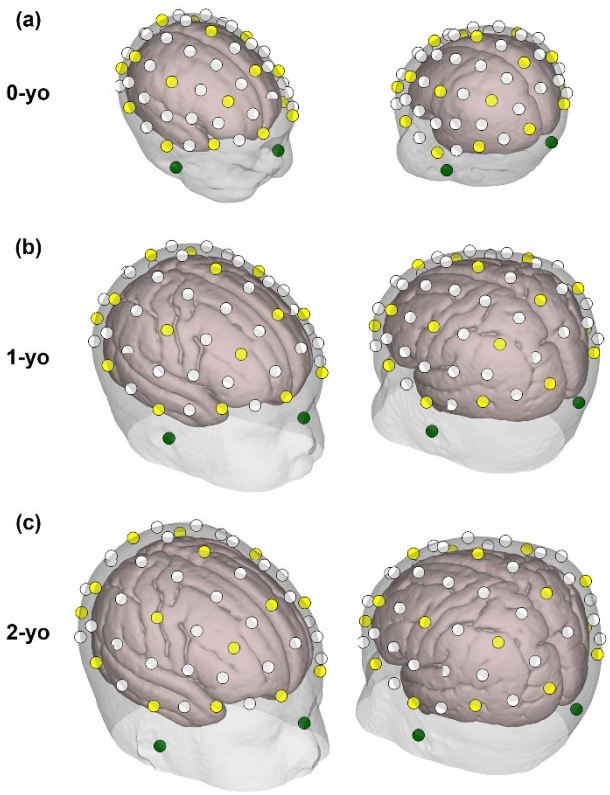

Figure 2. 6 Anatomical landmarks (in dark green), 10-20 fiducial points (in yellow), and 10-10 fiducial points (in white) on the head models of 0-yo (a), 1-yo (b), and 2-yo (c). In the left subfigure, the nasion and right periauricular point can be observed, while the left periauricular point and inion are visible in the right subfigure.

Because the SD distance significantly affects the sampling regions of SD pairs, the distances between sources and detectors were set as 10, 15, 20, 25, and 30 mm, where the midpoints of the SD pairs were set at the 10-10 fiducial points. Here, SD distances higher than 30 mm were not examined due to a SD distance higher than 30 mm showing extremely poor signal-to-noise ratio in 3-month-old infants (Taga et al., 2007). Two SD pairs were placed according to the circumferential and vertical orientations at each

fiducial point to examine whether the SD pair orientation influences the optics-based SCC for 0-, 1-, and 2-yo. The SD pair arrangements on the head models for five different SD distances for each age are shown in Fig. 2.7.

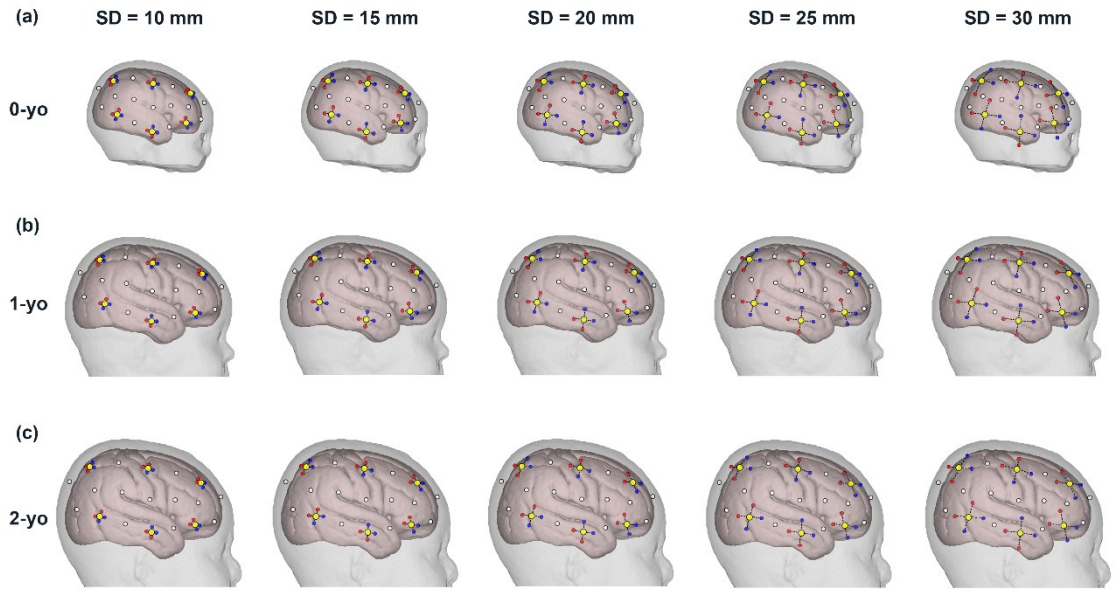

Figure 2. 7 SD pair arrangements on head models for five different SD distances for 0-yo (a), 1-yo (b), and 2-yo (c). The sources and detectors are indicated in red and blue dots, respectively. Two orientational SD pairs at the 10-20 fiducial points (yellow dots) are displayed only on the right hemisphere. Notably, SD pairs were also attached to the 10-10 fiducial points (white dots); however, the sources and detectors at these locations are not shown to avoid complications. The circumferential and vertical SD pairs at each fiducial point are indicated by two dashed black connections, respectively.

2.5.5 Calculation of optics-based SCC

Like section 2.4.6, I also adopted the SBM method to calculate the $L_{norm,M}$ to obtain the optics-based SCC using the FEM and MCM. Of note, the optical properties of each tissue type in the infant head models for a wavelength of 800 nm are specified in Table

2.5 according to previous studies on neonates (Dehaes et al., 2013; Fukui et al., 2003).

Table 2. 5 Infant optical properties of tissue types for light propagation analysis.

	μ_a (mm^{-1})	μ_s (mm^{-1})	g	n
Scalp	0.018	19	0.9	1.4
Skull	0.016	16	0.9	1.4
CSF	0.0041	0.32	0.9	1.4
Gray matter	0.048	5.0	0.9	1.4
White matter	0.037	10	0.9	1.4

2.6 Methodological verification in adult population

For an arbitrary adult subject, two fiducial points (i.e., T3 and P6) were selected to validate whether the optics-based SCC results from the FEM were comparable to those from the MCM. As shown in Fig. 2.8, the SSP obtained by the FEM is slightly localized than that obtained by the MCM, for both fiducial points T3 and P6. However, the same fiducial points are correlated with the highly similar brain regions, regardless of the methods of light propagation analysis. For instance, the circumferential SD pair set on T3 mainly corresponds to MTG_L (L_{norm,MTG_L} = 75.7%) and STG_L (L_{norm,STG_L} = 23.7%) for the FEM. Likewise, the MCM reveals that T3 is correlated with MTG_L (L_{norm,MTG_L} = 54.3%) and STG_L (L_{norm,STG_L} = 32.1%), although ITG_L ($L_{norm,ITG}$ = 9.3%) is a potential brain region. Taking the fiducial point P6 as another example, the

circumferential SD pair set on P6 has three main underlying brain regions, such as MOG_R (L_{norm,MOG_R} = 48.9%), MTG_R (L_{norm,MTG_R} = 38.6%), and ANG_R (L_{norm,ANG_R} = 11.8%) for the FEM. The broadened SSP obtained by the MCM shows P6 remains corresponding to these three brain regions (L_{norm,MOG_R} = 48.2%, L_{norm,MTG_R} = 13.4%, and L_{norm,ANG_R} = 23.5%), whereas other two brain regions are corresponded in relatively low probabilities (L_{norm,SMG_R} = 7.2%, and L_{norm,IPL_R} = 5.1%). Importantly, the brain regions with the maximum $L_{norm,M}$ corresponding to T3 or P6 are completely the same for the FEM and MCM, that is, MTG_L for T3 and MOG_R for P6. The values of the normalized PPL of underlying brain regions that are correlated with the circumferential SD pairs set on T3 and P6 obtained by the MCM and FEM for a representative adult are summarized in Table 2.6.

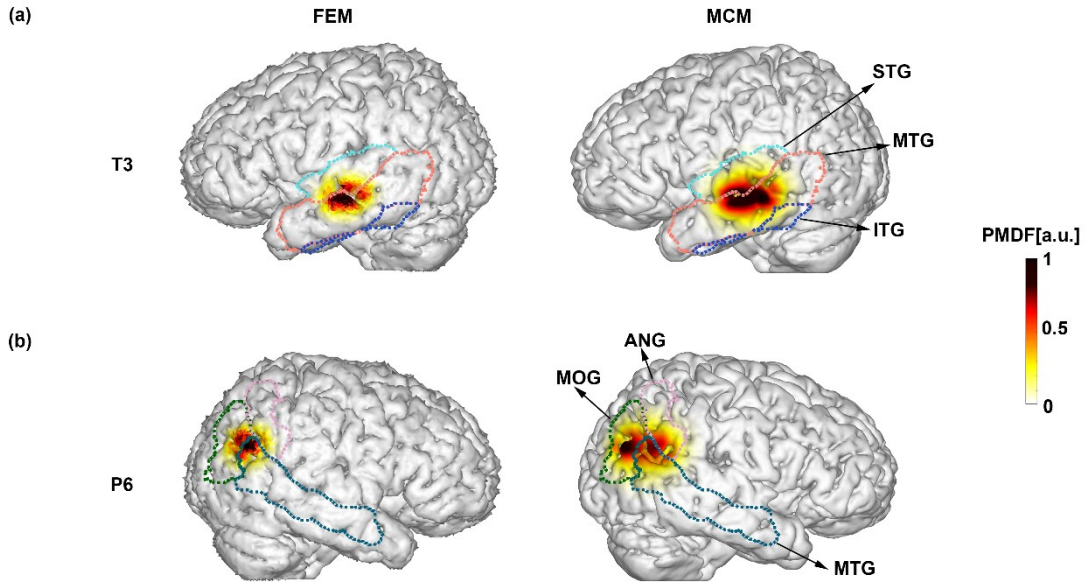

Figure 2. 8 Comparison between optics-based SCC derived from the FEM and MCM for two representative fiducial points T3 (a) and P6 (b). The PMDFs of the circumferential SD pairs set on the fiducial points T3 and P6 are shown for the same subject. Dashed contours in different colors denote the boundaries of brain regions.

Table 2. 6 $L_{norm,M}$ of brain regions that circumferential SD pairs set on T3 and P6 corresponded to obtained by the MCM and FEM for a representative adult.

Fiducial point	Brain region	MCM	FEM
T3	**MTG-L**	**54.3%**	**75.7%**
	STG-L	32.1%	23.7%
	ITG-L	9.3%	0.3%
P6	**MOG_R**	**48.2%**	**48.9%**
	MTG_R	13.4%	38.6%
	ANG_R	23.5%	11.8%
	SMG_R	7.2%	0.1%
	IPL_R	5.1%	0.1%

Note: The maximum $L_{norm,M}$ obtained by the FEM and MCM at each fiducial point are shown in bold.

2.7 Methodological verification in infant population

Given that the head structures of infants have a large discrepancy compared with those of adults, such as the smaller head size, thinner superficial layers, and different optical properties of infant head tissues, the optics-based SCC obtained by the FEM also should be verified by the MCM.

2.7.1 Comparison between optics-based SCC obtained by FEM and MCM

For the infant population, two representative fiducial points (i.e., T4 and P5) were chosen to examine the robustness of diffusion approximation to light propagation using the FEM. As the diffusion equation work not well when the SD distance is smaller than $10/\mu_s'$, the optics-based SCC results at all SD distances from 10 mm to 30 mm were assessed. Fig. 2.9 shows the PMDF of circumferential SD pairs on T4 over an SD distance of 10 mm. The SSP of T4 is slightly broadened for the FEM, compared with the MCM, for each age group. Specifically, T4 of 0-yo infants is correlated to MTG_R (L_{norm,MTG_R} = 63.6%) and ITG_R (L_{norm,ITG_R} = 34.6%) for the FEM. If the MCM is used, the $L_{norm,M}$ of MTG_R and ITG_R were 84.4% and 15.3%. Moreover, T4 of 1-yo infants has same corresponding brain regions with slightly different $L_{norm,M}$ for the FEM (MTG_R: 83.6%; ITG_R: 15.3%) and the MCM (MTG_R: 92.5%; ITG_R: 7.4%). Similarly, T4 of 2-yo infants corresponds to MTG_R (L_{norm,MTG_R} = 89.0%) and ITG_R (L_{norm,ITG_R} = 7.8%) for

the FEM, while it corresponded to MTG_R (L_{norm,MTG_R} = 96.9%) and ITG_R (L_{norm,ITG_R} = 2.4%) for the MCM. Similar results are found for 15, 20, 25, 30 mm SD distances, and the values of L_{norm,MTG_R} *and* L_{norm,ITG_R} are summarized in Table 2.7. To investigate whether the comparison between the FEM and MCM was dependent on the scalp location, the optics-based SCC of fiducial point P5 is also reported. The SSP of P5 replicated that of T4, that is, the SSP obtained by FEM is slightly broader than that by the MCM (Fig. 2.10). As summarized in Table 2.8, three brain regions are mainly correlated to SD pairs set on P5, and the $L_{norm,M}$ of these brain regions are similar for the FEM and MCM.

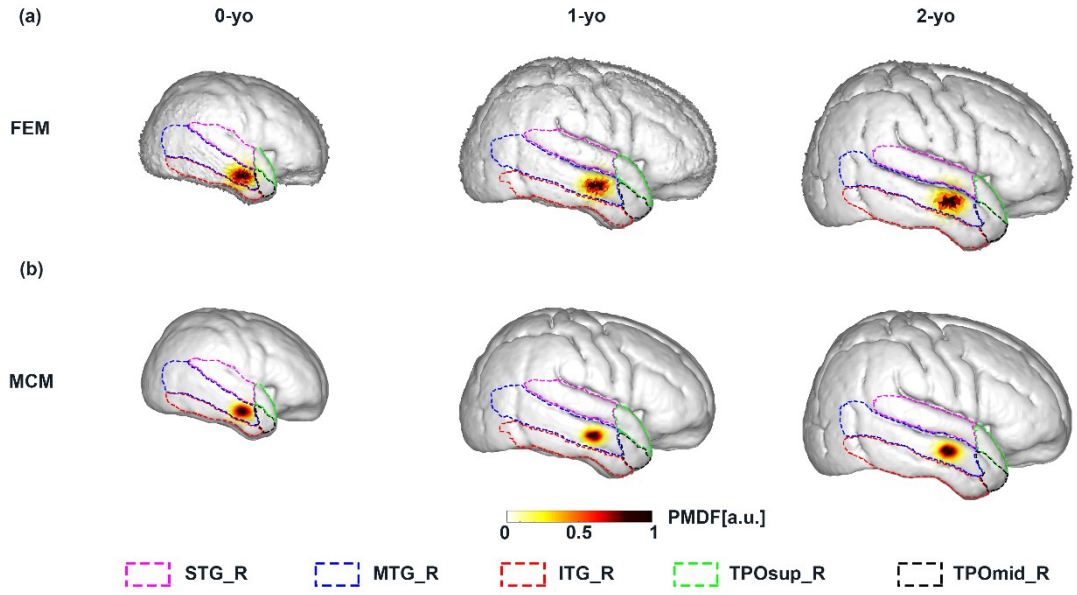

Figure 2. 9 The PMDF for the circumferential SD pair set on fiducial point T4 at 10 mm SD distance for 0-yo, 1-yo, and 2-yo when the FEM (a) or MCM (b) is used. Dashed lines in different colors indicate the AAL brain region boundaries.

Table 2. 7 $L_{norm,M}$ of two main brain regions that circumferential SD pairs set on T4 with five SD distances corresponded to obtained by the FEM and MCM for 0-, 1-, and 2-yo infants.

SD distance	Age	FEM		MCM	
		MTG-R	ITG-R	MTG-R	ITG-R
10 mm	0-yo	**63.6%**	34.6%	**84.4%**	15.3%
	1-yo	**83.6%**	15.3%	**92.5%**	7.4%
	2-yo	**89.0%**	7.8%	**96.7%**	2.5%
15 mm	0-yo	**65.1%**	31.8%	**78.3%**	20.8%
	1-yo	**81.8%**	16.8%	**87.1%**	12.7%
	2-yo	**86.9%**	9.7%	**94.5%**	4.3%
20 mm	0-yo	**59.3%**	36.6%	**67.7%**	30.3%
	1-yo	**78.6%**	19.6%	**81.3%**	18.4%
	2-yo	**86.1%**	9.4%	**93.3%**	4.8%
25 mm	0-yo	**61.1%**	33.2%	**66.4%**	29.0%
	1-yo	**78.6%**	18.8%	**81.7%**	17.7%
	2-yo	**82.4%**	12.4%	**90.3%**	7.3%
30 mm	0-yo	**56.2%**	36.6%	**58.0%**	32.9%
	1-yo	**74.6%**	22.4%	**78.6%**	20.4%
	2-yo	**81.9%**	11.7%	**87.9%**	8.5%

Note: The maximum $L_{norm,M}$ obtained by the FEM and MCM for five SD distances are shown in bold.

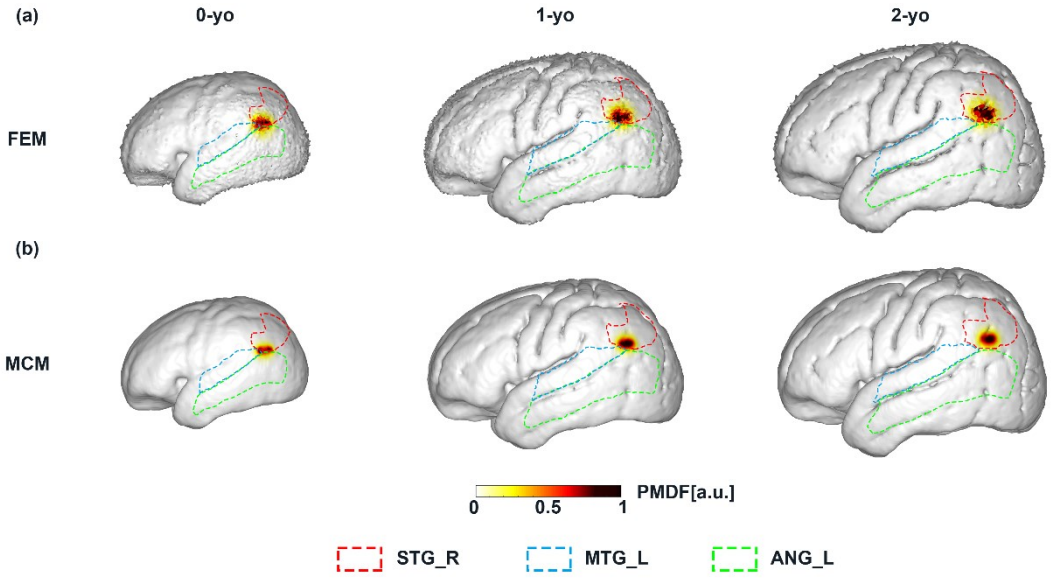

Figure 2. 10 The PMDF for the circumferential SD pair set on fiducial point P5 at 10 mm SD distance for 0-yo, 1-yo, and 2-yo when the FEM (a) or MCM (b) is used. Dashed lines in different colors indicate the AAL brain region boundaries.

Table 2. 8 $L_{norm,M}$ of three main brain regions that circumferential SD pairs set on T4 with five SD distances corresponded to obtained by the FEM and MCM for 0-, 1-, and 2-yo infants.

SD distance	Age	FEM			MCM		
		ANG-L	STG-L	MTG-L	ANG-L	STG-L	MTG-L
10 mm	0-yo	**45.6%**	19.6%	26.8%	**39.1%**	27.6%	29.3%
	1-yo	**78.9%**	6.7%	8.9%	**92.0%**	2.6%	4.4%
	2-yo	**80.1%**	3.3%	10.7%	**92.0%**	1.6%	4.7%
15 mm	0-yo	**33.0%**	25.7%	32.3%	32.3%	28.1%	**33.4%**
	1-yo	**72.6%**	8.5%	11.2%	**88.1%**	3.6%	6.1%
	2-yo	**73.0%**	5.7%	13.5%	**86.8%**	3.2%	7.2%
20 mm	0-yo	**36.0%**	24.1%	26.0%	**36.8%**	25.7%	28.0%
	1-yo	**71.1%**	8.6%	9.4%	**84.3%**	4.8%	6.2%
	2-yo	**67.8%**	7.6%	15.0%	**83.4%**	4.8%	7.6%
25 mm	0-yo	**29.2%**	24.7%	25.5%	**30.3%**	24.2%	28.6%
	1-yo	**61.0%**	11.2%	11.3%	**76.0%**	6.3%	7.0%
	2-yo	**61.3%**	10.6%	16.5%	**75.7%**	8.1%	9.8%
30 mm	0-yo	25.7%	24.4%	**28.7%**	21.4%	27.0%	**30.9%**
	1-yo	**55.9%**	12.6%	11.5%	**66.8%**	9.7%	9.5%
	2-yo	**53.4%**	13.8%	18.3%	**67.4%**	10.9%	10.5%

Note: The maximum $L_{norm,M}$ obtained by the FEM and MCM for five SD distances are shown in bold.

2.7.2 Influence of CSF layer and its optical properties

Other than verification of methodology of light propagation analysis, the CSF layer and its optical properties may affect the optics-based SCC that are calculated by the FEM. Firstly, the 5-layered infant head models with a CSF layer with the 4-layered head models without a CSF layer were compared in order to investigate the effect of the CSF layer on the optics-based SCC. Specifically, the CSF layer of the 5-layered infant head models was

replaced with the skull tissue. And then the light propagation analysis was conducted to obtain the optics-based SCC for 4-layered infant head models. The results as displayed in Fig. 2.11 at 20 mm SD distance show that infant head models without the CSF layer result in the weaker PMDF, compared with those with the CSF layer. By examining the values of $L_{norm,M}$ of the corresponding brain regions, two brain regions (i.e., MTG_R and ITG_R) are highly associated with the circumferential SD pair on T4, no matter which head models are used. Of note, the $L_{norm,M}$ of MTG_R and ITG_R for head models with and without a CSF layer over the five SD distances is highly similar (Table 2.9).

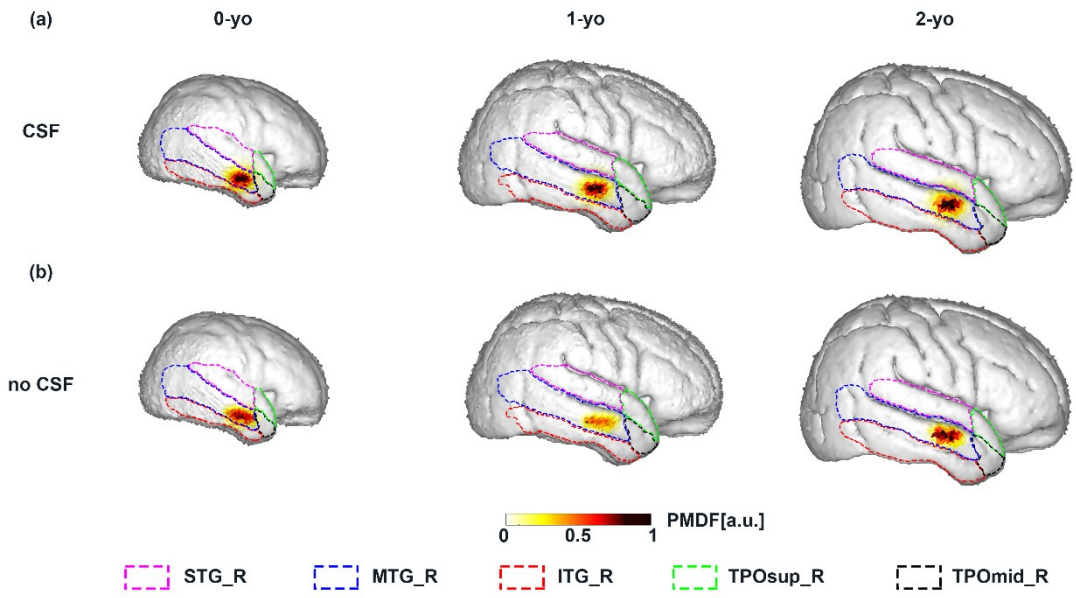

Figure 2. 11 The PMDF for the circumferential SD pair set on fiducial point T4 at 20 mm SD distance for 0-yo, 1-yo, and 2-yo when the 5-layered infant head models with the CSF layer (a) or 4-layered infant head models without the CSF layer (b) is used. Dashed lines in different colors indicate the AAL brain region boundaries.

Table 2. 9 $L_{norm,M}$ of two main brain regions that are correlated with circumferential SD pairs set on T4 over five SD distances, which are obtained by infant head models with and without the CSF layer for 0-, 1-, and 2-yo infants.

SD distance	Age	CSF		no CSF	
		MTG_R	STG-L	MTG_R	STG-L
10 mm	0-yo	63.6%	34.6%	76.6%	23.4%
	1-yo	83.6%	15.3%	95.8%	4.2%
	2-yo	89.0%	7.8%	99.2%	0.8%
15 mm	0-yo	65.1%	31.8%	77.1%	22.8%
	1-yo	81.8%	16.8%	92.4%	7.6%
	2-yo	86.9%	9.7%	98.3%	1.7%
20 mm	0-yo	59.3%	36.6%	67.3%	32.5%
	1-yo	78.6%	19.6%	89.6%	10.4%
	2-yo	86.1%	9.4%	98.1%	1.7%
25 mm	0-yo	61.1%	33.2%	69.3%	30.2%
	1-yo	78.6%	18.8%	91.2%	8.7%
	2-yo	82.4%	12.4%	96.0%	3.7%
30 mm	0-yo	56.2%	36.6%	60.1%	38.8%
	1-yo	74.6%	22.4%	88.5%	11.3%
	2-yo	81.9%	11.7%	95.7%	3.9%

Since there are no experimental results about the optical properties of the CSF layer for the infant population, previous simulation studies (Brigadoi et al., 2014; Fukui et al., 2003) used different values of μ_s' for the CSF layer. Therefore, I used $\mu_s' = 0.032$ mm^{-1} and $\mu_s' = 0.25$ mm^{-1} to examine the effect of the reduced scattering coefficients on the optics-based SCC. As shown in Fig. 2.12, the high scattering of the CSF layer results in a narrow SSP. However, the $L_{norm,M}$ of corresponding brain regions is almost equivalent

for low and high scattering conditions, by comparing the values of $L_{norm,M}$ from Table 2.10.

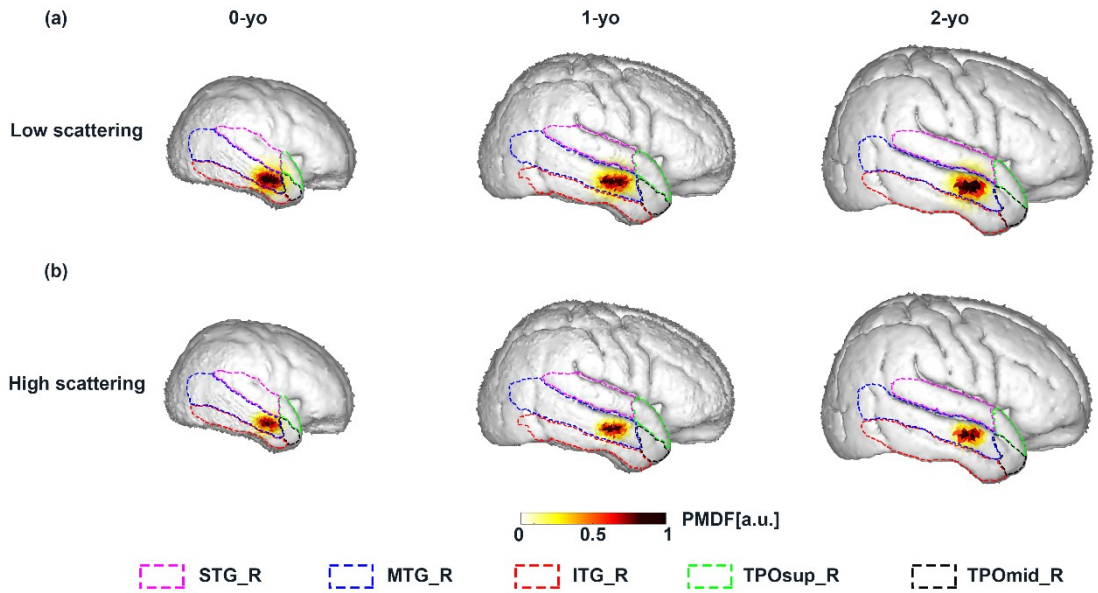

Figure 2. 12 The PMDF for the circumferential SD pair set on fiducial point T4 at 15 mm SD distance for 0-yo, 1-yo, and 2-yo when the μ_s' of CSF layer was 0.032 mm^{-1} (a) or the μ_s' of CSF layer was 0.25 mm^{-1} (b). Dashed lines in different colors indicate the AAL brain region boundaries.

Table 2. 10 $L_{norm,M}$ of two main brain regions that are correlated with circumferential SD pairs set on T4 over five SD distances, which is obtained by infant head models with a low or high scattering CSF layer for 0-, 1-, and 2-yo infants.

SD distance	Age	μ_s' = 0.032 mm^{-1}		μ_s' = 0.25 mm^{-1}	
		MTG_R	STG-L	MTG_R	STG-L
10 mm	0-yo	63.6%	34.6%	71.5%	28.3%
	1-yo	83.6%	15.3%	91.9%	8.0%
	2-yo	89.0%	7.8%	97.6%	2.1%
15 mm	0-yo	65.1%	31.8%	72.9%	26.7%
	1-yo	81.8%	16.8%	89.1%	10.9%
	2-yo	86.9%	9.7%	96.2%	3.4%
20 mm	0-yo	59.3%	36.6%	64.9%	34.4%
	1-yo	78.6%	19.6%	85.8%	14.0%
	2-yo	86.1%	9.4%	96.0%	3.4%
25 mm	0-yo	61.1%	33.2%	68.0%	30.7%
	1-yo	78.6%	18.8%	86.8%	12.9%
	2-yo	82.4%	12.4%	93.1%	6.0%
30 mm	0-yo	56.2%	36.6%	60.8%	37.1%
	1-yo	74.6%	22.4%	82.8%	16.8%
	2-yo	81.9%	11.7%	92.7%	5.8%

2.8 Discussion and conclusion

Previous studies on adults have shown that there is no significant difference in terms of the PPL between the FEM and MCM when the reduced scattering coefficient of the low-scattering CSF layer is more than 0.3 mm^{-1} (Koyama et al., 2005; Oki et al., 2009). In the current thesis, relative to the FEM, a more broadened SSP for an SD pair using the MCM is found for adults. Moreover, the corresponding brain regions underlying a fiducial

point have slightly different normalized PPL for the FEM and MCM. In addition, the optics-based SCC results of infant head models using different methods of light propagation analysis were also examined. Unlike the SSP results of adults, a similar range of SSP is observed no matter which method is used, suggesting that the error caused by diffusion approximation is smaller for infants than adults. The differences in the optics-based SCC between adults and infants may result from the different scattering coefficients for these two populations. Although the normalized PPL of corresponding brain regions of SD pairs at an SD distance of 10 mm was slightly different for the two methods, the normalized PPL of corresponding brain regions at 15-30 mm SD distances was almost the same for the two methods. These findings suggest that the diffusion approximation using FEM cannot estimate accurately the probabilities of corresponding brain regions. The inaccuracy mainly comes from the diffusion equation is a simplest approximation to the radiative transfer equation. According to a recent study (Capart et al., 2021), the diffusion equation is valid only when $\mu_a/\mu_s' = 1/100$ and the SD distance is greater than $10/\mu_s'$. Given that the optical properties of CSF and the SD distances in the current adult or infant study can not meet the prequsite of applying diffusion equation perfectly, the normalized PPL in each corresponding brain region for two light propagation methods is slightly distinct. In addition, the inaccuracy may also be caused by that the mesh size of

FEM is larger than that of MCM, even though the mesh elements of adult or infant head models show good quality on average. On the other hand, mesh-based head models have advantages in both improved boundary accuracy and high flexibility compared to voxel-based models (Tran et al., 2020), however, little is know about how the difference between mesh-based and voxel-based light propagation models affect on fNIRS signal in brain tissues. In the future work, when FEM is adopted to calculate the optics-based SCC, the optimal mesh size in adult and infant head models should be clarified respectively to obtain an equivalent optics-based SCC obtained by MCM. Since the main objective of the current thesis is to obtain more precise optics-based SCC by adopting the light propagation analysis instead of the conventional geometrical matching methods, the proposed SBM method can be regarded as a feasible methodology if main underlying brain regions for an SD pair on the scalp surface can be identified. More importantly, regardless of light propagation methods, the most likely corresponding brain region that has the maximum normalized PPL is consistent for the same fiducial point. This finding futher demonstrates that diffusion approximation using FEM is feasible and reliable. Although the MCM can solve the radiative transfer equation in any desired accuracy, it is not practical for the current study including many subjects and fiducial points due to the tremendous computation time. In the sense of practical application, the diffusion equation

solved by the FEM estimating the underlying brain regions for a SD pair is more suitable, because it can reliably localize the main brain regions, particularly, the brain regions with largest probability. To sum up, these findings demonstrate that the diffusion approximation using FEM is quite feasible and robust for the acquisition of optics-based SCC for adults and infants aged from 0 to 2 years.

On the basis of the robustness of the diffusion approximation, I also examined the effect of the CSF layer on results. Previous studies suggest that a low-scattering CSF layer is important for improving the fNIRS sensitivity to brain tissues (Firbank et al., 1996; Okada & Delpy, 2003a). I also found that compared with the model without the CSF layer, the model with the low-scattering CSF layer has larger values of PMDF. Moreover, the reduced scattering coefficient of the CSF layer affected the SSP. Specifically, compared to the high scattering coefficient, the low scattering coefficient can make more photons reach the brain tissues. However, the normalized PPL of underlying brain regions for the same fiducial points remains the same, regardless of the absence of the CSF layer or its scattering properties. These results suggest that the CSF layer and its scattering coefficient also have an influence on the optics-based SCC calculated by diffusion approximation to light propagation.

Chapter 3

3 Scalp-Cortex Correlation in Adult Population

In this chapter, to address whether the proposed SBM method using the FEM is superior to traditional geometrical matching (GM) methods when calculating the SCC, three GMs were defined according to the previous studies. Moreover, 45 subject-specific adult head models were utilized to analyze the SCC for the purpose of comparing the differences between the SBM and GMs at the individual and group levels.

3.1 Geometrical matching (GM) methods to analyze the SCC

The SCC was analyzed by a sensitivity-based matching (SBM) method using FEM and three GM methods (Fig. 3.1). The SCC was analyzed in two steps for either matching method. The SBM method provides the SCC based on the SSP of the SD pair at each scalp fiducial point (Details of method description see Chapter 2). In GM methods, SCC was obtained geometrically by using an approximated perpendicular line from the scalp surface at each fiducial point. There are three types of GM methods according to the space in which each step is executed. Details of each GM method are described below.

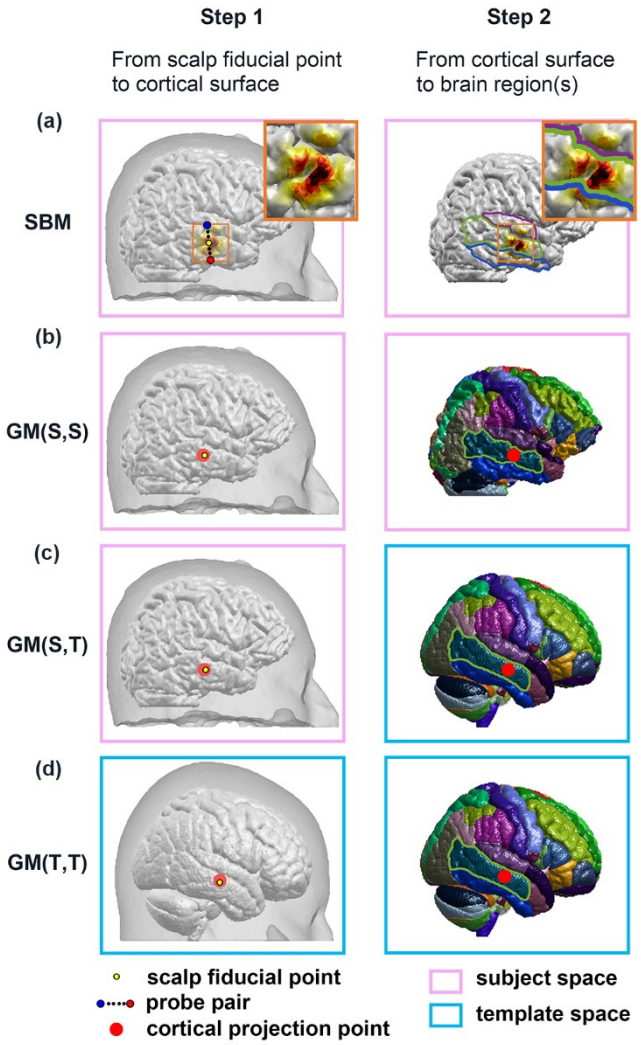

Figure 3. 1 Methods to analyze the SCC. (a) SBM, (b) GM (S,S), (c) GM (S,T), and (d) GM (T,T). In (a), the SSP of the SD pair is represented by magnification of the gray matter surface. The colors in descending order of sensitivity are black, red and yellow. The first and second character in the brackets of GM corresponds to the space in which the first and second steps of the SCC were executed, i.e., S and T denote the subject space and template space, respectively.

GM, which assumes the fNIRS signal is mainly contributed from the midpoint between the source and detector, has been widely adopted to analyze the SCC in fNIRS studies. GM consists of two steps to analyze the SCC (Fig. 3.1b-d). Initially, the scalp

position is projected onto the cortical surface location (Fig. 3.1b-d, left panel). Next, the brain region to which the cortical location belongs is determined according to the brain atlas (Fig. 3.1b-d, right panel). Based on whether these two steps are executed in the subject-specific spaces or the template space, I defined three GMs: GM (S,S), GM (S,T) and GM (T,T), in which S and T indicate subject-specific spaces and the template spaces, respectively. GM (S,S) corresponds to a traditional approach in which markers attached to probes are imaged with an MRI scan and then each marker position is projected onto the cortical surface along with the individual brain structure. GM (S,T) is included in the procedure to construct the transcranial brain atlas (Xiao et al., 2018). According to the definition of GM (T,T), it is assumed that GM (T,T) is a probabilistic registration (Singh et al., 2005; Tsuzuki & Dan, 2014).

GM (S,S) and GM (S,T) project the 10-10 fiducial points on the scalp surface of each individual subject to the cortical surface points in the individual space (Fig. 3.1b-c, left panels) by the balloon-inflation algorithm (Okamoto & Dan, 2005). For GM (S,S), the AAL brain region closest to the projected cortical surface point in the individual space is determined as the corresponding brain region for each fiducial point (Fig. 3.1b, right panel). For GM (S,T), however, a spatial normalization process is used to transfer the coordinates of cortical surface points to a MNI space by SPM DARTEL (Fig. 3.1c, right

panel), which was similar to the approach taken in a recent study (Xiao et al., 2018). Subsequently, the AAL brain region closest to the transferred point is searched in the ICBM-152 brain template. Finally, the closest region in the template is assigned as the corresponded brain region for each fiducial point. GM (S,S) and GM (S,T) make each fiducial point of individual subject correspond to a single brain region. In other words, the probability that the fNIRS signal is affected by brain activation in that single region is 100%. I employed these probabilities as a metric of the SCC for GM (S,S) and GM (S,T). I repeated the above steps for all 45 subjects to obtain the probability of the corresponding brain region at every fiducial point for GM (S,S) and GM (S,T), independently.

The SCC of GM (T,T) was analyzed using an NFRI toolbox (Okamoto et al., 2004; Okamoto & Dan, 2005; Singh et al., 2005). At the individual level, the coordinates of all 10-10 fiducial points were firstly affine-transformed to the corresponding coordinates on the scalp in the MNI space using the MRI database, which consists of 17 reference brains. Next, those transferred points were projected onto the cortical surfaces of those reference brains (Fig. 3.1d, left panel) by the balloon-inflation method (Okamoto & Dan, 2005). The spatial distribution of the projected cortical points was then quantified by the average and standard deviation from the 17 reference brains. Finally, the proportion of each brain

region covered by the spatial distribution as a metric of the SCC for GM(T,T) was provided using an AAL atlas (Fig. 3.1d, right panel).

Three GMs can be clearly ordered according to methodological differences from SBM (Fig. 3.1). As the PMDF of each brain region is calculated using SBM in the subject-specific model, the methodological dissociation for SBM and GM (S, S) is the difference in consideration of the light scattering (Fig. 3.1a-b). In addition the light scattering is not considered, GM (S,T) is different from SBM at the point that the brain labeling of the cortical location is determined using the template (Fig. 3.1a-c). In addition to the differences between SBM and GM (S,T), GM (T,T) differed from SBM at the point that the scalp position is projected onto the cortical surface in the template brain (Fig. 3.1a-d). Thus, the methodological dissociation between SBM and GMs increases in the order of GM (S,S), GM (S,T) and GM (T,T).

3.2 Comparisons between SBM and GM methods

3.2.1 Comparison at the individual level

The measures of the SCC obtained by SBM and GMs can be regarded as a probability showing which brain region the fNIRS signal derives from. That is, they can be compared directly at the individual level. In addition, it would be interesting for fNIRS users to know which brain region is the most likely source of the signal. The most likely

corresponding brain region (MLCBR) was defined for each matching method; that is the brain region with the largest $L_{norm,M}$ for SBM, the brain region obtained by the methods themselves for GM (S,S) and GM (S,T), and the brain region with the highest volumetric occupancy in the sphere centered on the centroid of the projected cortical points for GM (T,T).

3.2.2 Comparison at the group level

The group-level SCC indices were calculated at each fiducial point for the group-level comparisons of matching methods. One of the group-level SCC indices used was the group-wise probability of corresponding brain region for each matching method, i.e., the average of the $L_{norm,M}$ across all subjects for SBM, the number of subjects corresponding to a specific brain region divided by the total number of subjects for GM (S,S) and GM (S,T) and the score calculated by the group analysis of NFRI toolbox for GM (T,T). The group-wise probability of GM (T,T) was obtained from a multi-subject spatial distribution of cortical points corresponding to a given fiducial point by using spatial distribution results from all individual subjects. To statistically compare the group-wise probability between SBM and each GM, i.e. SBM vs. GM (S,S), SBM vs. GM (S,T), and SBM vs. GM (T,T), I used the chi-square test of independence, which is often used to determine if there is a significant relationship between two nominal variables. In this

study, the null hypothesis was that there would be no relationship between the group-wise probability between SBM and those from GMs. On the contrary, the alternative hypothesis was that there would be an association between the group-wise probabilities from different methods. The rejection of the null hypothesis meant that the proportion distribution of a series of corresponding AAL brain regions was distinct between SBM and GM at a fiducial point. Dunnett's test was adopted to hold the familywise error rate at or below alpha significant level (i.e., 0.05, 0.01, 0.001) when performing multiple comparisons of SBM with each GM (Dunnett, 1955). Moreover, in order to examine the effect of the SD pair orientation on the optics-based SCC, I also performed the chi-square test of independence between the group-wise probabilities from circumferential and vertical orientations for SBM.

The group-wise MLCBR was also obtained as another group-level SCC index. The group-wise MLCBR was the AAL region corresponding to the maximum group-wise probability of each matching method. In addition, I defined the concordance rate Q representing the extent of consistency of the MLCBR between SBM and each GM;

$$Q = \frac{n}{N} \times 100, \tag{21}$$

where n was the number of subjects that had the same MLCBR between SBM and GMs and N was the total number of subjects.

3.3 Results

3.3.1 Effect of SD pair orientation on the optics-based SCC

For an arbitrarily chosen subject 10, the PMDF of two orientational SD pairs (circumferential and vertical orientations) set at the fiducial point T4 are shown in Fig. 3.2a. For the circumferential SD pair (Fig. 3.2a, upper panel), it corresponds to three brain regions (MTG_R: 82.7%; STG_R: 8.9%; ITG_R: 6.4%). Likewise, the vertical SD pair (Fig. 3.2a, lower panel) corresponds to the same brain regions with similar $L_{norm,M}$ (MTG_R: 77.2%; STG_R: 10.4%; ITG_R: 11.0%). Moreover, for each of all 45 subjects, two orientational SD pairs set at the fiducial point T4 have the similar $L_{norm,M}$ distribution. For example, as shown in Fig. 3.2b, the color distribution in every column of left matrix is similar to that in the corresponding column of right matrix (each column of a matrix indicating the $L_{norm,M}$ distribution of one subject). The fiducial points F8 and O1 also show that two $L_{norm,M}$ matrices representing circumferential and vertical orientations are highly similar by visual examination (Figs. 3.2c-d). Similar spatial patterns of PMDF for one specific subject (Fig. 3.2a) and $L_{norm,M}$ distribution for all subjects (Fig. 3.2b) show that the optics-based SCC seems independent of the orientation of two SD pairs. Further chi-square test of independence at the group level shows that the orientation of two SD pairs set at every fiducial point has no significant effects on the $L_{norm,M}$ distribution (all ps >

0.05). In addition, the $L_{norm,MLCBR}$ for circumferential and vertical orientations at each fiducial point is approximately equivalent (Fig. 3.2e), which is further supported by the statistical results that interclass correlation coefficient (ICC(2,1)) between the $L_{norm,MLCBR}$ for circumferential and vertical orientations at all fiducial points is 0.964.

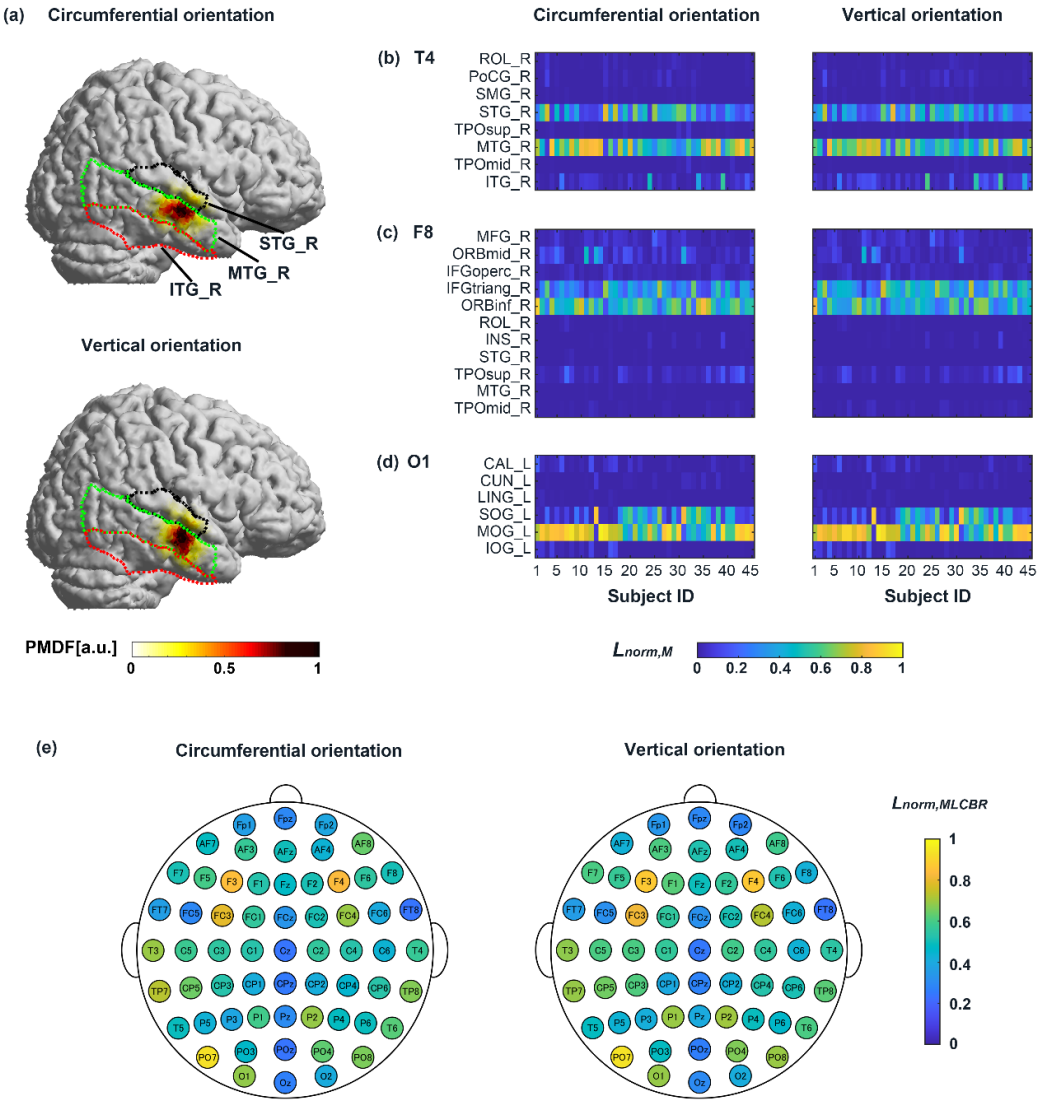

Figure 3. 2 The effect of SD pair orientation on the optics-based SCC. (a) The PMDF of two SD pairs attached according to circumferential and vertical orientations at the fiducial point T4 is shown for subject 10. Dashed contours in different colors denote the boundaries of brain regions (i.e., red: ITG_R; green: MTG_R; black: STG_R). Two-column panels of matrices at three fiducial points (b) T4, c) F8, and (d) O1 display the $L_{norm,M}$ distribution for circumferential and vertical SD pairs, respectively. The digits and characters in each $L_{norm,M}$ matrix represent the subject ID and brain regions, respectively. (e) $L_{norm,M}$ at all fiducial points for circumferential and vertical orientations.

3.3.2 Comparison between optics-based SCC and geometrical SCC at the individual level

Given that the two orientations of SD pairs have no significant influence on the optics-based SCC at all fiducial points, the optics-based SCC only from the circumferential orientation was used to compare with the geometrical SCC. To illustrate the distinction between the SCC obtained from SBM and that from GMs at the individual level, the SCC results from three representative subjects for a given fiducial point T3 were reported. The PMDF for the three subjects is shown in Figs. 3.3a-c, respectively. The number of corresponding brain regions (N_{CBR}) varies across three subjects for the same fiducial point T3. For instance, T3 of subject 01 corresponds to two brain regions (MTG_L: 75.7% and STG_L: 23.7%). However, T3 of subject 16 and subject 44 has four (MTG_L: 51.7%; STG_L: 44.5%; PoCG_L: 1.9% and ROL_L: 1.2%) and three corresponding brain regions (STG_L: 55.8%; MTG_L: 35.3% and PoCG_L: 7.1%), respectively. Notably, although the SD pair is placed at the same fiducial point T3, the MLCBR of T3 is not the same among the three subjects, i.e., MTG_L for subject 01 and subject 16, but STG_L for subject 44 (Fig. 3.3f). Moreover, T3 of subject 16 has almost equivalent $L_{norm,M}$ for the two brain regions, but one brain region dominates for the other two subjects. The cortical positions indicating the corresponding brain region of GM (S,S)

are located in the regions with the high PMDF (the green dots in Fig. 3.3a-c). Moreover, the corresponding brain region from GM (S,S) is the same as that with the largest $L_{norm,M}$ obtained by SBM for subject 01 and subject 44, except for subject 16. Nevertheless, once the spatial normalization is incorporated into the calculation of the SCC, as in GM (S,T), only the corresponding brain region of subject 01 is the same as that of the largest $L_{norm,M}$ (Fig. 3.3d). As shown in SCC results from GM (T,T) (Fig. 3.3e), T3 corresponds to the same brain region MTG_L for the three subjects, in which corresponding brain regions of subject 01 and subject 16 are congruent with those with the largest $L_{norm,M}$. Fig. 3.3f summarizes the results of MLCBR for each matching method and subject.

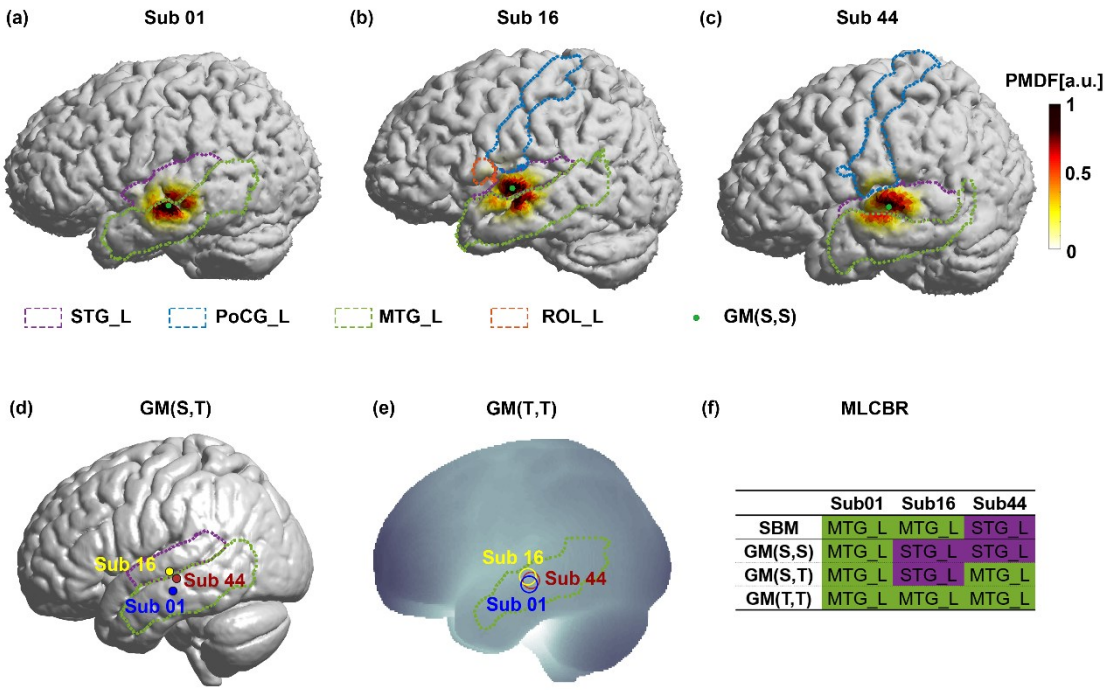

Figure 3. 3 The SCC for a given fiducial point T3 of three representative subjects. Dashed lines in different colors indicate the boundaries of AAL brain regions. The PMDF superimposed on three subject-brain structures is shown in (a), (b) and (c) when the SD pair is attached in a circumferential orientation. The PMDF is normalized by the maximum value for each subject. The position identified by GM (S,S) is indicated by a green dot in (a), (b) and (c). (d) Cortical surface points identified by GM (S,T) are shown as small dots on the ICBM-152 brain with different colors for three subjects. (e) The corresponding brain region obtained by GM (T,T) is displayed on the averaged reference brain. Centers and radii of circles indicate the mean values and one standard deviation of the most likely coordinates. (f) The MLCBR of T3 is shown as a table for each matching method and subject.

To investigate systematically the SCC obtained from each matching method across all 45 subjects, I selected three fiducial points (T3, Fpz, and Cz) that have widely been used as reference points to attach SD paris in cognitive neuroscience studies using fNIRS. For the fiducial point T3, N_{CBR} is different between subjects when SBM is used (max: 7

regions; min: 2 regions, see Fig. 3.4a upper panel). GM (S,S) and GM (S,T) provide the single corresponding brain region with a probability of 100% since these two geometrical matching methods are based on the point-to-point mapping at the individual level (Fig. 3.4a upper). GM (T,T) shows that T3 focuses on one or two specific brain regions, e.g. MTG_L, 84.7%; ITG_L, 15.3% for subject 13; MTG_L, 100% for subject 18. The SCC at fiducial points Fpz and Cz displays a large discrepancy compared to T3. Specifically, N_{CBR} of Fpz and Cz is much larger than that of T3, when SCC is calculated using SBM. In addition, the $L_{norm,M}$ of Fpz and Cz is not exclusively high in one region, but it is broadly distributed across several regions (Fig. 3.4b-c, upper panel). The corresponding brain region of GM (S,S) and GM (S,T) varies across subjects and the inter-subject variability differs at distinct fiducial points (Fig. 3.4b-c, upper panel). GM (T,T) shows that corresponding brain regions have more relatively limited and focused distribution across subjects (Fig. 3.4b-c, upper panel).

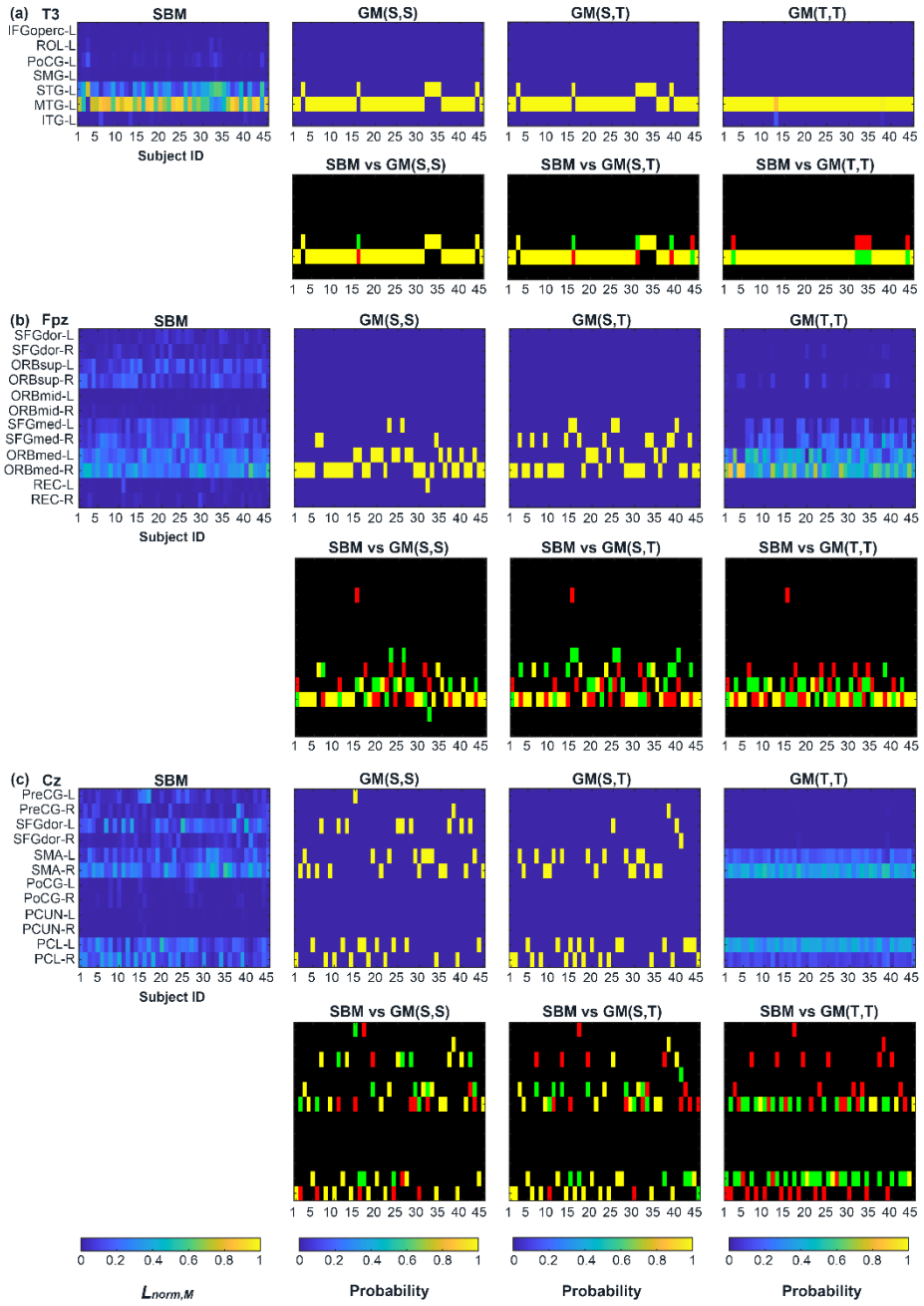

Figure 3. 4 The matrices indicating the SCC obtained by SBM and three GMs at three representative fiducial points (a) T3, (b) Fpz, and (c) Cz for 45 subjects. The digits and characters in each matrix represent the subject ID and brain regions, respectively. The color of the matrices in the upper panel of each subfigure for SBM and GMs indicates $L_{norm,M}$ and probability, respectively. Notably, GM(S,S) and GM(S,T) reveal one brain region for each subject. The lower panel of each subfigure shows the difference in MLCBR between SBM and GMs. Red and green blocks indicate the MLCBR of SBM and GMs, respectively. When the MLCBR is consistent between SBM and GMs, the block turns yellow due to the additive color of green and red.

The MLCBR at T3 between SBM and each GM is distinct only in a few subjects. (Fig. 3.4a, lower panel). In contrast, the MLCBR at Fpz or Cz is inconsistent between SBM and all GMs for most subjects (Fig. 3.4b-c, lower panel). Furthermore, the inconsistency of the MLCBR at each fiducial point increases with larger methodological dissociation between SBM and GMs. For instance, the number of subjects for whom the MLCBR is consistent between SBM and GMs (the number of yellow blocks in the lower panel of Fig. 3.4) decreases at T3, i.e. 44, 41, and 39 for SBM vs. GM (S,S), SBM vs. GM (S,T), and SBM vs. GM(T,T), respectively. On the other hand, the consistency of the MLCBR between SBM and each GM is different at chosen fiducial points, as indicated by the decrease in yellow blocks from T3, Fpz to Cz (Fig. 3.4a-c, lower panel).

3.3.3 Comparison between optics-based SCC and geometrical SCC at the group level

To examine the differences between optics-based SCC and geometrical SCC at the group level, I calculated group-level SCC indices across 45 subjects at three fiducial points T3, Fpz, and Cz (Table 3.1). Results show that fiducial point T3 is correlated with three brain regions using SBM, i.e., MTG_L: 69.3%; STG_L: 27.4%; PoCG_L: 1.8%. When GM (S,S) and GM (S,T) are used to calculate SCC, T3 corresponds two brain regions, i.e., MTG_L: 84.4% and 82.2%; STG_L: 15.6% and 17.8%, for GM (S,S) and GM (S,T), respectively. However, T3 is 100% mapped to MTG_L using GM (T,T). For

fiducial points Fpz and Cz, N_{CBR} obtained by SBM is greater than that obtained by GMs. At Fpz, the probabilities of a few brain regions are much greater than those of others when GMs are used. In contrast, the probabilities are relatively even across the corresponding brain regions when SBM is used (see Table 3.1). The group-wise MLCBR at T3 and Fpz is consistent whichever method is adopted. Nevertheless, the group-wise MLCBR of GM (S,T) at Cz is different from that of the other three methods. The group-wise probabilities of all 10-10 fiducial points at the group level could be found in Supplementary Table S1.

Table 3. 1 The group-wise probabilities of the SCC.

Fiducial point	AAL region	SBM (circumferential orientation)		GM (S,S)	GM (S,T)	GM (T,T)
		Mean	SD			
T3	MTG-L	**69.3%**	20.8%	**84.4%**	**82.2%**	**100.0%**
	STG-L	27.4%	18.1%	15.6%	17.8%	0.0%
	PoCG-L	1.8%	2.8%	0.0%	0.0%	0.0%
Fpz	ORBmed-R	**29.1%**	10.9%	**57.8%**	**48.9%**	**47.8%**
	ORBmed-L	20.3%	7.3%	28.9%	15.6%	35.7%
	SFGmed-R	12.2%	7.8%	6.7%	24.4%	12.2%
	SFGmed-L	10.2%	6.8%	4.4%	11.1%	2.6%
	ORBsup-L	10.2%	6.5%	0.0%	0.0%	0.0%
	ORBsup-R	9.8%	6.7%	0.0%	0.0%	1.7%
	SFGdor-L	2.5%	2.2%	0.0%	0.0%	0.0%
	SFGdor-R	2.4%	2.3%	0.0%	0.0%	0.0%
	REC-R	1.1%	1.7%	0.0%	0.0%	0.0%
	REC-L	0.0%	0.0%	2.2%	0.0%	0.0%
Cz	SMA-R	**24.0%**	12.1%	**22.2%**	20.0%	**36.7%**
	PCL-R	16.8%	12.1%	17.8%	**26.7%**	11.4%
	SFGdor-L	15.5%	12.1%	20.0%	4.4%	0.0%
	PCL-L	15.3%	10.2%	17.8%	24.4%	35.9%
	SMA-L	11.5%	8.2%	17.8%	20.0%	15.9%
	PreCG-L	6.0%	7.3%	2.2%	0.0%	0.0%
	PreCG-R	4.6%	5.9%	2.2%	2.2%	0.0%
	SFGdor-R	3.8%	4.6%	0.0%	2.2%	0.0%
	PoCG-L	0.0%	0.0%	0.0%	0.0%	0.0%

Note: SD stands for standard deviation. The maximum value obtained by each matching method at each fiducial point is shown in bold. The group-wise MLCBR is the AAL region corresponding to the maximum value of each matching method.

To evaluate the differences in SCCs obtained by matching methods quantitatively at all fiducial points at the group level, a chi-square test of independence was performed to examine whether group-wise probability for a given fiducial point derived from SBM and each GM is independent. When comparing results obtained from SBM and GM (S,S), the group-wise probability is significantly different for 9 of 61 fiducial points (Fig. 3.5a, fiducial points filled with color), which are mainly located in the anterior regions of the head. In addition, 23 fiducial points mainly in anterior and posterior regions display a significant difference between SBM and GM (S,T) (Fig. 3.5b). Importantly, the comparison between SBM and GM (T,T) shows that the group-wise probability is significantly different for 44 of 61 fiducial points, covering almost the whole head (Fig. 3.5c).

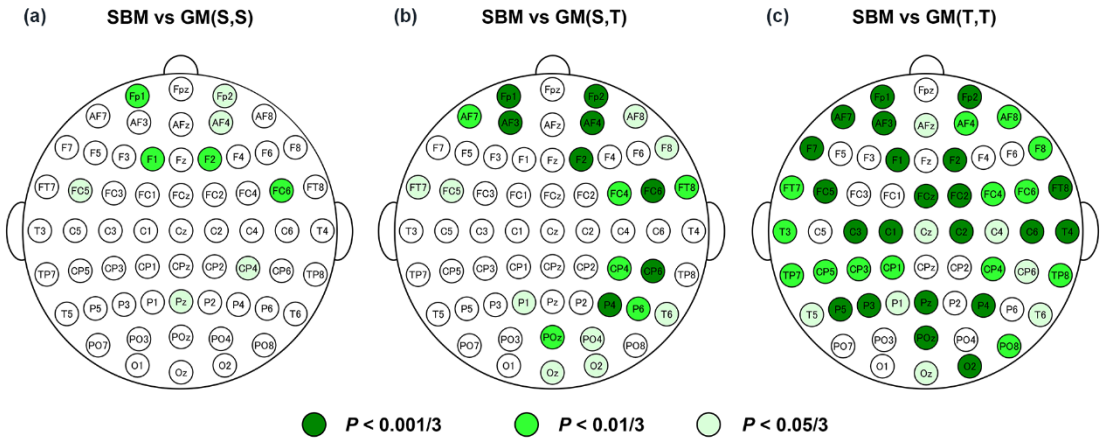

Figure 3. 5 The differences for the group-wise probability between SBM and each GM for all 10-10 fiducial points. (a) SBM vs. GM (S,S); (b) SBM vs. GM (S,T); (c) SBM vs. GM (T,T). The color indicates the significant level of the chi-square test of independence after Dunnett's multiple comparison procedure. White circles indicate $p >= 0.05/3$.

For all fiducial points, the consistency of the MLCBR between SBM and each GM is assessed by the concordance rate Q. As shown in Fig. 3.6, the MLCBR is moderately or highly consistent between SBM and GMs for most fiducial points. Importantly, the greater the methodological disassociation between SBM and GMs, the lower concordance rate Q is at almost all fiducial points. The mean and standard deviation of the concordance rate Q for all 10-10 fiducial points are 85.9 ± 11.2%, 74.0 ± 18.0%, and 65.5 ± 22.4% for SBM vs. GM (S,S), SBM vs. GM (S,T), and SBM vs. GM (T,T), respectively. The concordance rate Q shows the characteristic spatial distribution. The values are relatively low at frontal, central, and posterior fiducial points, particularly in SBM vs. GM (S,T) and SBM vs. GM (T,T).

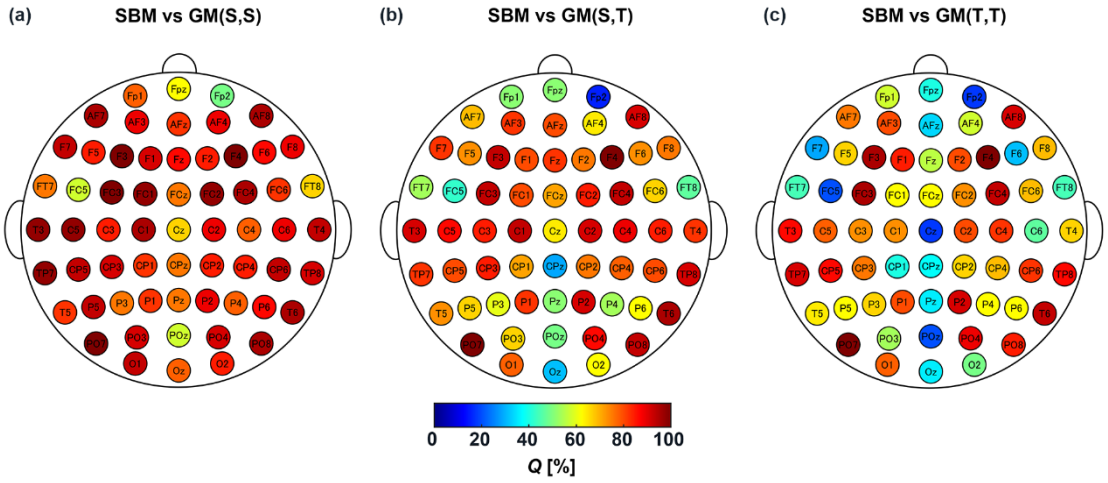

Figure 3. 6 The consistency for the MLCBR at all fiducial points between SBM and each GM. (a) SBM vs. GM (S,S), (b) SBM vs. GM (S,T), and (c) SBM vs. GM (T,T). A higher concordance rate Q correlated to a larger the number of subjects in which the MLCBR is the same between SBM and each GM.

3.4 Discussion

To date, most efforts to specify the cortical region under the scalp position in fNIRS studies have been based on a simple assumption that the signal originates from the brain region just below the midpoint of an SD pair. Additionally, few studies investigated the role of inter-subject variations in the anatomical structure of the head and brain in the SCC analysis. In this thesis, I established a precise optics-based SCC between the SD pairs on the 10-10 system positions on the head surface and underlying brain regions contributing to the detected hemodynamic changes by analyzing light propagation in 45 subject-specific head models. Results show that fNIRS sensitivity obtained by SBM is broadly distributed in several adjacent brain regions for all fiducial points on the scalp

surface, and the optics-based SCC is independent of orientations of SD pairs but varies across subjects for the same fiducial point. The comparisons between optics-based SCC and geometrical SCC demonstrate that matching methods have a significant influence on the SCC and that the level of influence is different for each fiducial point. In particular, the methodological dissociations between SBM and each GM determine the level of difference of the SCC. All of these findings demonstrate that it is necessary to consider both light scattering in head tissues and individual anatomical differences when estimating the brain region in which fNIRS signals originate.

The normalized PPL in a given brain region M ($L_{norm,M}$) represents the probability that an SD pair is sensitive to the brain region M. The accuracy of the $L_{norm,M}$ is also affected by the parcellation accuracy of the gray matter in the brain regions. Since the AAL atlas uses the sulcus as a boundary to parcellate brain regions, the accuracy of the parcellation on the individual brain can be easily evaluated by visual assessment. It should be noted that the AAL atlas is based on the Colin27 average brain, created by scanning a single subject 27 times (Holmes et al., 1998). Previous studies have demonstrated that the single-subject AAL atlas does not adequately represent the partition pattern of the human brain because it cannot capture the neuroanatomical variability across individuals (Devlin & Poldrack, 2007) and does not match the cytoarchitectonic borders well in most cases

(Amunts et al., 2007). Despite these limitations, the AAL atlas was still utilized to calculate the SCC for the purpose of direct comparison between SBM and GMs. Given that the AAL atlas is represented on standard brain structures, the individual gray matter was parcellated by transforming a standard brain structure into an individual brain structure using the DARTEL method. However, upon applying this method by itself, a brain region located in a certain sulcus in the standard brain was incorrectly transferred into several gyri in the individual brain (data not shown). To improve accuracy of parcellation, the RBFT was applied after using the DARTEL method to further align the 17 major cerebral sulci on the standard and individual brain structures. The application of DARTEL followed by RBFT provides accurate parcellation of the individual gray matter into the AAL brain regions. Therefore, the $L_{norm,M}$ is accurate for the current brain region parcellation.

3.4.1 Impact of light propagation in tissue on SCC

The SCC obtained from SBM always displays multiple corresponding brain regions for a fiducial point. Particularly, a certain single brain region dominates the $L_{norm,M}$ for some fiducial points such as T3 and T4, while several brain regions possess the equivalent $L_{norm,M}$ at fiducial points above the longitudinal fissure such as Fpz and Cz. Thus, the source of the fNIRS signal could be estimated exactly based on the scalp position when

the SD pair is attached around the former fiducial points, whereas such estimation is difficult when the probe pair is attached around the latter fiducial points. For the interpretation of fNIRS data measured around the latter points, meticulous attention should be paid to the brain region in which activity occurs.

Interestingly, the SD-pair orientation has no significant influence on the distribution of $L_{norm,M}$, which is consistent with findings from photon propagation in the Colin27 brain template (Strangman et al., 2014). Regardless of the SD-pair orientation, the PMDF value in the gray matter shows the local maximum at just below the midpoint of the source and detector and decreases with increasing distance from the maximum point. In addition, the contour lines of the PMDF on the gray matter surface resemble concentric circles centered at the maximum point. These spatial features of the PMDF explain the fact that the optics-based SCC is independent of the orientation of the probe pairs. It is a welcome relief for fNIRS users that the orientation of the SD pair has little effect on the optics-based SCC. On the other hand, the spatial features of the PMDF depend on the SD distance. Thus, it is uncertain whether such spatial features of the PMDF would change when the SD distances were not 30 mm. Previous studies have suggested that the optimal SD distance should be narrowed down to 30-35 mm (Chuang et al., 2013; Li et al., 2011; Strangman et al., 2013), while different adult brains have their own optimal SD distance (Chuang et

al., 2013). How the interaction between individual brain structure and SD distance affects SCC might be an interesting future research question.

In addition to the SD distance, the SSP of fNIRS is sensitive to individual anatomical differences associated with variations in head size, depth of the brain from the scalp, among other factors. Such individual anatomical difference is illustrated by evidence that each individual adult subject exhibits unique scalp and skull thickness (De Boer et al., 2016; Lillie et al., 2016), anatomical structures of the brain (Fleming et al., 2010; Hasan et al., 2007; Kanai & Rees, 2011; Li et al., 2007). Moreover, a recent study provides direct evidence supporting our findings, because the PPL in the brain decreases with an increase in the scalp-brain distance varying with individuals and across brain regions (Nakamura et al., 2016).

In particular, non-brain superficial head tissues, such as the scalp, skull, or CSF, could have a considerable influence on the SSP. Evidence from light propagation analysis in the adult head reveals that a low-scattering CSF layer could significantly broaden the SSP and confine the SSP of the sampling areas to the shallow regions of the gray matter (Firbank et al., 1998; Okada et al., 1997). In addition, the SSP is significantly affected by the thickness of the CSF layer (Okada & Delpy, 2003b). In older adults, changes in the thickness of the CSF layer due to brain atrophy could result in a decrease in sensitivity as

the scalp-brain distance increases. Similarly, Beauchamp et al. documented changes in the scalp-brain distance with age in 71 children aged 0 to 12 years old (Beauchamp et al., 2011). These age-related anatomical changes influence the optical path in tissue and the fraction of the signal coming from the actual brain compared to the superficial layers for 5-11 years old children (Whiteman et al., 2018). However, the optics-based SCC of the adult population in this thesis should be relatively constant, because the age range of 45 adult subjects was 21-58 years.

3.4.2 Comparison of SCCs between matching methods

In this thesis, the SCC of three GMs with that of SBM was compared. Remarkably, the smaller the methodological dissociation between SBM and GMs, the smaller the number of fiducial points that display significantly different group-wise probability of the SCC between SBM and GM, and the larger the number of subjects in which the MLCBR is consistent between SBM and GM. GM (S,S) is completely the same as SBM except for ignoring light scattering. There are the smallest differences between GM(S,S) and SBM in terms of the group-wise probability and the MLCBR. The group-wise probability shows statistically significant differences between SBM and GM (S,S) at 14.8% of all fiducial points. At such fiducial points, the influence of light propagation cannot be ignored to obtain the SCC accurately. On the other hand, the MLCBR of SBM and GM

(S,S) shows a relatively high consistency across almost all fiducial points and individual subjects. If we accept the assumption that brain activation is confined to a single brain region, GM (S,S) could provide a reasonable signal source for fNIRS.

GM (S,T) has a greater deviation from SBM than GM (S,S) with regards to the SCC. GM (S,T) is methodologically different from GM (S,S) at the point that assigning brain regions in the template space after the spatial normalization, which indicates that the accuracy of spatial normalization strongly affects the SCC. Similar spatial normalization was included in the process to construct the transcranial brain atlas (Jiang et al., 2020; Xiao et al., 2018). A more sophisticated transcranial brain atlas could be constructed by either replacing the spatial normalization with other more accurate techniques such as DARTEL followed by RBFT, or using the SCC from GM (S,S).

GM (T,T) displays the largest discrepancy with SBM. There are statistically significant differences in the group-wise probabilities between SBM and GM (T,T) at 72.1% of all fiducial points. Characteristically, GM (T,T) shows fewer individual differences on the SCC than the other matching methods. In other words, GM (T,T) eliminates the individual differences of the SCC that actually exist. In GM (T,T), a point on the scalp of the individual subject is transferred to the template space by the affine transformation that aligns the fiducial points in the individual space with those of the

template space. Then, the transferred point is projected onto the cortical surface in the template space. Noticeably, the head structures of the same 17 subjects are always used in GM (T,T), which indicates the positional relationship between the scalp and cortical surface is stationary on the SCC analysis by GM (T,T) for any subject.

3.4.3 Consideration of appropriate SCC for fNIRS

The SCC aims to identify cortical activation regions caused by changes in absorbance measured at the SD pairs attached to the scalp. Essentially, the SCC should be analyzed on the subject-specific anatomical structure because it is influenced by individual differences. However, the anatomical structures of individual subjects are not available in most fNIRS experiments. Techniques such as probabilistic registration and the transcranial brain atlas have been developed to estimate the activation region in such cases. Probabilistic registration is GM (T,T) itself, and a method equivalent to GM (S,T) was used to construct the transcranial brain atlas. The SCC obtained by these two methods is significantly different from that of SBM at a considerable number of fiducial points. Therefore, at those fiducial points, the reliability of the SCC obtained by GM (T,T) or GM (S,T) should be evaluated with great care.

The group-wise probability of the SCC obtained by SBM could be a promising alternative to the SCC on the individual subject. The group-wise probability of SBM

consists of individual SCCs considering the effects of light propagation in the head of 45 subjects. The full list of brain regions where the group-wise probability is greater than zero encompasses the brain regions that are potential sources of the fNIRS signal at each fiducial point. Thus, the possibility of ignoring the activation region must be extremely small by referring to the group-wise probability of SBM.

Chapter 4

4 Scalp-Cortex Correlation in Infant Population

4.1 Scalp-to-cortex distance

The depth of the head surface from the cortical surface, labeled as the scalp-to-cortex distance, is an important factor to be considered in actual fNIRS measurement. A previous simulation study shows that the shorter SD distances (e.g., 15 mm) may not allow near-infrared light to reach the gray matter of adults (Fukui et al., 2003; Okada et al., 1997). However, a simulation study on neonates reveals that an SD pair with an SD distance of 10 mm has the sensitivity to gray matter (Fukui et al., 2003). This finding must be associated with the very thin superficial layers of neonates. Given that age-related changes in the thickness of scalp and skull have been reported, the scalp-to-cortex distance must vary from birth to 2 years of life. A map of delineating the scalp-to-cortex distance that exhibits a global distribution of the cortical surface depth along the head surface can be beneficial to explain the age-related optics-based SCC and select the optimal SD distances for 0-, 1-, 2-yo infants. Hence, referencing a previous study (Nakamura et al., 2016), the scalp-to-cortex distance was calculated for all head surface points including 10-10 fiducial points for 0-, 1-, 2-yo infant head models.

4.2 Characterization of optics-based SCC

4.2.1 Definition of evaluation metrics

In addition to the establishment of the optics-based SCC at 10-10 fiducial points for 0-, 1-, 2-yo infants, the age-related changes of optics-based SCC deserve further evaluated quantitively. The reason is that fNIRS users who are involved in developmental neuroscience have been focusing on the following four questions most: 1) how many brain regions are associated with an SD pair; 2) which brain region is the MLCBR for a given SD pair and its probability; 3) whether the sensitivity is sufficient to measure brain activity in the MLCBR, and 4) whether the MLCBR for the same scalp location is consistent across the early development. Therefore, four evaluation metrics were defined, that is: N_{CBR}, the selectivity of the MLCBR, the sensitivity of the MLCBR, and the consistency of the MLCBR across physical development, to further characterize the optics-based SCC and to systematically investigate the effects of age and SD distance on the optics-based SCC.

The detailed definitions of the four metrics are described below. Due to the strong scattering of near-infrared light passing through head tissues, a fiducial point usually projects to more than one brain region. Hence, I simply counted the number of brain regions that are correlated to a given fiducial point as N_{CBR}. $L_{norm,M} = 0.05$ was used as a

threshold to calculate N_{CBR}. Moreover, I chose the brain region with the largest $L_{norm,M}$ as the MLCBR for a given fiducial point. $L_{norm,MLCBR}$ was defined as the metric of selectivity at the fiducial point. As for the sensitivity metric, I calculated the absolute PPL of the MLCBR. The absolute PPL in the MLCBR is obtained using the following equation:

$$L_{abs,MLCBR} = \frac{\ln(I_{base}/I_{pert})}{0.001\mu_{a,MLCBR}}, \quad (22)$$

where I_{base} and I_{pert} are the detected intensities when the absorption coefficient of the MLCBR ($\Delta\mu_{a,MLCBR}$) is the baseline and perturbed states (0.1% increase), respectively. Finally, to examine whether the MLCBR at the same fiducial point is consistent from 0- to 2-yo, all fiducial points are classified into five categories according to consistency: 1) completely consistent, that is, the MLCBR is the same for the brain region among the three age groups; 2) consistent between 0-yo and 1-yo; 3) consistent between 0-yo and 2-yo; 4) consistent between 1-yo and 2-yo; and 5) inconsistent between any age.

4.2.2 Statistical analysis

To examine the effects of age and SD distance on three evaluation metrics, i.e., N_{CBR}, the selectivity of the MLCBR, the sensitivity of the MLCBR, I used R to conduct all statistical analyses. Almost all analyses were performed using R version 3.6.3 in R Studio Version 1.2.5033 (RStudio Team, 2019), except for N_{CBR}, which was assessed using the nparLD package with R 3.5.1. In addition, the following packages were also used for data

manipulation, visualization, and statistical tests: dplyr v1.0.2, tidyverse v1.3.0, rstatix v0.6.0, magrittr v1.5, nparLD v2.1, and ggpubr v0.4.0. N_{CBR}, selectivity, and sensitivity values at each 10-10 fiducial point (61 in total) were treated as the dependent variables. Provided that the dependent variable N_{CBR} deviated from normality and equal variability, I applied a rank-based non-parametric mixed model statistical method, nparLD (Noguchi et al., 2012) with an F1-LD-F1 design, to investigate the effects of age and SD distance on N_{CBR}. I reported the Wald-type statistic (WTS) to assess the statistical significance of age, SD distance, and their interaction. If the interaction or main effects were significant, comparisons between two conditions were conducted using the nonparametric Mann-Whitney U test (independent samples) or Wilcoxon signed-rank test (dependent samples), followed by the Bonferroni method for multiple comparison adjustment. For the dependent variables of sensitivity or selectivity, a mixed design ANOVA was conducted to examine the effects of age and SD distance. Specifically, the sensitivity and selectivity were subjected to two 2-way mixed ANOVAs with the SD distance (10, 15, 20, 25, and 30 mm) as a within-subjects factor and age (0-yo, 1-yo, and 2-yo) as a between-subjects factor. If the interaction or main effects was significant, comparisons between two conditions were conducted using a two-sample t-test (independent samples) or paired t-test (dependent samples), followed by the Bonferroni

method for multiple comparison adjustment. In all ANOVA analyses, Greenhouse–Geisser corrections were applied on violation of the sphericity assumption. The generalized eta squared (Bakeman, 2005; Olejnik & Algina, 2003) served as estimates of the effect sizes.

4.3 Results

4.3.1 Distance from scalp to cortex

The spatial distribution of scalp-to-cortex distance (the sum of the scalp, skull, and CSF thicknesses) for 3 age groups is shown in Fig. 4.1. From the left and right view of Fig. 4.1, the scalp-to-cortex distance at temporal areas increases from 0 to 2 years of age. From the front view, Fig. 4.1 shows the scalp-to-cortex distance at frontal areas slightly decreases from 0 to 2 years of age. From the top and back views, the scalp-to-cortex distance at parietal areas increases from 0 to 2 years. Fig. 4.2 only shows the scalp-to-cortex distance at locations of 10-10 fiducial points. For each infant model, the scalp-to-cortex distance at frontal and midline fiducial points is relatively greater than other fiducial points. Importantly, the scalp-to-cortex distance in broad areas increases from 0 to 2 years of age.

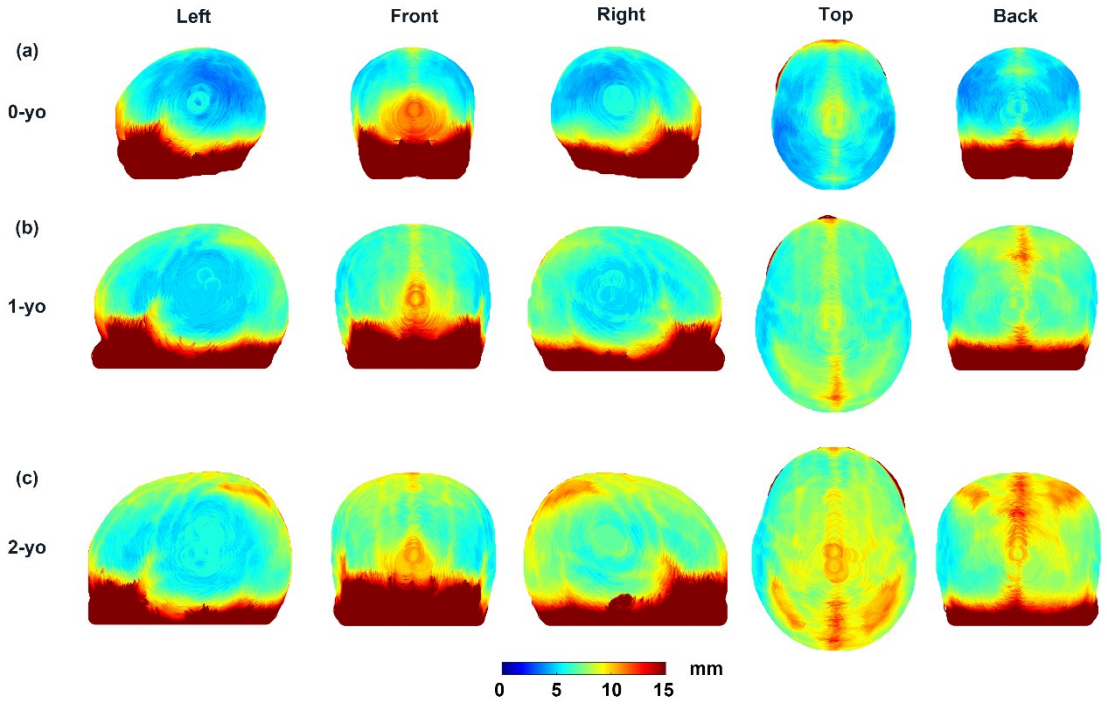

Figure 4. 1 The spatial distribution of the sum of the scalp, skull, and CSF thickness (i.e., scalp-to-cortex distance) in the 0-yo (a), 1-yo (b), and 2-yo (c) infant head models.

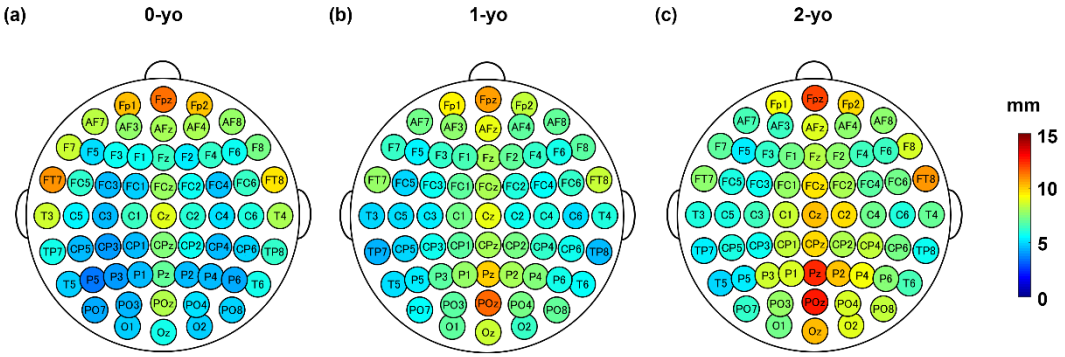

Figure 4. 2 The scalp-to-cortex distance at all 10-10 fiducial points in the 0-yo (a), 1-yo (b) and 2-yo (c) infant head models.

4.3.2 Optics-based SCC for a representative fiducial point

To illustrate the changes in SSP with age and SD distance, the PMDF of the circumferential SD pair at the fiducial point T4 is shown in Fig. 4.3. For each age group, the spatial distribution of the PMDF broadens as the SD distance increases, while changes a little with age. The values of $L_{norm,M}$ higher than 1% at the fiducial point T4 are shown in Table 4.1. According to the definition of the N_{CBR} (i.e., the number of brain regions whose $L_{norm,M}$ is greater than 5%), N_{CBR} of the fiducial point T4 is 2 for any age group and SD distance. Specifically, T4 mainly corresponds to two brain regions (MTG-R and ITG-R, indicated in boldface in Table 4.1). Among these two brain regions, MTG_R has the largest $L_{norm,M}$, so the MLCBR of T4 is MTG_R for any age group and SD distance, further suggesting the MLCBR is completely consistent across 3 age groups for each SD distance. Thus, when SD distance is 10 mm, the selectivity of MLCBR (i.e., $L_{norm,MLCBR}$) is 63.6%, 83.6%, 89.6% for 0-, 1-, and 2-yo, respectively (Table 4.1). In addition, other three brain regions, such as STG-R, TPOsup-R, and TPOmid-R, are also corresponded to T4 with the values of $L_{norm,M}$ lower than 5%. And $L_{norm,M}$ of these three brain regions increases as the SD distance increases (Table 4.1). The sensitivity of MLCBR (i.e., $L_{abs,MLCBR}$) is also shown in Table 4.1. I observed an increase in the $L_{abs,MLCBR}$ with increasing SD distance for each age group. The $L_{abs,MLCBR}$ of 0-yo is smaller than that of

1-yo and 2-yo, while $L_{abs,MLCBR}$ of 1-yo is almost similar or slightly larger than that of 2-yo.

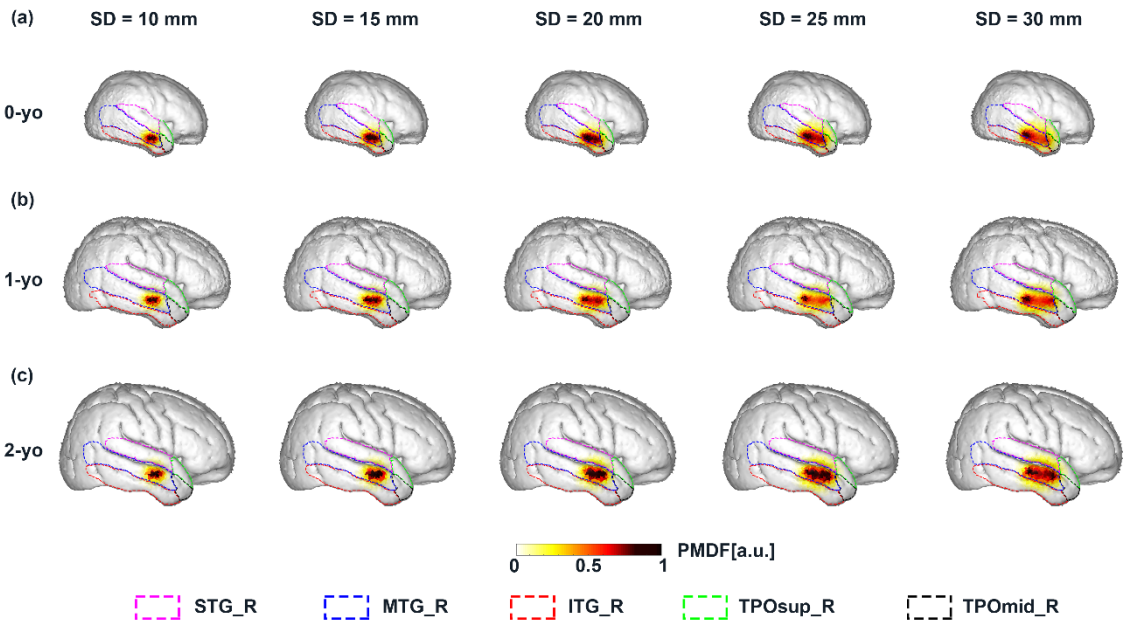

Figure 4. 3 The PMDF for a given fiducial point T4 at five SD distances for 0-yo, 1-yo, and 2-yo when the SD pair is attached in a circumferential orientation. Dashed lines in different colors indicate the AAL brain region boundaries. The PMDF superimposed on age-appropriate brain structures of 0-yo, 1-yo, and 2-yo are shown in (a), (b), and (c), respectively.

Table 4. 1 The normalized PPL of corresponding brain regions ($L_{norm,M}$) and the sensitivity of MLCBR ($L_{abs,MLCBR}$) for the circumferential SD pair set at the fiducial point T4 at five SD distances for 0-yo, 1-yo, and 2-yo.

Age	Brain region	SD distance				
		10 mm	15 mm	20 mm	25 mm	30 mm
0-yo	MTG_R	**63.6%**	**65.1%**	**59.3%**	**61.1%**	**56.2%**
	ITG_R	**34.6%**	**31.8%**	**36.6%**	**33.2%**	**36.6%**
	STG_R	0.9%	1.3%	1.4%	2.1%	2.2%
	TPOsup_R	0.4%	0.7%	0.9%	1.3%	1.7%
	TPOmid_R	0.3%	0.6%	1.0%	1.3%	2.0%
	$L_{abs,MLCBR}$ (mm)	1.9	4.6	5.9	7.9	9.1
1-yo	MTG_R	**83.6%**	**81.8%**	**78.6%**	**78.6%**	**74.6%**
	ITG_R	**15.3%**	**16.8%**	**19.6%**	**18.8%**	**22.4%**
	STG_R	0.9%	1.1%	1.4%	2.0%	2.2%
	TPOsup_R	0.1%	0.1%	0.1%	0.2%	0.3%
	TPOmid_R	0.0%	0.0%	0.1%	0.1%	0.2%
	$L_{abs,MLCBR}$ (mm)	4.6	6.2	8	10.4	11.3
2-yo	MTG_R	**89.0%**	**86.9%**	**86.1%**	**82.4%**	**81.9%**
	ITG_R	**7.8%**	**9.7%**	**9.4%**	**12.4%**	**11.7%**
	STG_R	2.6%	2.7%	3.4%	3.7%	4.6%
	TPOsup_R	0.2%	0.3%	0.4%	0.7%	0.9%
	TPOmid_R	0.1%	0.1%	0.1%	0.3%	0.3%
	$L_{abs,MLCBR}$ (mm)	3.9	5.8	7.6	9.8	11.3

Note: The $L_{norm,M}$ value higher than 0.05 is shown in bold. The MLCBR at T4 is MTG_R for all ages and SD distances.

To examine the effect of the orientation of SD pairs on SSP, the PMDF of the vertical SD pair set at T4 is shown in Fig. 4.4. When SD distance is 30 mm, the normalized PPL in STG_R corresponding to the vertical SD pair is 6.0%, 7.0%, and 9.4% for 0-yo, 1-yo,

and 2-yo, respectively. However, the vertical SD pair at T4 is also mainly correlated with the two brain regions (i.e., MTG_R and ITG_R) with a similar $L_{norm,M}$ for all SD distances. The brain regions correlated with the two orientational SD pairs at all 10-10 fiducial points and their normalized PPL from 0-yo, 1-yo, and 2-yo infants are provided in Supplementary Tables S2-6 for SD distances of 10 mm, 15 mm, 20 mm, 25 mm, and 30 mm, respectively.

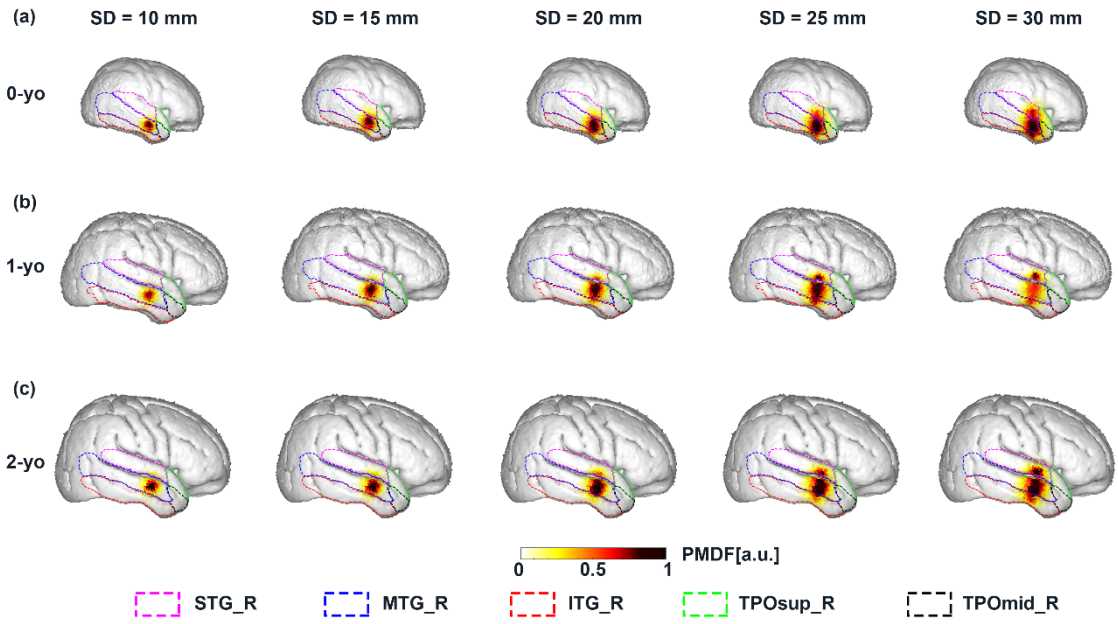

Figure 4. 4 The PMDF for a given fiducial point T4 at five SD distances for 0-yo, 1-yo, and 2-yo when the SD pair is attached in a vertical orientation. Dashed lines in different colors indicate the AAL brain region boundaries. The PMDF superimposed on age-appropriate brain structures of 0-yo, 1-yo, and 2-yo are shown in (a), (b), and (c), respectively.

4.3.3 The developmental changes in optics-based SCC

Fig. 4.5a-c shows the values of the N_{CBR} for circumferential SD pairs at all 10-10 fiducial points over five SD distances at three ages. Fiducial points neighboring the longitudinal fissure, for example, Fpz, FCz, Cz, CPz, and POz, are correlated with more corresponding brain regions for every SD distance and age. Furthermore, the larger the SD distance, the larger the N_{CBR} of the fiducial points for every age group. The N_{CBR} of 0-yo is larger than that of 1-yo and 2-yo, while the N_{CBR} of 1-yo and 2-yo is similar for each SD distance. According to a statistical analysis using the rank-based non-parametric mixed model, I found significant main effects of SD distance (WTS(4) = 195.88, $p < 0.001$) and age (WTS(2) = 10.37, $p < 0.01$), but none of interaction (WTS(8) = 9.01, $p = 0.34$). For the age factor (Fig. 4.5d-e left matrix), multiple comparisons with the Bonferroni adjustment showed that N_{CBR} of 0-yo is larger than that of 1-yo and 2-yo ($p < 0.001$, corrected); however, no significant differences are found between 1-yo and 2-yo ($p = 0.92$, corrected). For the SD distance factor (Fig. 4.5d-e right matrix), multiple comparisons between N_{CBR} of any two SD distances all produce significantly different values, and the N_{CBR} values of larger SD distances are greater than those of smaller SD distances ($p < 0.001$, corrected). Similar results for N_{CBR} of vertical SD pairs are shown in Fig. 4.6.

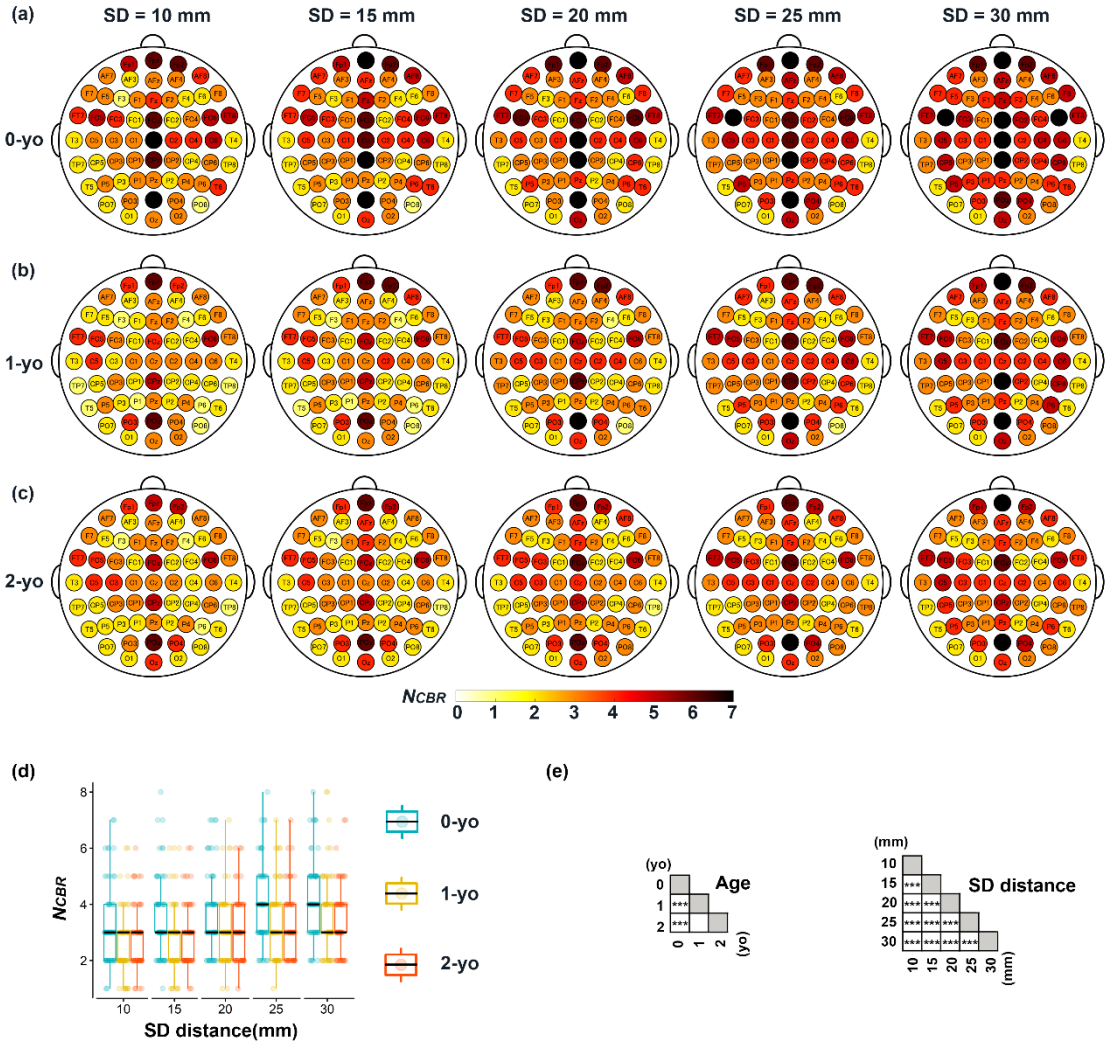

Figure 4. 5 N_{CBR} for circumferential SD pairs at all 10-10 fiducial points at five different SD distances for 0-yo (a), 1-yo (b), and 2-yo (c). Darker red regions indicate larger N_{CBR}. (d) Box plots of N_{CBR} at all 10-10 fiducial points for each condition of the age and the SD distance. The individual-colored dots indicate the N_{CBR} of each fiducial point. Boxes indicate the interquartile range. The black horizontal line within the boxes indicates the median. Whiskers extend 1.5 times above and below the interquartile range limits. (e) Statistical significance of post-hoc test for N_{CBR} is indicated by matrices. * $p < 0.05$, ** $p < 0.01$, *** $p < 0.001$, white and gray blank are not significant and not applicable, respectively.

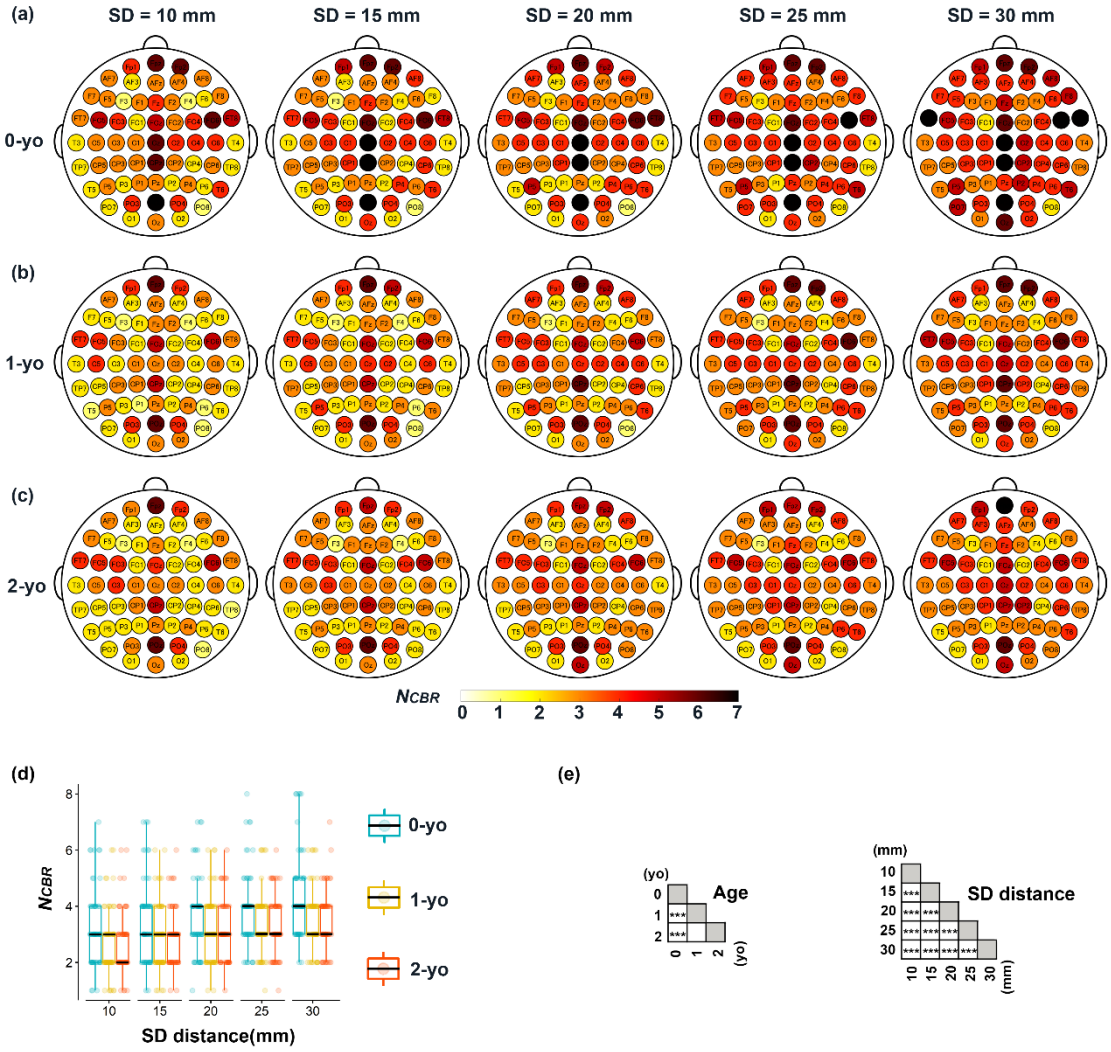

Figure 4. 6 N_{CBR} for vertical SD pairs at all 10-10 fiducial points at five different SD distances for 0-yo (a), 1-yo (b), and 2-yo (c). Darker red regions indicate larger N_{CBR}. (d) Box plots of N_{CBR} at all 10-10 fiducial points for each condition of the age and the SD distance. The individual-colored dots indicate the N_{CBR} of each fiducial point. Boxes indicate the interquartile range. The black horizontal line within the boxes indicates the median. Whiskers extend 1.5 times above and below the interquartile range limits. (e) Statistical significance of post-hoc test for N_{CBR} is indicated by matrices. * $p < 0.05$, ** $p < 0.01$, *** $p < 0.001$, white and gray blank are not significant and not applicable, respectively.

The selectivity of the MLCBR of circumferential SD pairs at all 10-10 fiducial points is shown in Fig. 4.7a-c. I found that most fiducial points at shorter SD distances have a higher selectivity for every age group. Moreover, the selectivity of 1-yo and 2-yo seems larger than that of 0-yo. These visually observable findings are proved by statistically significant main effects of age ($F(2, 180) = 4.89$, $p < 0.05$, $\eta_G^2 = 0.049$) and SD distance ($F(1.41, 253.25) = 266.11$, $p < 0.001$, $\eta_G^2 = 0.067$) on the selectivity; however, no statistically significant two-way interactions are found between age and SD distance on the selectivity, $F(2.81, 253.25) = 0.93$, $p = 0.42$, $\eta_G^2 = 0.001$ (Fig. 4.7d). The results of the post-hoc multiple comparisons are shown in Fig. 4.7e. For the age factor (Fig. 4.7e, left matrix), multiple pairwise independent sample t-tests show that the selectivity of 0-yo is lower than that of 1-yo and 2-yo for all fiducial points on average ($p < 0.001$, Bonferroni-corrected). In contrast, multiple pairwise paired t-tests for the SD distance (Fig. 4.7e, right matrix) showed that comparisons from any two SD distances are significantly different ($p < 0.001$, corrected) and that the selectivity decreases as SD distance increases. Similar results for the selectivity of vertical SD pairs are shown in Fig. 4.8.

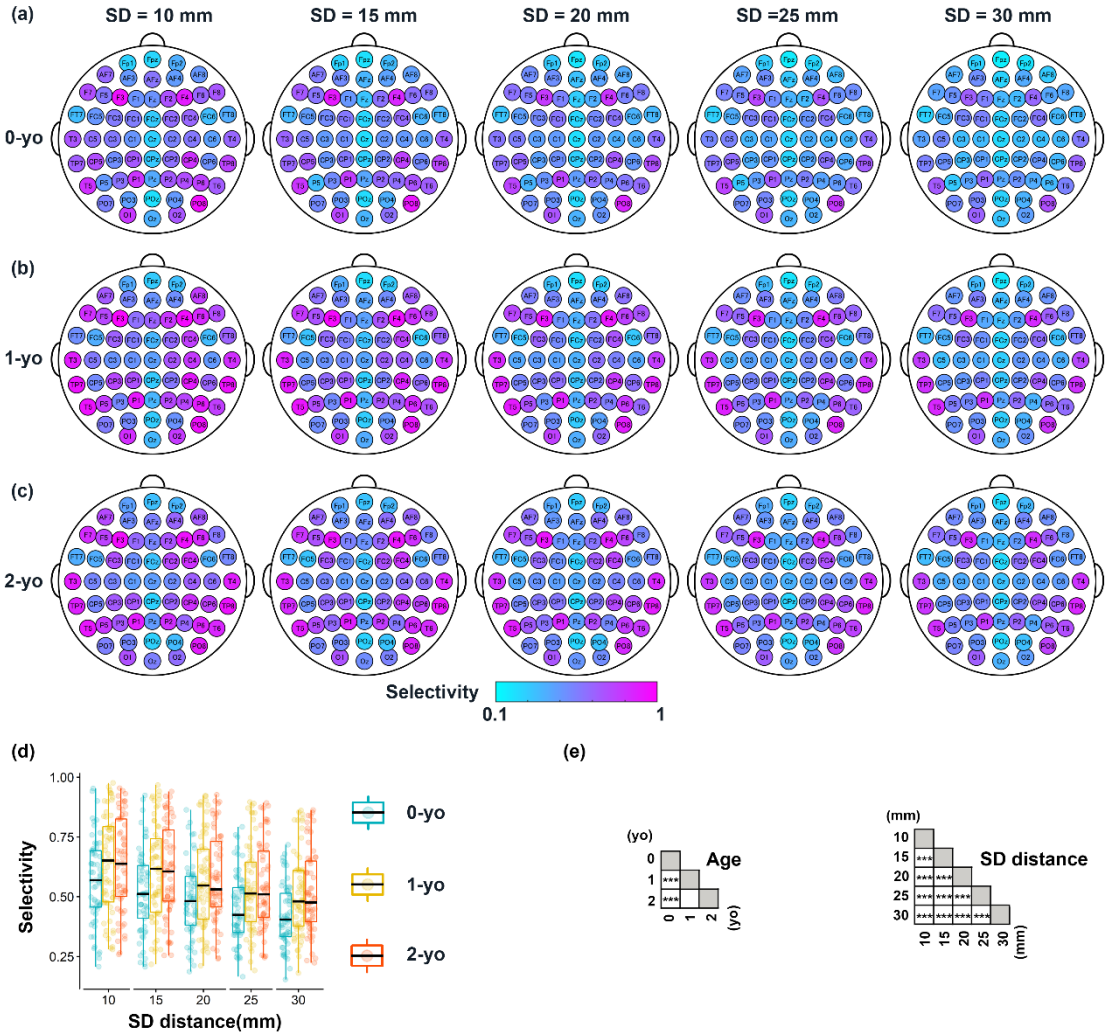

Figure 4. 7 Selectivity of the MLCBR for circumferential SD pairs at all 10-10 fiducial points at five different SD distances for 0-yo (a), 1-yo (b), and 2-yo (c). Magenta and blue indicate higher and lower selectivity, respectively. (d) Box plots of the selectivity at all 10-10 fiducial points for each condition of the age and the SD distance. The individual-colored dots indicate the selectivity of each fiducial point. Boxes indicate the interquartile range. The black horizontal line within the boxes indicates the median. Whiskers extend 1.5 times above and below the interquartile range limits. (e) Statistical significance of post-hoc test for the selectivity is indicated by matrices. * $p < 0.05$, ** $p < 0.01$, *** $p < 0.001$, white and gray blank are not significant and not applicable, respectively.

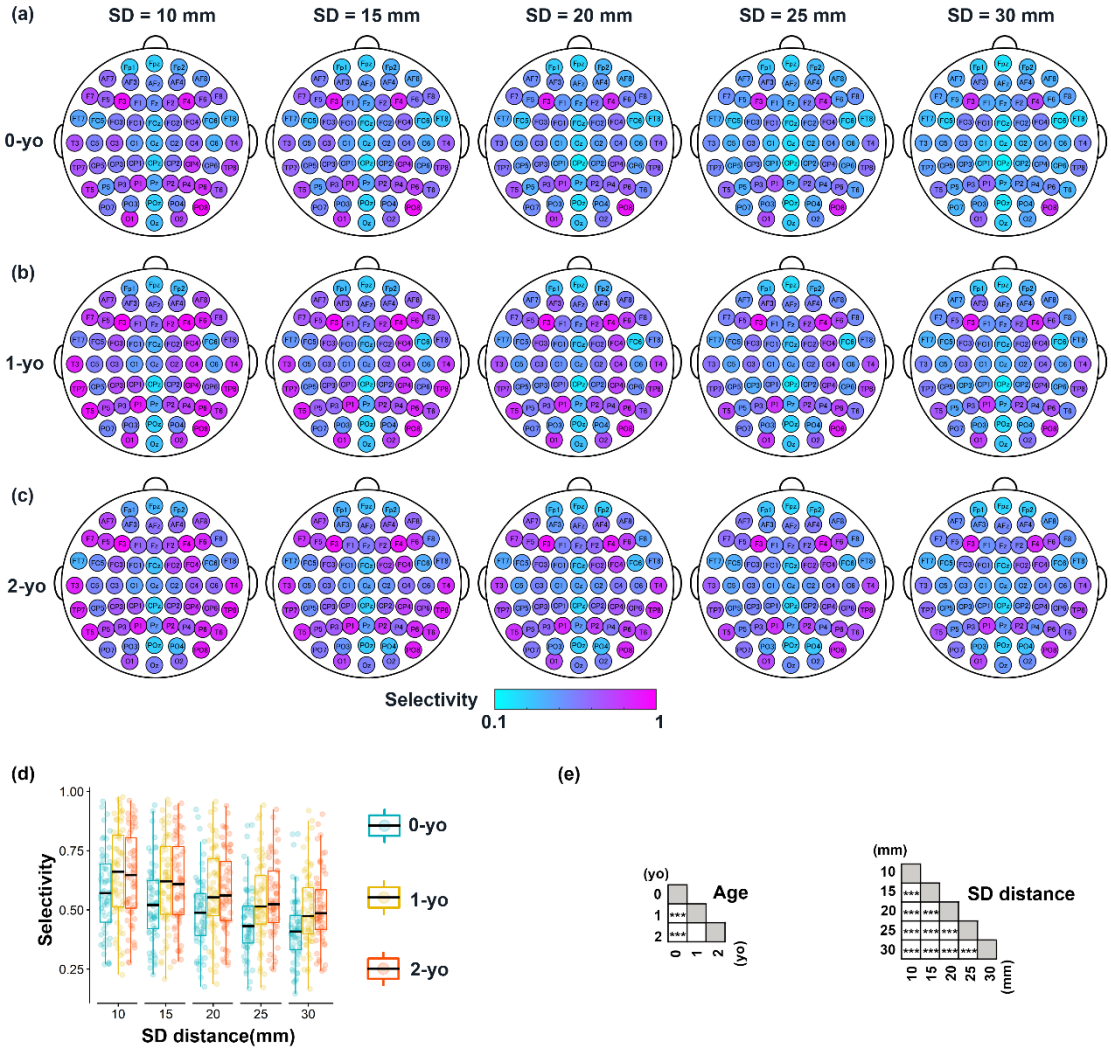

Figure 4. 8 Selectivity of the MLCBR for vertical SD pairs at all 10-10 fiducial points at five different SD distances for 0-yo (a), 1-yo (b), and 2-yo (c). Magenta and blue indicate higher and lower selectivity, respectively. (d) Box plots of the selectivity at all 10-10 fiducial points for each condition of the age and the SD distance. The individual-colored dots indicate the selectivity of each fiducial point. Boxes indicate the interquartile range. The black horizontal line within the boxes indicates the median. Whiskers extend 1.5 times above and below the interquartile range limits. (e) Statistical significance of post-hoc test for the selectivity is indicated by matrices. * $p < 0.05$, ** $p < 0.01$, *** $p < 0.001$, white and gray blank are not significant and not applicable, respectively.

Regarding the sensitivity of the MLCBR over all 10-10 fiducial points, I found an obvious increase in $L_{abs,\ MLCBR}$ with increasing SD distance for each age (Fig. 4.9a-c). However, no differences among the ages are observed during visual inspection. The 3 (age) × 5 (SD distance) mixed ANOVA reveals significant main effects of age ($F(2, 180) = 4.87$, $p < 0.01$, $\eta_G^2 = 0.047$) and SD distance ($F(1.37, 247.25) = 837.02$, $p < 0.001$, $\eta_G^2 = 0.306$). However, these main effects are further qualified by the presence of a significant interaction between age and SD distance, $F(2.75, 247.25) = 8.67$, $p < 0.001$, $\eta_G^2 = 0.009$ (Fig. 4.9d). The simple main effect of age is significant for all SD distances, that is, 10, 15, 20, 25, and 30 mm (all $p < 0.05$). The results of the post-hoc multiple comparisons are shown in Fig. 4.9e. At 10 mm SD distance, the mean sensitivity of 1-yo is significantly higher than that of 2-yo ($p < 0.05$, Bonferroni-corrected). The mean sensitivity of 1-yo is significantly higher than that of 0-yo at SD distances of 15 mm ($p < 0.05$, corrected), 20 mm ($p < 0.01$, corrected), 25 mm ($p < 0.01$, corrected), and 30 mm ($p < 0.01$, corrected). The simple main effect of the SD distance is also significant for any of the 0-yo, 1-yo, and 2-yo infants (all $p < 0.001$). At all years of age, the sensitivity of larger SD distances is significantly greater than that of smaller SD distances (Fig. 4.9d-e, $p < 0.001$, corrected). Similar results for the sensitivity of the vertical SD pairs are presented in Fig. 4.10.

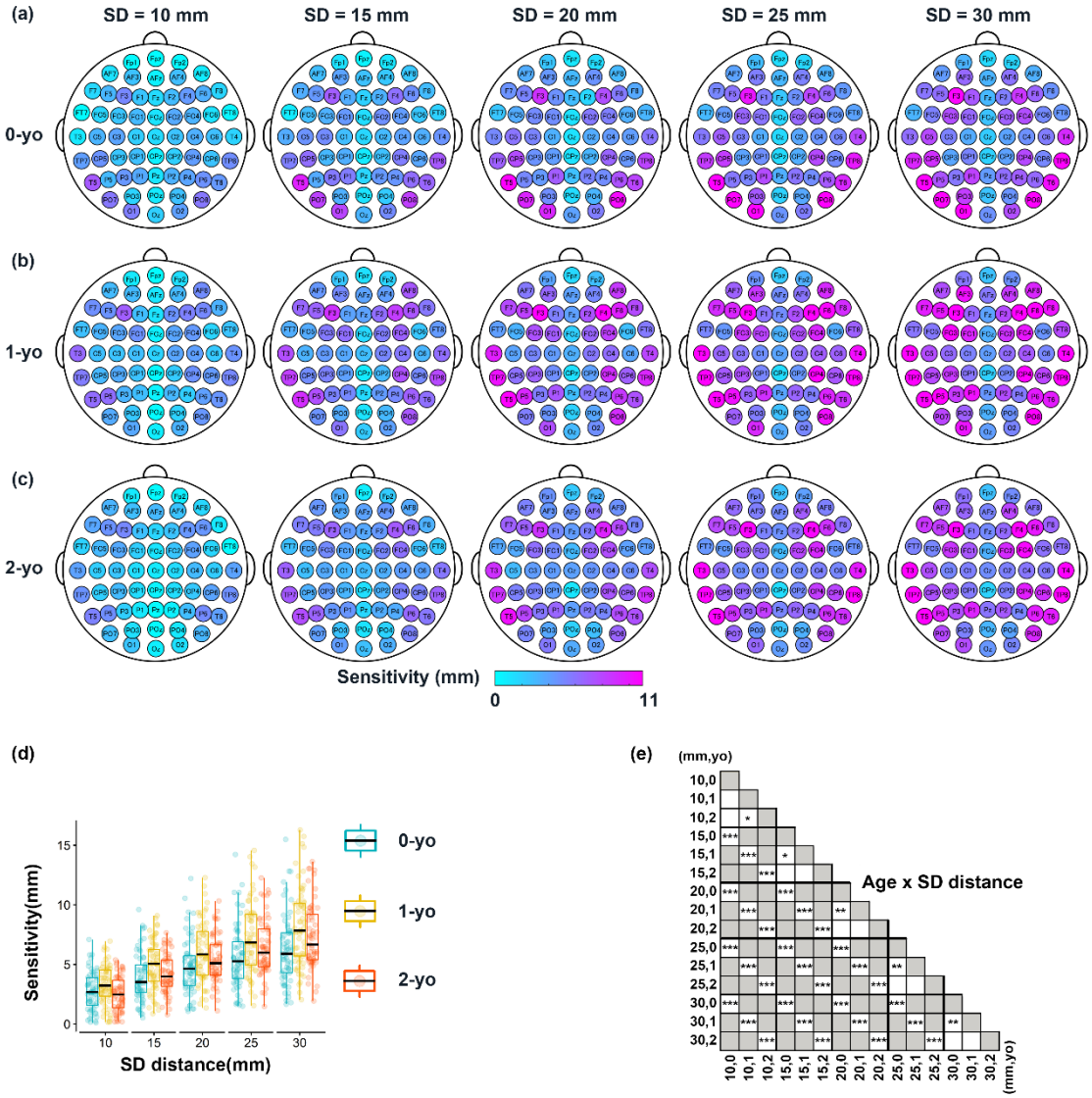

Figure 4. 9 Sensitivity of the MLCBR for circumferential SD pairs at all 10-10 fiducial points at five different SD distances for 0-yo (a), 1-yo (b), and 2-yo (c). Magenta and blue indicate higher and lower sensitivity, respectively. (d) Box plots of the sensitivity at all 10-10 fiducial points for each condition of the age and the SD distance. The individual-colored dots indicate the sensitivity of each fiducial point. Boxes indicate the interquartile range. The black horizontal line within the boxes indicates the median. Whiskers extend 1.5 times above and below the interquartile range limits. (e) Statistical significance of post-hoc test for the sensitivity is indicated by matrices. * $p < 0.05$, ** $p < 0.01$, *** $p < 0.001$, white and gray blank are not significant and not applicable, respectively.

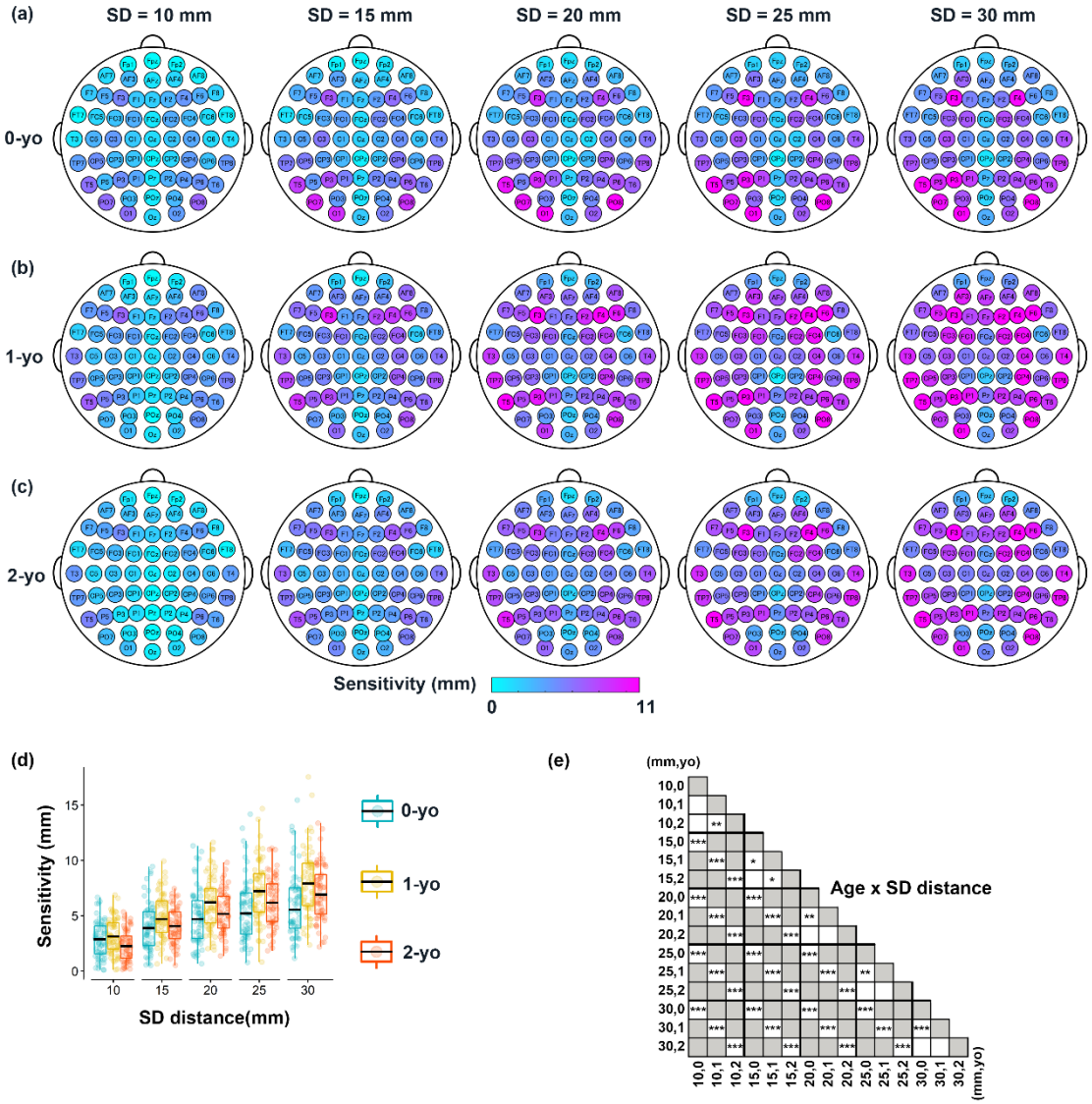

Figure 4. 10 Sensitivity of the MLCBR for vertical SD pairs at all 10-10 fiducial points at five different SD distances for 0-yo (a), 1-yo (b), and 2-yo (c). Magenta and blue indicate higher and lower sensitivity, respectively. (d) Box plots of the sensitivity at all 10-10 fiducial points for each condition of the age and the SD distance. The individual-colored dots indicate the sensitivity of each fiducial point. Boxes indicate the interquartile range. The black horizontal line within the boxes indicates the median. Whiskers extend 1.5 times above and below the interquartile range limits. (e) Statistical significance of post-hoc test for the sensitivity is indicated by matrices. * $p < 0.05$, ** $p < 0.01$, *** $p < 0.001$, white and gray blank are not significant and not applicable, respectively.

Almost half of 10-10 fiducial points are correlated with the completely consistent MLCBR across the three age groups for each SD distance (Fig. 4.11). The average number of fiducial points correlated with the completely consistent MLCBR for all SD distances is 41.6 ± 1.5 and 39.6 ± 0.9 for circumferential and vertical SD pairs, respectively, as shown in green circles in Fig. 4.11. However, fiducial points correlated with inconsistent MLCBR across the three ages (yellow and red circles) are found around the longitudinal fissure for both SD pair orientations. To help fNIRS researchers examining longitudinal functional development from 0-yo to 2-yo, I provided fiducial points whose MLCBR is completely consistent at certain SD distances for the circumferential and vertical SD pairs across 0-yo, 1-yo, and 2-yo infants (Table 4.2).

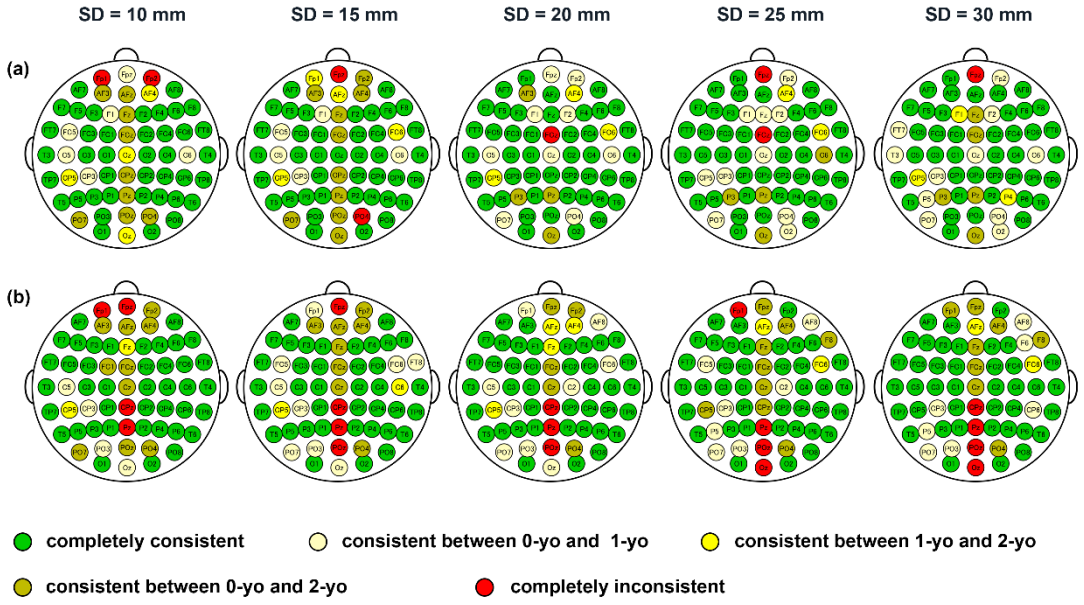

Figure 4. 11 Consistency of MLCBR at five SD distances for circumferential (a) and vertical (b) SD pairs. The consistency of the MLCBR among 0-yo, 1-yo, and 2-yo for every fiducial point is indicated by circles with different colors.

Table 4. 2 The summary of fiducial points whose the MLCBR is completely consistent at some SD distances for the circumferential and vertical SD pairs across 0-yo, 1-yo, and 2-yo infants.

Fiducial point	Circumferential SD pairs		Vertical SD pairs	
	MLCBR	SD distance (mm)	MLCBR	SD distance (mm)
Cz	SMA-R	15	-	-
AFz	SFGmed-R	20, 25, 30	-	-
Fz	SFGmed-R	20	-	-
CPz	PoCG-L	20, 25, 30	-	-
Poz	SPG-L	20, 25, 30	-	-
T3	MTG-L	10, 15, 20, 25	MTG-L	10, 15, 20, 25, 30
C5	STG-L	25, 30	PoCG-L	25, 30
C3	PoCG-L	10, 15, 20, 25, 30	PoCG-L	10, 15, 20, 25, 30
C1	PreCG-L	10, 15, 20, 25, 30	PreCG-L	10, 15, 20, 25, 30
C2	PreCG-R	10, 15, 20, 25, 30	PreCG-R	10, 15, 30
C4	PoCG-R	10, 15, 20, 25, 30	PoCG-R	10, 15, 20, 25, 30
C6	-	-	PoCG-R	10, 20, 25, 30
T4	MTG-R	10, 15, 20, 25, 30	MTG-R	10, 15, 20, 25, 30
FT7	TPOsup-L	10, 15, 20, 25	TPOsup-L	10, 15, 20, 25, 30
F7	ORBinf-L	10, 15, 20, 25, 30	ORBinf-L	10, 15, 20, 25, 30
AF7	ORBmid-L	10, 15, 20, 25, 30	ORBmid-L	10, 15, 20, 25, 30
Fp1	ORBmid-L	20, 25, 30	-	-
Fp2	-	-	SFGdor-R	25, 30
AF8	ORBmid-R	10, 15, 20, 25, 30	ORBmid-R	10, 15
F8	ORBinf-R	10, 15, 20, 25, 30	ORBinf-R	10, 15, 20
FT8	MTG-R	10, 15, 20, 25, 30	MTG-R	10, 20, 25, 30
TP7	MTG-L	10, 15, 20, 25, 30	MTG-L	10, 15, 20, 25, 30
T5	MTG-L	10, 15, 20, 25, 30	MTG-L	10, 15, 20, 25, 30
O1	MOG-L	10, 15, 20, 25, 30	MOG-L	10, 15, 20, 25, 30
O2	SOG-R	10, 15, 20	SOG-R	10, 15, 20, 25, 30
PO8	MOG-R	10, 15, 20, 25, 30	MOG-R	10, 15, 20, 25, 30
T6	MTG-R	10, 15, 20, 25, 30	MTG-R	10, 15, 20, 25, 30
TP8	MTG-R	10, 15, 20, 25, 30	MTG-R	10, 15, 20, 25, 30
FC5	IFGtriang-L	20, 25, 30	IFGoperc-L	10, 20, 30

Note: - not applicable. See Table 2.1 for abbreviations of brain regions.

Table 4. 2 The summary of fiducial points whose the MLCBR is completely consistent at some SD distances for the circumferential and vertical SD pairs across 0-yo, 1-yo, and 2-yo infants (Continued).

Fiducial point	Circumferential SD pairs		Vertical SD pairs	
	MLCBR	SD distance (mm)	MLCBR	SD distance (mm)
FC3	MFG-L	10, 15, 20, 25, 30	MFG-L	10, 15, 20, 25, 30
FC1	MFG-L	10, 15, 20, 25, 30	MFG-L	15, 20, 25, 30
FC2	MFG-R	10, 15, 20, 25, 30	MFG-R	10, 15, 20, 25, 30
FC4	MFG-R	10, 15, 20, 25, 30	MFG-R	10, 15, 20, 25, 30
FC6	IFGoperc-R	10, 30	IFGoperc-R	10
F5	IFGtriang-L	10, 15, 20, 25, 30	IFGtriang-L	10, 15, 20, 25, 30
F3	MFG-L	10, 15, 20, 25, 30	MFG-L	10, 15, 20, 25, 30
F1	-	-	SFGdor-L	10, 15, 20, 25, 30
F2	SFGdor-R	10, 15	SFGdor-R	10, 15, 20, 25, 30
F4	MFG-R	10, 15, 20, 25, 30	MFG-R	10, 15, 20, 25, 30
F6	IFGtriang-R	10, 15, 20, 25, 30	IFGtriang-R	10, 15, 20, 25
AF3	MFG-L	25, 30	MFG-L	20, 25, 30
AF4	MFG-R	30	-	-
CP3	IPL-L	20	-	-
CP1	PoCG-L	10, 15, 20, 25, 30	PoCG-L	10, 15, 20, 25, 30
CP2	PoCG-R	10, 15, 20, 25, 30	PoCG-R	10, 15, 20, 25, 30
CP4	IPL-R	10, 15, 20, 25, 30	IPL-R	10, 15, 20, 25, 30
CP6	SMG-R	10, 15, 20, 25, 30	SMG-R	10, 15, 20, 25
P5	ANG-L	10, 15, 20, 25	ANG-L	10, 15, 20
P3	ANG-L	10, 15	ANG-L	10, 15, 20, 25, 30
P1	SPG-L	10, 15, 20, 25, 30	SPG-L	10, 15, 20, 25, 30
P2	SPG-R	10, 15, 20, 25, 30	SPG-R	10, 15, 20, 25, 30
P4	ANG-R	10, 15, 20, 25	ANG-R	10, 15, 20, 25, 30
P6	ANG-R	10, 15, 20, 25, 30	ANG-R	10, 15, 20, 25, 30
PO3	ANG-L	10, 15, 20, 25, 30	-	-

Note: - not applicable. See Table 2.1 for abbreviations of brain regions.

4.3.4 Determination of optimal SD distance

Based on the results in Section 4.3.3, I found that the sensitivity and selectivity of the MLCBR increases and decreases, respectively, as the SD distance increases. In other words, there is a trade-off between the sensitivity and selectivity of the MLCBR in determining a suitable SD distance for targeting the brain regions of interest in infant fNIRS. Therefore, a suitable SD distance that achieves a good balance between the sensitivity and selectivity of the MLCBR in infant fNIRS was explored.

First, I drew a scatter plot of the selectivity and sensitivity for circumferential SD pairs set on all 10-10 fiducial points at five SD distances at each infant age (Fig. 4.12a-c). Then, I empirically chose thresholds 3.0 and 0.4 for the sensitivity and the selectivity, respectively, to categorize every point in the scatter plot into three zones. Because the sensitivity takes precedence over selectivity in fNIRS, I defined the red zone as the area with a sensitivity lower than 3.0. The remaining region was then divided into two zones according to the selectivity threshold. Fiducial points with a sensitivity lower and higher than 0.4 were classified into yellow and green zones, respectively. Therefore, the SD distance with a larger number of fiducial points categorized into the green zone indicates that both higher sensitivity and selectivity can be achieved.

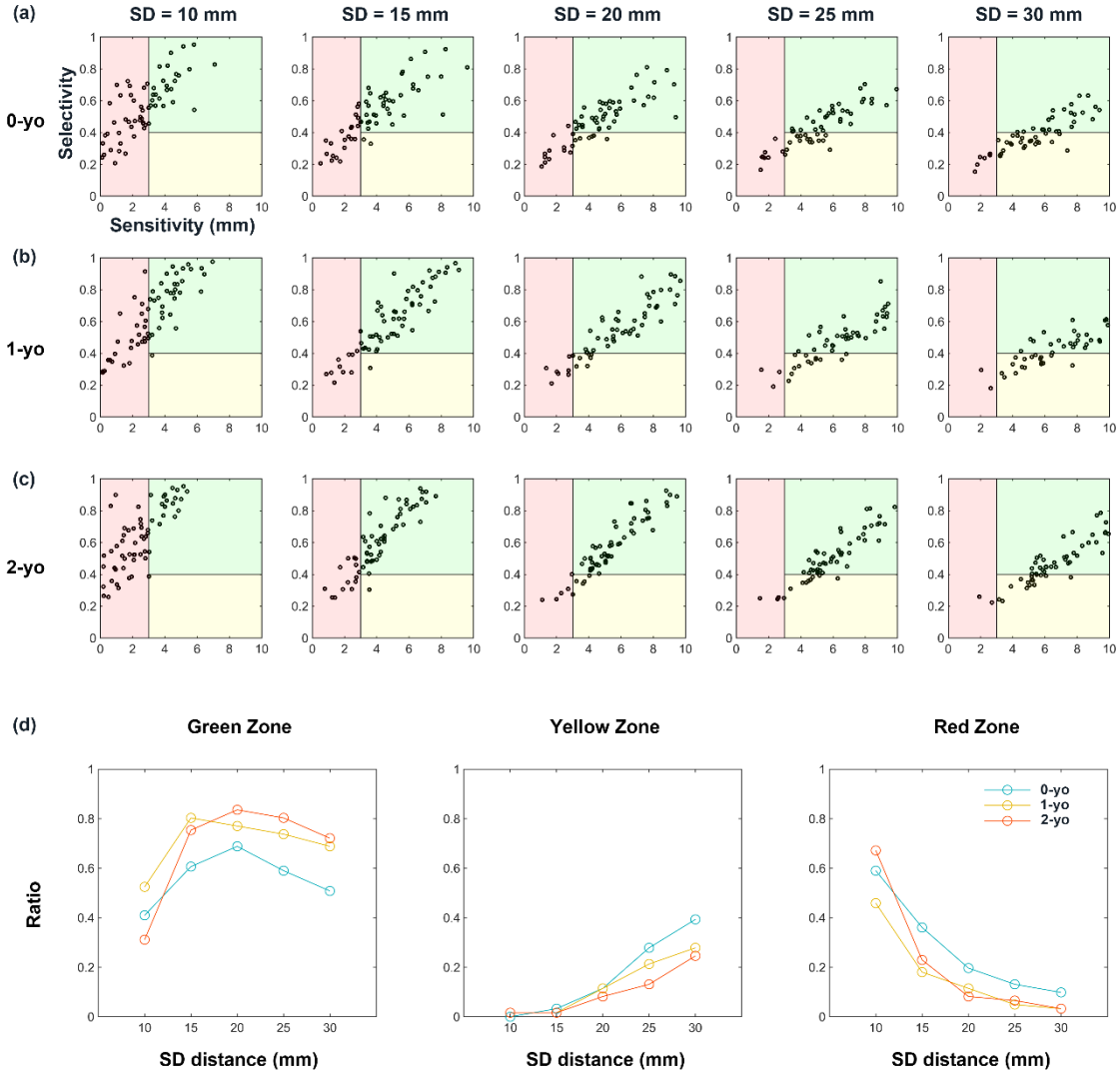

Figure 4. 12 The relation between sensitivity and selectivity for circumferential SD pairs over each SD distance for 0-yo (a), 1-yo (b), and 2-yo (c). Black circles in subfigures a-c indicate data from each 10-10 fiducial point. (d) The ratios of the number of fiducial points in the Green, Yellow and Red zones to the number of all 10-10 fiducial points.

As shown in Fig. 4.12, the distribution of points in the scatter plot varies with the SD distance for infants at all ages (Fig. 4.12a-c for 0-yo, 1-yo, and 2-yo infants, respectively). For shorter and longer SD distances, more fiducial points are observed in the red and yellow zones, respectively. The ratios of the number of fiducial points in each

zone to all fiducial points are shown in Fig. 4.12d. For the green zone, inverted U-shaped curves are observed for all three age groups. On the other hand, the ratio of fiducial points in the yellow and red zones shows a respective monotonic increase and decrease as the SD distance increases. These findings suggest that excessive short and long SD distances are unsuitable for infant fNIRS. Therefore, the SD distance between 15 mm and 25 mm is suitable for 0-yo, 1-yo, and 2-yo infants. A 25 mm SD distance is more suitable if the sensitivity is emphasized, whereas a 15 mm SD distance is more appropriate if selectivity is considered as a priority. A relatively balanced trade-off can be obtained when the SD distance is 20 mm. To validate the robustness of this finding, I examined the same problem with different thresholds 4.0 and 0.5 for sensitivity and selectivity, respectively. Although the thresholds change modestly, the shapes of the graph, as shown in Fig. 4.12d, are maintained (Fig. 4.13).

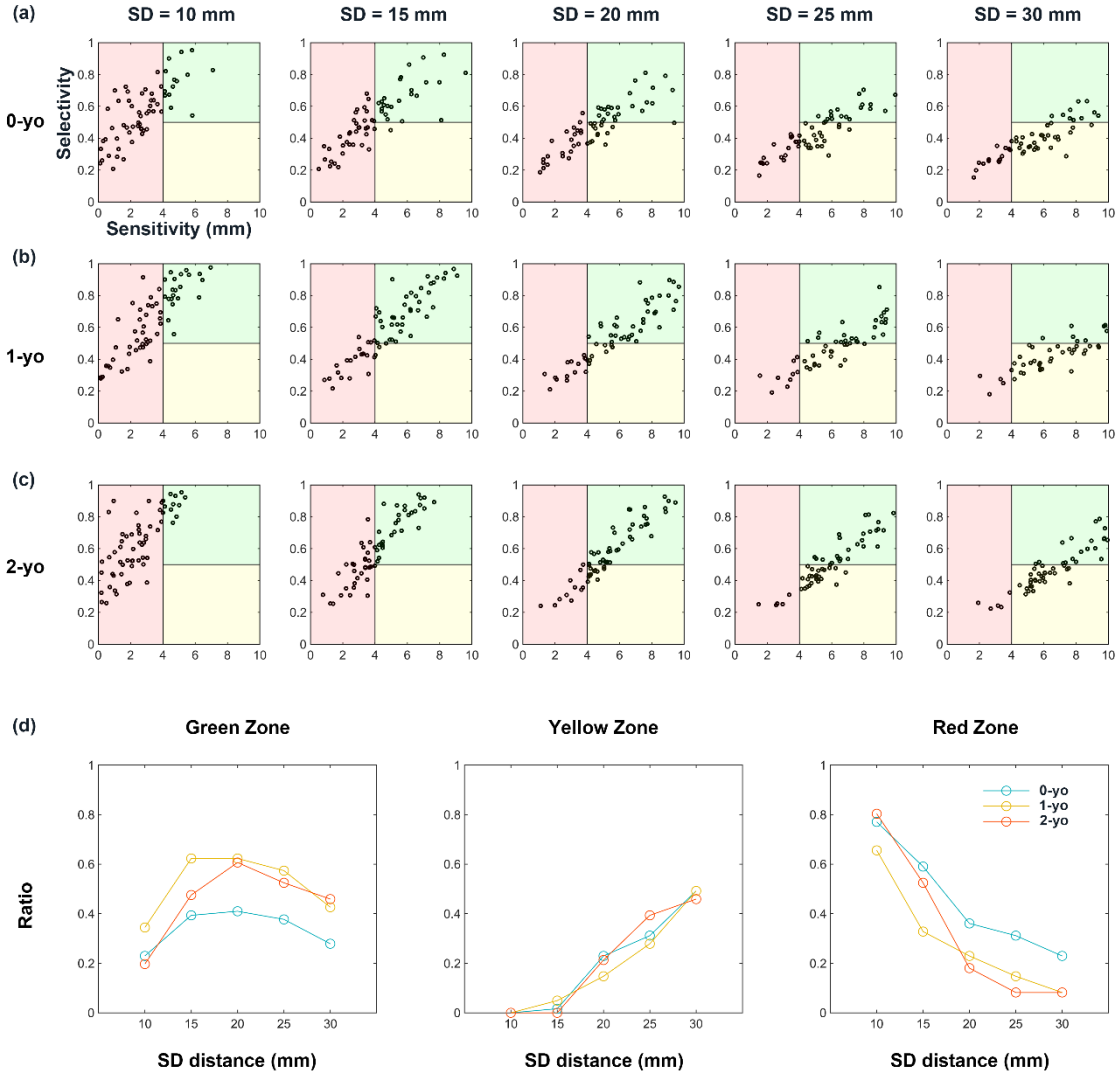

Figure 4. 13 The relation between sensitivity and selectivity for circumferential SD pairs over each SD distance for 0-yo (a), 1-yo (b), and 2-yo (c) at thresholds of 4 mm and 0.5 for the sensitivity and the selectivity, respectively. Black circles in subfigures a-c indicate data from each 10-10 fiducial point. (d) The ratios of the number of fiducial points in the Green, Yellow and Red zones to the number of all 10-10 fiducial points.

4.4 Discussion

fNIRS has contributed significantly to the advancement of developmental cognitive neuroscience; however, fNIRS data cannot provide any anatomical brain information, which is critical for data explanation and comparisons with other modalities. Although several methods have been proposed to obtain SCC in adults and infants, little is known about the influence of age and SD distance on the SCC with substantial physical development of the infant's head during the first 2 postnatal years. In this thesis, light propagation analysis was adopted to establish a precise optics-based SCC between the fNIRS measurement channels, that is, SD pairs, set on the 10-10 system scalp positions and AAL brain regions in three age-appropriate infant head models of 0-yo, 1-yo, and 2-yo. Importantly, four metrics: $N_{CBR,}$ and the selectivity, sensitivity, and consistency of the MLCBR, were provided to quantitatively evaluate the optics-based SCC for changes during a remarkable period of brain development. Moreover, the suitable SD distances for infant fNIRS were assessed by simultaneously considering the selectivity and sensitivity of the MLCBR.

4.4.1 Scalp-to-cortex distance increases during the first two years of life

As expected, the scalp-to-cortex distances at the most scalp locations increase from 0-yo to 2-yo, except for the frontal pole. This finding is in line with significant increases

in scalp-to-cortex distances in a larger age range from newborn to age 12 (Beauchamp et al., 2011). Furthermore, the scalp-to-cortex distance is dependent on the scalp locations for the same age group. For instance, the scalp-to-cortex distance over the parietal region is larger than that over the temporal region. The difference between scalp locations is also observed in adults and neonates (Brigadoi & Cooper, 2015). The increase in scalp-to-cortex distances during the first postnatal 2 years of life may be explained by changes in different head tissues. For example, increases in the skull thickness (Delye et al., 2015; Li et al., 2015), CSF volume (Makropoulos et al., 2016), and cortical folding (Li et al., 2014) during the first 2 years. Therefore, these findings suggest that SD pairs with larger distances can be set on the scalp surface of the parietal lobe and sensorimotor cortex because the scalp-to-cortex distance is greater there, particularly for 2-yo infants.

4.4.2 Optics-based SCC derived from age-appropriate sophisticated infant head models

Several studies have taken an important step toward the establishment of infant SCC (Emberson et al., 2017; Kabdebon et al., 2014; Lloyd-Fox et al., 2014; Tsuzuki et al., 2017); however, they only considered the head size of infants based on the simplified fNIRS principle that the signal comes from the cortical projection point below the midpoint of the SD pair. In fact, an fNIRS channel measures absorption changes in a

broad cortical area, rather than at a single point. Thus, to establish a precise optics-based SCC that reflects light diffusion in the brains of 0-yo, 1-yo, and 2-yo infants, the key step is to construct sophisticated realistic head models that comprise multiple biological tissues with distinct optical properties such as scalp, skull, CSF, and brain tissues. Therefore, a 5-layered head model was constructed for each age, distinguishable from a 4-layered model where the skull and scalp constitute a single extracerebral layer (Brigadoi et al., 2014; Dehaes et al., 2011b; Ferradal et al., 2016). Separating the scalp and skull in infantile light propagation analysis could guarantee more accurate SCC compared with using the 4-layered model, as these two types of infant tissues have their own optical properties (Dehaes et al., 2013; Fukui et al., 2003) and physical development (Li et al., 2015; Young, 1959). In addition, I employed template-based head models for light propagation analyses, because the acquisition of subject-specific MRI is generally challenging owing to the difficulty in controlling the motion of infants and undermines the intrinsic advantage of the fNIRS technique for facilitating functional brain measurements during early development. Notably, previous adult or infant studies have shown that the use of a template-based head model is useful for identifying the activation focus, although there are anatomical differences between subject-specific and template-based head models (Cooper et al., 2012; Custo et al., 2010; Emberson et al., 2017;

Ferradal et al., 2014; Lloyd-Fox et al., 2014). Furthermore, the template-based model used in this study was derived from anatomical images of 95 healthy infants and reflects the general anatomical structure of infants. Therefore, the optics-based SCC obtained by analyzing light propagation in template-based infant head models of 0-yo, 1-yo, and 2-yo could provide a reliable database to guide fNIRS users in designing probe geometry, as well as to explain fNIRS data.

Light propagation analysis depends on the optical properties of head tissues. The same optical properties of the neonate were assigned to all 3 age models because no established optical properties of head tissues are available for 1-yo and 2-yo infants. On the other hand, optical properties in these 3 age groups may change due to the alteration in tissue compositions, such as myelination and bone mineral density during the first 2 years of life. Since the level of bone mineral density was almost constant during the first year (Gallo et al., 2012) and slightly increase in the second year (Delye et al., 2015), the optical property of the skull may not so change during those years. In contrast, the substantial amount of myelination occurs in the wide ranges of the brain (Dietrich et al., 1988). Thus, the alteration of the optical properties of the gray matter and white matter should be considered. To address the effect of the change in optical properties on the optics-based SCC, I attempted to use optical properties of adult's gray matter and white

matter to calculate the optics-based SCC for the most aged 2-yo head model. Compared to results with infant's optical properties, additional simulation results revealed that optical properties of adults applied to 2-yo have little effect on the SCC. Although a slightly broadened SSP was observed due to stronger scattering (Fig. 4.14 for comparison between neonate' and adult's optical properties), the consistency of the MLCBR among 0-yo, 1-yo and 2-yo does not change due to the difference in the optical properties (see Fig. 4.15). The actual changes in optical properties with development from 0 to 2-yo would be smaller than those assumed here for neonates to adults. Therefore, I claim that our findings using same optical properties for three age groups could be used as a reference to contribute to developmental cognitive neuroscience. Meanwhile, the accuracy of optics-based SCC will be improved with the advance of in vivo measurement techniques for characterizing the optical properties of tissues (Spinelli et al., 2017). However, the measurement of accurate optical properties in vivo is still a challenging issue, as shown by the wide range of values reported by measurement techniques (Dehaes et al., 2011b).

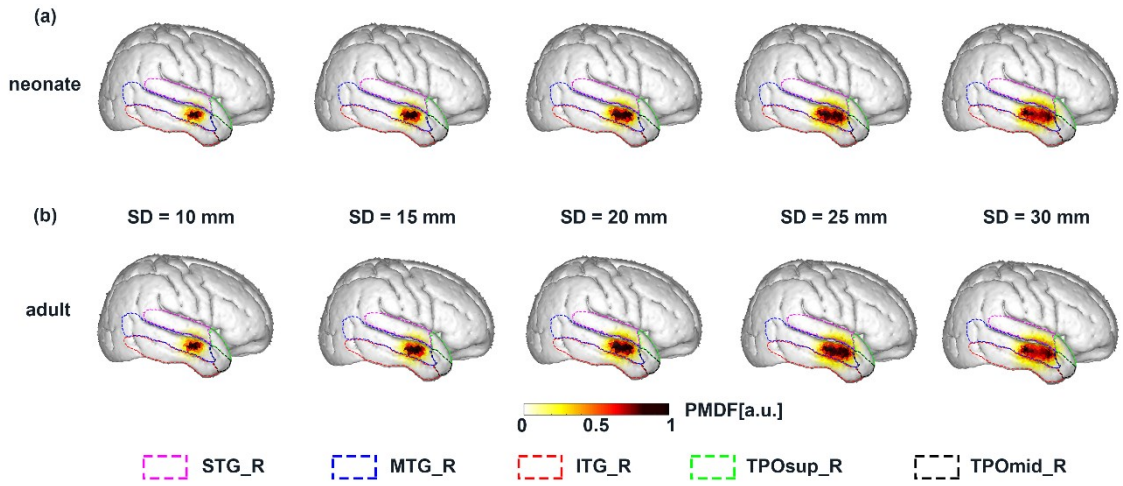

Figure 4. 14 Comparison of the PMDF obtained from neonate' (a) and adult's optical properties (b) for the fiducial point T4 at five SD distances for 2-yo when the SD pair was attached in a circumferential orientation. Dashed lines in different colors indicate the AAL brain region boundaries. Adult's absorption coefficients are 0.019 mm^{-1} and 0.011 mm^{-1} for gray matter and white matter, respectively. Adult's reduced scattering coefficients are 0.86 mm^{-1} and 4.16 mm^{-1} for gray matter and white matter, respectively.

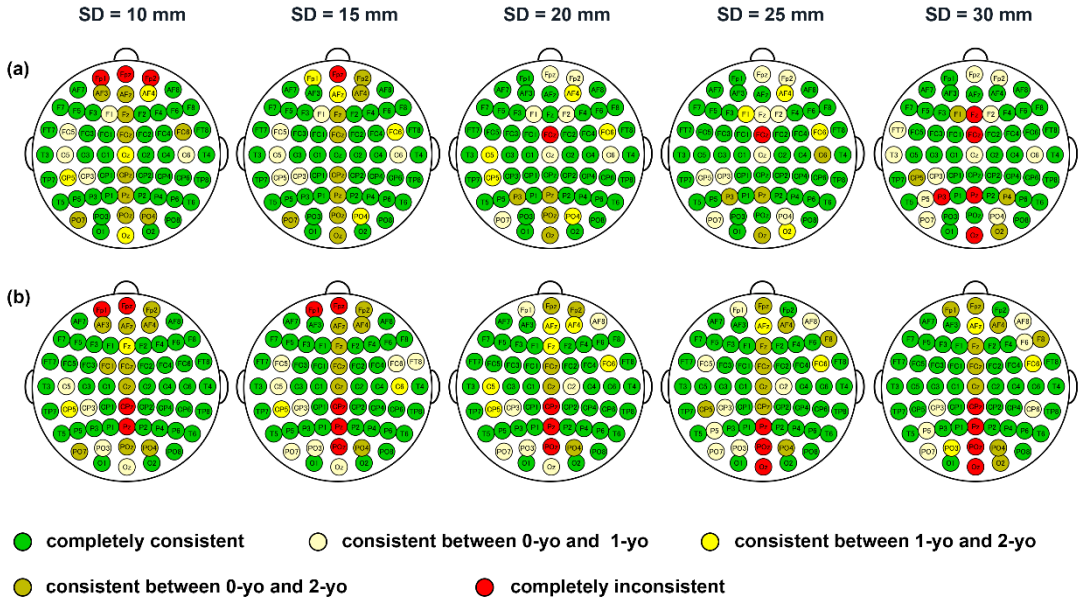

Figure 4. 15 Consistency of MLCBR at five SD distances for circumferential (a) and vertical (b) SD pairs. The consistency of the MLCBR among 0-yo, 1-yo, and 2-yo for every fiducial point is indicated by circles with different colors. Note: MLCBR for 2-yo was obtained by adult's optical properties of gray matter and white matter. Adult's absorption coefficients are 0.019 mm^{-1} and 0.011 mm^{-1} for gray matter and white matter, respectively. Adult's reduced scattering coefficients are 0.86 mm^{-1} and 4.16 mm^{-1} for gray matter and white matter, respectively.

4.4.3 Effect of SD distance and physical development on the optics-based SCC

For a given fiducial point, the SSP is a function of the SD distance, that is, the spatial range of the SSP broadens as the SD distance increases. This finding is consistent with previous studies, regardless of slab models (Okada et al., 1997; Wang et al., 2019b) or realistic head models (Strangman et al., 2013) being utilized. Intriguingly, the spatial distribution of SSP values is also affected by age for the consistent SD distance. Age-related alterations in the SSP may be caused by changes in the local anatomical structures across the three age groups.

The optics-based SCC results demonstrate that fNIRS signals interrogated by an SD pair always originate from multiple brain regions, even if the SD distance is 10 mm. The one-to-many relationship between an SD pair and cortical regions is due to strong light scattering in the head tissue. In addition, several aspects related to the N_{CBR} were found. As for the spatial characteristics, fiducial points around the longitudinal fissure are correlated with more brain regions than other points, which may be because the cortices around the longitudinal fissure are parcellated into a relatively large number of regions in the AAL atlas or the scalp-to-cortex distance is the largest in these areas. From the perspective of age-related change, although the N_{CBR} of 0-yo is larger than that of 1-yo and 2-yo, there are no significant differences between the N_{CBR} values of 1-yo and 2-yo,

which suggests that the similar spatial range of SSP for the same SD distance will occupy fewer brain regions when the head becomes larger owing to the physical development of the infant. In terms of the dependency on the SD distance, the finding that a larger SD distance has more corresponding brain regions could be clearly explained by the wider SSP at larger SD distances.

The selectivity of the MLCBR decreases as the SD distance increases. As mentioned before, the larger the SD distance, the wider the spatial range of the SSP in the brain. Hence, the increase in the normalized PPL of brain regions other than the MLCBR results in a relative decrease in the normalized PPL of the MLCBR. In addition, the selectivity of 1-yo and 2-yo is higher than that of 0-yo on average for all fiducial points. The relatively larger statistical dispersion in the values of selectivity is observed (e.g., Figs. 4.7d and 4.8d), however, the selectivity of the same fiducal point does not change dramatically across all five SD distances. Put another way, if the selectivity of the same fiducial point at a certain SD distance is low, it is also low at other four SD distances. Moreover, the relatively larger statistical dispersion in the selectivity of MLCBR suggest the selectivity is largely dependent on different scalp locations. Of note, the difference in the physical development of the head in each year may determine the degree of age-dependent change in the normalized PPL of the MLCBR. The 0-yo head size is obviously

smaller than that of 1-yo and 2-yo, while 1-yo and 2-yo have an almost similar head size. In other words, the constant area of the brain surface is occupied by a small number of brain regions in the large brains of 1-yo and 2-yo, but by a large number in the small brains of 0-yo. Furthermore, the spatial range of the SSP is almost constant for the same SD distance, regardless of age. Thus, the constant spatial range of SSP across age is mainly occupied by the MLCBR in the larger brains of 1-yo and 2-yo, but distributes across several brain regions in the smaller brain of the 0-yo. Therefore, the normalized PPL in the MLCBR of the 0-yo infants is significantly smaller than that of the 1-yo and 2-yo infants.

The sensitivity of the MLCBR significantly increases as the SD distance increases from 10 to 30 mm at 5 mm intervals for each age. This finding is in accordance with evidence obtained from the change in gray matter sensitivity as a function of SD distance in the neonatal and adult head models (Fukui et al., 2003). The sensitivity of 1-yo is significantly higher than that of 0-yo at 15-, 20-, 25-, and 30-mm SD distances; however, the sensitivity of 2-yo is significantly lower than that of 1-yo at 10 mm SD distance. One possible explanation for the increase or decrease in the sensitivity depending on the time of growth is that physical development differs between brain tissue and superficial layers such as the scalp and skull; the increase in the sensitivity from 0-yo to 1-yo may be caused

by the considerable expansion of the cortical surface during this period. Conversely, from 1-yo to 2-yo, the decrease in sensitivity may be owing to relatively smaller expansion of the cortical surface, although the thickness of the superficial layers continues to increase.

Importantly, the MLCBR is completely consistent at almost half of 10-10 fiducial points of 0-yo, 1-yo, and 2-yo for each SD distance. In other words, almost half of the fiducial points are correlated with one specific brain region with the largest normalized PPL. This finding indicates that it is possible to measure identical MLCBRs in longitudinal studies from 0-yo to 2-yo with fNIRS without the infant's own structural MRI when a probe of the same SD distance is attached at the scalp fiducial points. Thus, the finding is extremely uplifting for researchers who are interested in the functional development of such MLCBRs. On the other hand, the MLCBR corresponding to fiducial points just above the longitudinal fissure is mostly inconsistent across the three ages. The N_{CBR} and the $L_{norm,MLCBR}$ of the fiducial points are relatively larger and smaller than those of the other points, respectively, which suggests that the MLCBR at a certain age may easily be replaced by another brain region at another age due to the slight change in the light path. One possibility for age-related changes in the light path is that the thickness of the skull in the frontal, parietal, and occipital regions along with the longitudinal fissure changes more drastically than in other locations from 0-yo to 2-yo (Li et al., 2015).

Another possibility is that the cortical surface expands relatively more in regions of the superior parietal, prefrontal, occipital cortices, and postcentral gyrus than in other regions during the first two years (Li et al., 2013).

The consistency of the MLCBR could provide strong support for the reliability of findings from longitudinal developmental studies using fNIRS in which the probe is attached based on the scalp fiducial points. In recent years, by executing the longitudinal cohort study projects (e.g., Brain Imaging for Global Health (BRIGHT) project), several laboratories worldwide have devoted themselves to investigating functional brain development during the first two postnatal years, including studies of visual working memory (Reyes et al., 2020), social cognition (Lloyd-Fox et al., 2017; Miguel et al., 2019), as well as resting-state functional network (Bulgarelli et al., 2020). These findings will be especially useful for a large cohort of longitudinal or cross-sectional studies of early brain development, as structural MRI scanning, which is a demanding task for the infant population, is not necessarily required.

4.4.4 Consideration of suitable SD distances for infant fNIRS

The suitable SD distance for infants is still a matter of debate, as its choice is dependent on several factors. By considering a trade-off between the selectivity and the sensitivity of the MLCBR, I provided recommendations on suitable SD distances for 0-

yo, 1-yo, and 2-yo. The most desirable SD distance is the one that has both the maximum number of fiducial points with high selectivity and sensitivity, and a minimum number of fiducial points with low selectivity and sensitivity. Based on this perspective, I determined that the suitable SD distances in fNIRS for infants during the first 2 years range from 15 to 25 mm. This finding supports the results of a previous study in which the highest sensitivity was obtained at an SD distance of 20 mm in 3-month-old infants (Taga et al., 2007). In practical applications, I suggest that fNIRS users choose the SD distance according to the criteria (sensitivity or selectivity) more important to them. If the users focus on selectivity, an SD distance of 15 mm could be a better choice, whereas 25 mm is suitable for sensitivity as the priority. In addition, if fNIRS users pursue a relatively balanced trade-off between selectivity and sensitivity, I recommend an SD distance of 20 mm. These findings also reveal that the optimal SD distance for infants is different from that for adults. Previous adult studies have demonstrated that fNIRS probes should ideally be designed with 30-35 mm SD distances (Li et al., 2011; Strangman et al., 2013), as most light passes through the extra-cerebral superficial tissues at SD distances less than 20 mm (Wang et al., 2019b). Compared with that for adults, and the most suitable SD distances for infants are smaller than 30 mm, which indicates that thin superficial layers allow much more photons to pass through the brain tissue.

Chapter 5

5 Conclusion and Future Work

5.1 Conclusion

In the current thesis, compelling evidence demonstrates that light scattering should be considered when calculating the SCC for adult or infant populations. By comparing the optics-based SCC derived from the SBM and the geometrical SCC from the traditional point-to-point matching method, the proposed SBM method is demonstrated as a nonnegligible methodology to obtain the precise brain localization for the fNIRS measurement. More importantly, both individual anatomical differences in the adult heads and age-related changes in infant heads affect the optics-based SCC. For practical application, I recommended using group-wise probability consisting of individual optics-based SCCs over 10–10 system positions to design probe arrangements and explain fNIRS measurement data for the adult population, since this index considers the effects of light propagation in the head of 45 adult subjects. On the other hand, the fiducial points around the longitudinal fissure are correlated with different brain regions across 0, 1, and 2 years of age. Thus, it should be cautious when investigating the functional development of a certain specific brain region over the longitudinal fissure. Furthermore, SD distances

between 15 mm and 25 mm are recommended for infant fNIRS studies by considering the selectivity and sensitivity of the MLCBR. It is expected that the age-appropriate optics-based SCC will be a valuable reference to guide the probe design and provide convincing anatomical interpretations of fNIRS data for future infant developmental studies.

5.2 Future work

In the current thesis, 5-layered head models consisting of scalp, skull, CSF, gray matter, and white matter were constructed for adult and infant populations to obtain the optics-based SCC. However, the human head in fact comprises many other types of tissues, such as fat, muscle, soft bone, dura, and blood vessels (Baumann et al., 1997). Moreover, the optical heterogeneity of different head tissues has been reported to have an influence on light propagation. Particularly, the head models incorporating the fontal sinus and extra-cerebral vasculature show that fNIRS sensitivity is affected by these tissue types. For instance, Kurihara et al found that the shallow or deep frontal sinus identified by the computed tomography images tends to decrease or increase the sensitivity of fNIRS signal to the brain activation, respectively (Kurihara et al., 2012). In addition, the blood flow changes in the CSF and skin layers in an adult slab model also affect light prapogation, for example, larger vessel size can reduce the sensitivity to brain activity in

the gray matter (Wang et al., 2013). Similarly, a 5-layered realistic adult head model considering the effect of the extra-cerebral vasculature around the sagittal sinus can better estimate changes in hemoglobin concentration (Dehaes et al., 2011a). However, to date, there is no evidence showing how blood vessels or frontal sinus affect light propagation in infant head models. Along with the dramatic brain development during the first two years of life, the brain's vasculature also changes significantly morphologically and functionally, such as an increase in cross-sectional area of blood vessels and CBF volume during the early postnatal period (Kehrer & Schoning, 2009; Kozberg & Hillman, 2016). In the future, by combining several imaging techniques, like MR angiography and computed tomography, the immature extra-cerebral vasculature and frontal sinus can be recognized so as to construct more elaborated infant head models to establish the more accurate optics-based SCC.

According to the routine constructing the realistic head models, the established 5-layered subject-specific adult head models and age-appropriate infant head models indeed allow us to establish the optics-based SCC for fNIRS studies. Moreover, the currently proposed SBM method by solving the diffusion equation can be used to estimate underlying brain regions for an SD pair very efficiently. Notably, the SBM method is useful not only for fNIRS measurements but also for DOT, which utilizes a large number

of densely placed probe arrangements and allows the reconstruction of 3D images of brain activation by solving the inverse problem (Culver et al., 2003). Specifically, SBM will help correlate the reconstruction image of brain function by DOT and the underlying brain regions for a given probe arrangement. In addition, SBM could also contribute to the probe arrangement design for targeting specific brain regions in DOT, as well as to obtain the underlying brain regions for the long measurement channels. In some fNIRS measurements, the 3D coordinates of optodes on the scalp can be determined by instruments such as a 3D digitizer. By virtual positioning of the optodes on the heads of 45 adult subjects, SBM could be utilized to calculate the SCC based on light propagation from 45 subject-specific head models to approximately reach the required accuracy using the subject's own MRI. That is, it is possible to obtain a fairly accurate SCC even without the subject's head structure. Given that the 3D digitizer is not friendly to infants, a photo-based or video-based optode registration method (Hu et al., 2020; Jaffe-Dax et al., 2020) has been developed to localize scalp locations of SD pairs. Consequently, the optics-based SCC at any scalp position will be calculated only by virtually placing the SD pairs on the scalp of 45 subject-specific adult head models or age-appropriate infant head models.

There are several different brain atlases for the adult population, such as the Brodmann atlas (Brodmann, 2007) or the HCP-MMP1.0 atlas (Glasser et al., 2016), while

the LONI Probabilistic Brain Atlas (Shattuck et al., 2008) can also be used for the infant population. As the proposed SBM method is not only restricted to the AAL atlas, it is also suitable for other atlases when calculating the optics-based SCC. Thus, future work could use various brain atlases to establish the optics-based SCC to help understand human brain function.

Although the group-wise probability of the optics-based SCC could be used as a reference table to guide fNIRS users to design their probe geometry for targeting specific brain regions and to explain fNIRS data obtained according to the 10-10 system, the spatial density of the 10-10 fiducial points for analyzing the optics-based SCC is relatively sparse because a few brain regions had only a small chance of being corresponded. The group-wise probability obtained by SBM with a denser placement system (Oostenveld & Praamstra, 2001) will provide the corresponding brain regions of fNIRS probes placed anywhere on the scalp, because the denser fiducial points are expected to keep all brain regions with a high probability of being corresponded. For the 0-yo infant head model, as shown in the supplementary Fig. S1(a), the SSP of the circumferential SD pairs set at all 10-10 fiducial points distributes in almost all brain regions with relatively high values of PMDF. Nevertheless, not all brain regions have high values of PMDF for 1-yo and 2-yo infant head models (Fig. S1b-c). Hence, it is necessary to calculate the optics-based SCC

by using a denser placement system to estimate underlying brain regions 1-yo and 2yo infants in future work.

Notably, the head tissues within the first postnatal year undergo dramatic growth, such as the total volume of the brain expanding up to double its size (Gao et al., 2017; Li et al., 2019; Shi et al., 2011). Furthermore, several studies have discovered longitudinal functional brain developments during this period (Gao et al., 2015; Miguel et al., 2019; Wen et al., 2019). However, the 0-yo infant head model used in this study was constructed with a template-based MRI of an approximately 1-month-old infant. By establishing optics-based SCC at a finer temporal scale (every 3 months from birth to 12 months) that is in line with physical development during the first year after birth, it is expected to provide useful information for investigating the longitudinal development of the brain functions using the fNIRS technique.

References

Amunts, K., Schleicher, A., & Zilles, K. (2007). Cytoarchitecture of the cerebral cortex—more than localization. *Neuroimage, 37*(4), 1061-1065.

Anderson, C. A., Wiggins, I. M., Kitterick, P. T., & Hartley, D. E. H. (2017). Adaptive benefit of cross-modal plasticity following cochlear implantation in deaf adults. *Proc Natl Acad Sci U S A, 114*(38), 10256-10261. doi:10.1073/pnas.1704785114

Arridge, S. R. (1999). Optical tomography in medical imaging. *Inverse problems, 15*(2), R41.

Arridge, S. R., & Schweiger, M. (1995). Photon-measurement density functions. Part 2: Finite-element-method calculations. *Appl Opt, 34*(34), 8026-8037. doi:10.1364/AO.34.008026

Arridge, S. R., Schweiger, M., Hiraoka, M., & Delpy, D. T. (1993). A finite element approach for modeling photon transport in tissue. *Medical Physics, 20*(2 Pt 1), 299-309. doi:10.1118/1.597069

Ashburner, J. (2007). A fast diffeomorphic image registration algorithm. *Neuroimage, 38*(1), 95-113. doi:10.1016/j.neuroimage.2007.07.007

Auzias, G., Colliot, O., Glaunes, J. A., Perrot, M., Mangin, J. F., Trouve, A., & Baillet, S. (2011). Diffeomorphic brain registration under exhaustive sulcal constraints. *IEEE Trans Med Imaging, 30*(6), 1214-1227. doi:10.1109/TMI.2011.2108665

Baillet, S. (2017). Magnetoencephalography for brain electrophysiology and imaging. *Nature Neuroscience, 20*(3), 327-339.

Bakeman, R. (2005). Recommended effect size statistics for repeated measures designs. *Behav Res Methods, 37*(3), 379-384. doi:10.3758/bf03192707

Baumann, S. B., Wozny, D. R., Kelly, S. K., & Meno, F. M. (1997). The electrical conductivity of human cerebrospinal fluid at body temperature. *Ieee Transactions on Biomedical Engineering, 44*(3), 220-223.

Beauchamp, M. S., Beurlot, M. R., Fava, E., Nath, A. R., Parikh, N. A., Saad, Z. S., . . . Oghalai, J. S. (2011). The Developmental Trajectory of Brain-Scalp Distance from Birth through Childhood: Implications for Functional Neuroimaging. *Plos One, 6*(9). doi:ARTN e24981 10.1371/journal.pone.0024981

Bevilacqua, F., Piguet, D., Marquet, P., Gross, J. D., Tromberg, B. J., & Depeursinge, C. (1999). In vivo local determination of tissue optical properties: applications to human brain. *Applied Optics, 38*(22), 4939-4950. doi:Doi 10.1364/Ao.38.004939

Blume, W. T., Buza, R. C., & Okazaki, H. (1974). Anatomic correlates of the ten-twenty electrode placement system in infants. *Electroencephalogr Clin Neurophysiol, 36*(3), 303-307. doi:10.1016/0013-4694(74)90172-2

Boas, D. A., Elwell, C. E., Ferrari, M., & Taga, G. (2014). Twenty years of functional near-infrared

spectroscopy: introduction for the special issue. *Neuroimage, 85*, 1-5. doi:10.1016/j.neuroimage.2013.11.033

Brigadoi, S., Aljabar, P., Kuklisova-Murgasova, M., Arridge, S. R., & Cooper, R. J. (2014). A 4D neonatal head model for diffuse optical imaging of pre-term to term infants. *Neuroimage, 100*, 385-394. doi:10.1016/j.neuroimage.2014.06.028

Brigadoi, S., & Cooper, R. J. (2015). How short is short? Optimum source-detector distance for short-separation channels in functional near-infrared spectroscopy. *Neurophotonics, 2*(2), 025005. doi:10.1117/1.NPh.2.2.025005

Brodmann, K. (2007). *Brodmann's: Localisation in the cerebral cortex*: Springer Science & Business Media.

Bulgarelli, C., de Klerk, C. C., Richards, J. E., Southgate, V., Hamilton, A., & Blasi, A. (2020). The developmental trajectory of fronto-temporoparietal connectivity as a proxy of the default mode network: a longitudinal fNIRS investigation. *Human Brain Mapping*.

Buzsáki, G., Anastassiou, C. A., & Koch, C. (2012). The origin of extracellular fields and currents—EEG, ECoG, LFP and spikes. *Nature Reviews Neuroscience, 13*(6), 407-420.

Cai, L., Dong, Q., & Niu, H. J. (2018). The development of functional network organization in early childhood and early adolescence: A resting-state fNIRS study. *Developmental Cognitive Neuroscience, 30*, 223-235. doi:10.1016/j.dcn.2018.03.003

Cai, L., Dong, Q., Wang, M. J., & Niu, H. J. (2019). Functional near-infrared spectroscopy evidence for the development of topological asymmetry between hemispheric brain networks from childhood to adulthood. *Neurophotonics, 6*(2). doi:ARTN 025005 10.1117/1.NPh.6.2.025005

Capart, A., Ikegaya, S., Okada, E., Machida, M., & Hoshi, Y. (2021). Experimental tests of indicators for the degree of validness of the diffusion approximation. *Journal of Physics Communications, 5*(2), 025012.

Chen, M., Blumen, H. M., Izzetoglu, M., & Holtzer, R. (2017). Spatial coregistration of functional near-infrared spectroscopy to brain MRI. *Journal of Neuroimaging, 27*(5), 453-460.

Cheong, W.-F., Prahl, S. A., & Welch, A. J. (1990). A review of the optical properties of biological tissues. *IEEE journal of quantum electronics, 26*(12), 2166-2185.

Chuang, C. C., Chen, C. M., Hsieh, Y. S., Liu, T. C., & Sun, C. W. (2013). Brain structure and spatial sensitivity profile assessing by near-infrared spectroscopy modeling based on 3D MRI data. *Journal of Biophotonics, 6*(3), 267-274. doi:10.1002/jbio.201200025

Cooper, R. J., Caffini, M., Dubb, J., Fang, Q. Q., Custo, A., Tsuzuki, D., . . . Boas, D. A. (2012). Validating atlas-guided DOT: A comparison of diffuse optical tomography informed by atlas and subject-specific anatomies. *Neuroimage, 62*(3), 1999-2006. doi:10.1016/j.neuroimage.2012.05.031

Cope, M., Delpy, D. T., Reynolds, E. O., Wray, S., Wyatt, J., & van der Zee, P. (1988). Methods of quantitating cerebral near infrared spectroscopy data. *Advance in Experimental Medicine and Biology, 222*, 183-189.

Culver, J. P., Siegel, A. M., Stott, J. J., & Boas, D. A. (2003). Volumetric diffuse optical tomography of brain activity. *Optics letters, 28*(21), 2061-2063.

Custo, A., Boas, D. A., Tsuzuki, D., Dan, I., Mesquita, R., Fischl, B., . . . Wells, W. (2010). Anatomical atlas-guided diffuse optical tomography of brain activation. *Neuroimage, 49*(1), 561-567. doi:10.1016/j.neuroimage.2009.07.033

Cutini, S., Scatturin, P., & Zorzi, M. (2011). A new method based on ICBM152 head surface for probe placement in multichannel fNIRS. *Neuroimage, 54*(2), 919-927.

De Boer, H. H., Van der Merwe, A. L., & Soerdjbalie-Maikoe, V. V. (2016). Human cranial vault thickness in a contemporary sample of 1097 autopsy cases: relation to body weight, stature, age, sex and ancestry. *International journal of legal medicine, 130*(5), 1371-1377.

Dehaes, M., Gagnon, L., Lesage, F., Pélégrini-Issac, M., Vignaud, A., Valabrègue, R., . . . Benali, H. (2011a). Quantitative investigation of the effect of the extra-cerebral vasculature in diffuse optical imaging: a simulation study. *Biomedical Optics Express, 2*(3), 680-695.

Dehaes, M., Grant, P. E., Sliva, D. D., Roche-Labarbe, N., Pienaar, R., Boas, D. A., . . . Selb, J. (2011b). Assessment of the frequency-domain multi-distance method to evaluate the brain optical properties: Monte Carlo simulations from neonate to adult. *Biomedical Optics Express, 2*(3), 552-567. doi:Doi 10.1364/Boe.2.000552

Dehaes, M., Kazemi, K., Pelegrini-Issac, M., Grebe, R., Benali, H., & Wallois, F. (2013). Quantitative effect of the neonatal fontanel on synthetic near infrared spectroscopy measurements. *Human Brain Mapping, 34*(4), 878-889. doi:10.1002/hbm.21483

Dehghani, H., Eames, M. E., Yalavarthy, P. K., Davis, S. C., Srinivasan, S., Carpenter, C. M., . . . Paulsen, K. D. (2009). Near infrared optical tomography using NIRFAST: Algorithm for numerical model and image reconstruction. *Communications in Numerical Methods in Engineering, 25*(6), 711-732. doi:10.1002/cnm.1162

Delpy, D. T., Cope, M., Vanderzee, P., Arridge, S., Wray, S., & Wyatt, J. (1988). Estimation of Optical Pathlength through Tissue from Direct Time of Flight Measurement. *Physics in Medicine and Biology, 33*(12), 1433-1442. doi:Doi 10.1088/0031-9155/33/12/008

Delye, H., Clijmans, T., Mommaerts, M. Y., Sloten, J. V., & Goffin, J. (2015). Creating a normative database of age-specific 3D geometrical data, bone density, and bone thickness of the developing skull: a pilot study. *J Neurosurg Pediatr, 16*(6), 687-702. doi:10.3171/2015.4.PEDS1493

Devlin, J. T., & Poldrack, R. A. (2007). In praise of tedious anatomy. *Neuroimage, 37*(4), 1033-1041.

Dietrich, R. B., Bradley, W. G., Zaragoza, E. J. t., Otto, R. J., Taira, R. K., Wilson, G. H., & Kangarloo, H. (1988). MR evaluation of early myelination patterns in normal and developmentally delayed infants. *AJR Am J Roentgenol, 150*(4), 889-896. doi:10.2214/ajr.150.4.889

Dubois, J., Dehaene-Lambertz, G., Kulikova, S., Poupon, C., Hüppi, P. S., & Hertz-Pannier, L. (2014). The early development of brain white matter: a review of imaging studies in fetuses, newborns and

infants. *Neuroscience, 276*, 48-71.

Dunnett, C. W. (1955). A multiple comparison procedure for comparing several treatments with a control. *Journal of the American Statistical Association, 50*(272), 1096-1121.

Emberson, L. L., Cannon, G., Palmeri, H., Richards, J. E., & Aslin, R. N. (2017). Using fNIRS to examine occipital and temporal responses to stimulus repetition in young infants: Evidence of selective frontal cortex involvement. *Developmental Cognitive Neuroscience, 23*, 26-38. doi:10.1016/j.dcn.2016.11.002

Fang, Q. Q., & Boas, D. A. (2009). Tetrahedral Mesh Generation from Volumetric Binary and Gray-Scale Images. *2009 Ieee International Symposium on Biomedical Imaging: From Nano to Macro, Vols 1 and 2*, 1142-1145. doi:Doi 10.1109/Isbi.2009.5193259

Faro, S. H., & Mohamed, F. B. (2006). *Functional MRI: basic principles and clinical applications*: Springer Science & Business Media.

Ferradal, S. L., Eggebrecht, A. T., Hassanpour, M., Snyder, A. Z., & Culver, J. P. (2014). Atlas-based head modeling and spatial normalization for high-density diffuse optical tomography: In vivo validation against fMRI. *Neuroimage, 85*, 117-126. doi:10.1016/j.neuroimage.2013.03.069

Ferradal, S. L., Liao, S., Eggebrecht, A. T., Shimony, J. S., Inder, T. E., Culver, J. P., & Smyser, C. D. (2016). Functional Imaging of the Developing Brain at the Bedside Using Diffuse Optical Tomography. *Cerebral Cortex, 26*(4), 1558-1568. doi:10.1093/cercor/bhu320

Firbank, M. (1994). *The design, calibration and usage of a solid scattering and absorbing phantom for near infra red spectroscopy.* University of London,

Firbank, M., Arridge, S. R., Schweiger, M., & Delpy, D. T. (1996). An investigation of light transport through scattering bodies with non-scattering regions. *Physics in Medicine and Biology, 41*(4), 767-783. doi:Doi 10.1088/0031-9155/41/4/012

Firbank, M., Okada, E., & Delpy, D. T. (1998). A theoretical study of the signal contribution of regions of the adult head to near-infrared spectroscopy studies of visual evoked responses. *Neuroimage, 8*(1), 69-78. doi:10.1006/nimg.1998.0348

Fleming, S. M., Weil, R. S., Nagy, Z., Dolan, R. J., & Rees, G. (2010). Relating introspective accuracy to individual differences in brain structure. *Science, 329*(5998), 1541-1543. doi:10.1126/science.1191883

Flock, S. T., Patterson, M. S., Wilson, B. C., & Wyman, D. R. (1989). Monte Carlo modeling of light propagation in highly scattering tissue--I: Model predictions and comparison with diffusion theory. *IEEE Trans Biomed Eng, 36*(12), 1162-1168. doi:10.1109/tbme.1989.1173624

Fukui, Y., Ajichi, Y., & Okada, E. (2003). Monte Carlo prediction of near-infrared light propagation in realistic adult and neonatal head models. *Applied Optics, 42*(16), 2881-2887. doi:Doi 10.1364/Ao.42.002881

Gallo, S., Vanstone, C. A., & Weiler, H. A. (2012). Normative data for bone mass in healthy term infants

from birth to 1 year of age. *J Osteoporos, 2012*, 672403. doi:10.1155/2012/672403

Gao, W., Alcauter, S., Elton, A., Hernandez-Castillo, C. R., Smith, J. K., Ramirez, J., & Lin, W. (2015). Functional network development during the first year: relative sequence and socioeconomic correlations. *Cerebral Cortex, 25*(9), 2919-2928.

Gao, W., Lin, W., Grewen, K., & Gilmore, J. H. (2017). Functional Connectivity of the Infant Human Brain: Plastic and Modifiable. *Neuroscientist, 23*(2), 169-184. doi:10.1177/1073858416635986

Gebhart, S. C., Lin, W. C., & Mahadevan-Jansen, A. (2006). In vitro determination of normal and neoplastic human brain tissue optical properties using inverse adding-doubling. *Physics in Medicine and Biology, 51*(8), 2011-2027. doi:10.1088/0031-9155/51/8/004

Gilmore, J. H., Shi, F., Woolson, S. L., Knickmeyer, R. C., Short, S. J., Lin, W., . . . Shen, D. (2012). Longitudinal development of cortical and subcortical gray matter from birth to 2 years. *Cerebral Cortex, 22*(11), 2478-2485. doi:10.1093/cercor/bhr327

Glasser, M. F., Coalson, T. S., Robinson, E. C., Hacker, C. D., Harwell, J., Yacoub, E., . . . Jenkinson, M. (2016). A multi-modal parcellation of human cerebral cortex. *Nature, 536*(7615), 171-178.

Hakuno, Y., Hata, M., Naoi, N., Hoshino, E. I., & Minagawa, Y. (2020). Interactive live fNIRS reveals engagement of the temporoparietal junction in response to social contingency in infants. *Neuroimage, 218*, 116901. doi:10.1016/j.neuroimage.2020.116901

Hale, G. M., & Querry, M. R. (1973). Optical Constants of Water in the 200-nm to 200-microm Wavelength Region. *Appl Opt, 12*(3), 555-563. doi:10.1364/AO.12.000555

Hasan, K. M., Sankar, A., Halphen, C., Kramer, L. A., Brandt, M. E., Juranek, J., . . . Ewing-Cobbs, L. (2007). Development and organization of the human brain tissue compartments across the lifespan using diffusion tensor imaging. *Neuroreport, 18*(16), 1735-1739.

Hiraoka, M., Firbank, M., Essenpreis, M., Cope, M., Arridge, S. R., van der Zee, P., & Delpy, D. T. (1993). A Monte Carlo investigation of optical pathlength in inhomogeneous tissue and its application to near-infrared spectroscopy. *Physics in Medicine and Biology, 38*(12), 1859-1876. doi:10.1088/0031-9155/38/12/011

Holmes, C. J., Hoge, R., Collins, L., Woods, R., Toga, A. W., & Evans, A. C. (1998). Enhancement of MR images using registration for signal averaging. *Journal of Computer Assisted Tomography, 22*(2), 324-333.

Homan, R. W., Herman, J., & Purdy, P. (1987). Cerebral Location of International 10-20 System Electrode Placement. *Electroencephalography and Clinical Neurophysiology, 66*(4), 376-382. doi:Doi 10.1016/0013-4694(87)90206-9

Hu, X.-S., Wagley, N., Rioboo, A. T., DaSilva, A. F., & Kovelman, I. (2020). Photogrammetry-based stereoscopic optode registration method for functional near-infrared spectroscopy. *Journal of biomedical optics, 25*(9), 095001.

Huang, Y., Parra, L. C., & Haufe, S. (2016). The New York Head—A precise standardized volume

conductor model for EEG source localization and tES targeting. *Neuroimage, 140*, 150-162.

Jacques, S. L. (2013). Optical properties of biological tissues: a review. *Physics in Medicine & Biology, 58*(11), R37.

Jacques, S. L., & Wang, L. (1995). Monte Carlo modeling of light transport in tissues. In *Optical-thermal response of laser-irradiated tissue* (pp. 73-100): Springer.

Jaffe-Dax, S., Bermano, A. H., Erel, Y., & Emberson, L. L. (2020). Video-based motion-resilient reconstruction of three-dimensional position for functional near-infrared spectroscopy and electroencephalography head mounted probes. *Neurophotonics, 7*(3), 035001.

Jasper, H. H. (1958). The ten-twenty electrode system of the International Federation. *Electroencephalogr. Clin. Neurophysiol., 10*, 370-375.

Jermyn, M., Ghadyani, H., Mastanduno, M. A., Turner, W., Davis, S. C., Dehghani, H., & Pogue, B. W. (2013). Fast segmentation and high-quality three-dimensional volume mesh creation from medical images for diffuse optical tomography. *Journal of biomedical optics, 18*(8). doi:Artn 086007 10.1117/1.Jbo.18.8.086007

Jiang, J., Chen, C., Dai, B., Shi, G., Ding, G., Liu, L., & Lu, C. (2015). Leader emergence through interpersonal neural synchronization. *Proc Natl Acad Sci U S A, 112*(14), 4274-4279. doi:10.1073/pnas.1422930112

Jiang, Y., Li, Z., Zhao, Y., Xiao, X., Zhang, W., Sun, P., . . . Zhu, C. (2020). Targeting brain functions from the scalp: Transcranial brain atlas based on large-scale fMRI data synthesis. *Neuroimage, 210*, 116550.

Jobsis, F. F. (1977). Noninvasive, infrared monitoring of cerebral and myocardial oxygen sufficiency and circulatory parameters. *Science, 198*(4323), 1264-1267.

Jurcak, V., Tsuzuki, D., & Dan, I. (2007). 10/20, 10/10, and 10/5 systems revisited: Their validity as relative head-surface-based positioning systems. *Neuroimage, 34*(4), 1600-1611. doi:10.1016/j.neuroimage.2006.09.024

Kabdebon, C., Leroy, F., Simmonet, H., Perrot, M., Dubois, J., & Dehaene-Lambertz, G. (2014). Anatomical correlations of the international 10-20 sensor placement system in infants. *Neuroimage, 99*, 342-356. doi:10.1016/j.neuroimage.2014.05.046

Kalos, M. H., & Whitlock, P. A. (2009). *Monte carlo methods*: John Wiley & Sons.

Kanai, R., & Rees, G. (2011). The structural basis of inter-individual differences in human behaviour and cognition. *Nature Reviews Neuroscience, 12*(4), 231-242. doi:10.1038/nrn3000

Kawaguchi, H., Koyama, T., & Okada, E. (2007). Effect of probe arrangement on reproducibility of images by near-infrared topography evaluated by a virtual head phantom. *Applied Optics, 46*(10), 1658-1668. doi:Doi 10.1364/Ao.46.001658

Kehrer, M., & Schoning, M. (2009). A longitudinal study of cerebral blood flow over the first 30 months. *Pediatric Research, 66*(5), 560-564. doi:10.1203/PDR.0b013e3181ba1a29

Keller, P. J., Hunter Jr, W., & Schmalbrock, P. (1987). Multisection fat-water imaging with chemical shift selective presaturation. *Radiology, 164*(2), 539-541.

Klem, G. H., Luders, H. O., Jasper, H. H., & Elger, C. (1999). The ten-twenty electrode system of the International Federation. The International Federation of Clinical Neurophysiology. *Electroencephalogr Clin Neurophysiol Suppl, 52*, 3-6.

Knaus, T. A., Bollich, A. M., Corey, D. M., Lemen, L. C., & Foundas, A. L. (2006). Variability in perisylvian brain anatomy in healthy adults. *Brain and Language, 97*(2), 219-232. doi:10.1016/j.bandl.2005.10.008

Koessler, L., Maillard, L., Benhadid, A., Vignal, J. P., Felblinger, J., Vespignani, H., & Braun, M. (2009). Automated cortical projection of EEG sensors: anatomical correlation via the international 10-10 system. *Neuroimage, 46*(1), 64-72. doi:10.1016/j.neuroimage.2009.02.006

Kovelman, I., Shalinsky, M. H., White, K. S., Schmitt, S. N., Berens, M. S., Paymer, N., & Petitto, L. A. (2009). Dual language use in sign-speech bimodal bilinguals: fNIRS brain-imaging evidence. *Brain and Language, 109*(2-3), 112-123. doi:10.1016/j.bandl.2008.09.008

Koyama, T., Iwasaki, A., Ogoshi, Y., & Okada, E. (2005). Practical and adequate approach to modeling light propagation in an adult head with low-scattering regions by use of diffusion theory. *Applied Optics, 44*(11), 2094-2103. doi:Doi 10.1364/Ao.44.002094

Kozberg, M., & Hillman, E. (2016). Neurovascular coupling and energy metabolism in the developing brain. *Progress in brain research, 225*, 213-242.

Kumar, V., Shivakumar, V., Chhabra, H., Bose, A., Venkatasubramanian, G., & Gangadhar, B. N. (2017). Functional near infra-red spectroscopy (fNIRS) in schizophrenia: A review. *Asian Journal of Psychiatry, 27*, 18-31. doi:10.1016/j.ajp.2017.02.009

Kurihara, K., Kawaguchi, H., Obata, T., Ito, H., & Okada, E. (2015). Magnetic resonance imaging appropriate for construction of subject-specific head models for diffuse optical tomography. *Biomedical Optics Express, 6*(9), 3197-3209. doi:10.1364/Boe.6.003197

Kurihara, K., Kawaguchi, H., Obata, T., Ito, H., Sakatani, K., & Okada, E. (2012). The influence of frontal sinus in brain activation measurements by near-infrared spectroscopy analyzed by realistic head models. *Biomedical Optics Express, 3*(9), 2121-2130. doi:Doi 10.1364/Boe.3.002121

Li, G., Nie, J. X., Wang, L., Shi, F., Lin, W. L., Gilmore, J. H., & Shen, D. G. (2013). Mapping Region-Specific Longitudinal Cortical Surface Expansion from Birth to 2 Years of Age. *Cerebral Cortex, 23*(11), 2724-2733. doi:10.1093/cercor/bhs265

Li, G., Wang, L., Shi, F., Lyall, A. E., Lin, W. L., Gilmore, J. H., & Shen, D. G. (2014). Mapping Longitudinal Development of Local Cortical Gyrification in Infants from Birth to 2 Years of Age. *Journal of Neuroscience, 34*(12), 4228-4238. doi:10.1523/Jneurosci.3976-13.2014

Li, G., Wang, L., Yap, P. T., Wang, F., Wu, Z. W., Meng, Y., . . . Shen, D. G. (2019). Computational neuroanatomy of baby brains: A review. *Neuroimage, 185*, 906-925.

doi:10.1016/j.neuroimage.2018.03.042

Li, H., Ruan, J., Xie, Z., Wang, H., & Liu, W. (2007). Investigation of the critical geometric characteristics of living human skulls utilising medical image analysis techniques. *International Journal of Vehicle Safety, 2*(4), 345-367.

Li, T., Gong, H., & Luo, Q. (2011). Visualization of light propagation in visible Chinese human head for functional near-infrared spectroscopy. *Journal of biomedical optics, 16*(4), 045001.

Li, Z. G., Park, B. K., Liu, W., Zhang, J., Reed, M. P., Rupp, J. D., . . . Hu, J. (2015). A statistical skull geometry model for children 0-3 years old. *Plos One, 10*(5), e0127322. doi:10.1371/journal.pone.0127322

Lillie, E. M., Urban, J. E., Lynch, S. K., Weaver, A. A., & Stitzel, J. D. (2016). Evaluation of Skull Cortical Thickness Changes With Age and Sex From Computed Tomography Scans. *J Bone Miner Res, 31*(2), 299-307. doi:10.1002/jbmr.2613

Lloyd-Fox, S., Begus, K., Halliday, D., Pirazzoli, L., Blasi, A., Papademetriou, M., . . . Moore, S. (2017). Cortical specialisation to social stimuli from the first days to the second year of life: A rural Gambian cohort. *Developmental Cognitive Neuroscience, 25*, 92-104.

Lloyd-Fox, S., Blasi, A., & Elwell, C. E. (2010). Illuminating the developing brain: The past, present and future of functional near infrared spectroscopy. *Neuroscience and Biobehavioral Reviews, 34*(3), 269-284. doi:10.1016/j.neubiorev.2009.07.008

Lloyd-Fox, S., Richards, J. E., Blasi, A., Murphy, D. G. M., Elwell, C. E., & Johnson, M. H. (2014). Coregistering functional near-infrared spectroscopy with underlying cortical areas in infants. *Neurophotonics, 1*(2). doi:ARTN 025006 10.1117/1.NPh.1.2.025006

Logothetis, N. K. (2008). What we can do and what we cannot do with fMRI. *Nature, 453*(7197), 869-878.

Luck, S. J. (2014). *An introduction to the event-related potential technique*: MIT press.

Maki, A., Yamashita, Y., Ito, Y., Watanabe, E., Mayanagi, Y., & Koizumi, H. (1995). Spatial and temporal analysis of human motor activity using noninvasive NIR topography. *Medical Physics, 22*(12), 1997-2005.

Makropoulos, A., Aljabar, P., Wright, R., Hüning, B., Merchant, N., Arichi, T., . . . Counsell, S. J. (2016). Regional growth and atlasing of the developing human brain. *Neuroimage, 125*, 456-478.

Mansouri, C., L'Huillier, J.-P., Kashou, N. H., & Humeau, A. (2010). Depth sensitivity analysis of functional near-infrared spectroscopy measurement using three-dimensional Monte Carlo modelling-based magnetic resonance imaging. *Lasers in medical science, 25*(3), 431-438.

Miguel, H. O., Gonçalves, Ó. F., Cruz, S., & Sampaio, A. (2019). Infant brain response to affective and discriminative touch: A longitudinal study using fNIRS. *Social neuroscience, 14*(5), 571-582.

Minagawa-Kawai, Y., Mori, K., Naoi, N., & Kojima, S. (2007). Neural attunement processes in infants during the acquisition of a language-specific phonemic contrast. *Journal of Neuroscience, 27*(2), 315-321. doi:10.1523/Jneurosci.1984-06.2007

Minagawa, Y., Hakuno, Y., Kobayashi, A., Naoi, N., & Kojima, S. (2017). Infant word segmentation recruits the cerebral network of phonological short-term memory. *Brain and Language, 170*, 39-49. doi:10.1016/j.bandl.2017.03.005

Moriguchi, Y., & Hiraki, K. (2009). Neural origin of cognitive shifting in young children. *Proc Natl Acad Sci U S A, 106*(14), 6017-6021. doi:10.1073/pnas.0809747106

Nakamura, K., Kurihara, K., Kawaguchi, H., Obata, T., Ito, H., & Okada, E. (2016). Estimation of partial optical path length in the brain in subject-specific head models for near-infrared spectroscopy. *Optical Review, 23*(2), 316-322. doi:10.1007/s10043-016-0179-9

Noguchi, K., Gel, Y. R., Brunner, E., & Konietschke, F. (2012). nparLD: an R software package for the nonparametric analysis of longitudinal data in factorial experiments. *Journal of Statistical Software, 50*(12).

Nuwer, M. R. (2018). 10-10 electrode system for EEG recording. *Clinical neurophysiology: official journal of the International Federation of Clinical Neurophysiology, 129*(5), 1103.

Okada, E., & Delpy, D. T. (2003a). Near-infrared light propagation in an adult head model. I. Modeling of low-level scattering in the cerebrospinal fluid layer. *Applied Optics, 42*(16), 2906-2914. doi:Doi 10.1364/Ao.42.002906

Okada, E., & Delpy, D. T. (2003b). Near-infrared light propagation in an adult head model. II. Effect of superficial tissue thickness on the sensitivity of the near-infrared spectroscopy signal. *Applied Optics, 42*(16), 2915-2922. doi:Doi 10.1364/Ao.42.002915

Okada, E., Firbank, M., Schweiger, M., Arridge, S. R., Cope, M., & Delpy, D. T. (1997). Theoretical and experimental investigation of near-infrared light propagation in a model of the adult head. *Appl Opt, 36*(1), 21-31. doi:10.1364/ao.36.000021

Okamoto, M., Dan, H., Sakamoto, K., Takeo, K., Shimizu, K., Kohno, S., . . . Dan, I. (2004). Three-dimensional probabilistic anatomical cranio-cerebral correlation via the international 10-20 system oriented for transcranial functional brain mapping. *Neuroimage, 21*(1), 99-111. doi:10.1016/j.neuroimage.2003.08.026

Okamoto, M., & Dan, I. (2005). Automated cortical projection transcranial functional brain of head-surface locations for mapping. *Neuroimage, 26*(1), 18-28. doi:10.1016/j.neuroimage.2005.01.018

Oki, Y., Kawaguchi, H., & Okada, E. (2009). Validation of practical diffusion approximation for virtual near infrared spectroscopy using a digital head phantom. *Optical Review, 16*(2), 153-159.

Olejnik, S., & Algina, J. (2003). Generalized eta and omega squared statistics: measures of effect size for some common research designs. *Psychol Methods, 8*(4), 434-447. doi:10.1037/1082-989X.8.4.434

Oostenveld, R., & Praamstra, P. (2001). The five percent electrode system for high-resolution EEG and ERP measurements. *Clinical Neurophysiology, 112*(4), 713-719. doi:Doi 10.1016/S1388-2457(00)00527-7

Papadelis, C., Poghosyan, V., Fenwick, P. B., & Ioannides, A. A. (2009). MEG's ability to localise accurately weak transient neural sources. *Clinical Neurophysiology, 120*(11), 1958-1970.

Phillips, A. A., Chan, F. H., Zheng, M. M. Z., Krassioukov, A. V., & Ainslie, P. N. (2016). Neurovascular coupling in humans: physiology, methodological advances and clinical implications. *Journal of Cerebral Blood Flow & Metabolism, 36*(4), 647-664.

Pighin, F., Hecker, J., Lischinski, D., Szeliski, R., & Salesin, D. H. (2006). *Synthesizing realistic facial expressions from photographs.* Paper presented at the ACM SIGGRAPH 2006 Courses.

Pinti, P., Tachtsidis, I., Hamilton, A., Hirsch, J., Aichelburg, C., Gilbert, S., & Burgess, P. W. (2020). The present and future use of functional near-infrared spectroscopy (fNIRS) for cognitive neuroscience. *Annals of the New York Academy of Sciences, 1464*(1), 5.

Quaresima, V., & Ferrari, M. (2019a). Functional near-infrared spectroscopy (fNIRS) for assessing cerebral cortex function during human behavior in natural/social situations: a concise review. *Organizational Research Methods, 22*(1), 46-68.

Quaresima, V., & Ferrari, M. (2019b). A Mini-Review on Functional Near-Infrared Spectroscopy (fNIRS): Where Do We Stand, and Where Should We Go? *Photonics, 6*(3). doi:ARTN 87 10.3390/photonics6030087

Reyes, L. D., Wijeakumar, S., Magnotta, V. A., Forbes, S. H., & Spencer, J. P. (2020). The functional brain networks that underlie visual working memory in the first two years of life. *Neuroimage*, 116971.

Ruan, J., & Prasad, P. (2001). *The effects of skull thickness variations on human head dynamic impact responses*. Retrieved from

Schmitz, B., Hagen, T., & Reith, W. (2003). Three-dimensional true FISP for high-resolution imaging of the whole brain. *European radiology, 13*(7), 1577-1582.

Sharma, S. D., Park, E., Purcell, P. L., Gordon, K. A., Papsin, B. C., & Cushing, S. L. (2020). Age-related variability in pediatric scalp thickness: Implications for auditory prostheses. *International Journal of Pediatric Otorhinolaryngology, 130*, 109853.

Shattuck, D. W., Mirza, M., Adisetiyo, V., Hojatkashani, C., Salamon, G., Narr, K. L., . . . Toga, A. W. (2008). Construction of a 3D probabilistic atlas of human cortical structures. *Neuroimage, 39*(3), 1064-1080.

Shi, F., Yap, P. T., Wu, G. R., Jia, H. J., Gilmore, J. H., Lin, W. L., & Shen, D. G. (2011). Infant Brain Atlases from Neonates to 1-and 2-Year-Olds. *Plos One, 6*(4). doi:ARTN e18746 10.1371/journal.pone.0018746

Singh, A. K., Okamoto, M., Dan, H., Jurcak, V., & Dan, I. (2005). Spatial registration of multichannel multi-subject fNIRS data to MNI space without MRI. *Neuroimage, 27*(4), 842-851. doi:10.1016/j.neuroimage.2005.05.019

Singh, S. P. (2014). Magnetoencephalography: basic principles. *Annals of Indian Academy of Neurology, 17*(Suppl 1), S107.

Spinelli, L., Zucchelli, L., Contini, D., Caffini, M., Mehler, J., Flo, A., . . . Torricelli, A. (2017). In vivo measure of neonate brain optical properties and hemodynamic parameters by time-domain near-infrared spectroscopy. *Neurophotonics, 4*(4). doi:ARTN 041414 10.1117/1.NPh.4.4.041414

Strangman, G. E., Li, Z., & Zhang, Q. (2013). Depth sensitivity and source-detector separations for near infrared spectroscopy based on the Colin27 brain template. *Plos One, 8*(8), e66319. doi:10.1371/journal.pone.0066319

Strangman, G. E., Zhang, Q., & Li, Z. (2014). Scalp and skull influence on near infrared photon propagation in the Colin27 brain template. *Neuroimage, 85*, 136-149. doi:10.1016/j.neuroimage.2013.04.090

Taga, G., Homae, F., & Watanabe, H. (2007). Effects of source-detector distance of near infrared spectroscopy on the measurement of the cortical hemodynamic response in infants. *Neuroimage, 38*(3), 452-460. doi:10.1016/j.neuroimage.2007.07.050

Teplan, M. (2002). Fundamentals of EEG measurement. *Measurement science review, 2*(2), 1-11.

Timmler, S., & Simons, M. (2019). Grey matter myelination. *Glia, 67*(11), 2063-2070.

Torricelli, A., Pifferi, A., Taroni, P., Giambattistelli, E., & Cubeddu, R. (2001). In vivo optical characterization of human tissues from 610 to 1010 nm by time-resolved reflectance spectroscopy. *Physics in Medicine and Biology, 46*(8), 2227-2237. doi:Doi 10.1088/0031-9155/46/8/313

Tran, A. P., Yan, S., & Fang, Q. (2020). Improving model-based functional near-infrared spectroscopy analysis using mesh-based anatomical and light-transport models. *Neurophotonics, 7*(1), 015008.

Tsuyuki. (2016). Anatomical Structure-based Identification of the Functional Areas in the Brain Models and Application to fNIRS Group Analysis. *Unpublished master's thesis*.

Tsuzuki, D., & Dan, I. (2014). Spatial registration for functional near-infrared spectroscopy: From channel position on the scalp to cortical location in individual and group analyses. *Neuroimage, 85*, 92-103. doi:10.1016/j.neuroimage.2013.07.025

Tsuzuki, D., Homae, F., Taga, G., Watanabe, H., Matsui, M., & Dan, I. (2017). Macroanatomical Landmarks Featuring Junctions of Major Sulci and Fissures and Scalp Landmarks Based on the International 10-10 System for Analyzing Lateral Cortical Development of Infants. *Frontiers in Neuroscience, 11*. doi:ARTN 394 10.3389/fnins.2017.00394

Tsuzuki, D., Jurcak, V., Singh, A. K., Okamoto, M., Watanabe, E., & Dan, I. (2007). Virtual spatial registration of stand-alone MRS data to MNI space. *Neuroimage, 34*(4), 1506-1518. doi:10.1016/j.neuroimage.2006.10.043

Tzourio-Mazoyer, N., Landeau, B., Papathanassiou, D., Crivello, F., Etard, O., Delcroix, N., . . . Joliot, M. (2002). Automated anatomical labeling of activations in SPM using a macroscopic anatomical parcellation of the MNI MRI single-subject brain. *Neuroimage, 15*(1), 273-289. doi:10.1006/nimg.2001.0978

Uchida-Ota, M., Arimitsu, T., Tsuzuki, D., Dan, I., Ikeda, K., Takahashi, T., & Minagawa, Y. (2019). Maternal speech shapes the cerebral frontotemporal network in neonates: A hemodynamic

functional connectivity study. *Developmental Cognitive Neuroscience, 39*. doi:UNSP 100701 10.1016/j.dcn.2019.100701

Van der Zee, P. (1993). *Measurement and modelling of the optical properties of human tissue in the near infrared.* UCL (University College London),

Van der Zee, P., Essenpreis, M., & Delpy, D. T. (1993). *Optical properties of brain tissue.* Paper presented at the Photon Migration and Imaging in Random Media and Tissues.

Vanderwert, R. E., & Nelson, C. A. (2014). The use of near-infrared spectroscopy in the study of typical and atypical development. *Neuroimage, 85*, 264-271. doi:10.1016/j.neuroimage.2013.10.009

Wang, F., Lian, C. F., Wu, Z. W., Zhang, H., Li, T. F., Meng, Y., . . . Li, G. (2019a). Developmental topography of cortical thickness during infancy. *Proceedings of the National Academy of Sciences of the United States of America, 116*(32), 15855-15860. doi:10.1073/pnas.1821523116

Wang, L., Ayaz, H., & Izzetoglu, M. (2019b). Investigation of the source-detector separation in near infrared spectroscopy for healthy and clinical applications. *Journal of Biophotonics, 12*(11), e201900175.

Wang, S., Hoshi, Y., & Yamada, Y. (2013). *Influences of blood flow changes in cerebrospinal fluid and skin layers on optical mapping.* Paper presented at the 2013 35th Annual International Conference of the IEEE Engineering in Medicine and Biology Society (EMBC).

Watanabe, H., Homae, F., Nakano, T., Tsuzuki, D., Enkhtur, L., Nemoto, K., . . . Taga, G. (2013). Effect of auditory input on activations in infant diverse cortical regions during audiovisual processing. *Human Brain Mapping, 34*(3), 543-565. doi:10.1002/hbm.21453

Wen, X. Y., Zhang, H., Li, G., Liu, M. X., Yin, W. Y., Lin, W. L., . . . Shen, D. G. (2019). First-year development of modules and hubs in infant brain functional networks. *Neuroimage, 185*, 222-235. doi:10.1016/j.neuroimage.2018.10.019

Whiteman, A. C., Santosa, H., Chen, D. F., Perlman, S., & Huppert, T. (2018). Investigation of the sensitivity of functional near-infrared spectroscopy brain imaging to anatomical variations in 5- to 11-year-old children. *Neurophotonics, 5*(1). doi:ARTN 011009 10.1117/1.NPh.5.1.011009

Xiao, X., Yu, X. T., Zhang, Z., Zhao, Y., Jiang, Y. H., Li, Z., . . . Zhu, C. Z. (2018). Transcranial brain atlas. *Science Advances, 4*(9). doi:ARTN eaar6904 10.1126/sciadv.aar6904

Young, R. W. (1959). Age changes in the thickness of the scalp in white males. *Hum Biol, 31*(1), 74-79.

Zhang, Y. Y., Brady, M., & Smith, S. (2001). Segmentation of brain MR images through a hidden Markov random field model and the expectation-maximization algorithm. *Ieee Transactions on Medical Imaging, 20*(1), 45-57. doi:Doi 10.1109/42.906424

Zhu, C., & Liu, Q. (2013). Review of Monte Carlo modeling of light transport in tissues. *Journal of biomedical optics, 18*(5), 050902.

Acknowledgments

I owe many people an immense debt of gratitude for the help and support they have provided me during the past three years. First and foremost, I would like to thank my supervisor Prof. Eiji Okada, from whom I received invaluable guidance on my thesis. He also enriched my life in Japan by organizing various lab activities, such as the welcome party, rowing competition, and training camp.

I also owe a debt of gratitude to the other members of my thesis committee, Prof. Masaaki Ikehara, Prof. Yasue Mitsukura, Prof. Junichi Ushiba, and Dr. Hiroshi Kawaguchi for agreeing to take their valuable time to read and evaluate this thesis. I would particularly like to thank Dr. Hiroshi Kawaguchi with whom I worked on two publications during the past two years, and he gave me many valuable suggestions and comments on these publications. This thesis would not have been possible if not for the stimulating environment created by the other members in Okada Lab, in particular: Tomonori Nitta, Sho Yokota, Taiki Shirai, Yoshinori Ueno, Gennya Nakamura, Ryosuke Mochizuki, Kohei Yamamoto, and Yusei Maeda. I thank each of them for their selfless help and countless suggestions. I would also like to thank Prof. Yasuyo Minagawa in Keio Baby Lab, who instructed me to design and conduct infant experiments, and provided many opportunities for me to attend the domestic and international conferences. It has been a great privilege to work with Yoko Hakuno, Masahiro Hata, Eiichi Hoshino, Satoshi Morimoto, Mingdi Xu, and Na Jiang from Keio Baby Lab. I would also like to thank my friend Dr. Jiaming Lu for helping me all the time. I would furthermore like to thank Keio University and Heiwa Nakajima Foundation, from which I received the scholarships and research grants, which made me concentrate on my Ph.D. studies. Finally, I would particularly like to thank my parents and family members for supporting me along the way, and this thesis is dedicated to them.

List of publications

Original papers related to this doctoral thesis

1. Cai, L., Okada, E., Minagawa, Y., & Kawaguchi, H. (2021). Correlating functional near-infrared spectroscopy with underlying cortical regions of 0-, 1-, and 2-year-olds using theoretical light propagation analysis. *Neurophotonics*, 8(2), 025009.
2. Cai, L., Nitta, T., Yokota, S., Obata, T., Okada, E., & Kawaguchi, H. (2021). Targeting brain regions of interest in functional near-infrared spectroscopy-Scalp-cortex correlation using subject-specific light propagation models. *Human Brain Mapping*, 42 (7), 1-18.

Other articles

1. Cai, L., Dong, Q., Wang, M., & Niu, H. (2019). Functional near-infrared spectroscopy evidence for the development of topological asymmetry between hemispheric brain networks from childhood to adulthood. *Neurophotonics*, 6 (2), 025005.
2. Cai, L., Dong, Q., & Niu, H. (2018). The development of functional network organization in early childhood and early adolescence: a resting-state fNIRS study. *Developmental Cognitive Neuroscience*, 30, 223-235.
3. Arduino, L. S., Veronelli, L., Cai, L., Xue, S., Corbo, M., & Zhang, Y. (2016). Pseudoneglect in sentence bisection: a comparison between Italian and Chinese. *Journal of Cognitive Psychology*, 28 (5), 575-584.
4. Yu, J., Zhang, Y., Boland, J. E., & Cai, L. (2015). The interplay between referential processing and local syntactic/semantic processing: ERPs to written Chinese discourse. *Brain Research*, 1597, 139-158.
5. Cai, L., & Zhang, Y. (2014). EEG Time-Frequency Analysis of Syntactic and Semantic Processing in Sentence Comprehension. *Advances in Psychological Science*, 22 (7), 1112-1121.

Appendix

Fig. S1 Spatial sensitivity profile for all circumferential SD pairs over all 10-10 fiducial points for 0-, 1-, and 2-yo infants

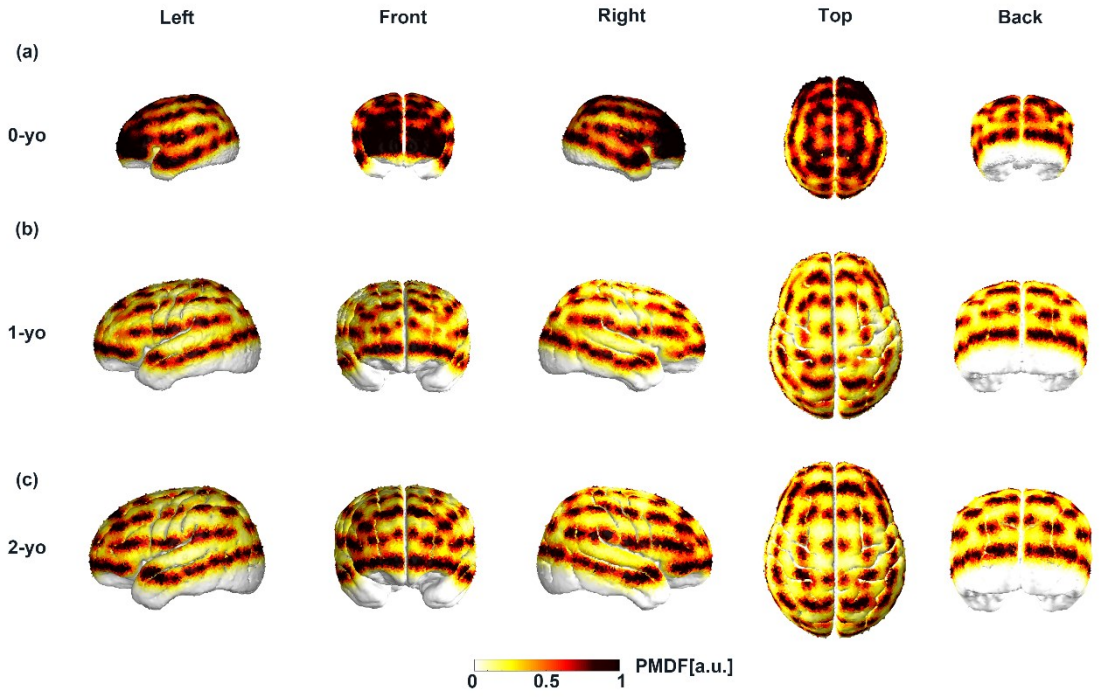

Table S1-1 Group-wise SCC between scalp fiducial points and AAL brain regions in 45 subjects for SBM and three GMs

Fiducial point	AAL region	Scalp-cortex correlation (%)						
		SBM				GM(S,S)	GM(S,T)	GM(T,T)
		Circumferential orientation		Vertical orientation				
		Mean	SD	Mean	SD			
Cz	SMA-R	24	12.1	24.7	12.5	22.2	20	36.7
	PCL-R	16.8	12.1	18.4	12.1	17.8	26.7	11.4
	SFGdor-L	15.5	12.1	12.6	11.1	20	4.4	0
	PCL-L	15.3	10.2	16.9	10.6	17.8	24.4	35.9
	SMA-L	11.5	8.2	14.7	9.6	17.8	20	15.9
	PreCG-L	6	7.3	4.2	5.4	2.2	0	0
	PreCG-R	4.6	5.9	2.9	4.4	2.2	2.2	0
	SFGdor-R	3.8	4.6	2.7	3.2	0	2.2	0
	PoCG-L	0	0	1.1	1.9	0	0	0
Fpz	ORBmed-R	29.1	10.9	29.1	12.3	57.8	48.9	47.8
	ORBmed-L	20.3	7.3	19	7.4	28.9	15.6	35.7
	SFGmed-R	12.2	7.8	17.8	9	6.7	24.4	12.2
	SFGmed-L	10.2	6.8	13.8	9	4.4	11.1	2.6
	ORBsup-L	10.2	6.5	6.5	5	0	0	0
	ORBsup-R	9.8	6.7	6.6	5.3	0	0	1.7
	SFGdor-L	2.5	2.2	2.1	2.2	0	0	0
	SFGdor-R	2.4	2.3	1.7	1.8	0	0	0
	REC-R	1.1	1.7	1.4	2.4	0	0	0
	REC-L	0	0	1.2	2.4	2.2	0	0
AFz	SFGmed-R	49.9	13.4	52.2	17.1	57.8	60	48.5
	SFGmed-L	30.8	10.3	34.6	13.2	35.6	40	51.5
	SFGdor-L	14	11.1	9.2	9.3	6.7	0	0
	SFGdor-R	4.2	3.2	2.4	1.7	0	0	0
Fz	SFGmed-R	47	12.7	49.4	15.7	57.8	62.2	47.5
	SFGmed-L	34.7	9.1	37.9	12.3	42.2	37.8	52.5
	SFGdor-L	9.4	9	7.3	9.2	0	0	0
	SFGdor-R	7.3	4.5	4.1	2.9	0	0	0

Table S1-2 Group-wise SCC between scalp fiducial points and AAL brain regions in 45 subjects for SBM and three GMs

Fiducial point	AAL region	Scalp-cortex correlation (%)						
		SBM				GM(S,S)	GM(S,T)	GM(T,T)
		Circumferential orientation		Vertical orientation				
		Mean	SD	Mean	SD			
FCz	SMA-R	32.9	15.2	31.7	15.3	40	46.7	48.7
	SMA-L	26.1	10.8	27.8	11.8	42.2	35.6	51.3
	SFGmed-R	12.7	10	14.7	9.9	8.9	11.1	0
	SFGdor-L	11.5	9.6	8.9	9.4	2.2	0	0
	SFGmed-L	8.7	7.5	10.9	7	6.7	6.7	0
	SFGdor-R	7.2	4.8	5.2	4.1	0	0	0
CPz	PCL-R	25.1	15.1	27.4	14.9	35.6	26.7	35.4
	PCUN-L	19.3	13.7	20.2	13.6	17.8	15.6	21.8
	PCUN-R	18.4	13.9	18.1	13.4	24.4	2.2	20.4
	PCL-L	13.8	11	16.8	11.8	13.3	8.9	22.4
	PoCG-L	9.1	10	6.7	7.7	4.4	11.1	0
	PoCG-R	7.3	8	4.9	5.9	2.2	35.6	0
	SPG-L	2.6	4.4	1.8	2.9	2.2	0	0
	SPG-R	2	2.4	1.5	1.8	0	0	0
	PreCG-L	1.2	3.2	1.1	2.5	0	0	0
Pz	PCUN-L	30.3	16.7	39.9	15	51.1	51.1	65.1
	PCUN-R	28.5	18.3	35.7	13.6	42.2	31.1	34.9
	SPG-L	19.2	24.7	8.1	7.8	2.2	0	0
	SPG-R	15.5	18.9	8.8	7.7	4.4	17.8	0
	CUN-R	1.2	2.1	2.2	2.7	0	0	0
	SOG-L	0	0	1.6	2.3	0	0	0
	CUN-L	0	0	1	2.7	0	0	0

Table S1-3 Group-wise SCC between scalp fiducial points and AAL brain regions in 45 subjects for SBM and three GMs

Fiducial point	AAL region	Scalp-cortex correlation (%)						
		SBM				GM(S,S)	GM(S,T)	GM(T,T)
		Circumferential orientation		Vertical orientation				
		Mean	SD	Mean	SD			
POz	CUN-R	24	9.4	23.4	9.5	17.8	22.2	3.2
	SOG-L	22.6	11.4	19.6	11.5	13.3	0	28.6
	CUN-L	20.5	12.4	26.4	13.6	44.4	37.8	66.4
	PCUN-L	10.1	10.2	11.4	10.2	11.1	28.9	1.8
	SOG-R	9.4	9.3	6.3	7.5	6.7	0	0
	PCUN-R	5.7	6.7	6.7	7.7	6.7	8.9	0
	SPG-L	3.7	4.8	2.6	3.5	0	0	0
	SPG-R	3.3	4.4	2.2	2.7	0	2.2	0
Oz	SOG-L	26.9	18.1	26.4	17.1	37.8	33.3	59.9
	CAL-L	24.2	17.1	30	19.2	33.3	17.8	12.8
	MOG-L	17.1	14.4	13.9	12.3	15.6	2.2	12.2
	CUN-L	9	10.7	11.3	11.4	6.7	22.2	15.1
	CUN-R	8.7	6.7	7.9	6.7	2.2	24.4	0
	SOG-R	6.4	9.1	4.4	6.9	2.2	0	0
	CAL-R	6.2	8	4.7	6.3	2.2	0	0
	LING-R	1	2.3	0	0	0	0	0
T3	MTG-L	69.3	20.8	68.1	18.4	84.4	82.2	100
	STG-L	27.4	18.1	26.9	14.8	15.6	17.8	0
	PoCG-L	1.8	2.8	3	4.6	0	0	0
C5	PoCG-L	58.1	19.9	60.2	22.1	77.8	80	76.9
	SMG-L	29.6	20.9	27.1	22.1	22.2	20	23.1
	PreCG-L	5.8	6.3	4.4	5	0	0	0
	STG-L	4.7	6.3	6.7	7.9	0	0	0
C3	PoCG-L	55.2	20.6	60.3	17.5	73.3	71.1	100
	PreCG-L	29	15.3	28	17.2	22.2	28.9	0
	MFG-L	8.4	15.7	3.7	5.9	0	0	0
	IPL-L	4.9	7	4.5	7.1	4.4	0	0
	SMG-L	2.1	3.2	3.4	4.4	0	0	0

Table S1-4 Group-wise SCC between scalp fiducial points and AAL brain regions in 45 subjects for SBM and three GMs

Fiducial point	AAL region	Scalp-cortex correlation (%)						
		SBM				GM(S,S)	GM(S,T)	GM(T,T)
		Circumferential orientation		Vertical orientation				
		Mean	SD	Mean	SD			
C1	PreCG-L	53.4	18.5	56.3	17.9	77.8	80	100
	SFGdor-L	28.3	20.6	26	20.8	22.2	20	0
	PoCG-L	9.7	9	10.7	9.7	0	0	0
	MFG-L	5.1	5.4	3.5	4.1	0	0	0
	PCL-L	1.8	2.1	2	2.2	0	0	0
C2	PreCG-R	56.1	16.4	59.2	16.1	73.3	80	99
	SFGdor-R	22.1	18.1	18.4	17.2	24.4	20	1
	PoCG-R	10.5	10.2	11.9	12.6	2.2	0	0
	SMA-R	4.6	5	5.1	5	0	0	0
	MFG-R	3.2	4.1	1.8	2.6	0	0	0
	PCL-R	2.6	2.6	2.8	2.5	0	0	0
C4	PoCG-R	53.2	13.9	56.2	13.8	75.6	86.7	88.4
	PreCG-R	26.3	15.2	25.3	16.5	15.6	11.1	11.6
	IPL-R	10	12	6.2	7	2.2	0	0
	SMG-R	6.8	8.7	10.3	12	6.7	2.2	0
	MFG-R	2	3	1.4	2.3	0	0	0
	SPG-R	1.5	4	0	0	0	0	0
C6	SMG-R	43.7	22.5	41.7	24.6	48.9	62.2	97
	PoCG-R	42.9	18.4	43.3	21.9	51.1	37.8	3
	STG-R	6.6	8.7	9.7	9.4	0	0	0
	PreCG-R	5	5.8	3.4	4.4	0	0	0
	ROL-R	1	1.3	0	0	0	0	0
T4	MTG-R	57.1	21.8	54.6	19	71.1	77.8	98
	STG-R	33.3	22	32	18.8	24.4	22.2	2
	ITG-R	6.6	12.2	10.2	14.6	4.4	0	0
	PoCG-R	1	1.8	1.5	2.3	0	0	0

Table S1-5 Group-wise SCC between scalp fiducial points and AAL brain regions in 45 subjects for SBM and three GMs

Fiducial point	AAL region	Scalp-cortex correlation (%)						
		SBM				GM(S,S)	GM(S,T)	GM(T,T)
		Circumferential orientation		Vertical orientation				
		Mean	SD	Mean	SD			
FT7	MTG-L	36.1	21.1	35.8	20.4	48.9	31.1	11.3
	STG-L	35.7	13.8	30.4	12.3	42.2	24.4	72.2
	IFGoperc-L	8.4	7.5	12.5	10.3	2.2	2.2	0
	IFGtriang-L	6.8	6.5	5.7	5.9	2.2	2.2	0
	TPOsup-L	5.3	4.5	5.6	4.9	2.2	40	16.5
	ROL-L	4.3	4.3	5.5	5.3	2.2	0	0
	PoCG-L	2.1	1.9	3.2	3.4	0	0	0
F7	IFGtriang-L	50.8	17.7	60.4	16.2	75.6	71.1	13.2
	ORBinf-L	34.4	17	26.5	15.3	24.4	28.9	86.8
	MFG-L	4.1	3.3	4.5	3.8	0	0	0
	ORBmid-L	3.5	4.4	1.8	3.3	0	0	0
	TPOsup-L	2.8	2.8	2.5	2.6	0	0	0
	IFGoperc-L	1.9	2.8	2.1	3.4	0	0	0
	STG-L	1.2	1.6	0	0	0	0	0
AF7	ORBmid-L	48.2	16.8	42.7	18.8	75.6	91.1	100
	ORBinf-L	23.1	14.8	18.8	14	17.8	0	0
	MFG-L	17.8	10.2	29	13	4.4	8.9	0
	IFGtriang-L	7.4	8.2	6.8	9.7	2.2	0	0
	SFGdor-L	1.8	2.3	1.7	2	0	0	0
	ORBsup-L	1.6	1.5	0	0	0	0	0
Fp1	ORBsup-L	36.3	11.9	33.5	11.5	77.8	62.2	68.4
	ORBmid-L	27.4	11.2	19.3	9.7	8.9	0	0
	SFGdor-L	17.2	9.3	30.7	11.4	13.3	35.6	31.6
	ORBmed-L	8.2	5.8	5.2	4.6	0	2.2	0
	SFGmed-L	5	3.4	5.5	4.3	0	0	0
	MFG-L	4.6	3.4	4.9	3.9	0	0	0

Table S1-6 Group-wise SCC between scalp fiducial points and AAL brain regions in 45 subjects for SBM and three GMs

Fiducial point	AAL region	Scalp-cortex correlation (%)						
		SBM				GM(S,S)	GM(S,T)	GM(T,T)
		Circumferential orientation		Vertical orientation				
		Mean	SD	Mean	SD			
Fp2	ORBmid-R	38.7	13.8	28.7	12.8	22.2	6.7	0
	ORBsup-R	27.8	9.7	26.1	10.4	55.6	35.6	75.4
	SFGdor-R	15.1	8.9	26.7	11.5	22.2	57.8	24.6
	ORBmed-R	7.7	5.3	4.8	4.2	0	0	0
	SFGmed-R	5.3	5.9	6.7	6.3	0	0	0
	MFG-R	4.9	4.1	6.7	6.7	0	0	0
AF8	ORBmid-R	63.8	15.7	58.6	15.9	91.1	95.6	100
	ORBinf-R	18.1	15.7	13.6	13.9	4.4	0	0
	MFG-R	13.1	9.7	23.2	12.1	4.4	4.4	0
	IFGtriang-R	3	4.6	3.1	5.8	0	0	0
	SFGdor-R	1	1.4	0	0	0	0	0
F8	ORBinf-R	50.4	17.9	42.3	17.1	68.9	86.7	92.9
	IFGtriang-R	29.7	16.8	41.5	17.1	24.4	13.3	7.1
	ORBmid-R	8.4	11.2	4.8	8.8	6.7	0	0
	TPOsup-R	4.4	5.2	3.8	4.6	0	0	0
	MFG-R	3.1	3.5	3.5	3.9	0	0	0
	IFGoperc-R	2	2	2.1	2.4	0	0	0
FT8	TPOsup-R	23.9	13.7	24	13.1	37.8	73.3	27.1
	STG-R	23.8	13.2	16.7	13	33.3	6.7	72.9
	MTG-R	22.1	14.6	20.4	13.1	13.3	11.1	0
	ROL-R	9.5	8.3	13	10	6.7	4.4	0
	TPOmid-R	5.9	7.6	9.6	11	6.7	0	0
	IFGoperc-R	5.8	5.2	7	5.5	2.2	4.4	0
	IFGtriang-R	4.3	4.7	3.4	3.8	0	0	0
	PoCG-R	1.2	1.4	1.6	1.9	0	0	0
	ORBinf-R	1.2	1.5	0	0	0	0	0
	PreCG-R	0	0	1.7	2.2	0	0	0
	ITG-R	0	0	1	1.8	0	0	0

Table S1-7 Group-wise SCC between scalp fiducial points and AAL brain regions in 45 subjects for SBM and three GMs

Fiducial point	AAL region	Scalp-cortex correlation (%)						
		SBM				GM(S,S)	GM(S,T)	GM(T,T)
		Circumferential orientation		Vertical orientation				
		Mean	SD	Mean	SD			
TP7	MTG-L	73	20.8	69.1	18.6	88.9	86.7	100
	STG-L	21	19.1	22.7	16.7	11.1	13.3	0
	SMG-L	3.2	4.6	5	6	0	0	0
	ITG-L	2.2	3.9	2.7	4.4	0	0	0
T5	MTG-L	49.1	19.1	48.1	19.5	64.4	84.4	88.7
	MOG-L	30.7	19	28	20.6	24.4	15.6	11.3
	IOG-L	5.2	8.2	6.3	7.9	2.2	0	0
	ANG-L	4.9	7.7	7.5	9	4.4	0	0
	SMG-L	4.9	7.3	5.7	7.9	2.2	0	0
	STG-L	3.1	6.5	1.8	4.2	2.2	0	0
	ITG-L	1.9	3.1	2.2	3.2	0	0	0
PO7	MOG-L	93.2	7.7	93.6	7.6	100	100	100
	IOG-L	3	6.3	3.5	6.2	0	0	0
	MTG-L	1.8	3	1	2	0	0	0
O1	MOG-L	68.6	23	69	22.2	80	60	89.8
	SOG-L	26.3	24.5	25.4	24.1	20	40	10.2
	CAL-L	2.3	4.1	2.1	3.7	0	0	0
	IOG-L	1.6	3.6	2.4	4.6	0	0	0
O2	SOG-R	40.2	27.4	40.8	25.8	44.4	80	88.3
	CAL-R	22.6	18.7	25.4	17.7	28.9	8.9	0
	CUN-R	14.7	13.3	14.3	11.9	20	0	11.7
	MOG-R	8.8	10.7	6.4	10	2.2	8.9	0
	IOG-R	6.4	10.5	5.2	7.7	2.2	2.2	0
	LING-R	4.2	7	5.7	8	2.2	0	0
	CAL-L	2.5	3.6	1.6	2.5	0	0	0

Table S1-8 Group-wise SCC between scalp fiducial points and AAL brain regions in 45 subjects for SBM and three GMs

Fiducial point	AAL region	Scalp-cortex correlation (%)						
		SBM				GM(S,S)	GM(S,T)	GM(T,T)
		Circumferential orientation		Vertical orientation				
		Mean	SD	Mean	SD			
PO8	MOG-R	66.3	21.6	69.1	19	80	91.1	100
	IOG-R	17.7	22.8	19.5	18.9	17.8	8.9	0
	SOG-R	8.2	8.9	6	7.2	2.2	0	0
	MTG-R	4.1	4.3	2.2	2.9	0	0	0
	CAL-R	1.9	2.9	1.2	2.9	0	0	0
T6	MTG-R	61.8	13.9	60.4	12.4	88.9	93.3	94.6
	MOG-R	16.4	14	13.3	13.6	4.4	0	5.4
	ITG-R	7.8	10.9	9.5	10.4	6.7	4.4	0
	IOG-R	4.7	7.2	4.7	6.1	0	0	0
	STG-R	4.2	6.1	3	4.2	0	0	0
	ANG-R	4.1	5.1	7.5	8	0	2.2	0
	CERCRU1-R	0	0	1.1	2.5	0	0	0
TP8	MTG-R	66.9	16.2	62.3	12.7	86.7	91.1	100
	STG-R	24.5	19.2	24.7	15.6	13.3	8.9	0
	ITG-R	6.9	8.8	10	9.4	0	0	0
	SMG-R	1.1	1.5	2.4	2.9	0	0	0
FC5	PreCG-L	29.1	10.8	31.6	13.6	46.7	46.7	12.7
	IFGtriang-L	21.9	13.8	19.4	14.4	13.3	13.3	6.4
	IFGoperc-L	21.9	11	27.1	12.7	40	40	80.9
	PoCG-L	16.3	12.9	10.7	10.7	0	0	0
	MFG-L	8.6	8.1	8.6	8.5	0	0	0
	ROL-L	1.2	2	1.5	2.4	0	0	0
FC3	MFG-L	79.1	15.7	81.5	14.8	95.6	97.8	97.8
	PreCG-L	17.1	14.1	13.9	13.9	4.4	2.2	2.2
	IFGtriang-L	1.5	3	2.3	2.7	0	0	0
	IFGoperc-L	0	0	1	1.2	0	0	0

Table S1-9 Group-wise SCC between scalp fiducial points and AAL brain regions in 45 subjects for SBM and three GMs

Fiducial point	AAL region	Scalp-cortex correlation (%)						
		SBM				GM(S,S)	GM(S,T)	GM(T,T)
		Circumferential orientation		Vertical orientation				
		Mean	SD	Mean	SD			
FC1	SFGdor-L	56	16.7	55.8	16.9	77.8	82.2	57
	MFG-L	34.1	20.2	35	20.7	22.2	15.6	43
	SMA-L	5.7	4.8	6.5	5.4	0	2.2	0
	SFGmed-L	2.6	2.3	1.6	1.5	0	0	0
	PreCG-L	1.2	1.6	0	0	0	0	0
FC2	SFGdor-R	51.1	14.1	51	13	71.1	80	99
	MFG-R	33.7	19.3	34.4	18.7	26.7	20	1
	SMA-R	8.2	7.7	9.9	8.3	2.2	0	0
	SFGmed-R	4.5	4.5	3.1	3.9	0	0	0
	PreCG-R	2.1	2.8	1.1	1.5	0	0	0
FC4	MFG-R	69.5	16.7	72.6	16.5	88.9	100	100
	PreCG-R	24.2	15.4	19.1	15.4	8.9	0	0
	IFGoperc-R	2.9	4.5	4.9	7.2	2.2	0	0
	SFGdor-R	1.6	3.9	1.9	4.6	0	0	0
	PoCG-R	1.3	1.5	0	0	0	0	0
FC6	PreCG-R	39.9	13.7	43	18.7	64.4	82.2	78.3
	IFGoperc-R	20.3	15	24.3	19	33.3	2.2	21.7
	IFGtriang-R	13.8	10	10.7	10.7	2.2	15.6	0
	PoCG-R	13.1	10.5	7.9	8.9	0	0	0
	MFG-R	6.5	6.4	5.8	5.8	0	0	0
	ROL-R	5.2	3.9	7.3	4.7	0	0	0
F5	MFG-L	59.4	21	57.1	22.4	60	84.4	50.6
	IFGtriang-L	36.8	20.4	38.5	22.2	40	15.6	49.4
	IFGoperc-L	1.4	2.1	0	0	0	0	0
	ORBinf-L	0	0	2	3.1	0	0	0
	ORBmid-L	0	0	1.3	2.7	0	0	0

Table S1-10 Group-wise SCC between scalp fiducial points and AAL brain regions in 45 subjects for SBM and three GMs

Fiducial point	AAL region	Scalp-cortex correlation (%)						
		SBM				GM(S,S)	GM(S,T)	GM(T,T)
		Circumferential orientation		Vertical orientation				
		Mean	SD	Mean	SD			
F3	MFG-L	84.2	12.6	87.3	11	95.6	97.8	98.9
	SFGdor-L	13.6	12.3	10.7	10.9	4.4	2.2	1.1
	IFGtriang-L	1.7	4.2	1.7	4.1	0	0	0
F1	SFGdor-L	53.1	15.1	62.1	12.5	88.9	77.8	100
	SFGmed-L	25.6	13.4	20.6	13.3	6.7	20	0
	MFG-L	17	15.2	16.3	15.6	4.4	2.2	0
	SFGmed-R	3.8	11.3	0	0	0	0	0
F2	SFGdor-R	50.8	10.3	56.6	10.3	86.7	95.6	100
	SFGmed-R	29.4	11.6	27.4	12.6	11.1	4.4	0
	MFG-R	18.5	12.1	14.9	12.1	2.2	0	0
F4	MFG-R	83.5	10.2	87	9.1	100	100	100
	SFGdor-R	14	10	10.9	8.9	0	0	0
	IFGtriang-R	1.2	1.6	1.4	2	0	0	0
F6	MFG-R	55.2	18.5	52	18.6	62.2	71.1	50.9
	IFGtriang-R	38.6	18.3	39	19.3	37.8	28.9	49.1
	ORBinf-R	2.4	2.9	5.4	5.4	0	0	0
	IFGoperc-R	1.7	1.6	1	1	0	0	0
	ORBmid-R	1.4	3.3	2.2	5.4	0	0	0
AF3	SFGdor-L	57.3	12	60.6	14	73.3	97.8	98.9
	MFG-L	32.2	15.2	28.6	17.1	26.7	2.2	1.1
	SFGmed-L	7.4	5.8	5	3.8	0	0	0
	ORBmid-L	1.3	1.9	2.6	2.4	0	0	0
	ORBsup-L	1.1	1.5	2.6	2.3	0	0	0
AF4	SFGdor-R	43.5	13.7	50.7	14.7	75.6	100	79.7
	MFG-R	35.8	16.8	30.7	18.2	24.4	0	20.3
	SFGmed-R	17.6	8.6	12.3	6.9	0	0	0
	ORBmid-R	1.6	1.7	3.8	3.4	0	0	0
	ORBsup-R	0	0	1.9	1.9	0	0	0

Table S1-11 Group-wise SCC between scalp fiducial points and AAL brain regions in 45 subjects for SBM and three GMs

Fiducial point	AAL region	Scalp-cortex correlation (%)						
		SBM				GM(S,S)	GM(S,T)	GM(T,T)
		Circumferential orientation		Vertical orientation				
		Mean	SD	Mean	SD			
CP5	SMG-L	64.7	13	65	12.4	82.2	86.7	100
	IPL-L	21.7	12.9	21.3	11.7	17.8	11.1	0
	ANG-L	6.5	6.8	4.3	5.2	0	0	0
	STG-L	3.3	4.3	5.6	5.9	0	2.2	0
	PoCG-L	3	4.8	2.1	3.8	0	0	0
	MTG-L	0	0	1.5	2.8	0	0	0
CP3	IPL-L	52.8	24.7	61	20.2	77.8	75.6	94.2
	PoCG-L	27.8	23	24.6	20.9	20	24.4	5.8
	SPG-L	11.8	11.9	9.2	8	2.2	0	0
	ANG-L	3.6	5.2	2.8	4.1	0	0	0
	PreCG-L	2.4	8.5	0	0	0	0	0
	SMG-L	1.2	1.2	1.6	1.5	0	0	0
CP1	PoCG-L	41	19.6	39.5	18.6	33.3	57.8	18.5
	SPG-L	37.2	25	38.8	23.9	55.6	42.2	81.5
	PCUN-L	10.7	14.4	9	12.7	6.7	0	0
	PreCG-L	7.3	10.2	7.7	10.3	4.4	0	0
	PCL-L	2.3	3.2	3.3	4.3	0	0	0
CP2	SPG-R	41.1	22.8	42.1	21.3	53.3	66.7	55.1
	PoCG-R	36.4	16.1	35.1	15.3	35.6	31.1	44.9
	PCUN-R	9	7.9	7.3	6.9	0	0	0
	PreCG-R	7	9.5	6.9	9.8	6.7	2.2	0
	PCL-R	5	6.3	6.8	7.2	4.4	0	0
CP4	IPL-R	44.9	18.8	52.8	16.2	80	88.9	61.7
	SPG-R	21.6	18.1	16.4	13.7	13.3	6.7	38.3
	PoCG-R	18.2	15.1	15.6	12.6	2.2	2.2	0
	ANG-R	11.4	10.9	11.4	11.3	4.4	0	0
	SMG-R	2.8	3.7	2.9	3.2	0	2.2	0

Table S1-12 Group-wise SCC between scalp fiducial points and AAL brain regions in 45 subjects for SBM and three GMs

Fiducial point	AAL region	Scalp-cortex correlation (%)						
		SBM				GM(S,S)	GM(S,T)	GM(T,T)
		Circumferential orientation		Vertical orientation				
		Mean	SD	Mean	SD			
CP6	SMG-R	53.7	16.4	50.9	18.8	77.8	100	71.4
	ANG-R	21.1	13	19.1	11.7	15.6	0	28.6
	IPL-R	16.5	12	16.8	11	4.4	0	0
	STG-R	5.3	6.8	8.9	8.3	0	0	0
	MTG-R	2.2	6.8	3.5	8.8	2.2	0	0
P5	ANG-L	43.2	16	43.6	16.3	60	57.8	100
	MOG-L	35.2	22.7	35.6	22.9	33.3	37.8	0
	IPL-L	11.4	13.6	10.8	12.9	4.4	4.4	0
	SMG-L	5.9	6	3.9	4.9	0	0	0
	MTG-L	3.9	6.2	5.7	7.8	2.2	0	0
P3	ANG-L	38.8	17.7	41.6	16.7	68.9	62.2	100
	SPG-L	23.1	19.9	19.8	17	6.7	4.4	0
	IPL-L	21.3	13.5	16.6	11.9	11.1	24.4	0
	MOG-L	14.7	16.1	20.6	19	13.3	8.9	0
	SOG-L	1.3	1.9	0	0	0	0	0
P4	ANG-R	48.2	19.9	48.9	19.8	73.3	66.7	91.5
	SPG-R	26.4	21.5	23.5	19.2	11.1	2.2	8.5
	MOG-R	14.3	18.9	19.9	21.6	15.6	0	0
	SOG-R	5.3	5.4	4.3	4.7	0	0	0
	IPL-R	5.2	5.4	2.8	3.3	0	31.1	0
P1	SPG-L	59	22.6	69.4	15.1	91.1	97.8	95.8
	PCUN-L	13.1	13.8	15.5	12.3	4.4	0	4.2
	IPL-L	9.5	14	3.3	6.8	4.4	2.2	0
	PoCG-L	7.8	14.4	1.9	3.6	0	0	0
	ANG-L	4.1	5.3	2.9	4	0	0	0
	SOG-L	2.4	3.9	4.2	5.5	0	0	0
	PCUN-R	1.9	7.7	0	0	0	0	0
	MOG-L	1	2	2.2	3.7	0	0	0

Table S1-13 Group-wise SCC between scalp fiducial points and AAL brain regions in 45 subjects for SBM and three GMs

Fiducial point	AAL region	Scalp-cortex correlation (%)						
		SBM				GM(S,S)	GM(S,T)	GM(T,T)
		Circumferential orientation		Vertical orientation				
		Mean	SD	Mean	SD			
P2	SPG-R	68.9	18.8	70.1	13.7	97.8	100	100
	PCUN-R	14.8	11.3	12.4	10.3	0	0	0
	SOG-R	4	6	7	8.7	2.2	0	0
	ANG-R	3.7	5.9	3.7	6.2	0	0	0
	CUN-R	2.7	4.4	3.3	4.9	0	0	0
	SPG-L	1.6	7.9	0	0	0	0	0
	PCUN-L	1.6	5.7	0	0	0	0	0
	PoCG-R	1.4	3.2	1.4	3.3	0	0	0
	MOG-R	1	2.6	1.5	3.1	0	0	0
P6	ANG-R	48.9	23.4	45.9	23.5	53.3	86.7	74.7
	MOG-R	35.9	21.6	37.6	22.3	37.8	4.4	25.3
	MTG-R	8	9.9	10.9	10.2	8.9	8.9	0
	IPL-R	5.2	6.1	4.2	5.2	0	0	0
PO3	MOG-L	46.4	22.8	48.4	24.8	55.6	48.9	62.6
	SOG-L	40.7	17.1	39.1	19.6	42.2	40	37.4
	SPG-L	6.8	11.2	7.8	11.8	0	2.2	0
	ANG-L	2.6	4.7	1.8	3.5	0	0	0
	IPL-L	1.6	2.8	1.5	2.6	2.2	8.9	0
	CUN-L	1.5	2.2	1	1.6	0	0	0
PO4	SOG-R	63	15.6	66.5	15.4	88.9	93.3	87.2
	MOG-R	19.7	16	16.4	15.4	11.1	6.7	12.8
	CUN-R	10.3	9.9	9.1	9.1	0	0	0
	SPG-R	4.2	8.1	4.9	8.5	0	0	0
	ANG-R	1.9	2.5	1.3	1.8	0	0	0
	CAL-R	0	0	1.3	2.7	0	0	0

Table S2-1 Normalized PPL of corresponding brain regions ($L_{norm,M}$) for the circumferential and vertical SD pairs set at 10/10 fiducial points at 10-mm SD distance from 0-yo, 1-yo, and 2-yo.

SD distance = 10 mm		Circumferential SD pair			Vertical channel SD pair		
10/10 Points	AAL regions	0 year	1 year	2 year	0 year	1 year	2 year
Cz	PreCG-R	1.9%	0.3%	0.4%	1.2%	0.3%	0.3%
	PreCG-L	5.2%	1.6%	0.9%	6.6%	1.9%	0.9%
	SFGdor-R	8.8%	2.5%	3.8%	4.5%	1.8%	3.1%
	SFGdor-L	14.7%	13.4%	7.2%	14.5%	11.2%	6.1%
	SMA-R	26.8%	34.6%	44.1%	17.6%	29.2%	46.2%
	SMA-L	22.8%	43.4%	40.5%	35.4%	50.2%	39.7%
	PoCG-L	6.0%	0.2%	0.1%	6.0%	0.3%	0.1%
	SPG-L	2.8%	0.0%	0.0%	2.5%	0.0%	0.0%
	PCL-R	6.4%	2.9%	2.1%	5.7%	3.8%	2.4%
	PCL-L	2.0%	0.7%	0.5%	2.9%	1.1%	0.7%
Fpz	SFGdor-R	3.8%	1.7%	2.1%	2.8%	1.2%	2.3%
	SFGdor-L	7.5%	5.4%	1.4%	6.1%	5.2%	1.1%
	ORBsup-R	2.8%	2.2%	4.6%	2.3%	1.7%	5.0%
	ORBsup-L	7.5%	11.7%	7.0%	7.1%	10.4%	5.6%
	ORBmid-L	1.6%	0.8%	0.8%	1.5%	0.8%	0.7%
	SFGmed-R	21.2%	10.5%	7.6%	20.2%	9.9%	9.5%
	SFGmed-L	24.3%	19.1%	8.7%	27.2%	22.8%	8.2%
	ORBmed-R	13.4%	18.3%	31.6%	13.2%	15.6%	35.1%
	ORBmed-L	14.9%	28.6%	32.3%	16.7%	30.8%	27.7%
	REC-R	0.9%	1.0%	2.5%	1.0%	1.0%	3.3%
AFz	SFGdor-R	4.0%	1.9%	6.2%	4.1%	1.4%	5.0%
	SFGdor-L	5.4%	10.2%	3.8%	5.7%	9.3%	2.9%
	SFGmed-R	30.2%	39.4%	54.2%	39.5%	31.3%	59.7%
	SFGmed-L	58.5%	47.4%	34.9%	48.3%	56.8%	31.4%
Fz	SFGdor-R	4.5%	1.3%	5.9%	5.4%	1.8%	5.8%
	SFGdor-L	6.8%	9.5%	4.6%	6.8%	6.9%	3.0%
	SMA-R	3.6%	0.0%	0.0%	1.9%	0.1%	0.0%
	SMA-L	8.1%	0.0%	0.0%	2.6%	0.1%	0.0%
	SFGmed-R	27.7%	23.7%	52.6%	47.4%	33.0%	59.8%
	SFGmed-L	48.2%	65.1%	36.3%	34.5%	57.8%	30.9%

Table S2-2 Normalized PPL of corresponding brain regions ($L_{norm,M}$) for the circumferential and vertical SD pairs set at 10/10 fiducial points at 10-mm SD distance from 0-yo, 1-yo, and 2-yo.

SD distance = 10 mm		Circumferential SD pair			Vertical channel SD pair		
10/10 Points	AAL regions	0 year	1 year	2 year	0 year	1 year	2 year
FCz	SFGdor-R	7.7%	1.6%	5.1%	4.9%	1.3%	4.5%
	SFGdor-L	9.1%	3.9%	3.3%	9.4%	5.6%	2.9%
	SMA-R	28.3%	35.7%	21.5%	22.0%	15.7%	23.6%
	SMA-L	25.0%	30.2%	11.8%	31.3%	37.6%	11.1%
	SFGmed-R	10.0%	10.7%	31.4%	10.3%	11.3%	32.6%
	SFGmed-L	13.3%	17.7%	26.3%	19.8%	28.2%	24.8%
	PCL-R	4.6%	0.0%	0.0%	0.4%	0.0%	0.0%
CPz	PreCG-L	4.3%	1.8%	1.6%	4.7%	1.7%	1.8%
	SMA-L	1.3%	0.9%	0.9%	1.4%	1.0%	1.3%
	PoCG-R	3.7%	0.9%	1.7%	2.1%	0.7%	1.3%
	PoCG-L	29.0%	29.0%	15.5%	26.9%	21.7%	12.7%
	SPG-R	1.4%	0.6%	0.8%	1.0%	0.5%	0.6%
	SPG-L	5.1%	4.0%	2.2%	7.6%	4.0%	2.1%
	PCUN-R	18.5%	14.7%	21.3%	12.9%	13.6%	19.1%
	PCUN-L	6.2%	12.5%	9.4%	13.4%	18.4%	10.2%
	PCL-R	15.8%	15.2%	25.8%	10.1%	15.0%	27.9%
	PCL-L	11.4%	19.9%	20.0%	17.2%	22.5%	21.9%
Pz	PoCG-L	1.1%	0.4%	0.4%	1.6%	0.5%	0.4%
	SPG-R	3.1%	1.1%	1.7%	1.5%	0.7%	1.3%
	SPG-L	39.8%	35.8%	18.8%	40.1%	36.4%	15.5%
	PCUN-R	31.9%	27.2%	44.9%	22.7%	21.8%	45.5%
	PCUN-L	22.1%	34.9%	33.7%	32.1%	40.0%	36.9%

Table S2-3 Normalized PPL of corresponding brain regions ($L_{norm,M}$) for the circumferential and vertical SD pairs set at 10/10 fiducial points at 10-mm SD distance from 0-yo, 1-yo, and 2-yo.

SD distance = 10 mm		Circumferential SD pair			Vertical channel SD pair		
10/10 Points	AAL regions	0 year	1 year	2 year	0 year	1 year	2 year
POz	CUN-R	15.8%	8.1%	10.1%	13.2%	8.3%	11.2%
	CUN-L	16.2%	25.6%	14.2%	18.4%	25.7%	14.4%
	SOG-R	15.2%	7.0%	9.4%	6.9%	5.7%	7.9%
	SOG-L	5.4%	3.7%	1.2%	5.9%	3.1%	1.1%
	MOG-L	1.0%	0.2%	0.1%	1.1%	0.2%	0.1%
	SPG-R	1.8%	1.8%	2.6%	1.1%	1.5%	2.0%
	SPG-L	20.8%	27.9%	24.3%	27.2%	27.1%	22.5%
	PCUN-R	15.3%	16.4%	26.5%	14.4%	16.9%	27.6%
	PCUN-L	7.0%	9.0%	11.2%	10.5%	11.2%	13.0%
Oz	CAL-R	3.8%	2.0%	3.1%	3.7%	2.4%	3.7%
	CUN-R	37.6%	31.3%	54.6%	28.4%	31.7%	54.7%
	CUN-L	20.7%	26.3%	20.9%	27.7%	30.6%	22.7%
	SOG-R	4.4%	3.0%	5.7%	2.2%	2.8%	4.2%
	SOG-L	29.7%	34.8%	13.8%	34.2%	29.8%	12.8%
	MOG-L	2.2%	1.6%	0.5%	2.1%	1.4%	0.5%
T3	STG-L	2.5%	5.8%	3.3%	3.5%	7.3%	4.1%
	TPOsup-L	1.1%	0.5%	0.4%	1.2%	0.4%	0.3%
	MTG-L	70.0%	89.8%	90.1%	71.2%	88.2%	88.7%
	TPOmid-L	2.3%	0.5%	0.5%	2.1%	0.4%	0.4%
	ITG-L	23.8%	3.4%	5.7%	21.8%	3.5%	6.3%
C5	PreCG-L	1.4%	1.5%	1.5%	1.4%	0.9%	1.0%
	ROL-L	9.7%	9.8%	6.7%	7.2%	6.1%	3.9%
	PoCG-L	19.6%	56.7%	52.4%	27.9%	55.8%	53.0%
	SMG-L	4.2%	7.6%	8.3%	3.6%	6.9%	7.5%
	STG-L	60.3%	23.8%	30.1%	54.5%	29.9%	33.7%
	TPOsup-L	1.5%	0.1%	0.3%	1.2%	0.1%	0.2%
	MTG-L	2.4%	0.2%	0.4%	3.3%	0.2%	0.5%

Table S2-4 Normalized PPL of corresponding brain regions ($L_{norm,M}$) for the circumferential and vertical SD pairs set at 10/10 fiducial points at 10-mm SD distance from 0-yo, 1-yo, and 2-yo.

SD distance = 10 mm		Circumferential SD pair			Vertical channel SD pair		
10/10 Points	AAL regions	0 year	1 year	2 year	0 year	1 year	2 year
C3	PreCG-L	33.8%	46.8%	36.3%	23.9%	31.8%	33.5%
	MFG-L	1.6%	3.8%	5.3%	1.2%	3.0%	5.8%
	PoCG-L	56.7%	47.3%	52.6%	69.3%	62.5%	55.4%
	SMG-L	7.4%	2.0%	5.4%	5.1%	2.6%	5.1%
C1	PreCG-L	47.3%	47.4%	44.0%	45.4%	44.6%	43.4%
	SFGdor-L	27.9%	35.3%	27.5%	33.1%	38.3%	32.5%
	MFG-L	20.0%	14.4%	25.9%	15.3%	14.3%	21.2%
	PoCG-L	3.7%	2.3%	2.2%	4.9%	2.1%	2.4%
C2	PreCG-R	53.9%	69.5%	49.9%	51.8%	69.6%	48.7%
	SFGdor-R	23.7%	16.1%	27.3%	31.0%	21.2%	31.2%
	MFG-R	12.7%	10.5%	18.9%	8.0%	5.1%	16.5%
	SMA-R	1.1%	0.5%	0.9%	1.2%	0.5%	1.0%
	PoCG-R	6.9%	3.2%	2.6%	6.5%	3.3%	2.2%
C4	PreCG-R	18.7%	8.3%	26.2%	12.8%	8.2%	27.5%
	MFG-R	1.3%	0.2%	1.2%	0.9%	0.2%	1.3%
	PoCG-R	56.9%	79.3%	66.0%	62.2%	82.8%	65.8%
	IPL-R	9.7%	8.8%	3.6%	6.0%	4.8%	2.3%
	SMG-R	12.9%	3.3%	2.8%	17.8%	4.0%	3.0%
C6	PreCG-R	0.8%	0.2%	1.2%	1.0%	0.2%	1.4%
	ROL-R	5.4%	1.9%	1.9%	4.1%	1.5%	2.1%
	PoCG-R	28.8%	45.7%	59.8%	37.2%	42.5%	61.8%
	SMG-R	6.9%	14.3%	13.9%	5.2%	11.1%	10.0%
	STG-R	42.8%	35.6%	21.0%	36.9%	41.6%	22.4%
	MTG-R	12.9%	2.1%	1.7%	13.2%	3.0%	1.8%
T4	STG-R	0.9%	0.9%	2.6%	1.1%	1.1%	2.9%
	MTG-R	63.6%	83.6%	89.0%	67.3%	82.9%	88.3%
	ITG-R	34.6%	15.3%	7.8%	30.5%	15.9%	8.1%

Table S2-5 Normalized PPL of corresponding brain regions ($L_{norm,M}$) for the circumferential and vertical SD pairs set at 10/10 fiducial points at 10-mm SD distance from 0-yo, 1-yo, and 2-yo.

SD distance = 10 mm		Circumferential SD pair			Vertical channel SD pair		
10/10 Points	AAL regions	0 year	1 year	2 year	0 year	1 year	2 year
FT7	IFGoperc-L	0.9%	1.0%	0.6%	1.3%	1.0%	0.6%
	IFGtriang-L	1.6%	0.8%	0.7%	1.9%	0.8%	0.7%
	ORBinf-L	5.6%	1.5%	1.6%	4.9%	1.3%	1.3%
	STG-L	3.3%	11.5%	7.0%	2.9%	7.0%	5.4%
	TPOsup-L	33.3%	49.5%	38.5%	41.9%	51.9%	36.2%
	MTG-L	18.5%	13.6%	20.9%	12.9%	11.7%	21.4%
	TPOmid-L	32.2%	20.2%	29.5%	29.4%	24.6%	33.1%
	ITG-L	3.3%	0.5%	0.6%	2.9%	0.5%	0.8%
F7	MFG-L	2.0%	0.4%	0.4%	1.9%	0.4%	0.4%
	ORBmid-L	7.6%	0.7%	1.3%	6.4%	0.5%	1.0%
	IFGtriang-L	14.2%	10.5%	5.6%	14.6%	13.9%	6.8%
	ORBinf-L	72.3%	83.4%	84.2%	72.7%	81.0%	85.2%
	TPOsup-L	2.9%	4.5%	7.5%	3.3%	3.7%	5.8%
AF7	SFGdor-L	1.9%	0.3%	0.4%	1.6%	0.2%	0.4%
	ORBsup-L	1.4%	0.4%	0.8%	1.2%	0.3%	0.8%
	MFG-L	17.2%	8.5%	5.6%	18.3%	10.1%	6.6%
	ORBmid-L	63.4%	67.9%	73.9%	62.3%	68.8%	74.9%
	IFGtriang-L	3.3%	2.0%	1.5%	3.4%	1.9%	1.6%
	ORBinf-L	12.3%	20.9%	17.6%	12.8%	18.7%	15.5%
Fp1	SFGdor-L	26.0%	17.2%	7.4%	27.7%	20.9%	9.6%
	ORBsup-L	21.9%	39.7%	37.5%	20.5%	40.4%	38.1%
	MFG-L	14.8%	7.8%	2.5%	15.4%	6.8%	3.1%
	ORBmid-L	25.7%	32.0%	43.1%	27.3%	28.5%	42.0%
	SFGmed-L	5.4%	1.6%	2.0%	4.2%	1.6%	1.7%
	ORBmed-L	3.4%	1.4%	6.5%	2.5%	1.5%	4.5%

Table S2-6 Normalized PPL of corresponding brain regions ($L_{norm,M}$) for the circumferential and vertical SD pairs set at 10/10 fiducial points at 10-mm SD distance from 0-yo, 1-yo, and 2-yo.

SD distance = 10 mm		Circumferential SD pair			Vertical channel SD pair		
10/10 Points	AAL regions	0 year	1 year	2 year	0 year	1 year	2 year
Fp2	SFGdor-R	38.3%	29.3%	18.1%	39.5%	33.7%	19.6%
	ORBsup-R	16.4%	32.3%	32.1%	18.3%	30.7%	30.1%
	MFG-R	10.6%	4.7%	5.5%	8.2%	5.0%	6.4%
	ORBmid-R	13.4%	22.9%	35.8%	13.4%	22.0%	37.2%
	SFGmed-R	10.2%	3.4%	1.9%	9.7%	3.0%	1.6%
	SFGmed-L	1.2%	0.1%	0.1%	1.1%	0.1%	0.1%
	ORBmed-R	6.9%	6.6%	5.1%	6.8%	4.9%	3.6%
AF8	SFGdor-R	3.7%	0.3%	0.6%	3.8%	0.3%	0.6%
	ORBsup-R	1.5%	0.2%	0.7%	1.7%	0.2%	0.7%
	MFG-R	28.8%	8.4%	8.7%	33.2%	13.0%	10.5%
	ORBmid-R	46.3%	78.2%	67.7%	44.8%	73.0%	68.3%
	IFGtriang-R	5.9%	2.3%	3.8%	4.3%	2.4%	3.5%
	ORBinf-R	13.0%	10.6%	18.3%	11.5%	10.9%	16.1%
F8	MFG-R	2.3%	0.1%	0.6%	2.6%	0.1%	0.6%
	ORBmid-R	6.2%	0.3%	1.8%	5.2%	0.3%	1.7%
	IFGtriang-R	18.0%	20.1%	29.4%	26.5%	26.0%	35.2%
	ORBinf-R	69.3%	73.3%	57.8%	62.0%	69.3%	53.6%
	TPOsup-R	2.9%	5.0%	8.7%	2.4%	3.4%	7.4%
FT8	IFGoperc-R	1.4%	0.4%	1.2%	2.3%	0.4%	1.4%
	IFGtriang-R	2.5%	0.5%	1.5%	3.1%	0.5%	1.5%
	ORBinf-R	7.0%	0.7%	1.5%	6.0%	0.7%	1.4%
	ROL-R	1.1%	0.6%	1.2%	1.8%	0.7%	1.4%
	STG-R	7.5%	14.0%	13.6%	10.0%	18.1%	14.3%
	TPOsup-R	27.9%	15.4%	25.8%	28.4%	14.7%	26.9%
	MTG-R	39.3%	65.0%	51.8%	35.6%	61.5%	49.0%
	TPOmid-R	9.4%	2.4%	2.6%	8.9%	2.3%	3.1%
	ITG-R	3.0%	0.9%	0.6%	2.9%	1.0%	0.6%
TP7	STG-L	3.0%	2.9%	1.7%	4.2%	3.3%	2.2%
	MTG-L	66.8%	93.0%	87.9%	70.4%	91.2%	86.7%
	ITG-L	30.1%	4.0%	10.4%	25.3%	5.5%	11.1%

Table S2-7 Normalized PPL of corresponding brain regions ($L_{norm,M}$) for the circumferential and vertical SD pairs set at 10/10 fiducial points at 10-mm SD distance from 0-yo, 1-yo, and 2-yo.

SD distance = 10 mm		Circumferential SD pair			Vertical channel SD pair		
10/10 Points	AAL regions	0 year	1 year	2 year	0 year	1 year	2 year
T5	STG-L	0.6%	1.0%	0.7%	0.9%	1.4%	0.7%
	MTG-L	82.8%	93.5%	92.2%	80.1%	93.6%	90.7%
	ITG-L	16.2%	4.8%	6.6%	18.6%	4.3%	7.9%
PO7	MOG-L	44.2%	42.0%	54.4%	40.4%	46.4%	54.4%
	ANG-L	0.6%	1.5%	0.6%	0.7%	1.9%	0.7%
	MTG-L	54.2%	55.9%	44.3%	55.2%	51.1%	44.1%
O1	SOG-L	18.4%	14.9%	26.6%	10.5%	11.4%	26.6%
	MOG-L	79.8%	84.0%	71.8%	87.9%	87.5%	71.7%
O2	CUN-R	5.8%	8.1%	4.0%	3.9%	6.7%	3.6%
	SOG-R	69.4%	79.0%	61.1%	73.3%	80.2%	61.1%
	MOG-R	23.0%	12.1%	34.3%	21.1%	12.2%	34.7%
PO8	SOG-R	0.7%	1.2%	0.5%	0.5%	1.3%	0.5%
	MOG-R	95.3%	94.6%	89.9%	95.8%	95.3%	90.4%
	ANG-R	1.3%	2.4%	3.8%	1.3%	2.0%	4.4%
	MTG-R	1.9%	1.2%	5.5%	1.3%	0.8%	4.3%
T6	MOG-R	10.7%	12.5%	6.2%	7.9%	9.0%	5.3%
	IOG-R	7.7%	4.2%	1.5%	9.3%	3.7%	1.6%
	ANG-R	1.3%	2.3%	2.4%	1.7%	2.8%	2.5%
	STG-R	0.4%	0.3%	1.1%	0.4%	0.4%	1.0%
	MTG-R	67.3%	77.9%	86.4%	67.8%	81.5%	86.9%
	ITG-R	12.4%	2.5%	2.0%	12.7%	2.3%	2.1%
TP8	STG-R	0.7%	1.5%	3.8%	1.1%	1.7%	3.9%
	MTG-R	75.8%	93.4%	93.1%	75.4%	91.5%	91.9%
	ITG-R	23.2%	4.9%	2.7%	23.3%	6.5%	3.8%

Table S2-8 Normalized PPL of corresponding brain regions ($L_{norm,M}$) for the circumferential and vertical SD pairs set at 10/10 fiducial points at 10-mm SD distance from 0-yo, 1-yo, and 2-yo.

SD distance = 10 mm		Circumferential SD pair			Vertical channel SD pair		
10/10 Points	AAL regions	0 year	1 year	2 year	0 year	1 year	2 year
FC5	PreCG-L	7.8%	14.5%	16.3%	13.2%	10.3%	14.4%
	IFGoperc-L	22.1%	38.8%	38.7%	37.9%	57.6%	49.6%
	IFGtriang-L	46.7%	23.6%	23.7%	28.2%	20.0%	20.4%
	ORBinf-L	2.2%	0.3%	0.3%	1.5%	0.3%	0.3%
	ROL-L	9.3%	18.6%	16.0%	7.9%	8.7%	10.7%
	PoCG-L	2.3%	1.6%	1.2%	2.5%	0.8%	0.8%
	STG-L	2.1%	0.7%	0.8%	1.8%	0.4%	0.7%
	TPOsup-L	6.1%	1.5%	2.6%	5.8%	1.4%	2.8%
FC3	PreCG-L	15.8%	14.9%	10.1%	10.9%	8.1%	9.2%
	MFG-L	56.2%	65.6%	71.6%	55.2%	71.0%	66.9%
	IFGoperc-L	19.7%	15.7%	13.4%	24.4%	17.7%	18.3%
	IFGtriang-L	6.9%	3.5%	4.3%	8.5%	3.0%	5.0%
	PoCG-L	1.0%	0.2%	0.3%	0.8%	0.1%	0.3%
FC1	PreCG-L	4.9%	0.2%	0.1%	1.2%	0.1%	0.1%
	SFGdor-L	37.2%	42.8%	48.8%	39.0%	48.0%	52.2%
	MFG-L	55.6%	55.8%	49.1%	57.4%	50.5%	45.3%
	SFGmed-L	1.1%	0.4%	1.2%	0.9%	0.5%	1.4%
FC2	PreCG-R	3.1%	0.1%	0.2%	7.0%	0.1%	0.2%
	SFGdor-R	31.5%	34.6%	23.1%	32.5%	33.6%	24.9%
	MFG-R	61.4%	62.3%	74.6%	57.1%	63.5%	72.9%
	SMA-R	1.8%	1.3%	0.7%	1.7%	1.5%	0.7%
	SFGmed-R	1.4%	1.6%	1.2%	1.0%	1.2%	1.2%
FC4	PreCG-R	21.9%	16.5%	9.0%	15.8%	13.1%	8.4%
	MFG-R	63.8%	77.9%	82.6%	63.1%	81.0%	82.5%
	IFGoperc-R	6.8%	2.8%	4.1%	12.4%	3.3%	4.7%
	IFGtriang-R	4.9%	2.2%	3.9%	5.8%	2.1%	4.0%
	PoCG-R	2.2%	0.5%	0.3%	2.5%	0.4%	0.3%

Table S2-9 Normalized PPL of corresponding brain regions ($L_{norm,M}$) for the circumferential and vertical SD pairs set at 10/10 fiducial points at 10-mm SD distance from 0-yo, 1-yo, and 2-yo.

SD distance = 10 mm		Circumferential SD pair			Vertical channel SD pair		
10/10 Points	AAL regions	0 year	1 year	2 year	0 year	1 year	2 year
FC6	PreCG-R	5.1%	12.9%	9.2%	6.9%	17.6%	8.6%
	MFG-R	1.8%	0.5%	1.1%	1.9%	0.7%	1.1%
	IFGoperc-R	33.2%	33.8%	37.7%	35.1%	35.8%	43.2%
	IFGtriang-R	32.0%	13.5%	35.2%	26.6%	12.2%	30.8%
	ORBinf-R	1.2%	0.1%	0.1%	1.3%	0.1%	0.1%
	ROL-R	7.7%	9.6%	5.3%	7.9%	11.4%	6.0%
	PoCG-R	10.2%	26.9%	9.3%	9.9%	19.4%	7.7%
	STG-R	4.5%	1.8%	1.2%	5.2%	2.0%	1.5%
	TPOsup-R	2.6%	0.6%	0.7%	3.3%	0.7%	0.9%
	MTG-R	1.2%	0.2%	0.1%	1.4%	0.2%	0.1%
F5	MFG-L	33.9%	23.0%	18.8%	23.6%	22.4%	15.8%
	ORBmid-L	2.0%	0.3%	0.6%	1.9%	0.3%	0.5%
	IFGtriang-L	57.0%	74.6%	76.2%	64.9%	74.5%	79.2%
	ORBinf-L	5.7%	1.9%	3.9%	8.1%	2.5%	4.2%
F3	SFGdor-L	1.3%	0.5%	1.0%	1.4%	0.6%	1.0%
	MFG-L	94.2%	97.6%	95.4%	93.4%	97.7%	96.2%
	IFGtriang-L	3.9%	1.8%	3.4%	4.4%	1.6%	2.6%
F1	SFGdor-L	44.8%	60.6%	62.5%	53.8%	65.2%	63.6%
	MFG-L	47.7%	35.5%	31.0%	38.4%	31.5%	31.0%
	SFGmed-R	1.0%	0.1%	0.5%	1.1%	0.1%	0.5%
	SFGmed-L	6.0%	3.8%	6.0%	6.2%	3.1%	4.9%
F2	SFGdor-R	70.7%	80.1%	69.4%	67.0%	83.7%	71.3%
	MFG-R	18.6%	11.1%	25.1%	20.0%	9.9%	23.7%
	SFGmed-R	9.0%	8.5%	5.1%	10.7%	6.1%	4.7%
	SFGmed-L	1.1%	0.2%	0.3%	1.4%	0.2%	0.3%
F4	SFGdor-R	3.9%	0.8%	1.7%	3.8%	0.9%	1.4%
	MFG-R	90.1%	96.0%	94.3%	90.4%	96.8%	94.0%
	IFGtriang-R	5.1%	3.1%	3.8%	4.8%	2.2%	4.5%

Table S2-10 Normalized PPL of corresponding brain regions ($L_{norm,M}$) for the circumferential and vertical SD pairs set at 10/10 fiducial points at 10-mm SD distance from 0-yo, 1-yo, and 2-yo.

SD distance = 10 mm		Circumferential SD pair			Vertical channel SD pair		
10/10 Points	AAL regions	0 year	1 year	2 year	0 year	1 year	2 year
F6	MFG-R	28.8%	12.8%	13.6%	27.4%	9.7%	13.2%
	ORBmid-R	1.8%	0.3%	0.6%	1.8%	0.4%	0.6%
	IFGoperc-R	1.1%	0.5%	0.2%	1.0%	0.5%	0.2%
	IFGtriang-R	63.9%	85.4%	84.6%	64.9%	88.1%	84.9%
	ORBinf-R	3.3%	0.8%	0.8%	3.8%	1.1%	0.9%
AF3	SFGdor-L	44.9%	44.3%	50.1%	38.2%	38.8%	52.6%
	ORBsup-L	1.1%	0.8%	1.4%	1.2%	0.5%	1.4%
	MFG-L	46.1%	52.4%	43.8%	53.3%	58.7%	41.7%
	ORBmid-L	2.5%	1.5%	2.0%	2.9%	1.1%	2.0%
	SFGmed-L	3.7%	0.8%	2.3%	2.9%	0.7%	2.0%
AF4	SFGdor-R	44.6%	49.6%	32.6%	52.3%	60.5%	32.9%
	MFG-R	44.8%	47.2%	63.8%	37.6%	36.0%	63.2%
	ORBmid-R	1.7%	0.5%	1.2%	1.8%	0.5%	1.4%
	SFGmed-R	6.0%	2.2%	1.5%	5.4%	2.5%	1.4%
CP5	PoCG-L	1.5%	0.2%	0.2%	1.0%	0.2%	0.2%
	SMG-L	21.0%	50.9%	44.6%	30.4%	50.9%	44.5%
	STG-L	72.4%	46.5%	52.3%	61.4%	46.5%	52.3%
	MTG-L	4.6%	1.3%	1.9%	6.8%	1.6%	2.1%
CP3	PoCG-L	5.7%	6.4%	5.9%	6.5%	5.4%	4.9%
	SPG-L	0.8%	0.8%	1.3%	0.8%	1.2%	1.2%
	IPL-L	43.0%	75.0%	67.9%	36.0%	74.2%	68.8%
	SMG-L	49.8%	17.6%	24.1%	56.0%	18.9%	24.3%
CP1	PreCG-L	8.7%	4.6%	6.7%	9.9%	5.2%	7.0%
	PoCG-L	68.1%	71.1%	69.1%	58.0%	70.3%	68.3%
	SPG-L	19.6%	22.4%	21.9%	27.5%	22.5%	22.2%
	IPL-L	2.5%	1.6%	1.8%	3.4%	1.6%	2.0%

Table S2-11 Normalized PPL of corresponding brain regions ($L_{norm,M}$) for the circumferential and vertical SD pairs set at 10/10 fiducial points at 10-mm SD distance from 0-yo, 1-yo, and 2-yo.

SD distance = 10 mm		Circumferential SD pair			Vertical channel SD pair		
10/10 Points	AAL regions	0 year	1 year	2 year	0 year	1 year	2 year
CP2	PreCG-R	8.2%	2.3%	4.5%	7.2%	2.6%	4.8%
	PoCG-R	60.1%	57.5%	64.7%	57.6%	58.3%	64.7%
	SPG-R	24.8%	35.1%	26.1%	28.1%	34.2%	25.6%
	IPL-R	1.4%	1.1%	1.7%	1.8%	1.5%	1.9%
	PCUN-R	2.3%	2.4%	1.2%	1.9%	1.8%	1.1%
	PCL-R	1.9%	1.4%	1.4%	2.1%	1.4%	1.5%
CP4	PoCG-R	11.9%	7.5%	15.1%	14.3%	9.1%	17.1%
	IPL-R	82.1%	90.4%	82.5%	80.1%	88.9%	80.4%
	SMG-R	3.4%	0.6%	1.0%	3.1%	0.5%	1.1%
	ANG-R	1.3%	0.8%	0.4%	1.2%	0.8%	0.4%
CP6	PoCG-R	1.2%	0.3%	0.7%	1.1%	0.2%	0.7%
	IPL-R	2.9%	4.8%	5.0%	4.4%	6.1%	4.9%
	SMG-R	48.8%	64.4%	77.0%	52.8%	61.0%	73.9%
	ANG-R	2.2%	1.6%	1.1%	1.4%	1.6%	0.9%
	STG-R	33.7%	26.5%	14.9%	31.3%	28.3%	18.2%
	MTG-R	11.1%	2.3%	1.3%	8.9%	2.7%	1.5%
P5	MOG-L	3.9%	0.8%	1.4%	1.4%	0.8%	1.3%
	IPL-L	0.7%	3.1%	3.2%	1.0%	3.9%	3.4%
	SMG-L	3.4%	1.7%	1.3%	2.9%	1.1%	1.2%
	ANG-L	45.6%	78.9%	80.1%	43.7%	75.7%	75.1%
	STG-L	19.6%	6.7%	3.3%	14.5%	6.0%	3.0%
	MTG-L	26.8%	8.9%	10.7%	36.5%	12.5%	16.0%
P3	SPG-L	2.6%	3.0%	2.5%	2.4%	2.8%	2.7%
	IPL-L	37.1%	45.1%	28.1%	33.8%	30.7%	27.9%
	ANG-L	59.1%	51.6%	68.9%	62.6%	66.2%	69.1%

Table S2-12 Normalized PPL of corresponding brain regions ($L_{norm,M}$) for the circumferential and vertical SD pairs set at 10/10 fiducial points at 10-mm SD distance from 0-yo, 1-yo, and 2-yo.

SD distance = 10 mm		Circumferential SD pair			Vertical channel SD pair		
10/10 Points	AAL regions	0 year	1 year	2 year	0 year	1 year	2 year
P1	SPG-L	81.5%	91.5%	90.0%	80.7%	91.9%	89.2%
	IPL-L	6.8%	2.9%	3.4%	5.5%	2.3%	3.3%
	ANG-L	9.3%	4.5%	5.1%	11.6%	4.8%	6.0%
P2	SPG-R	68.0%	74.0%	83.0%	72.7%	73.9%	83.7%
	IPL-R	2.2%	0.7%	1.6%	2.3%	0.8%	2.2%
	ANG-R	1.7%	0.4%	1.0%	1.6%	0.4%	1.3%
	PCUN-R	24.5%	24.2%	13.4%	20.0%	24.1%	11.9%
P4	MOG-R	1.9%	0.5%	0.6%	3.5%	0.6%	0.6%
	SPG-R	6.6%	11.7%	10.8%	7.5%	12.5%	10.7%
	IPL-R	18.2%	12.3%	24.4%	12.1%	10.8%	22.5%
	ANG-R	72.5%	75.3%	63.8%	76.3%	75.9%	65.8%
P6	MOG-R	6.8%	3.0%	1.3%	4.5%	3.0%	1.1%
	IPL-R	1.5%	2.2%	4.3%	2.2%	2.7%	6.0%
	SMG-R	4.4%	1.1%	3.9%	1.7%	0.8%	3.3%
	ANG-R	76.7%	90.1%	87.3%	83.4%	90.8%	86.7%
	MTG-R	9.7%	3.5%	3.0%	7.9%	2.6%	2.7%
PO3	SOG-L	14.1%	21.7%	19.6%	11.3%	16.1%	16.0%
	MOG-L	37.2%	20.3%	23.5%	49.2%	23.8%	28.3%
	SPG-L	4.3%	5.6%	4.5%	5.3%	5.8%	4.4%
	ANG-L	43.6%	51.8%	51.7%	33.4%	53.8%	50.7%
PO4	CUN-R	1.5%	1.0%	0.4%	1.6%	0.9%	0.4%
	SOG-R	45.7%	47.8%	25.0%	50.7%	49.2%	25.3%
	MOG-R	31.7%	24.9%	32.8%	23.4%	24.2%	31.1%
	SPG-R	2.9%	4.9%	5.3%	5.3%	6.7%	6.9%
	IPL-R	15.5%	19.8%	33.6%	15.8%	17.6%	33.9%
	ANG-R	1.3%	0.8%	2.3%	1.4%	0.7%	1.6%

Table S3-1 Normalized PPL of corresponding brain regions ($L_{norm,M}$) for the circumferential and vertical SD pairs set at 10/10 fiducial points at 15-mm SD distance from 0-yo, 1-yo, and 2-yo.

SD distance = 15 mm		Circumferential SD pair			Vertical SD pair		
10/10 Point	AAL regions	0 year	1 year	2 year	0 year	1 year	2 year
Cz	PreCG-R	2.1%	0.5%	0.5%	1.4%	0.3%	0.4%
	PreCG-L	6.0%	1.9%	1.1%	7.8%	2.4%	1.5%
	SFGdor-R	11.0%	4.0%	5.0%	5.1%	2.1%	3.3%
	SFGdor-L	20.8%	15.1%	9.9%	15.1%	11.5%	7.0%
	SMA-R	21.9%	41.5%	41.5%	17.2%	29.0%	42.7%
	SMA-L	19.1%	32.2%	38.5%	30.7%	47.0%	38.9%
	PoCG-L	4.4%	0.3%	0.2%	5.1%	0.4%	0.3%
	SPG-L	3.9%	0.0%	0.0%	2.5%	0.0%	0.0%
	PCL-R	6.1%	3.3%	2.3%	7.7%	5.1%	4.1%
	PCL-L	2.0%	0.8%	0.6%	4.6%	1.7%	1.3%
Fpz	SFGdor-R	5.2%	2.3%	2.7%	2.9%	1.3%	2.5%
	SFGdor-L	8.4%	7.2%	1.4%	6.6%	5.1%	1.3%
	ORBsup-R	3.8%	2.9%	6.2%	2.4%	2.0%	5.0%
	ORBsup-L	8.5%	13.8%	7.6%	7.5%	11.0%	5.8%
	ORBmid-L	1.9%	1.1%	0.9%	1.7%	1.0%	0.7%
	SFGmed-R	20.7%	11.7%	7.8%	19.6%	10.3%	11.1%
	SFGmed-L	20.7%	18.6%	8.0%	27.6%	22.5%	10.1%
	ORBmed-R	13.7%	19.0%	31.0%	12.6%	16.1%	32.6%
	ORBmed-L	13.4%	21.7%	30.0%	15.8%	28.3%	25.8%
	REC-R	1.0%	1.1%	2.8%	1.1%	1.4%	3.5%
AFz	SFGdor-R	8.7%	2.7%	8.2%	4.5%	1.8%	5.1%
	SFGdor-L	18.5%	15.9%	5.8%	7.5%	9.4%	3.7%
	MFG-L	1.9%	0.9%	0.4%	1.3%	0.7%	0.3%
	SFGmed-R	35.9%	38.5%	49.3%	39.0%	33.2%	55.7%
	SFGmed-L	33.1%	41.3%	35.4%	45.7%	54.0%	34.2%

Table S3-2 Normalized PPL of corresponding brain regions ($L_{norm,M}$) for the circumferential and vertical SD pairs set at 10/10 fiducial points at 15-mm SD distance from 0-yo, 1-yo, and 2-yo.

SD distance = 15 mm		Circumferential SD pair			Vertical SD pair		
10/10 Point	AAL regions	0 year	1 year	2 year	0 year	1 year	2 year
Fz	SFGdor-R	8.3%	2.5%	8.5%	5.9%	2.0%	5.9%
	SFGdor-L	19.8%	25.0%	6.2%	9.3%	8.9%	4.1%
	MFG-L	1.2%	0.3%	0.3%	1.3%	0.4%	0.3%
	SMA-R	9.1%	0.1%	0.0%	1.6%	0.1%	0.0%
	SMA-L	3.0%	0.1%	0.0%	1.4%	0.1%	0.0%
	SFGmed-R	27.5%	29.2%	48.6%	39.4%	33.0%	55.3%
	SFGmed-L	30.4%	42.6%	35.9%	40.3%	55.3%	34.1%
FCz	SFGdor-R	10.3%	3.0%	6.4%	6.0%	1.5%	5.2%
	SFGdor-L	19.4%	6.8%	4.7%	10.9%	6.3%	3.0%
	SMA-R	24.1%	31.7%	17.8%	22.7%	15.1%	23.4%
	SMA-L	22.9%	23.8%	11.2%	26.7%	34.7%	12.4%
	SFGmed-R	8.0%	14.5%	30.7%	12.0%	12.2%	32.7%
	SFGmed-L	11.2%	19.8%	28.4%	18.6%	29.8%	22.7%
	PCL-R	1.2%	0.0%	0.0%	0.5%	0.0%	0.0%
CPz	PreCG-R	1.4%	0.2%	0.3%	0.7%	0.2%	0.3%
	PreCG-L	5.1%	1.7%	2.0%	6.0%	2.1%	1.9%
	SMA-R	1.1%	0.4%	0.5%	1.1%	0.5%	0.8%
	SMA-L	1.5%	0.8%	1.0%	2.0%	1.4%	1.7%
	PoCG-R	5.8%	1.4%	2.2%	2.0%	0.7%	1.6%
	PoCG-L	26.6%	27.0%	19.1%	22.6%	20.1%	11.3%
	SPG-R	1.8%	1.0%	1.0%	1.0%	0.6%	0.8%
	SPG-L	5.6%	4.4%	2.5%	9.4%	4.9%	2.4%
	PCUN-R	18.0%	19.2%	20.0%	11.1%	14.3%	20.6%
	PCUN-L	5.4%	11.6%	7.8%	12.3%	18.7%	10.7%
	PCL-R	16.0%	16.7%	25.4%	10.2%	15.5%	28.2%
	PCL-L	9.7%	15.4%	17.9%	19.8%	20.8%	19.5%

Table S3-3 Normalized PPL of corresponding brain regions ($L_{norm,M}$) for the circumferential and vertical SD pairs set at 10/10 fiducial points at 15-mm SD distance from 0-yo, 1-yo, and 2-yo.

SD distance = 15 mm		Circumferential SD pair			Vertical SD pair		
10/10 Point	AAL regions	0 year	1 year	2 year	0 year	1 year	2 year
Pz	PoCG-L	1.4%	0.6%	0.5%	2.4%	0.6%	0.5%
	SPG-R	4.2%	1.6%	2.1%	1.7%	0.9%	1.4%
	SPG-L	41.0%	36.1%	21.7%	40.3%	33.2%	16.1%
	PCUN-R	32.9%	31.7%	44.5%	22.7%	25.3%	44.4%
	PCUN-L	18.1%	29.4%	30.5%	30.2%	39.1%	37.0%
POz	CUN-R	13.8%	7.9%	9.4%	14.4%	9.4%	11.7%
	CUN-L	15.6%	23.6%	13.5%	18.0%	25.8%	13.9%
	SOG-R	15.2%	8.1%	11.6%	6.5%	5.9%	8.2%
	SOG-L	7.2%	4.7%	1.5%	6.5%	3.4%	1.2%
	MOG-L	1.3%	0.3%	0.1%	1.3%	0.2%	0.1%
	SPG-R	2.0%	2.4%	3.8%	1.0%	1.6%	2.3%
POz	SPG-L	22.4%	27.9%	23.7%	25.5%	24.3%	19.2%
	PCUN-R	14.2%	16.5%	25.6%	13.8%	17.3%	29.0%
	PCUN-L	6.5%	8.4%	10.4%	11.5%	11.9%	14.3%
Oz	CAL-R	3.4%	2.1%	3.0%	5.4%	3.5%	4.7%
	CUN-R	32.8%	29.7%	49.9%	27.4%	32.0%	54.6%
	CUN-L	17.2%	20.3%	20.1%	26.9%	29.1%	22.1%
	SOG-R	5.2%	4.7%	7.0%	2.9%	3.3%	5.0%
	SOG-L	35.7%	39.3%	17.7%	31.7%	28.9%	11.5%
	MOG-L	3.8%	2.7%	0.8%	2.9%	1.7%	0.5%
T3	STG-L	3.1%	6.3%	4.2%	5.0%	13.1%	6.3%
	TPOsup-L	1.6%	0.6%	0.5%	1.6%	0.7%	0.5%
	MTG-L	64.7%	88.2%	87.4%	64.0%	80.9%	83.6%
	TPOmid-L	3.7%	0.7%	0.8%	2.6%	0.6%	0.6%
	ITG-L	26.4%	4.2%	6.9%	26.4%	4.5%	8.9%

Table S3-4 Normalized PPL of corresponding brain regions ($L_{norm,M}$) for the circumferential and vertical SD pairs set at 10/10 fiducial points at 15-mm SD distance from 0-yo, 1-yo, and 2-yo.

SD distance = 15 mm		Circumferential SD pair			Vertical SD pair		
10/10 Point	AAL regions	0 year	1 year	2 year	0 year	1 year	2 year
C5	PreCG-L	2.4%	2.3%	2.0%	1.9%	1.3%	1.4%
	ROL-L	9.8%	12.9%	7.4%	6.6%	5.4%	4.0%
	PoCG-L	20.3%	43.5%	46.0%	31.8%	47.8%	48.3%
	SMG-L	5.7%	9.3%	11.6%	3.8%	8.8%	9.4%
	STG-L	54.9%	31.1%	31.6%	49.2%	35.9%	35.6%
	TPOsup-L	2.0%	0.3%	0.3%	1.4%	0.2%	0.2%
	MTG-L	3.2%	0.4%	0.6%	4.2%	0.5%	0.8%
C3	PreCG-L	32.9%	43.2%	32.0%	17.5%	31.0%	30.8%
	MFG-L	2.6%	4.0%	4.9%	11.8%	8.8%	7.4%
	PoCG-L	45.1%	47.7%	52.4%	62.2%	57.1%	55.0%
	SMG-L	18.1%	4.8%	10.1%	7.7%	2.9%	6.4%
C1	PreCG-L	49.3%	50.6%	44.5%	42.1%	48.1%	45.7%
	SFGdor-L	19.9%	25.1%	26.8%	33.0%	38.7%	33.3%
	MFG-L	23.5%	20.4%	25.4%	16.4%	8.9%	16.8%
	PoCG-L	5.9%	3.4%	2.8%	6.6%	3.1%	3.5%
C2	PreCG-R	46.6%	66.0%	48.4%	48.0%	61.9%	47.6%
	SFGdor-R	24.0%	14.2%	24.6%	32.8%	25.5%	32.2%
	MFG-R	18.8%	12.9%	22.1%	6.9%	5.5%	15.2%
	SMA-R	1.5%	0.6%	1.0%	1.5%	0.8%	1.5%
	PoCG-R	7.1%	5.8%	3.3%	8.8%	5.8%	2.9%
C4	PreCG-R	20.9%	19.0%	30.6%	13.5%	12.8%	31.9%
	MFG-R	1.8%	0.5%	1.7%	1.0%	0.5%	1.7%
	PoCG-R	45.8%	66.2%	59.1%	53.1%	76.8%	60.3%
	IPL-R	13.0%	11.2%	5.0%	8.1%	4.9%	2.5%
	SMG-R	17.9%	3.1%	3.5%	23.8%	5.0%	3.4%

Table S3-5 Normalized PPL of corresponding brain regions ($L_{norm,M}$) for the circumferential and vertical SD pairs set at 10/10 fiducial points at 15-mm SD distance from 0-yo, 1-yo, and 2-yo.

SD distance = 15 mm		Circumferential SD pair			Vertical SD pair		
10/10 Point	AAL regions	0 year	1 year	2 year	0 year	1 year	2 year
C6	PreCG-R	0.9%	0.4%	2.1%	1.5%	0.3%	1.6%
	IFGoperc-R	1.1%	0.1%	0.6%	0.9%	0.0%	0.4%
	ROL-R	5.9%	3.6%	2.7%	3.6%	1.3%	2.3%
	PoCG-R	24.2%	43.0%	60.9%	39.1%	40.1%	55.1%
	SMG-R	6.5%	12.7%	13.2%	5.7%	10.2%	8.8%
	STG-R	42.5%	37.1%	18.6%	30.5%	42.3%	28.6%
	MTG-R	16.9%	2.9%	1.7%	16.8%	5.7%	2.9%
T4	STG-R	1.3%	1.1%	2.7%	1.8%	1.6%	3.4%
	MTG-R	65.1%	81.8%	86.9%	66.2%	79.2%	85.4%
	ITG-R	31.8%	16.8%	9.7%	30.5%	19.0%	10.4%
FT7	IFGoperc-L	1.2%	1.1%	0.7%	2.1%	1.1%	1.0%
	IFGtriang-L	2.5%	1.1%	0.9%	3.2%	0.8%	1.1%
	ORBinf-L	8.9%	2.4%	2.2%	7.1%	1.3%	1.9%
	STG-L	3.9%	13.5%	7.8%	3.1%	8.8%	6.4%
	TPOsup-L	35.0%	42.4%	35.5%	42.1%	46.0%	41.9%
	MTG-L	17.4%	18.0%	25.0%	11.1%	15.6%	19.0%
	TPOmid-L	26.3%	19.5%	26.6%	25.6%	24.1%	27.3%
	ITG-L	2.9%	0.7%	0.8%	3.3%	0.8%	0.8%
F7	MFG-L	2.1%	0.6%	0.5%	2.3%	0.5%	0.4%
	ORBmid-L	10.0%	1.1%	1.9%	6.4%	0.7%	1.0%
	IFGtriang-L	13.2%	11.7%	7.7%	19.9%	24.1%	10.3%
	ORBinf-L	68.0%	79.6%	81.1%	65.7%	68.9%	80.8%
	TPOsup-L	5.0%	6.1%	7.7%	4.2%	4.9%	6.6%
AF7	SFGdor-L	2.1%	0.4%	0.5%	2.3%	0.4%	0.5%
	ORBsup-L	1.6%	0.5%	1.0%	1.5%	0.5%	1.0%
	MFG-L	15.3%	9.3%	6.3%	25.9%	16.1%	9.8%
	ORBmid-L	56.2%	60.3%	64.3%	53.4%	63.9%	71.2%
	IFGtriang-L	5.5%	2.8%	2.3%	4.4%	2.7%	2.1%
	ORBinf-L	18.7%	26.6%	25.3%	11.9%	16.3%	15.2%

Table S3-6 Normalized PPL of corresponding brain regions ($L_{norm,M}$) for the circumferential and vertical SD pairs set at 10/10 fiducial points at 15-mm SD distance from 0-yo, 1-yo, and 2-yo.

SD distance = 15 mm		Circumferential SD pair			Vertical SD pair		
10/10 Point	AAL regions	0 year	1 year	2 year	0 year	1 year	2 year
Fp1	SFGdor-L	24.5%	15.7%	6.6%	28.5%	22.4%	13.1%
	ORBsup-L	20.3%	39.2%	36.1%	21.6%	33.6%	37.3%
	MFG-L	14.3%	6.9%	2.4%	12.4%	8.2%	3.6%
	ORBmid-L	25.3%	32.5%	40.5%	25.5%	32.1%	37.2%
	SFGmed-R	1.3%	0.1%	0.2%	1.0%	0.1%	0.2%
	SFGmed-L	7.3%	2.3%	2.5%	5.6%	1.7%	2.3%
	ORBmed-L	4.6%	2.8%	10.3%	3.5%	1.7%	5.3%
Fp2	SFGdor-R	33.3%	28.3%	18.3%	37.8%	36.7%	22.4%
	ORBsup-R	14.7%	27.4%	29.4%	17.3%	26.9%	27.2%
	MFG-R	13.1%	6.2%	6.8%	9.3%	5.8%	8.8%
	ORBmid-R	15.6%	22.9%	35.1%	14.0%	19.7%	34.8%
	ORBinf-R	1.1%	0.1%	0.5%	0.8%	0.1%	0.5%
	SFGmed-R	10.9%	5.0%	2.3%	10.1%	4.1%	1.7%
	SFGmed-L	1.4%	0.2%	0.2%	1.3%	0.2%	0.1%
	ORBmed-R	7.1%	9.2%	6.2%	6.6%	5.8%	3.5%
	ORBmed-L	1.1%	0.2%	0.4%	1.0%	0.2%	0.3%
AF8	SFGdor-R	5.4%	0.7%	0.9%	4.2%	0.4%	0.8%
	ORBsup-R	2.3%	0.4%	1.0%	1.8%	0.3%	0.8%
	MFG-R	26.1%	15.2%	9.3%	34.9%	17.3%	16.6%
	ORBmid-R	43.6%	66.7%	64.0%	40.6%	62.8%	62.5%
	IFGtriang-R	6.9%	5.1%	4.3%	5.4%	4.0%	4.7%
	ORBinf-R	14.7%	11.8%	20.1%	12.3%	15.1%	14.3%
F8	MFG-R	3.4%	0.2%	0.7%	2.7%	0.2%	0.8%
	ORBmid-R	8.4%	0.4%	2.2%	4.8%	0.4%	1.9%
	IFGtriang-R	24.2%	16.7%	31.3%	28.6%	28.8%	38.0%
	ORBinf-R	58.1%	74.2%	53.1%	58.4%	64.1%	49.5%
	TPOsup-R	3.7%	6.9%	10.5%	3.5%	5.1%	8.0%

Table S3-7 Normalized PPL of corresponding brain regions ($L_{norm,M}$) for the circumferential and vertical SD pairs set at 10/10 fiducial points at 15-mm SD distance from 0-yo, 1-yo, and 2-yo.

SD distance = 15 mm		Circumferential SD pair			Vertical SD pair		
10/10 Point	AAL regions	0 year	1 year	2 year	0 year	1 year	2 year
FT8	IFGoperc-R	2.1%	0.4%	1.4%	3.2%	0.6%	1.7%
	IFGtriang-R	4.4%	0.6%	1.9%	4.5%	0.7%	1.9%
	ORBinf-R	11.2%	1.0%	2.1%	7.7%	0.9%	1.7%
	ROL-R	1.6%	0.6%	1.4%	2.3%	0.9%	1.7%
	STG-R	9.3%	11.0%	13.0%	9.4%	18.3%	13.4%
	TPOsup-R	25.6%	17.5%	25.8%	29.6%	15.7%	26.3%
	MTG-R	35.5%	64.0%	50.1%	28.6%	58.0%	48.0%
	TPOmid-R	6.4%	3.3%	3.2%	10.2%	3.2%	4.1%
	ITG-R	2.6%	1.3%	0.7%	3.1%	1.5%	0.9%
TP7	STG-L	3.9%	3.7%	2.2%	7.9%	8.1%	2.8%
	MTG-L	63.5%	90.7%	85.2%	64.0%	81.8%	78.5%
	ITG-L	32.4%	5.6%	12.5%	27.9%	10.0%	18.7%
T5	STG-L	1.0%	1.8%	0.7%	1.8%	2.2%	1.0%
	MTG-L	81.0%	92.5%	89.2%	74.7%	89.7%	85.7%
	ITG-L	17.2%	4.7%	9.2%	22.9%	6.8%	12.4%
PO7	MOG-L	45.5%	47.1%	52.0%	37.7%	50.4%	57.3%
	IOG-L	1.1%	0.3%	0.5%	3.9%	0.5%	0.8%
	ANG-L	0.7%	2.2%	0.9%	1.4%	3.2%	1.2%
	MTG-L	51.3%	50.0%	46.3%	53.1%	45.4%	40.3%
	ITG-L	1.2%	0.3%	0.2%	3.7%	0.4%	0.3%
O1	SOG-L	22.0%	19.1%	27.4%	16.3%	11.6%	23.1%
	MOG-L	75.2%	79.3%	70.5%	80.6%	86.8%	74.7%
O2	CAL-R	1.4%	0.6%	0.2%	1.5%	0.7%	0.2%
	CUN-R	8.4%	10.7%	4.8%	4.4%	8.7%	3.6%
	SOG-R	59.7%	72.0%	53.6%	62.2%	75.4%	56.4%
	MOG-R	29.1%	16.1%	40.8%	30.6%	14.4%	39.2%

Table S3-8 Normalized PPL of corresponding brain regions ($L_{norm,M}$) for the circumferential and vertical SD pairs set at 10/10 fiducial points at 15-mm SD distance from 0-yo, 1-yo, and 2-yo.

SD distance = 15 mm		Circumferential SD pair			Vertical SD pair		
10/10 Point	AAL regions	0 year	1 year	2 year	0 year	1 year	2 year
PO8	SOG-R	1.4%	1.8%	0.6%	0.6%	1.2%	0.6%
	MOG-R	92.4%	92.1%	87.2%	94.3%	92.1%	89.2%
	IOG-R	1.0%	0.6%	0.4%	1.2%	0.6%	0.3%
	ANG-R	1.9%	3.4%	4.3%	2.0%	4.2%	5.3%
	MTG-R	3.0%	1.9%	7.4%	1.6%	1.5%	4.5%
T6	MOG-R	12.6%	17.4%	7.2%	9.7%	13.6%	6.6%
	IOG-R	6.4%	4.9%	1.3%	13.4%	7.1%	2.3%
	ANG-R	1.9%	2.8%	3.3%	3.1%	4.1%	3.5%
	STG-R	0.8%	0.4%	1.5%	0.6%	0.4%	1.3%
	MTG-R	66.6%	71.4%	84.2%	59.3%	71.3%	83.1%
	ITG-R	11.3%	2.8%	1.7%	13.4%	3.0%	2.3%
TP8	STG-R	1.2%	2.0%	4.3%	1.5%	2.5%	5.5%
	MTG-R	75.1%	91.3%	91.8%	68.6%	87.6%	89.4%
	ITG-R	23.2%	6.4%	3.6%	29.5%	9.6%	4.7%
FC5	PreCG-L	8.7%	17.0%	14.2%	12.6%	13.9%	12.2%
	MFG-L	1.1%	0.4%	0.4%	1.0%	0.5%	0.4%
	IFGoperc-L	17.0%	30.8%	30.5%	30.9%	49.8%	48.4%
	IFGtriang-L	44.1%	28.2%	27.6%	32.2%	18.0%	22.9%
	ORBinf-L	2.6%	0.4%	0.4%	2.6%	0.5%	0.4%
	ROL-L	12.5%	17.7%	20.4%	7.0%	12.2%	10.0%
	PoCG-L	4.1%	2.8%	2.0%	2.7%	1.5%	1.1%
	STG-L	2.9%	0.9%	1.2%	2.1%	0.8%	0.8%
	TPOsup-L	6.0%	1.8%	3.1%	7.9%	2.7%	3.6%
FC3	PreCG-L	22.9%	20.7%	13.0%	11.3%	10.4%	8.1%
	MFG-L	51.1%	61.8%	68.5%	56.6%	65.9%	63.7%
	IFGoperc-L	16.2%	13.0%	12.9%	19.9%	19.1%	20.1%
	IFGtriang-L	7.6%	4.1%	4.8%	10.7%	4.2%	7.5%
	PoCG-L	1.7%	0.3%	0.5%	1.0%	0.2%	0.3%

Table S3-9 Normalized PPL of corresponding brain regions ($L_{norm,M}$) for the circumferential and vertical SD pairs set at 10/10 fiducial points at 15-mm SD distance from 0-yo, 1-yo, and 2-yo.

SD distance = 15 mm		Circumferential SD pair			Vertical SD pair		
10/10 Point	AAL regions	0 year	1 year	2 year	0 year	1 year	2 year
FC1	PreCG-L	7.8%	0.2%	0.2%	3.8%	0.2%	0.1%
	SFGdor-L	32.4%	43.4%	48.3%	39.5%	45.5%	48.4%
	MFG-L	56.8%	54.6%	48.6%	52.8%	52.3%	48.5%
	SFGmed-L	1.4%	0.8%	1.7%	1.3%	0.6%	1.6%
FC2	PreCG-R	2.9%	0.2%	0.3%	2.7%	0.2%	0.3%
	SFGdor-R	38.4%	38.3%	26.5%	43.9%	36.1%	24.8%
	MFG-R	51.9%	57.4%	70.5%	47.4%	60.0%	72.5%
	SMA-R	2.9%	1.7%	0.8%	3.1%	2.2%	0.9%
	SFGmed-R	2.5%	2.2%	1.6%	1.5%	1.4%	1.3%
FC4	PreCG-R	23.8%	18.6%	11.2%	12.9%	11.7%	7.1%
	MFG-R	62.1%	75.9%	81.1%	61.3%	80.8%	81.5%
	IFGoperc-R	5.7%	2.3%	3.4%	14.8%	4.0%	5.1%
	IFGtriang-R	5.3%	2.5%	3.7%	8.4%	3.1%	5.8%
	PoCG-R	2.5%	0.6%	0.4%	2.0%	0.4%	0.3%
FC6	PreCG-R	5.8%	10.3%	9.2%	9.0%	20.3%	9.2%
	MFG-R	2.5%	0.6%	1.3%	3.1%	0.8%	1.5%
	IFGoperc-R	24.1%	28.0%	31.0%	29.4%	27.5%	39.1%
	IFGtriang-R	36.0%	20.3%	38.2%	30.0%	11.0%	33.3%
	ORBinf-R	1.4%	0.1%	0.1%	1.6%	0.1%	0.1%
	ROL-R	7.4%	9.6%	6.2%	6.7%	14.6%	6.3%
	PoCG-R	13.5%	27.4%	11.2%	9.5%	20.4%	7.2%
	STG-R	4.8%	2.5%	1.7%	5.1%	3.6%	1.8%
	TPOsup-R	2.6%	0.8%	0.9%	3.7%	1.3%	1.3%
	MTG-R	1.3%	0.3%	0.2%	1.4%	0.3%	0.2%
F5	MFG-L	29.1%	25.8%	23.8%	26.9%	24.1%	19.3%
	ORBmid-L	2.7%	0.4%	0.6%	2.7%	0.4%	0.7%
	IFGoperc-L	1.1%	0.5%	0.4%	0.8%	0.3%	0.3%
	IFGtriang-L	58.6%	70.7%	71.3%	57.4%	71.3%	73.2%
	ORBinf-L	7.3%	2.4%	3.7%	11.3%	3.8%	6.3%

Table S3-10 Normalized PPL of corresponding brain regions ($L_{norm,M}$) for the circumferential and vertical SD pairs set at 10/10 fiducial points at 15-mm SD distance from 0-yo, 1-yo, and 2-yo.

SD distance = 15 mm		Circumferential SD pair			Vertical SD pair		
10/10 Point	AAL regions	0 year	1 year	2 year	0 year	1 year	2 year
F3	SFGdor-L	2.6%	0.8%	1.1%	2.1%	0.9%	1.2%
	MFG-L	90.7%	96.7%	94.0%	91.7%	96.7%	95.0%
	IFGtriang-L	5.5%	2.4%	4.6%	5.0%	2.3%	3.5%
F1	SFGdor-L	40.1%	51.7%	54.2%	47.6%	64.9%	59.8%
	MFG-L	46.8%	41.9%	35.2%	42.8%	31.3%	32.6%
	SFGmed-R	1.9%	0.2%	0.9%	1.5%	0.2%	0.7%
	SFGmed-L	10.5%	6.0%	9.6%	7.4%	3.6%	6.7%
F2	SFGdor-R	59.4%	70.4%	63.3%	59.0%	76.8%	66.1%
	MFG-R	23.3%	17.3%	29.1%	26.1%	13.8%	28.2%
	SFGmed-R	14.6%	11.9%	7.1%	11.9%	9.0%	5.3%
	SFGmed-L	1.8%	0.3%	0.4%	1.7%	0.4%	0.3%
F4	SFGdor-R	5.0%	2.3%	2.1%	4.9%	1.6%	2.0%
	MFG-R	86.2%	94.2%	92.0%	87.5%	94.8%	93.1%
	IFGtriang-R	7.3%	3.3%	5.6%	6.3%	3.5%	4.7%
F6	MFG-R	30.6%	15.3%	14.8%	31.8%	11.7%	17.6%
	ORBmid-R	2.2%	0.5%	1.0%	3.0%	0.7%	0.8%
	IFGoperc-R	1.6%	0.8%	0.3%	1.1%	0.6%	0.2%
	IFGtriang-R	60.3%	81.9%	82.5%	56.9%	84.3%	79.9%
	ORBinf-R	3.7%	1.2%	1.1%	5.6%	2.4%	1.2%
AF3	SFGdor-L	37.4%	44.1%	48.1%	36.4%	33.3%	47.1%
	ORBsup-L	1.2%	0.8%	1.3%	1.9%	0.9%	2.1%
	MFG-L	50.8%	52.2%	44.9%	51.5%	62.9%	45.0%
	ORBmid-L	2.6%	1.2%	1.9%	4.0%	1.7%	2.8%
	SFGmed-L	5.6%	1.4%	3.3%	4.0%	0.9%	2.5%
AF4	SFGdor-R	42.9%	50.2%	34.9%	47.0%	57.0%	32.0%
	MFG-R	42.7%	45.0%	60.6%	41.9%	38.4%	63.2%
	ORBmid-R	1.8%	0.5%	1.4%	2.4%	0.8%	1.9%
	SFGmed-R	8.7%	3.7%	1.9%	5.3%	3.0%	1.7%

Table S3-11 Normalized PPL of corresponding brain regions ($L_{norm,M}$) for the circumferential and vertical SD pairs set at 10/10 fiducial points at 15-mm SD distance from 0-yo, 1-yo, and 2-yo.

SD distance = 15 mm		Circumferential SD pair			Vertical SD pair		
10/10 Point	AAL regions	0 year	1 year	2 year	0 year	1 year	2 year
CP5	PoCG-L	1.9%	0.5%	0.4%	1.4%	0.4%	0.3%
	SMG-L	23.2%	52.3%	47.6%	35.0%	48.2%	45.6%
	ANG-L	0.7%	1.7%	1.5%	0.3%	0.7%	0.9%
	STG-L	67.7%	43.5%	47.9%	52.3%	47.7%	49.6%
	MTG-L	6.4%	1.7%	2.3%	10.8%	2.8%	3.3%
CP3	PoCG-L	8.4%	11.2%	7.0%	9.3%	8.9%	7.4%
	SPG-L	1.1%	1.4%	1.5%	1.0%	1.3%	1.5%
	IPL-L	42.8%	61.9%	62.3%	33.0%	59.9%	62.0%
	SMG-L	46.8%	25.1%	28.2%	55.5%	29.5%	27.9%
CP1	PreCG-L	11.9%	7.1%	6.8%	14.6%	7.8%	8.6%
	PoCG-L	56.9%	66.9%	63.6%	48.6%	66.0%	63.1%
	SPG-L	26.4%	23.7%	26.7%	30.0%	23.7%	24.9%
	IPL-L	3.0%	1.7%	2.2%	5.1%	2.0%	2.7%
CP2	PreCG-R	9.7%	3.0%	5.0%	8.6%	3.5%	5.6%
	PoCG-R	51.3%	53.9%	60.9%	47.2%	55.6%	61.4%
	SPG-R	29.6%	36.2%	28.4%	34.2%	34.1%	26.9%
	IPL-R	2.0%	1.4%	2.3%	2.8%	1.9%	2.3%
	PCUN-R	3.4%	3.6%	1.5%	2.5%	2.3%	1.3%
	PCL-R	2.1%	1.7%	1.5%	2.8%	2.2%	1.9%
CP4	PoCG-R	14.8%	9.6%	19.0%	15.1%	15.2%	20.2%
	SPG-R	1.5%	0.8%	0.8%	0.9%	1.0%	0.8%
	IPL-R	77.1%	87.5%	78.0%	76.5%	82.1%	76.7%
	SMG-R	3.6%	0.9%	1.2%	4.7%	0.7%	1.3%
	ANG-R	2.1%	1.1%	0.5%	2.1%	0.9%	0.5%

Table S3-12 Normalized PPL of corresponding brain regions ($L_{norm,M}$) for the circumferential and vertical SD pairs set at 10/10 fiducial points at 15-mm SD distance from 0-yo, 1-yo, and 2-yo.

SD distance = 15 mm		Circumferential SD pair			Vertical SD pair		
10/10 Point	AAL regions	0 year	1 year	2 year	0 year	1 year	2 year
CP6	PoCG-R	1.8%	0.3%	1.0%	1.2%	0.3%	0.9%
	IPL-R	4.5%	5.5%	6.0%	5.2%	7.3%	6.3%
	SMG-R	51.3%	61.7%	76.0%	46.1%	54.3%	69.1%
	ANG-R	3.6%	2.9%	1.5%	1.5%	1.6%	1.0%
	STG-R	27.3%	26.5%	14.0%	30.8%	32.6%	20.6%
	MTG-R	11.3%	3.0%	1.5%	15.0%	3.9%	2.0%
P5	MOG-L	3.3%	1.4%	1.8%	1.4%	1.3%	1.9%
	IPL-L	0.8%	3.6%	3.5%	2.5%	6.3%	5.5%
	SMG-L	4.9%	2.8%	2.3%	4.0%	1.4%	1.4%
	ANG-L	33.0%	72.6%	73.0%	43.2%	66.2%	69.0%
	STG-L	25.7%	8.5%	5.7%	11.4%	5.1%	2.7%
	MTG-L	32.3%	11.2%	13.5%	37.3%	19.7%	19.5%
P3	SPG-L	3.2%	4.5%	3.5%	3.2%	4.0%	3.5%
	IPL-L	44.0%	44.0%	33.8%	32.0%	33.1%	28.9%
	SMG-L	1.3%	0.2%	0.2%	0.8%	0.2%	0.1%
	ANG-L	50.6%	51.1%	62.2%	62.5%	62.2%	67.1%
P1	PoCG-L	1.2%	0.6%	0.5%	1.4%	0.6%	0.5%
	SPG-L	78.3%	90.2%	88.1%	76.1%	88.3%	87.7%
	IPL-L	8.1%	3.5%	4.3%	5.3%	3.3%	3.4%
	ANG-L	9.8%	4.8%	5.5%	15.0%	7.2%	7.1%
	PCUN-L	1.5%	0.6%	1.1%	0.9%	0.4%	0.9%
P2	PoCG-R	1.4%	0.1%	0.6%	1.4%	0.1%	0.5%
	SPG-R	63.1%	69.4%	78.4%	66.1%	74.4%	81.6%
	IPL-R	2.9%	1.0%	2.0%	3.9%	1.0%	2.5%
	ANG-R	2.5%	0.6%	1.3%	2.5%	0.5%	1.5%
	PCUN-R	26.5%	28.0%	17.0%	21.6%	23.1%	13.3%
	PCUN-L	1.2%	0.5%	0.4%	0.9%	0.4%	0.3%

Table S3-13 Normalized PPL of corresponding brain regions ($L_{norm,M}$) for the circumferential and vertical SD pairs set at 10/10 fiducial points at 15-mm SD distance from 0-yo, 1-yo, and 2-yo.

SD distance = 15 mm		Circumferential SD pair			Vertical SD pair		
10/10 Point	AAL regions	0 year	1 year	2 year	0 year	1 year	2 year
P4	MOG-R	2.6%	0.5%	0.5%	5.1%	0.8%	0.8%
	SPG-R	8.8%	15.2%	13.5%	9.7%	17.0%	12.9%
	IPL-R	26.3%	17.6%	28.0%	14.6%	12.9%	24.9%
	ANG-R	60.8%	66.4%	57.4%	69.6%	68.9%	60.9%
P6	MOG-R	9.1%	4.7%	1.9%	6.3%	3.6%	1.5%
	IPL-R	2.4%	3.5%	5.6%	4.6%	3.6%	5.9%
	SMG-R	7.3%	2.4%	5.4%	2.5%	1.4%	3.5%
	ANG-R	70.2%	84.7%	83.5%	76.0%	86.3%	84.6%
	MTG-R	9.9%	4.4%	3.3%	10.0%	4.9%	4.2%
PO3	SOG-L	14.3%	23.4%	19.9%	11.8%	17.5%	15.3%
	MOG-L	33.4%	18.6%	23.6%	46.4%	27.4%	30.8%
	SPG-L	4.6%	6.4%	5.1%	8.8%	8.7%	5.7%
	ANG-L	46.2%	50.7%	50.4%	31.7%	45.7%	47.4%
PO4	CUN-R	2.3%	1.3%	0.6%	2.1%	1.2%	0.6%
	SOG-R	37.4%	46.4%	28.7%	46.8%	47.0%	25.4%
	MOG-R	37.5%	27.0%	30.5%	24.4%	24.6%	32.7%
	SPG-R	3.4%	4.9%	6.1%	7.5%	9.1%	8.0%
	IPL-R	15.2%	18.3%	30.7%	15.1%	16.3%	30.5%
	ANG-R	2.0%	1.1%	2.7%	1.7%	0.9%	2.0%
	PCUN-R	1.3%	0.7%	0.6%	1.6%	0.7%	0.7%

Table S4-1 Normalized PPL of corresponding brain regions ($L_{norm,M}$) for the circumferential and vertical SD pairs set at 10/10 fiducial points at 20-mm SD distance from 0-yo, 1-yo, and 2-yo.

SD distance = 20 mm		Circumferential SD pair			Vertical SD pair		
10/10 Points	AAL regions	0 year	1 year	2 year	0 year	1 year	2 year
Cz	PreCG-R	2.7%	0.8%	0.7%	1.5%	0.4%	0.6%
	PreCG-L	5.9%	2.4%	1.5%	7.9%	3.1%	1.7%
	SFGdor-R	18.7%	6.5%	7.6%	5.6%	2.4%	3.8%
	SFGdor-L	21.2%	18.3%	13.4%	13.7%	11.1%	7.2%
	SMA-R	16.8%	37.1%	39.2%	17.3%	27.8%	41.8%
	SMA-L	14.9%	29.1%	33.3%	26.8%	44.2%	36.9%
	PoCG-R	1.1%	0.2%	0.1%	0.9%	0.1%	0.1%
	PoCG-L	3.3%	0.3%	0.2%	4.8%	0.6%	0.3%
	SPG-L	5.9%	0.0%	0.0%	1.9%	0.0%	0.0%
	PCL-R	6.0%	3.9%	2.6%	9.3%	6.9%	5.4%
	PCL-L	1.8%	0.9%	0.7%	7.8%	2.8%	1.6%
Fpz	SFGdor-R	6.0%	3.4%	3.4%	3.1%	1.5%	2.4%
	SFGdor-L	10.3%	7.0%	1.7%	6.6%	5.9%	1.5%
	ORBsup-R	4.5%	4.0%	7.3%	2.9%	2.0%	4.9%
	ORBsup-L	10.0%	12.3%	9.1%	9.1%	11.8%	7.1%
	ORBmid-R	1.1%	0.4%	0.7%	0.7%	0.2%	0.5%
	ORBmid-L	2.6%	1.0%	1.2%	2.1%	1.3%	0.9%
	SFGmed-R	18.7%	13.4%	8.4%	18.6%	11.2%	11.3%
	SFGmed-L	18.6%	17.3%	8.4%	24.8%	24.7%	10.6%
	ORBmed-R	12.7%	21.1%	28.2%	12.6%	14.1%	29.1%
	ORBmed-L	12.2%	18.3%	27.7%	15.7%	24.6%	26.1%
	REC-R	1.1%	1.2%	2.7%	1.7%	1.7%	4.2%
AFz	SFGdor-R	11.9%	4.4%	11.8%	6.5%	2.0%	5.9%
	SFGdor-L	28.2%	19.5%	7.6%	9.8%	10.5%	4.5%
	MFG-R	1.1%	0.1%	0.4%	0.7%	0.1%	0.3%
	MFG-L	2.9%	1.5%	0.6%	1.9%	0.8%	0.4%
	SFGmed-R	31.6%	39.4%	45.6%	42.0%	31.7%	53.6%
	SFGmed-L	23.0%	34.5%	33.3%	36.7%	53.8%	34.3%

Table S4-2 Normalized PPL of corresponding brain regions ($L_{norm,M}$) for the circumferential and vertical SD pairs set at 10/10 fiducial points at 20-mm SD distance from 0-yo, 1-yo, and 2-yo.

SD distance = 20 mm		Circumferential SD pair			Vertical SD pair		
10/10 Points	AAL regions	0 year	1 year	2 year	0 year	1 year	2 year
Fz	SFGdor-R	18.8%	4.6%	11.3%	6.9%	2.8%	7.1%
	SFGdor-L	21.8%	22.7%	9.0%	8.9%	8.7%	4.5%
	MFG-R	1.2%	0.1%	0.5%	0.8%	0.1%	0.4%
	MFG-L	2.2%	0.5%	0.5%	1.4%	0.4%	0.3%
	SMA-R	2.5%	0.1%	0.0%	2.0%	0.1%	0.1%
	SMA-L	1.8%	0.1%	0.0%	4.9%	0.1%	0.0%
	SFGmed-R	27.5%	37.2%	43.9%	40.2%	37.6%	55.8%
	SFGmed-L	24.2%	34.6%	34.8%	34.6%	49.9%	31.7%
FCz	SFGdor-R	13.2%	3.8%	9.6%	6.8%	2.2%	5.8%
	SFGdor-L	24.6%	12.6%	5.9%	12.1%	6.7%	3.8%
	MFG-R	1.2%	0.2%	0.8%	0.8%	0.1%	0.6%
	MFG-L	1.1%	0.3%	0.2%	0.8%	0.2%	0.2%
	SMA-R	19.4%	27.3%	17.3%	19.3%	16.7%	23.0%
	SMA-L	17.1%	24.3%	13.1%	27.1%	30.4%	14.2%
	SFGmed-R	8.7%	14.3%	27.4%	13.5%	14.6%	30.5%
	SFGmed-L	11.0%	17.0%	25.6%	17.5%	28.8%	22.1%
	PCL-R	2.5%	0.0%	0.0%	0.6%	0.0%	0.0%
CPz	PreCG-R	1.5%	0.2%	0.3%	1.0%	0.2%	0.3%
	PreCG-L	5.9%	2.1%	2.2%	6.0%	2.7%	2.4%
	SFGdor-L	1.1%	0.2%	0.2%	1.4%	0.2%	0.3%
	SMA-R	1.1%	0.4%	0.5%	1.5%	0.7%	1.2%
	SMA-L	1.5%	0.8%	1.0%	2.8%	2.1%	2.3%
	PoCG-R	7.5%	1.9%	3.0%	2.6%	0.9%	1.7%
	PoCG-L	26.7%	30.8%	24.0%	17.5%	18.4%	11.9%
	SPG-R	1.9%	1.4%	1.3%	1.4%	0.7%	0.9%
	SPG-L	6.9%	6.4%	3.6%	10.3%	5.8%	3.0%
	PCUN-R	17.4%	19.8%	19.8%	13.3%	15.2%	19.1%
	PCUN-L	4.5%	9.8%	7.2%	12.9%	17.6%	11.2%
	PCL-R	14.9%	14.7%	22.4%	11.6%	16.6%	26.6%
	PCL-L	8.0%	11.6%	14.3%	16.8%	18.7%	18.7%

Table S4-3 Normalized PPL of corresponding brain regions ($L_{norm,M}$) for the circumferential and vertical SD pairs set at 10/10 fiducial points at 20-mm SD distance from 0-yo, 1-yo, and 2-yo.

SD distance = 20 mm		Circumferential SD pair			Vertical SD pair		
10/10 Points	AAL regions	0 year	1 year	2 year	0 year	1 year	2 year
Pz	PoCG-L	1.8%	0.6%	0.6%	4.1%	0.9%	0.7%
	SPG-R	5.2%	2.4%	3.1%	2.4%	1.1%	1.6%
	SPG-L	44.2%	38.1%	25.0%	34.1%	31.4%	15.6%
	PCUN-R	30.6%	34.3%	43.5%	26.2%	27.1%	45.0%
	PCUN-L	15.4%	23.7%	27.0%	29.5%	38.4%	36.2%
POz	CUN-R	12.4%	7.0%	8.8%	16.5%	10.0%	12.8%
	CUN-L	14.3%	20.3%	14.6%	17.2%	26.5%	14.8%
	SOG-R	15.8%	9.0%	12.9%	6.9%	5.5%	8.1%
	SOG-L	9.5%	5.5%	2.5%	7.2%	4.2%	1.4%
	MOG-L	1.7%	0.3%	0.2%	1.5%	0.3%	0.1%
	SPG-R	2.3%	3.6%	4.6%	1.3%	1.6%	2.3%
	SPG-L	23.3%	28.4%	24.4%	21.5%	22.1%	17.7%
	ANG-L	1.3%	0.3%	0.3%	1.0%	0.2%	0.1%
	PCUN-R	12.6%	17.1%	22.5%	14.5%	16.8%	27.9%
	PCUN-L	5.8%	8.2%	9.1%	11.8%	12.8%	14.6%
Oz	CAL-R	3.6%	2.0%	2.8%	6.7%	4.4%	6.4%
	CUN-R	28.5%	31.1%	46.6%	25.3%	32.3%	52.1%
	CUN-L	14.5%	17.6%	18.8%	26.4%	29.4%	21.7%
	SOG-R	8.3%	6.1%	8.9%	3.4%	3.8%	5.6%
	SOG-L	36.7%	38.6%	20.2%	29.9%	26.2%	11.3%
	MOG-L	5.9%	3.4%	1.0%	3.9%	1.8%	0.6%
T3	STG-L	3.9%	7.2%	4.6%	6.5%	19.8%	10.7%
	TPOsup-L	2.4%	0.7%	0.8%	1.5%	0.8%	0.8%
	MTG-L	58.1%	85.6%	83.1%	56.9%	71.2%	76.5%
	TPOmid-L	5.3%	1.0%	1.5%	2.2%	0.6%	0.9%
	ITG-L	29.6%	5.4%	9.9%	32.3%	7.4%	11.0%

Table S4-4 Normalized PPL of corresponding brain regions ($L_{norm,M}$) for the circumferential and vertical SD pairs set at 10/10 fiducial points at 20-mm SD distance from 0-yo, 1-yo, and 2-yo.

SD distance = 20 mm		Circumferential SD pair			Vertical SD pair		
10/10 Points	AAL regions	0 year	1 year	2 year	0 year	1 year	2 year
C5	PreCG-L	2.7%	3.7%	2.4%	3.1%	1.9%	1.6%
	IFGoperc-L	1.7%	0.4%	0.3%	0.9%	0.2%	0.2%
	ROL-L	9.7%	13.6%	8.3%	6.1%	5.6%	3.3%
	PoCG-L	15.7%	40.6%	40.1%	33.7%	43.6%	42.4%
	SMG-L	6.4%	11.4%	12.3%	3.6%	8.5%	11.9%
	STG-L	55.0%	29.3%	35.3%	41.7%	38.6%	38.5%
	TPOsup-L	3.0%	0.4%	0.4%	2.0%	0.3%	0.3%
	MTG-L	4.6%	0.5%	0.8%	8.0%	1.1%	1.8%
C3	PreCG-L	24.6%	41.2%	34.0%	19.7%	26.8%	26.4%
	MFG-L	3.5%	7.0%	6.0%	13.3%	9.0%	9.4%
	PoCG-L	43.1%	44.7%	47.5%	55.6%	58.5%	53.1%
	SMG-L	26.4%	6.6%	11.6%	9.9%	5.4%	10.4%
C1	PreCG-L	44.8%	41.9%	43.1%	38.1%	47.8%	43.8%
	SFGdor-L	20.2%	32.5%	25.1%	32.6%	36.6%	32.6%
	MFG-L	23.1%	21.0%	26.8%	19.3%	9.7%	18.2%
	PoCG-L	9.6%	3.6%	4.1%	7.3%	4.4%	4.5%
C2	PreCG-R	44.8%	60.5%	46.4%	37.2%	56.4%	46.2%
	SFGdor-R	19.1%	13.4%	23.6%	42.1%	26.8%	32.1%
	MFG-R	19.7%	16.7%	23.8%	8.5%	7.3%	15.0%
	SMA-R	1.7%	0.7%	1.2%	0.6%	1.3%	2.1%
	PoCG-R	11.9%	7.9%	4.2%	10.6%	7.7%	3.9%
	PCL-R	1.2%	0.4%	0.5%	0.4%	0.4%	0.5%
C4	PreCG-R	24.2%	23.5%	34.3%	20.2%	14.6%	32.9%
	MFG-R	2.9%	0.8%	2.5%	2.0%	0.6%	2.1%
	PoCG-R	38.1%	53.9%	53.0%	52.3%	71.8%	56.1%
	IPL-R	15.2%	15.9%	6.3%	6.2%	5.4%	3.4%
	SMG-R	18.5%	5.8%	3.7%	18.4%	7.6%	5.4%

Table S4-5 Normalized PPL of corresponding brain regions ($L_{norm,M}$) for the circumferential and vertical SD pairs set at 10/10 fiducial points at 20-mm SD distance from 0-yo, 1-yo, and 2-yo.

SD distance = 20 mm		Circumferential SD pair			Vertical SD pair		
10/10 Points	AAL regions	0 year	1 year	2 year	0 year	1 year	2 year
C6	PreCG-R	1.3%	0.7%	2.4%	2.3%	0.5%	2.2%
	IFGoperc-R	1.9%	0.1%	1.0%	1.1%	0.1%	0.5%
	ROL-R	6.9%	4.7%	4.4%	3.4%	1.5%	2.2%
	PoCG-R	24.4%	40.6%	51.4%	37.2%	43.1%	52.1%
	SMG-R	7.7%	12.6%	13.6%	5.8%	9.1%	9.0%
	STG-R	37.5%	37.5%	24.1%	24.6%	38.2%	29.4%
	MTG-R	17.6%	3.7%	2.6%	23.5%	7.4%	4.3%
T4	STG-R	1.4%	1.4%	3.4%	2.2%	2.3%	4.6%
	MTG-R	59.3%	78.6%	86.1%	61.6%	76.7%	80.6%
	TPOmid-R	1.0%	0.1%	0.1%	0.6%	0.0%	0.1%
	ITG-R	36.6%	19.6%	9.4%	34.1%	20.7%	13.8%
FT7	IFGoperc-L	1.4%	1.3%	0.9%	3.0%	1.4%	1.4%
	IFGtriang-L	3.8%	1.5%	1.4%	4.9%	1.0%	1.5%
	ORBinf-L	14.6%	4.2%	3.5%	8.8%	1.5%	2.2%
	ROL-L	0.7%	1.0%	0.5%	1.2%	1.3%	0.7%
	STG-L	5.3%	13.4%	9.9%	3.3%	9.8%	6.7%
	TPOsup-L	30.7%	39.4%	35.5%	40.7%	42.8%	40.0%
	MTG-L	19.7%	20.0%	26.8%	9.8%	18.2%	19.5%
	TPOmid-L	19.0%	17.8%	20.2%	22.8%	22.4%	26.5%
	ITG-L	3.1%	0.9%	0.9%	3.6%	1.2%	1.1%
F7	MFG-L	2.9%	0.8%	0.6%	3.1%	0.9%	0.7%
	ORBmid-L	14.3%	1.8%	2.5%	6.8%	1.0%	1.3%
	IFGtriang-L	14.6%	12.7%	8.2%	27.4%	31.7%	17.2%
	ORBinf-L	59.3%	75.1%	75.2%	56.5%	59.4%	74.7%
	TPOsup-L	6.6%	8.3%	11.8%	4.3%	5.8%	5.2%
	TPOmid-L	0.6%	0.5%	1.1%	0.6%	0.5%	0.6%

Table S4-6 Normalized PPL of corresponding brain regions ($L_{norm,M}$) for the circumferential and vertical SD pairs set at 10/10 fiducial points at 20-mm SD distance from 0-yo, 1-yo, and 2-yo.

SD distance = 20 mm		Circumferential SD pair			Vertical SD pair		
10/10 Points	AAL regions	0 year	1 year	2 year	0 year	1 year	2 year
AF7	SFGdor-L	2.7%	0.6%	0.6%	2.6%	0.6%	0.7%
	ORBsup-L	2.3%	1.0%	1.4%	1.6%	0.7%	1.1%
	MFG-L	15.6%	10.9%	6.5%	28.8%	24.7%	15.1%
	ORBmid-L	50.0%	54.8%	60.2%	48.7%	50.1%	64.6%
	IFGtriang-L	7.1%	4.2%	2.7%	5.1%	5.4%	2.8%
	ORBinf-L	21.3%	28.5%	28.3%	12.5%	18.4%	15.5%
Fp1	SFGdor-L	20.4%	17.8%	7.7%	28.2%	25.5%	19.6%
	ORBsup-L	17.3%	32.0%	31.9%	18.0%	26.7%	32.8%
	MFG-L	15.0%	11.5%	3.5%	14.1%	11.4%	4.9%
	ORBmid-L	28.7%	32.1%	40.5%	27.3%	32.1%	32.9%
	ORBinf-L	1.1%	0.2%	0.4%	0.9%	0.2%	0.2%
	SFGmed-R	1.7%	0.1%	0.3%	1.1%	0.1%	0.3%
	SFGmed-L	8.3%	2.9%	3.1%	5.5%	1.9%	3.1%
	ORBmed-R	1.1%	0.1%	0.8%	0.7%	0.1%	0.5%
	ORBmed-L	5.2%	3.1%	11.2%	3.3%	1.9%	5.2%
Fp2	SFGdor-R	28.6%	24.3%	16.5%	36.0%	36.0%	25.7%
	ORBsup-R	13.6%	24.1%	27.7%	15.7%	26.3%	28.0%
	MFG-R	14.7%	7.7%	7.1%	13.7%	5.8%	8.6%
	ORBmid-R	16.6%	26.7%	35.7%	18.4%	19.4%	27.5%
	ORBinf-R	1.3%	0.2%	0.7%	1.3%	0.1%	0.5%
	SFGmed-R	12.0%	5.4%	2.6%	6.8%	4.7%	2.6%
	SFGmed-L	1.8%	0.3%	0.2%	1.0%	0.2%	0.2%
	ORBmed-R	7.9%	10.5%	7.8%	4.7%	6.5%	5.1%
	ORBmed-L	1.3%	0.3%	0.5%	0.7%	0.2%	0.4%

Table S4-7 Normalized PPL of corresponding brain regions ($L_{norm,M}$) for the circumferential and vertical SD pairs set at 10/10 fiducial points at 20-mm SD distance from 0-yo, 1-yo, and 2-yo.

SD distance = 20 mm		Circumferential SD pair			Vertical SD pair		
10/10 Points	AAL regions	0 year	1 year	2 year	0 year	1 year	2 year
AF8	SFGdor-R	5.7%	1.1%	1.2%	4.6%	0.7%	1.0%
	ORBsup-R	2.5%	0.8%	1.4%	2.0%	0.5%	0.9%
	MFG-R	22.2%	15.5%	10.4%	36.9%	23.4%	21.4%
	ORBmid-R	39.1%	60.1%	57.7%	35.9%	54.6%	54.3%
	IFGtriang-R	9.8%	6.6%	6.5%	6.6%	5.1%	6.6%
	ORBinf-R	19.5%	15.9%	22.4%	13.0%	15.5%	15.5%
F8	MFG-R	3.5%	0.2%	0.9%	3.8%	0.2%	1.0%
	ORBmid-R	10.0%	0.8%	3.0%	5.7%	0.4%	2.1%
	IFGoperc-R	1.0%	0.6%	0.7%	0.8%	0.8%	0.6%
	IFGtriang-R	20.9%	16.6%	28.1%	32.1%	30.6%	42.5%
	ORBinf-R	55.8%	69.9%	51.9%	52.0%	57.1%	43.0%
	TPOsup-R	6.3%	9.9%	13.2%	3.9%	8.8%	9.1%
FT8	IFGoperc-R	2.0%	0.5%	1.4%	4.2%	1.1%	2.2%
	IFGtriang-R	4.6%	0.8%	2.5%	5.1%	1.1%	2.1%
	ORBinf-R	15.5%	1.6%	3.1%	7.5%	1.3%	1.7%
	ROL-R	1.6%	0.7%	1.4%	3.0%	2.1%	2.4%
	STG-R	8.5%	9.6%	11.2%	10.1%	21.2%	14.6%
	TPOsup-R	22.0%	18.9%	25.5%	26.2%	17.7%	24.6%
	MTG-R	35.2%	61.5%	49.9%	28.1%	49.3%	46.0%
	TPOmid-R	6.2%	4.4%	3.6%	10.1%	3.8%	4.8%
	ITG-R	3.1%	1.8%	1.0%	4.0%	1.8%	1.2%
TP7	STG-L	4.8%	6.2%	2.8%	11.4%	12.2%	4.5%
	MTG-L	60.1%	88.3%	85.3%	58.0%	71.7%	70.5%
	ITG-L	34.8%	5.4%	11.8%	30.2%	16.1%	24.8%
T5	STG-L	1.8%	1.9%	1.2%	4.6%	4.3%	1.9%
	MTG-L	76.1%	90.2%	89.7%	69.7%	83.5%	82.2%
	ITG-L	20.8%	6.5%	7.8%	24.5%	10.3%	14.7%

Table S4-8 Normalized PPL of corresponding brain regions ($L_{norm,M}$) for the circumferential and vertical SD pairs set at 10/10 fiducial points at 20-mm SD distance from 0-yo, 1-yo, and 2-yo.

SD distance = 20 mm		Circumferential SD pair			Vertical SD pair		
10/10 Points	AAL regions	0 year	1 year	2 year	0 year	1 year	2 year
PO7	MOG-L	46.0%	50.9%	51.7%	37.7%	51.3%	56.9%
	IOG-L	1.1%	0.4%	0.8%	4.9%	0.7%	1.6%
	ANG-L	1.6%	3.1%	0.9%	2.9%	4.9%	1.9%
	MTG-L	49.7%	45.0%	46.2%	50.2%	42.5%	39.0%
	ITG-L	1.2%	0.4%	0.4%	4.0%	0.5%	0.4%
O1	CUN-L	1.4%	0.7%	1.2%	1.1%	0.7%	1.0%
	SOG-L	25.3%	20.5%	27.2%	16.5%	13.8%	22.5%
	MOG-L	70.3%	77.2%	70.0%	78.9%	83.6%	74.7%
O2	CAL-R	1.8%	0.7%	0.2%	2.6%	0.9%	0.3%
	CUN-R	12.5%	13.6%	5.9%	6.3%	9.2%	4.1%
	SOG-R	47.1%	62.5%	50.4%	56.1%	70.9%	53.4%
	MOG-R	36.3%	22.2%	42.7%	32.6%	17.9%	41.3%
PO8	SOG-R	2.3%	2.9%	1.0%	1.0%	1.6%	0.7%
	MOG-R	86.4%	89.7%	84.6%	92.3%	91.3%	85.3%
	IOG-R	1.9%	0.8%	0.3%	1.8%	0.8%	0.4%
	ANG-R	2.8%	3.6%	5.5%	2.8%	4.4%	8.0%
	MTG-R	6.0%	2.6%	8.3%	1.6%	1.4%	5.4%
T6	MOG-R	16.0%	23.8%	9.6%	9.6%	15.0%	7.7%
	IOG-R	7.2%	5.6%	1.7%	17.1%	9.4%	3.5%
	ANG-R	1.9%	3.6%	3.3%	4.5%	5.4%	5.3%
	STG-R	1.1%	0.6%	1.8%	1.1%	0.6%	1.8%
	MTG-R	61.9%	62.9%	80.6%	50.5%	65.5%	77.2%
	ITG-R	11.3%	3.0%	2.3%	16.4%	3.4%	3.0%
TP8	STG-R	1.4%	2.0%	4.5%	2.4%	4.1%	7.6%
	MTG-R	71.7%	88.5%	90.0%	62.0%	79.3%	84.9%
	ITG-R	26.3%	8.9%	4.9%	35.1%	16.0%	6.9%

Table S4-9 Normalized PPL of corresponding brain regions ($L_{norm,M}$) for the circumferential and vertical SD pairs set at 10/10 fiducial points at 20-mm SD distance from 0-yo, 1-yo, and 2-yo.

SD distance = 20 mm		Circumferential SD pair			Vertical SD pair		
10/10 Points	AAL regions	0 year	1 year	2 year	0 year	1 year	2 year
FC5	PreCG-L	8.8%	15.1%	13.1%	14.5%	15.7%	13.2%
	MFG-L	1.6%	0.5%	0.6%	1.5%	0.7%	0.5%
	IFGoperc-L	14.6%	24.7%	24.0%	29.7%	47.5%	45.5%
	IFGtriang-L	43.5%	31.8%	34.2%	29.0%	18.0%	22.2%
	ORBinf-L	3.3%	0.5%	0.6%	3.2%	0.6%	0.6%
	ROL-L	12.4%	19.3%	19.5%	6.3%	11.3%	10.3%
	PoCG-L	5.7%	4.3%	2.7%	3.2%	1.7%	1.4%
	STG-L	3.4%	1.3%	1.5%	2.3%	0.9%	1.1%
	TPOsup-L	5.8%	2.2%	3.5%	9.1%	3.4%	5.0%
FC3	PreCG-L	25.0%	21.4%	16.9%	10.9%	9.5%	8.3%
	MFG-L	51.7%	65.2%	63.2%	54.9%	65.8%	60.2%
	IFGoperc-L	12.0%	9.5%	13.0%	16.0%	17.3%	20.9%
	IFGtriang-L	7.9%	3.3%	5.9%	16.4%	7.0%	9.9%
	PoCG-L	2.6%	0.3%	0.7%	1.1%	0.2%	0.4%
FC1	PreCG-L	2.2%	0.3%	0.2%	4.2%	0.2%	0.2%
	SFGdor-L	34.3%	46.1%	47.1%	36.9%	48.0%	47.2%
	MFG-L	58.5%	51.3%	48.5%	54.0%	48.9%	48.8%
	SMA-L	1.5%	1.1%	1.1%	2.4%	2.0%	1.6%
	SFGmed-L	2.5%	1.1%	2.8%	1.4%	0.8%	2.0%
FC2	PreCG-R	4.6%	0.3%	0.4%	2.8%	0.2%	0.3%
	SFGdor-R	35.0%	40.1%	28.9%	36.3%	36.1%	30.3%
	MFG-R	51.3%	54.3%	67.4%	51.4%	58.6%	65.8%
	SMA-R	3.5%	2.0%	1.0%	5.1%	3.0%	1.4%
	SFGmed-R	3.6%	3.1%	2.1%	2.0%	1.8%	1.9%
FC4	PreCG-R	25.5%	23.3%	16.1%	14.3%	14.1%	8.3%
	MFG-R	58.9%	69.8%	75.1%	59.3%	76.0%	76.1%
	IFGoperc-R	5.0%	2.5%	3.5%	9.8%	5.0%	6.3%
	IFGtriang-R	5.9%	3.2%	4.4%	13.2%	4.2%	8.6%
	PoCG-R	3.6%	1.0%	0.6%	2.4%	0.6%	0.4%

Table S4-10 Normalized PPL of corresponding brain regions ($L_{norm,M}$) for the circumferential and vertical SD pairs set at 10/10 fiducial points at 20-mm SD distance from 0-yo, 1-yo, and 2-yo.

SD distance = 20 mm		Circumferential SD pair			Vertical SD pair		
10/10 Points	AAL regions	0 year	1 year	2 year	0 year	1 year	2 year
FC6	PreCG-R	5.3%	10.1%	9.6%	11.1%	23.3%	11.0%
	MFG-R	2.9%	0.8%	1.8%	3.9%	1.2%	2.0%
	IFGoperc-R	17.1%	21.7%	22.9%	25.8%	23.8%	33.4%
	IFGtriang-R	36.3%	24.6%	42.4%	27.4%	11.9%	32.0%
	ORBinf-R	2.0%	0.2%	0.2%	2.1%	0.2%	0.2%
	ROL-R	7.5%	9.0%	6.1%	6.4%	14.3%	8.0%
	PoCG-R	16.7%	29.3%	13.6%	9.7%	18.0%	8.1%
	STG-R	6.4%	3.1%	2.1%	6.2%	4.9%	2.9%
	TPOsup-R	3.0%	0.9%	1.0%	4.9%	1.9%	2.1%
	MTG-R	1.9%	0.3%	0.2%	1.9%	0.5%	0.3%
F5	MFG-L	30.3%	26.2%	28.3%	33.2%	28.1%	21.1%
	ORBmid-L	3.5%	0.6%	0.9%	3.5%	0.7%	0.8%
	IFGoperc-L	1.8%	0.9%	0.6%	0.9%	0.4%	0.4%
	IFGtriang-L	55.4%	68.9%	65.9%	47.3%	64.6%	67.8%
	ORBinf-L	7.2%	3.0%	4.0%	13.8%	6.0%	9.7%
F3	SFGdor-L	3.1%	0.9%	1.8%	3.2%	1.2%	1.5%
	MFG-L	79.2%	92.2%	92.6%	89.2%	95.7%	94.0%
	IFGoperc-L	1.1%	0.2%	0.2%	0.4%	0.1%	0.1%
	IFGtriang-L	15.4%	6.5%	5.1%	5.8%	2.9%	4.1%
F1	SFGdor-L	29.4%	48.9%	47.4%	46.4%	57.4%	53.3%
	MFG-L	54.3%	39.1%	37.1%	41.4%	37.3%	38.9%
	SFGmed-R	2.4%	0.5%	1.3%	2.1%	0.3%	0.8%
	SFGmed-L	12.9%	11.5%	14.0%	9.1%	4.9%	6.8%
F2	SFGdor-R	29.9%	57.8%	58.5%	54.7%	72.5%	62.7%
	MFG-R	26.9%	22.0%	28.8%	28.8%	15.9%	28.9%
	SFGmed-R	38.4%	19.3%	11.9%	12.8%	11.0%	7.8%
	SFGmed-L	3.0%	0.8%	0.8%	2.1%	0.5%	0.6%

Table S4-11 Normalized PPL of corresponding brain regions ($L_{norm,M}$) for the circumferential and vertical SD pairs set at 10/10 fiducial points at 20-mm SD distance from 0-yo, 1-yo, and 2-yo.

SD distance = 20 mm		Circumferential SD pair			Vertical SD pair		
10/10 Points	AAL regions	0 year	1 year	2 year	0 year	1 year	2 year
F4	SFGdor-R	7.2%	3.2%	2.7%	6.7%	2.1%	2.4%
	MFG-R	81.1%	92.2%	89.0%	84.2%	92.4%	90.9%
	IFGtriang-R	9.3%	4.3%	7.9%	7.2%	5.2%	6.5%
F6	MFG-R	35.3%	19.1%	21.4%	33.1%	16.4%	18.2%
	ORBmid-R	2.4%	0.9%	1.1%	3.4%	1.2%	1.2%
	IFGoperc-R	2.7%	1.3%	0.5%	1.5%	0.7%	0.4%
	IFGtriang-R	53.4%	76.5%	75.5%	52.3%	77.4%	77.7%
	ORBinf-R	3.7%	1.8%	1.1%	7.7%	3.9%	2.1%
AF3	SFGdor-L	35.7%	42.8%	46.1%	35.2%	29.3%	43.6%
	ORBsup-L	1.3%	0.9%	1.5%	2.4%	1.4%	3.2%
	MFG-L	49.3%	52.4%	44.3%	50.4%	65.2%	45.2%
	ORBmid-L	2.7%	1.3%	2.1%	4.7%	2.7%	4.3%
	SFGmed-R	1.4%	0.1%	0.3%	1.0%	0.1%	0.2%
	SFGmed-L	7.8%	2.3%	5.4%	4.8%	1.1%	3.0%
AF4	SFGdor-R	39.3%	48.9%	35.1%	40.9%	52.2%	31.5%
	ORBsup-R	1.1%	0.4%	0.6%	1.8%	0.6%	1.2%
	MFG-R	42.1%	44.1%	59.4%	44.6%	42.2%	62.1%
	ORBmid-R	2.0%	0.6%	1.5%	3.7%	1.2%	2.7%
	IFGtriang-R	1.3%	0.2%	0.5%	0.9%	0.1%	0.3%
	SFGmed-R	11.6%	5.6%	2.6%	6.0%	3.3%	1.9%
	SFGmed-L	1.2%	0.2%	0.1%	0.7%	0.1%	0.1%
CP5	PoCG-L	2.3%	0.6%	0.7%	1.5%	0.5%	0.5%
	SMG-L	24.2%	52.9%	41.9%	35.3%	50.0%	40.9%
	ANG-L	1.7%	3.0%	2.2%	0.4%	1.0%	1.0%
	STG-L	62.5%	40.9%	51.3%	44.5%	44.1%	50.6%
	MTG-L	8.9%	2.1%	3.5%	18.0%	4.1%	6.8%

Table S4-12 Normalized PPL of corresponding brain regions ($L_{norm,M}$) for the circumferential and vertical SD pairs set at 10/10 fiducial points at 20-mm SD distance from 0-yo, 1-yo, and 2-yo.

SD distance = 20 mm		Circumferential SD pair			Vertical SD pair		
10/10 Points	AAL regions	0 year	1 year	2 year	0 year	1 year	2 year
CP3	PoCG-L	15.6%	15.1%	9.5%	16.4%	14.2%	10.3%
	SPG-L	1.9%	1.7%	2.0%	1.3%	1.3%	2.1%
	IPL-L	42.7%	55.4%	58.0%	26.4%	49.3%	59.8%
	SMG-L	38.1%	27.2%	29.2%	53.7%	34.4%	26.1%
CP1	PreCG-L	14.3%	7.7%	9.1%	21.5%	8.8%	9.9%
	PoCG-L	49.2%	60.8%	57.7%	39.9%	55.3%	55.0%
	SPG-L	30.5%	28.6%	30.0%	28.5%	32.1%	29.6%
	IPL-L	3.4%	2.1%	2.2%	7.1%	3.1%	4.5%
CP2	PreCG-R	11.3%	4.3%	6.2%	11.4%	4.3%	8.1%
	SFGdor-R	1.0%	0.2%	0.4%	1.5%	0.2%	0.5%
	PoCG-R	46.7%	54.2%	56.7%	43.4%	49.7%	58.3%
	SPG-R	30.1%	32.8%	29.9%	29.4%	36.9%	25.6%
	IPL-R	2.3%	1.9%	2.4%	4.6%	2.9%	3.3%
	PCUN-R	4.8%	4.4%	2.2%	3.1%	2.6%	1.3%
	PCL-R	2.4%	1.9%	1.9%	4.8%	2.9%	2.6%
CP4	PreCG-R	1.2%	0.1%	0.7%	1.0%	0.2%	0.8%
	PoCG-R	20.7%	16.2%	22.3%	22.9%	19.9%	26.3%
	SPG-R	2.0%	1.4%	1.1%	1.4%	1.4%	0.8%
	IPL-R	68.2%	80.1%	73.8%	63.7%	76.2%	69.5%
	SMG-R	4.6%	0.8%	1.3%	7.5%	0.9%	2.0%
	ANG-R	2.9%	1.4%	0.7%	3.2%	1.4%	0.6%
CP6	PoCG-R	2.7%	0.7%	1.5%	1.4%	0.4%	1.2%
	IPL-R	4.3%	8.0%	6.8%	7.7%	10.1%	9.1%
	SMG-R	46.2%	60.6%	72.0%	43.0%	49.5%	66.5%
	ANG-R	5.7%	4.6%	2.4%	1.9%	1.8%	1.3%
	STG-R	26.4%	22.8%	15.2%	23.3%	32.2%	19.5%
	MTG-R	14.5%	3.2%	2.1%	22.3%	6.0%	2.4%

Table S4-13 Normalized PPL of corresponding brain regions ($L_{norm,M}$) for the circumferential and vertical SD pairs set at 10/10 fiducial points at 20-mm SD distance from 0-yo, 1-yo, and 2-yo.

SD distance = 20 mm		Circumferential SD pair			Vertical SD pair		
10/10 Points	AAL regions	0 year	1 year	2 year	0 year	1 year	2 year
P5	MOG-L	4.7%	1.8%	2.5%	1.6%	1.4%	2.2%
	IPL-L	1.3%	4.8%	3.8%	5.3%	11.9%	7.7%
	SMG-L	7.8%	4.4%	3.3%	5.3%	2.7%	1.8%
	ANG-L	36.0%	71.1%	67.8%	39.2%	55.0%	59.9%
	STG-L	24.1%	8.6%	7.6%	9.9%	5.5%	3.0%
	MTG-L	26.0%	9.4%	15.0%	38.6%	23.5%	25.4%
P3	SPG-L	5.2%	5.7%	4.0%	4.9%	5.7%	4.3%
	IPL-L	47.6%	47.6%	36.3%	29.4%	31.9%	31.9%
	SMG-L	2.3%	0.4%	0.3%	0.8%	0.3%	0.2%
	ANG-L	43.8%	45.8%	58.9%	62.4%	61.6%	63.1%
P1	PoCG-L	2.6%	0.8%	0.6%	1.9%	0.9%	0.7%
	SPG-L	76.2%	88.3%	84.7%	73.5%	85.6%	84.8%
	IPL-L	8.8%	4.4%	5.6%	4.1%	3.3%	3.9%
	ANG-L	7.8%	5.2%	6.9%	17.7%	9.2%	9.0%
	PCUN-L	2.7%	1.0%	1.5%	1.2%	0.6%	1.0%
P2	SOG-R	1.0%	0.3%	0.1%	3.3%	0.4%	0.2%
	PoCG-R	2.2%	0.2%	0.7%	1.9%	0.2%	0.6%
	SPG-R	59.7%	66.1%	73.2%	60.3%	71.5%	77.5%
	IPL-R	3.8%	1.4%	2.5%	4.4%	1.8%	3.0%
	ANG-R	3.2%	1.1%	1.5%	2.5%	0.8%	1.6%
	PCUN-R	26.5%	29.8%	21.1%	24.5%	24.4%	16.4%
	PCUN-L	1.6%	0.8%	0.6%	1.2%	0.6%	0.4%
P4	MOG-R	3.0%	0.6%	0.7%	11.1%	1.4%	1.2%
	SPG-R	11.4%	20.3%	14.9%	11.8%	18.6%	13.8%
	IPL-R	33.0%	23.5%	32.4%	14.0%	15.0%	27.4%
	ANG-R	50.1%	55.0%	51.2%	61.7%	64.5%	56.9%

Table S4-14 Normalized PPL of corresponding brain regions ($L_{norm,M}$) for the circumferential and vertical SD pairs set at 10/10 fiducial points at 20-mm SD distance from 0-yo, 1-yo, and 2-yo.

SD distance = 20 mm		Circumferential SD pair			Vertical SD pair		
10/10 Points	AAL regions	0 year	1 year	2 year	0 year	1 year	2 year
P6	MOG-R	13.3%	6.0%	2.5%	7.6%	4.9%	2.0%
	IPL-R	4.8%	5.2%	6.8%	8.2%	5.4%	9.3%
	SMG-R	12.3%	4.1%	7.8%	3.4%	1.6%	4.5%
	ANG-R	57.2%	79.9%	79.0%	66.9%	81.2%	77.7%
	STG-R	1.8%	0.3%	0.3%	0.6%	0.2%	0.3%
	MTG-R	10.3%	4.3%	3.5%	12.9%	6.5%	6.2%
PO3	CUN-L	1.4%	1.0%	1.0%	1.0%	0.6%	0.6%
	SOG-L	13.4%	23.6%	19.8%	11.8%	14.1%	13.8%
	MOG-L	31.1%	17.4%	22.7%	45.0%	29.7%	31.2%
	SPG-L	4.9%	8.0%	6.1%	11.1%	10.3%	8.4%
	ANG-L	48.2%	49.5%	50.0%	30.3%	44.9%	45.5%
PO4	CUN-R	2.9%	1.7%	0.8%	2.6%	1.2%	0.7%
	SOG-R	29.5%	42.6%	30.9%	42.2%	40.9%	25.4%
	MOG-R	42.4%	25.9%	28.9%	24.3%	26.3%	32.5%
	SPG-R	3.9%	6.3%	6.7%	11.0%	12.3%	9.6%
	IPL-R	14.7%	20.3%	27.7%	14.2%	16.8%	28.4%
	ANG-R	3.7%	1.8%	3.8%	2.2%	1.3%	2.3%
	PCUN-R	1.7%	1.0%	0.9%	2.3%	0.9%	0.8%

Table S5-1 Normalized PPL of corresponding brain regions ($L_{norm,M}$) for the circumferential and vertical SD pairs set at 10/10 fiducial points at 25-mm SD distance from 0-yo, 1-yo, and 2-yo.

SD distance = 25 mm		Circumferential SD pair			Vertical SD pair		
10/10 Points	AAL regions	0 year	1 year	2 year	0 year	1 year	2 year
Cz	PreCG-R	3.0%	1.1%	1.0%	1.7%	0.5%	0.7%
	PreCG-L	8.1%	3.5%	1.7%	7.8%	3.9%	2.0%
	SFGdor-R	20.6%	9.2%	10.7%	6.0%	2.4%	4.2%
	SFGdor-L	24.7%	22.7%	15.8%	12.0%	11.4%	7.1%
	SMA-R	14.5%	32.0%	36.6%	17.5%	25.5%	40.8%
	SMA-L	12.3%	24.6%	29.5%	23.1%	43.5%	34.8%
	PoCG-R	1.1%	0.2%	0.1%	1.1%	0.2%	0.2%
	PoCG-L	3.3%	0.5%	0.2%	5.0%	0.9%	0.4%
	SPG-L	3.3%	0.0%	0.0%	1.7%	0.0%	0.0%
	PCL-R	5.4%	4.5%	2.7%	9.3%	7.3%	6.9%
	PCL-L	1.9%	1.1%	0.7%	11.8%	3.7%	2.1%
Fpz	SFGdor-R	7.7%	4.4%	4.1%	3.6%	1.8%	3.2%
	SFGdor-L	12.2%	8.4%	2.0%	7.1%	5.3%	1.8%
	ORBsup-R	5.4%	4.8%	9.3%	3.0%	3.1%	4.9%
	ORBsup-L	11.1%	15.0%	11.1%	9.3%	11.2%	7.2%
	MFG-L	1.5%	0.2%	0.1%	0.9%	0.1%	0.1%
	ORBmid-R	1.5%	0.5%	1.1%	0.7%	0.3%	0.6%
	ORBmid-L	3.5%	1.6%	1.7%	2.4%	1.4%	1.0%
	SFGmed-R	16.6%	13.1%	7.9%	20.4%	12.1%	15.3%
	SFGmed-L	16.2%	15.3%	8.0%	24.4%	22.9%	12.6%
	ORBmed-R	11.2%	19.1%	25.2%	11.3%	16.1%	25.3%
	ORBmed-L	10.2%	15.7%	25.5%	13.4%	21.5%	22.1%
	REC-R	1.2%	1.3%	2.9%	1.9%	3.0%	4.4%
AFz	SFGdor-R	17.7%	7.1%	15.4%	7.3%	2.5%	6.7%
	SFGdor-L	22.1%	23.7%	10.6%	10.4%	9.3%	4.8%
	MFG-R	2.0%	0.2%	0.6%	0.9%	0.1%	0.3%
	MFG-L	5.5%	2.8%	0.9%	2.2%	0.9%	0.5%
	SFGmed-R	29.2%	36.3%	41.0%	40.7%	34.7%	52.5%
	SFGmed-L	20.9%	29.2%	30.8%	34.7%	51.0%	33.5%

Table S5-2 Normalized PPL of corresponding brain regions ($L_{norm,M}$) for the circumferential and vertical SD pairs set at 10/10 fiducial points at 25-mm SD distance from 0-yo, 1-yo, and 2-yo.

SD distance = 25 mm		Circumferential SD pair			Vertical SD pair		
10/10 Points	AAL regions	0 year	1 year	2 year	0 year	1 year	2 year
Fz	SFGdor-R	16.4%	8.6%	15.8%	6.9%	3.2%	7.9%
	SFGdor-L	36.2%	23.6%	13.1%	10.3%	9.3%	5.1%
	MFG-R	1.8%	0.1%	0.8%	0.9%	0.1%	0.5%
	MFG-L	3.5%	0.8%	0.7%	1.8%	0.5%	0.4%
	SMA-R	1.7%	0.2%	0.1%	2.4%	0.2%	0.1%
	SMA-L	1.2%	0.2%	0.0%	3.4%	0.2%	0.1%
	SFGmed-R	20.5%	37.1%	38.4%	37.0%	37.9%	54.2%
	SFGmed-L	18.5%	29.4%	31.1%	37.2%	48.3%	31.7%
FCz	PreCG-L	1.2%	0.0%	0.0%	0.9%	0.0%	0.0%
	SFGdor-R	15.7%	6.4%	13.4%	7.5%	2.7%	6.6%
	SFGdor-L	27.6%	19.7%	8.5%	13.5%	7.5%	4.1%
	MFG-R	1.6%	0.4%	1.2%	1.0%	0.2%	0.7%
	MFG-L	1.6%	0.6%	0.4%	1.0%	0.3%	0.2%
	SMA-R	16.8%	18.8%	15.1%	18.6%	18.8%	24.9%
	SMA-L	16.0%	22.8%	11.6%	24.1%	31.8%	15.6%
	SFGmed-R	8.1%	16.4%	24.7%	14.3%	14.8%	28.2%
	SFGmed-L	9.5%	15.0%	25.1%	17.1%	23.7%	19.8%
	PCL-R	1.4%	0.0%	0.0%	1.0%	0.0%	0.0%

Table S5-3 Normalized PPL of corresponding brain regions ($L_{norm,M}$) for the circumferential and vertical SD pairs set at 10/10 fiducial points at 25-mm SD distance from 0-yo, 1-yo, and 2-yo.

SD distance = 25 mm		Circumferential SD pair			Vertical SD pair		
10/10 Points	AAL regions	0 year	1 year	2 year	0 year	1 year	2 year
CPz	PreCG-R	2.0%	0.3%	0.5%	1.1%	0.3%	0.4%
	PreCG-L	6.6%	2.3%	3.1%	7.6%	3.4%	2.7%
	SFGdor-R	1.1%	0.1%	0.2%	1.2%	0.2%	0.2%
	SFGdor-L	1.2%	0.2%	0.3%	2.3%	0.4%	0.4%
	SMA-R	1.2%	0.4%	0.7%	2.2%	1.1%	1.4%
	SMA-L	1.5%	0.9%	1.2%	4.9%	3.2%	2.7%
	PoCG-R	13.0%	3.1%	4.4%	2.6%	1.0%	1.7%
	PoCG-L	24.7%	29.7%	25.0%	16.7%	17.2%	11.7%
	SPG-R	3.6%	2.1%	1.6%	1.4%	0.9%	1.0%
	SPG-L	8.1%	6.6%	3.8%	12.6%	7.6%	3.7%
	PCUN-R	13.8%	20.1%	17.3%	12.4%	15.2%	20.0%
	PCUN-L	4.0%	8.4%	5.8%	12.1%	16.6%	11.9%
	PCL-R	12.5%	15.7%	23.0%	11.2%	16.5%	24.7%
	PCL-L	6.6%	10.0%	13.0%	11.4%	16.6%	17.4%
Pz	PoCG-L	2.5%	0.8%	0.8%	6.3%	1.4%	1.0%
	SPG-R	9.5%	3.4%	4.4%	2.5%	1.3%	1.8%
	SPG-L	42.4%	41.3%	27.9%	34.7%	30.5%	15.7%
	PCUN-R	29.6%	34.0%	42.4%	24.2%	28.3%	44.6%
	PCUN-L	12.5%	19.6%	23.6%	26.9%	37.2%	35.8%
POz	CUN-R	10.0%	6.8%	8.3%	17.8%	11.4%	14.5%
	CUN-L	11.7%	19.0%	13.9%	16.3%	25.2%	15.5%
	SOG-R	17.0%	10.4%	14.8%	6.8%	5.6%	7.8%
	SOG-L	12.0%	7.4%	3.0%	7.8%	4.3%	1.8%
	MOG-L	2.3%	0.4%	0.2%	1.6%	0.3%	0.1%
	SPG-R	2.9%	4.4%	5.3%	1.4%	1.8%	2.2%
	SPG-L	24.3%	28.4%	24.5%	19.6%	19.3%	15.9%
	ANG-L	2.1%	0.5%	0.4%	1.0%	0.2%	0.1%
	PCUN-R	11.4%	15.3%	20.8%	14.8%	17.7%	26.9%
	PCUN-L	5.2%	7.0%	8.3%	12.1%	14.0%	15.0%

Table S5-4 Normalized PPL of corresponding brain regions ($L_{norm,M}$) for the circumferential and vertical SD pairs set at 10/10 fiducial points at 25-mm SD distance from 0-yo, 1-yo, and 2-yo.

SD distance = 25 mm		Circumferential SD pair			Vertical SD pair		
10/10 Points	AAL regions	0 year	1 year	2 year	0 year	1 year	2 year
Oz	CAL-R	3.7%	2.3%	2.9%	8.3%	5.1%	7.2%
	CUN-R	24.4%	28.2%	41.4%	23.9%	28.5%	49.5%
	CUN-L	12.5%	14.4%	16.5%	24.5%	29.6%	22.3%
	SOG-R	11.3%	9.5%	12.6%	4.0%	3.9%	5.9%
	SOG-L	35.8%	39.1%	23.1%	28.0%	27.8%	11.5%
	MOG-L	9.3%	5.1%	1.6%	4.8%	2.5%	0.7%
T3	STG-L	4.2%	8.3%	5.8%	11.0%	29.2%	18.4%
	TPOsup-L	2.8%	1.1%	1.1%	2.3%	1.3%	1.0%
	MTG-L	52.1%	82.3%	79.9%	50.4%	59.6%	67.1%
	TPOmid-L	6.1%	1.8%	2.1%	2.7%	0.8%	0.9%
	ITG-L	34.0%	6.4%	10.9%	32.6%	8.6%	12.2%
C5	PreCG-L	3.2%	4.5%	4.2%	3.9%	2.7%	3.0%
	IFGoperc-L	2.7%	0.8%	0.8%	1.0%	0.3%	0.4%
	IFGtriang-L	1.3%	0.1%	0.1%	0.5%	0.0%	0.1%
	ROL-L	9.0%	18.3%	12.0%	4.7%	5.2%	4.1%
	PoCG-L	13.8%	30.0%	32.4%	36.7%	41.6%	43.1%
	SMG-L	6.4%	8.7%	10.9%	5.5%	8.0%	9.1%
	STG-L	53.4%	36.0%	37.4%	34.1%	39.9%	37.1%
	TPOsup-L	3.5%	0.7%	0.8%	1.8%	0.4%	0.4%
	MTG-L	6.0%	0.8%	1.1%	11.0%	1.9%	2.6%
C3	PreCG-L	26.3%	36.8%	33.8%	18.8%	26.6%	27.1%
	MFG-L	5.3%	7.6%	6.4%	11.4%	7.7%	11.6%
	IFGoperc-L	1.8%	0.4%	0.4%	0.5%	0.1%	0.2%
	PoCG-L	35.0%	41.7%	42.6%	50.5%	58.6%	49.8%
	IPL-L	1.2%	0.5%	0.8%	0.5%	0.2%	0.3%
	SMG-L	29.1%	12.8%	15.7%	16.6%	6.7%	10.8%

Table S5-5 Normalized PPL of corresponding brain regions ($L_{norm,M}$) for the circumferential and vertical SD pairs set at 10/10 fiducial points at 25-mm SD distance from 0-yo, 1-yo, and 2-yo.

SD distance = 25 mm		Circumferential SD pair			Vertical SD pair		
10/10 Points	AAL regions	0 year	1 year	2 year	0 year	1 year	2 year
C1	PreCG-L	41.1%	42.3%	42.0%	32.2%	45.8%	43.0%
	SFGdor-L	19.6%	25.7%	22.0%	28.4%	36.2%	31.4%
	MFG-L	23.6%	25.8%	28.9%	21.4%	10.2%	18.2%
	SMA-L	1.1%	1.0%	0.6%	2.1%	1.8%	0.9%
	PoCG-L	12.7%	4.9%	6.1%	10.5%	5.6%	6.1%
C2	PreCG-R	37.7%	51.0%	43.2%	33.9%	51.3%	45.3%
	SFGdor-R	18.4%	14.1%	23.0%	34.0%	28.4%	31.8%
	MFG-R	20.7%	21.6%	25.7%	7.4%	7.4%	14.5%
	SMA-R	2.2%	1.0%	1.6%	4.8%	2.2%	2.7%
	PoCG-R	16.6%	11.2%	5.4%	15.2%	9.7%	4.8%
	PCL-R	1.8%	0.7%	0.7%	2.0%	0.7%	0.6%
C4	PreCG-R	25.0%	24.1%	37.6%	22.8%	18.8%	33.1%
	MFG-R	4.5%	1.1%	3.7%	2.8%	0.9%	2.4%
	PoCG-R	34.0%	49.3%	47.2%	46.7%	67.1%	53.4%
	IPL-R	19.2%	18.0%	7.4%	6.3%	4.6%	3.8%
	SMG-R	15.7%	7.2%	3.8%	19.9%	8.4%	7.0%
C6	PreCG-R	1.6%	0.9%	2.8%	3.0%	0.8%	3.7%
	IFGoperc-R	3.2%	0.2%	1.4%	1.1%	0.1%	0.7%
	IFGtriang-R	1.4%	0.1%	0.2%	0.7%	0.0%	0.2%
	ROL-R	6.6%	6.1%	4.8%	2.9%	1.3%	2.8%
	PoCG-R	20.6%	35.8%	46.2%	36.0%	44.0%	51.3%
	SMG-R	8.1%	12.0%	15.2%	6.6%	10.2%	6.7%
	STG-R	34.9%	39.6%	25.7%	20.5%	32.0%	28.4%
	TPOsup-R	1.1%	0.1%	0.1%	0.5%	0.0%	0.1%
	MTG-R	21.0%	5.2%	3.2%	27.2%	11.3%	6.0%

Table S5-6 Normalized PPL of corresponding brain regions ($L_{norm,M}$) for the circumferential and vertical SD pairs set at 10/10 fiducial points at 25-mm SD distance from 0-yo, 1-yo, and 2-yo.

SD distance = 25 mm		Circumferential SD pair			Vertical SD pair		
10/10 Points	AAL regions	0 year	1 year	2 year	0 year	1 year	2 year
T4	STG-R	2.1%	2.0%	3.7%	3.8%	3.7%	6.9%
	TPOsup-R	1.3%	0.2%	0.7%	1.1%	0.1%	0.4%
	MTG-R	61.1%	78.6%	82.4%	58.7%	72.9%	74.5%
	TPOmid-R	1.3%	0.1%	0.3%	0.9%	0.1%	0.1%
	ITG-R	33.2%	18.8%	12.4%	34.0%	22.9%	17.2%
FT7	IFGoperc-L	1.5%	1.6%	1.2%	3.3%	3.1%	2.1%
	IFGtriang-L	4.3%	2.5%	2.1%	3.5%	1.9%	2.1%
	ORBinf-L	15.9%	7.5%	6.0%	5.4%	2.3%	2.6%
	ROL-L	0.8%	1.5%	0.6%	2.1%	3.9%	1.2%
	STG-L	6.6%	16.4%	10.2%	6.0%	10.5%	6.8%
	TPOsup-L	26.2%	36.1%	35.9%	38.9%	40.4%	39.5%
	MTG-L	24.3%	20.1%	25.8%	12.3%	16.3%	19.5%
	TPOmid-L	14.8%	12.7%	17.0%	21.5%	19.2%	24.3%
	ITG-L	3.9%	0.9%	0.9%	4.7%	1.6%	1.6%
F7	MFG-L	3.1%	1.1%	0.7%	3.5%	1.2%	0.9%
	ORBmid-L	16.3%	3.4%	2.9%	6.2%	1.3%	1.4%
	IFGtriang-L	13.8%	15.1%	9.6%	32.0%	36.0%	27.9%
	ORBinf-L	53.9%	67.0%	65.3%	49.2%	53.6%	61.2%
	TPOsup-L	9.4%	11.1%	18.5%	5.9%	6.1%	7.1%
	TPOmid-L	1.0%	0.8%	1.9%	1.1%	0.6%	1.0%
AF7	SFGdor-L	3.8%	1.0%	0.8%	3.0%	0.7%	0.8%
	ORBsup-L	3.4%	1.8%	2.1%	1.8%	0.8%	1.3%
	MFG-L	16.6%	12.8%	7.2%	31.3%	27.0%	20.7%
	ORBmid-L	41.6%	49.2%	55.3%	43.3%	47.1%	57.1%
	IFGtriang-L	9.5%	5.6%	3.4%	6.2%	5.7%	3.9%
	ORBinf-L	23.7%	29.5%	30.6%	13.5%	18.6%	15.8%

Table S5-7 Normalized PPL of corresponding brain regions ($L_{norm,M}$) for the circumferential and vertical SD pairs set at 10/10 fiducial points at 25-mm SD distance from 0-yo, 1-yo, and 2-yo.

SD distance = 25 mm		Circumferential SD pair			Vertical SD pair		
10/10 Points	AAL regions	0 year	1 year	2 year	0 year	1 year	2 year
Fp1	SFGdor-L	18.7%	17.1%	8.5%	30.2%	26.8%	21.5%
	ORBsup-L	16.0%	30.5%	29.1%	16.2%	24.9%	31.1%
	MFG-L	15.0%	9.4%	4.5%	14.0%	12.1%	5.6%
	ORBmid-L	28.0%	33.9%	39.3%	24.8%	30.9%	30.9%
	ORBinf-L	1.3%	0.3%	0.4%	0.9%	0.3%	0.3%
	SFGmed-R	2.2%	0.2%	0.4%	1.5%	0.1%	0.3%
	SFGmed-L	9.4%	3.9%	3.7%	6.7%	2.2%	3.4%
	ORBmed-R	1.5%	0.2%	1.0%	0.8%	0.1%	0.6%
	ORBmed-L	6.2%	4.3%	12.3%	3.6%	2.2%	5.6%
Fp2	SFGdor-R	24.1%	22.8%	15.5%	34.1%	35.9%	28.7%
	ORBsup-R	11.9%	20.6%	24.7%	15.7%	25.9%	25.1%
	MFG-R	16.1%	9.4%	8.0%	11.6%	5.9%	10.8%
	ORBmid-R	16.6%	27.2%	34.7%	15.5%	17.0%	24.2%
	ORBinf-R	1.6%	0.3%	0.9%	1.2%	0.1%	0.5%
	SFGmed-R	13.4%	6.5%	3.3%	10.4%	5.6%	3.2%
	SFGmed-L	2.7%	0.4%	0.3%	1.7%	0.3%	0.3%
	ORBmed-R	8.7%	11.6%	10.3%	6.1%	7.6%	5.3%
	ORBmed-L	2.0%	0.5%	0.8%	1.2%	0.4%	0.5%
	REC-R	0.8%	0.6%	1.1%	1.1%	1.0%	1.2%
AF8	SFGdor-R	7.9%	1.8%	1.7%	5.0%	1.0%	1.1%
	ORBsup-R	3.8%	1.4%	2.0%	2.3%	0.7%	1.0%
	MFG-R	21.0%	16.2%	11.5%	36.4%	26.6%	24.7%
	ORBmid-R	33.8%	55.5%	53.1%	33.8%	49.4%	48.6%
	IFGtriang-R	11.4%	7.5%	8.4%	7.4%	6.2%	8.5%
	ORBinf-R	20.1%	17.4%	22.6%	13.8%	15.8%	15.8%

Table S5-8 Normalized PPL of corresponding brain regions ($L_{norm,M}$) for the circumferential and vertical SD pairs set at 10/10 fiducial points at 25-mm SD distance from 0-yo, 1-yo, and 2-yo.

SD distance = 25 mm		Circumferential SD pair			Vertical SD pair		
10/10 Points	AAL regions	0 year	1 year	2 year	0 year	1 year	2 year
F8	MFG-R	4.2%	0.4%	1.0%	4.5%	0.2%	1.2%
	ORBmid-R	11.9%	1.7%	3.7%	5.7%	0.5%	2.0%
	IFGoperc-R	1.5%	0.8%	0.8%	1.0%	1.3%	0.8%
	IFGtriang-R	19.5%	16.9%	25.1%	33.4%	33.2%	45.6%
	ORBinf-R	49.4%	63.3%	50.0%	47.8%	50.5%	37.2%
	STG-R	1.1%	0.8%	0.5%	0.4%	0.5%	0.3%
	TPOsup-R	9.1%	13.5%	16.2%	5.0%	11.3%	10.7%
	TPOmid-R	0.8%	1.0%	1.2%	0.7%	1.3%	1.2%
FT8	IFGoperc-R	1.8%	0.7%	2.0%	4.8%	1.4%	3.3%
	IFGtriang-R	4.9%	1.4%	3.9%	4.7%	1.3%	2.9%
	ORBinf-R	18.9%	3.2%	4.8%	6.5%	1.3%	2.0%
	ROL-R	1.5%	1.1%	1.9%	3.9%	3.3%	3.8%
	STG-R	7.6%	10.5%	12.2%	11.1%	21.7%	14.8%
	TPOsup-R	19.5%	21.3%	27.4%	23.2%	15.9%	24.7%
	MTG-R	34.9%	55.1%	42.9%	28.3%	47.6%	40.8%
	TPOmid-R	5.7%	4.3%	3.4%	10.5%	4.0%	5.4%
	ITG-R	3.6%	1.8%	0.9%	4.9%	2.8%	1.5%
TP7	STG-L	6.2%	6.6%	3.4%	17.1%	18.8%	6.6%
	MTG-L	58.5%	85.1%	82.2%	52.0%	61.8%	66.4%
	ITG-L	34.8%	8.2%	14.3%	30.3%	19.2%	26.9%
T5	MOG-L	1.5%	0.8%	1.1%	0.3%	0.6%	0.5%
	STG-L	2.5%	3.0%	1.5%	10.1%	8.0%	2.9%
	MTG-L	75.9%	88.1%	87.5%	62.9%	75.8%	76.9%
	ITG-L	19.0%	7.1%	9.1%	25.1%	13.1%	18.6%
PO7	MOG-L	43.6%	51.6%	53.5%	38.3%	53.5%	59.0%
	IOG-L	1.7%	0.4%	1.0%	9.0%	1.2%	2.6%
	ANG-L	1.9%	4.5%	1.0%	6.0%	8.8%	3.1%
	MTG-L	50.1%	42.8%	43.8%	41.5%	35.8%	34.6%
	ITG-L	1.8%	0.4%	0.5%	4.7%	0.6%	0.6%

Table S5-9 Normalized PPL of corresponding brain regions ($L_{norm,M}$) for the circumferential and vertical SD pairs set at 10/10 fiducial points at 25-mm SD distance from 0-yo, 1-yo, and 2-yo.

SD distance = 25 mm		Circumferential SD pair			Vertical SD pair		
10/10 Points	AAL regions	0 year	1 year	2 year	0 year	1 year	2 year
O1	CUN-L	2.3%	1.2%	1.8%	1.6%	1.0%	1.2%
	SOG-L	23.8%	27.0%	29.3%	17.6%	16.2%	21.9%
	MOG-L	68.4%	69.4%	66.8%	72.6%	79.8%	74.4%
	ANG-L	1.1%	1.1%	0.5%	1.7%	1.5%	0.8%
	MTG-L	1.8%	0.4%	0.3%	0.2%	0.2%	0.2%
O2	CAL-R	2.8%	1.0%	0.3%	4.1%	1.6%	0.4%
	CUN-R	17.2%	17.2%	8.1%	6.5%	10.3%	4.5%
	CUN-L	1.8%	0.9%	0.4%	0.8%	0.7%	0.3%
	SOG-R	37.7%	53.5%	47.1%	47.3%	64.5%	50.2%
	MOG-R	38.3%	26.4%	43.3%	38.5%	21.9%	43.7%
PO8	SOG-R	3.7%	4.0%	1.3%	1.3%	1.8%	0.9%
	MOG-R	79.3%	87.1%	81.1%	85.9%	88.7%	83.8%
	IOG-R	2.3%	0.9%	0.5%	3.2%	1.3%	0.5%
	ANG-R	4.1%	4.1%	5.7%	6.7%	5.9%	9.5%
	MTG-R	9.8%	3.4%	11.1%	1.9%	1.7%	4.9%
T6	MOG-R	17.8%	21.9%	12.1%	10.2%	16.5%	9.2%
	IOG-R	7.9%	4.5%	1.8%	23.8%	12.9%	5.7%
	ANG-R	1.8%	4.4%	3.9%	6.2%	8.1%	6.3%
	STG-R	1.5%	1.0%	2.5%	1.2%	0.8%	2.2%
	MTG-R	57.2%	64.5%	76.6%	42.0%	56.8%	70.1%
	ITG-R	13.2%	3.0%	2.2%	15.1%	3.8%	4.1%
TP8	STG-R	2.0%	2.5%	5.1%	5.0%	6.7%	10.0%
	MTG-R	67.3%	85.1%	88.0%	59.3%	74.1%	79.7%
	ITG-R	29.6%	11.5%	6.2%	34.7%	18.3%	9.4%

Table S5-10 Normalized PPL of corresponding brain regions ($L_{norm,M}$) for the circumferential and vertical SD pairs set at 10/10 fiducial points at 25-mm SD distance from 0-yo, 1-yo, and 2-yo.

SD distance = 25 mm		Circumferential SD pair			Vertical SD pair		
10/10 Points	AAL regions	0 year	1 year	2 year	0 year	1 year	2 year
FC5	PreCG-L	7.1%	15.1%	13.3%	13.8%	14.3%	15.9%
	MFG-L	1.9%	0.8%	0.8%	2.4%	1.3%	0.7%
	IFGoperc-L	11.1%	20.3%	20.8%	27.6%	43.9%	38.7%
	IFGtriang-L	38.4%	34.9%	34.9%	28.6%	23.9%	19.6%
	ORBinf-L	4.8%	0.7%	0.8%	4.6%	1.1%	0.8%
	ROL-L	10.8%	16.5%	17.0%	5.1%	8.7%	11.7%
	PoCG-L	11.1%	7.7%	5.7%	3.4%	1.7%	2.2%
	STG-L	6.2%	1.6%	2.3%	2.3%	0.9%	1.8%
	TPOsup-L	6.9%	2.3%	4.0%	10.4%	4.1%	8.3%
FC3	PreCG-L	25.6%	25.2%	21.2%	14.4%	11.8%	9.1%
	MFG-L	53.8%	60.2%	59.3%	47.6%	58.6%	54.1%
	IFGoperc-L	8.7%	9.2%	12.0%	16.5%	18.3%	20.6%
	IFGtriang-L	7.4%	4.6%	6.0%	18.4%	10.6%	15.2%
	PoCG-L	3.4%	0.5%	1.0%	1.8%	0.3%	0.5%
FC1	PreCG-L	3.0%	0.5%	0.4%	3.9%	0.3%	0.3%
	SFGdor-L	31.1%	45.9%	45.8%	34.1%	44.5%	44.3%
	MFG-L	56.8%	49.7%	47.8%	54.6%	51.6%	50.3%
	SMA-L	2.2%	1.7%	1.4%	3.7%	2.5%	2.4%
	SFGmed-L	5.0%	2.0%	4.1%	1.9%	0.9%	2.2%
FC2	PreCG-R	6.0%	0.5%	0.6%	2.5%	0.3%	0.4%
	SFGdor-R	33.2%	41.5%	32.6%	30.8%	34.9%	28.9%
	MFG-R	47.0%	51.0%	61.4%	46.8%	58.0%	66.8%
	SMA-R	4.7%	2.2%	1.3%	7.0%	4.6%	1.8%
	SFGmed-R	6.0%	4.6%	3.5%	2.2%	1.8%	1.8%
FC4	PreCG-R	24.9%	26.7%	19.1%	16.8%	16.8%	10.4%
	MFG-R	58.0%	65.2%	71.5%	58.4%	71.3%	70.6%
	IFGoperc-R	4.4%	2.6%	3.2%	8.0%	5.1%	6.5%
	IFGtriang-R	6.1%	3.7%	4.9%	12.3%	5.7%	11.6%
	PoCG-R	4.9%	1.7%	0.9%	2.8%	0.9%	0.6%

Table S5-11 Normalized PPL of corresponding brain regions ($L_{norm,M}$) for the circumferential and vertical SD pairs set at 10/10 fiducial points at 25-mm SD distance from 0-yo, 1-yo, and 2-yo.

SD distance = 25 mm		Circumferential SD pair			Vertical SD pair		
10/10 Points	AAL regions	0 year	1 year	2 year	0 year	1 year	2 year
FC6	PreCG-R	5.4%	9.3%	9.9%	12.7%	24.1%	11.7%
	MFG-R	3.9%	0.9%	1.9%	5.0%	1.9%	2.7%
	IFGoperc-R	13.3%	18.0%	20.1%	22.7%	20.4%	29.0%
	IFGtriang-R	35.8%	25.6%	40.8%	26.5%	13.1%	33.9%
	ORBinf-R	2.5%	0.2%	0.2%	2.4%	0.3%	0.4%
	ROL-R	6.7%	9.4%	6.4%	6.0%	13.3%	7.8%
	PoCG-R	18.7%	30.7%	16.7%	9.5%	16.0%	7.6%
	STG-R	7.4%	4.2%	2.6%	6.4%	6.9%	3.5%
	TPOsup-R	2.9%	1.1%	1.0%	5.7%	3.3%	2.9%
	MTG-R	2.2%	0.5%	0.3%	2.2%	0.8%	0.4%
F5	MFG-L	26.2%	29.6%	29.7%	35.1%	24.3%	24.4%
	ORBmid-L	4.5%	0.9%	1.3%	4.5%	0.8%	1.3%
	IFGoperc-L	4.0%	1.9%	0.8%	1.7%	0.8%	0.5%
	IFGtriang-L	52.2%	63.0%	62.7%	43.0%	64.1%	59.8%
	ORBinf-L	9.3%	3.9%	4.9%	14.0%	9.6%	13.6%
	TPOsup-L	1.4%	0.3%	0.3%	0.6%	0.2%	0.2%
F3	SFGdor-L	5.0%	1.4%	2.5%	4.4%	1.7%	2.1%
	MFG-L	75.0%	89.0%	89.3%	85.6%	94.2%	92.4%
	IFGoperc-L	1.6%	0.4%	0.4%	0.6%	0.1%	0.2%
	IFGtriang-L	16.5%	9.0%	7.5%	7.2%	3.7%	4.9%
F1	SFGdor-L	26.2%	44.8%	41.0%	43.5%	49.7%	50.5%
	MFG-L	50.4%	36.8%	38.7%	40.7%	43.7%	40.4%
	SFGmed-R	4.1%	0.9%	2.0%	2.9%	0.4%	1.1%
	SFGmed-L	17.6%	17.3%	18.1%	11.3%	5.9%	7.8%
F2	SFGdor-R	30.4%	51.3%	51.0%	51.7%	68.4%	57.2%
	MFG-R	33.9%	24.3%	31.3%	28.2%	19.0%	34.6%
	SFGmed-R	29.1%	23.0%	16.3%	14.6%	11.7%	7.5%
	SFGmed-L	4.2%	1.2%	1.2%	2.7%	0.7%	0.6%

Table S5-12 Normalized PPL of corresponding brain regions ($L_{norm,M}$) for the circumferential and vertical SD pairs set at 10/10 fiducial points at 25-mm SD distance from 0-yo, 1-yo, and 2-yo.

SD distance = 25 mm		Circumferential SD pair			Vertical SD pair		
10/10 Points	AAL regions	0 year	1 year	2 year	0 year	1 year	2 year
F4	SFGdor-R	10.0%	5.2%	3.7%	8.0%	3.6%	2.9%
	MFG-R	70.4%	89.6%	87.1%	81.0%	90.0%	89.1%
	IFGoperc-R	1.3%	0.2%	0.2%	0.4%	0.1%	0.1%
	IFGtriang-R	16.1%	4.7%	8.8%	8.4%	6.0%	7.7%
F6	SFGdor-R	1.1%	0.1%	0.1%	0.9%	0.1%	0.1%
	MFG-R	35.4%	22.5%	24.1%	40.0%	18.4%	19.7%
	ORBmid-R	3.0%	1.1%	1.8%	4.7%	1.5%	1.6%
	IFGoperc-R	4.6%	2.5%	0.7%	1.6%	1.0%	0.5%
	IFGtriang-R	48.4%	71.1%	71.4%	42.0%	72.3%	74.5%
	ORBinf-R	4.7%	2.0%	1.4%	9.3%	6.3%	3.1%
AF3	SFGdor-L	30.4%	39.5%	41.3%	30.2%	31.1%	38.3%
	ORBsup-L	1.7%	1.1%	1.5%	3.4%	2.4%	4.5%
	MFG-L	49.7%	53.7%	46.7%	50.5%	60.5%	47.1%
	ORBmid-L	3.4%	1.5%	2.4%	7.6%	3.8%	5.9%
	IFGtriang-L	1.3%	0.2%	0.3%	0.7%	0.1%	0.2%
	SFGmed-R	1.9%	0.2%	0.4%	1.2%	0.1%	0.3%
	SFGmed-L	10.1%	3.6%	7.0%	5.0%	1.8%	3.3%
AF4	SFGdor-R	35.0%	45.1%	37.7%	43.2%	54.6%	34.5%
	ORBsup-R	1.1%	0.5%	0.9%	2.2%	1.2%	1.8%
	MFG-R	41.2%	43.7%	53.5%	38.4%	36.6%	56.6%
	ORBmid-R	2.0%	0.8%	1.8%	4.3%	2.0%	3.7%
	IFGtriang-R	1.7%	0.4%	0.6%	0.9%	0.1%	0.4%
	SFGmed-R	15.4%	9.0%	4.9%	8.0%	4.9%	2.5%
	SFGmed-L	1.8%	0.3%	0.2%	1.1%	0.2%	0.2%
CP5	PoCG-L	4.0%	1.2%	1.1%	2.0%	0.7%	0.7%
	SMG-L	23.3%	50.1%	45.0%	38.9%	49.8%	41.2%
	ANG-L	1.7%	5.6%	4.4%	0.5%	1.1%	1.1%
	STG-L	61.2%	39.7%	45.0%	35.3%	40.9%	46.2%
	MTG-L	9.1%	2.8%	3.7%	22.7%	7.0%	10.3%

Table S5-13 Normalized PPL of corresponding brain regions ($L_{norm,M}$) for the circumferential and vertical SD pairs set at 10/10 fiducial points at 25-mm SD distance from 0-yo, 1-yo, and 2-yo.

SD distance = 25 mm		Circumferential SD pair			Vertical SD pair		
10/10 Points	AAL regions	0 year	1 year	2 year	0 year	1 year	2 year
CP3	PreCG-L	1.0%	0.4%	0.7%	0.8%	0.5%	0.7%
	PoCG-L	20.9%	20.5%	12.1%	23.5%	21.5%	13.4%
	SPG-L	2.1%	2.1%	2.4%	1.1%	1.7%	2.2%
	IPL-L	36.4%	52.9%	53.9%	20.9%	39.3%	53.2%
	SMG-L	37.9%	23.7%	29.7%	50.8%	36.3%	28.9%
	ANG-L	1.3%	0.3%	1.1%	1.6%	0.7%	1.5%
CP1	PreCG-L	13.9%	8.3%	9.5%	24.5%	12.6%	12.1%
	PoCG-L	46.7%	56.7%	54.6%	34.3%	50.4%	51.2%
	SPG-L	31.3%	31.6%	31.6%	23.6%	30.9%	29.6%
	IPL-L	4.8%	2.5%	3.1%	13.3%	4.8%	5.8%
CP2	PreCG-R	12.4%	5.1%	6.8%	12.5%	5.7%	11.2%
	SFGdor-R	1.3%	0.2%	0.4%	2.0%	0.4%	0.8%
	PoCG-R	40.6%	51.4%	53.7%	40.0%	47.3%	51.9%
	SPG-R	29.9%	32.6%	30.2%	25.5%	34.9%	25.6%
	IPL-R	2.4%	2.1%	2.8%	7.3%	4.2%	4.5%
	PCUN-R	8.6%	6.1%	3.3%	3.4%	2.8%	1.6%
	PCL-R	2.9%	2.1%	2.3%	6.6%	4.3%	3.8%
CP4	PreCG-R	1.8%	0.2%	1.0%	2.0%	0.3%	1.1%
	PoCG-R	24.1%	19.6%	24.5%	26.7%	26.2%	31.0%
	SPG-R	2.8%	2.0%	1.3%	2.0%	2.0%	1.1%
	IPL-R	59.2%	74.7%	70.7%	53.6%	68.4%	63.4%
	SMG-R	6.4%	1.2%	1.6%	10.3%	1.2%	2.5%
	ANG-R	5.2%	2.2%	0.9%	4.9%	1.9%	0.8%
CP6	PoCG-R	4.5%	1.1%	2.6%	2.5%	0.5%	1.4%
	IPL-R	4.6%	7.4%	8.3%	10.5%	17.1%	10.6%
	SMG-R	38.9%	53.1%	69.4%	40.2%	44.1%	60.9%
	ANG-R	10.8%	7.2%	3.4%	1.6%	2.2%	1.7%
	STG-R	23.5%	26.5%	13.9%	18.9%	27.6%	21.1%
	MTG-R	17.1%	4.7%	2.3%	25.8%	8.4%	4.2%

Table S5-14 Normalized PPL of corresponding brain regions ($L_{norm,M}$) for the circumferential and vertical SD pairs set at 10/10 fiducial points at 25-mm SD distance from 0-yo, 1-yo, and 2-yo.

SD distance = 25 mm		Circumferential SD pair			Vertical SD pair		
10/10 Points	AAL regions	0 year	1 year	2 year	0 year	1 year	2 year
P5	MOG-L	7.1%	2.6%	3.1%	1.2%	1.8%	2.7%
	IPL-L	1.7%	4.9%	3.8%	9.7%	17.0%	11.0%
	SMG-L	11.7%	9.0%	4.6%	7.3%	3.4%	2.2%
	ANG-L	29.2%	61.0%	61.3%	32.4%	47.3%	51.0%
	STG-L	24.7%	11.2%	10.6%	11.3%	5.4%	3.0%
	MTG-L	25.5%	11.3%	16.5%	38.0%	25.2%	30.0%
P3	SPG-L	7.5%	9.0%	6.3%	7.1%	8.5%	5.9%
	IPL-L	43.5%	50.8%	40.3%	29.3%	31.4%	33.1%
	SMG-L	5.0%	0.8%	0.5%	1.1%	0.4%	0.3%
	ANG-L	41.9%	38.8%	52.3%	57.9%	58.8%	59.9%
P1	PoCG-L	3.3%	1.1%	0.9%	3.4%	1.4%	1.0%
	SPG-L	67.8%	85.3%	81.4%	69.8%	82.4%	82.5%
	IPL-L	12.7%	5.5%	7.4%	4.0%	3.6%	3.8%
	ANG-L	9.7%	5.7%	7.4%	18.0%	11.4%	10.5%
	PCUN-R	1.3%	0.4%	0.6%	0.7%	0.2%	0.4%
	PCUN-L	3.6%	1.7%	2.0%	1.7%	0.7%	1.3%
P2	SOG-R	1.2%	0.3%	0.1%	3.8%	0.6%	0.3%
	PoCG-R	3.0%	0.3%	1.0%	2.3%	0.3%	0.9%
	SPG-R	54.3%	63.3%	69.0%	57.9%	68.8%	76.1%
	SPG-L	1.1%	0.3%	0.1%	0.8%	0.2%	0.1%
	IPL-R	6.0%	1.9%	3.0%	6.4%	2.2%	4.4%
	ANG-R	4.8%	1.5%	1.7%	3.1%	1.0%	2.3%
	PCUN-R	25.9%	30.9%	24.0%	22.4%	25.8%	15.3%
	PCUN-L	2.1%	1.3%	0.8%	1.4%	0.8%	0.5%
P4	SOG-R	1.8%	0.3%	0.1%	0.8%	0.2%	0.1%
	MOG-R	3.4%	0.6%	0.8%	19.2%	2.6%	1.7%
	SPG-R	14.2%	25.6%	15.3%	14.3%	23.2%	17.5%
	IPL-R	36.5%	27.8%	35.0%	14.5%	16.2%	27.4%
	ANG-R	41.9%	45.0%	47.9%	49.5%	57.2%	52.5%

Table S5-15 Normalized PPL of corresponding brain regions ($L_{norm,M}$) for the circumferential and vertical SD pairs set at 10/10 fiducial points at 25-mm SD distance from 0-yo, 1-yo, and 2-yo.

SD distance = 25 mm		Circumferential SD pair			Vertical SD pair		
10/10 Points	AAL regions	0 year	1 year	2 year	0 year	1 year	2 year
P6	MOG-R	21.6%	10.0%	3.8%	9.3%	6.8%	2.4%
	IPL-R	4.3%	6.0%	8.4%	11.0%	7.3%	11.9%
	SMG-R	12.7%	7.0%	11.1%	4.0%	1.9%	5.1%
	ANG-R	45.4%	71.2%	72.2%	58.3%	75.0%	72.2%
	STG-R	2.8%	0.5%	0.5%	0.8%	0.2%	0.4%
	MTG-R	12.8%	4.9%	3.9%	15.8%	8.5%	8.0%
PO3	CUN-L	2.6%	1.7%	1.5%	1.1%	0.6%	0.8%
	SOG-L	11.5%	23.4%	19.8%	11.4%	11.4%	14.1%
	MOG-L	24.7%	16.7%	22.0%	43.6%	31.0%	33.1%
	SPG-L	7.3%	9.4%	7.1%	13.5%	10.6%	10.8%
	ANG-L	51.9%	48.3%	49.0%	29.2%	45.9%	40.6%
PO4	CUN-R	3.2%	2.2%	1.1%	3.0%	1.8%	0.9%
	SOG-R	24.0%	38.8%	31.0%	38.6%	39.7%	26.3%
	MOG-R	37.8%	24.6%	26.2%	23.5%	24.1%	30.0%
	SPG-R	5.1%	7.6%	7.9%	14.2%	17.0%	13.2%
	IPL-R	15.5%	21.4%	25.7%	12.9%	14.2%	25.2%
	ANG-R	10.5%	3.3%	6.5%	2.9%	1.4%	2.6%
	PCUN-R	2.3%	1.4%	1.3%	3.4%	1.4%	1.4%

Table S6-1 Normalized PPL of corresponding brain regions ($L_{norm,M}$) for the circumferential and vertical SD pairs set at 10/10 fiducial points at 30-mm SD distance from 0-yo, 1-yo, and 2-yo.

SD distance = 30 mm		Circumferential SD pair			Vertical SD pair		
10/10 Points	AAL regions	0 year	1 year	2 year	0 year	1 year	2 year
Cz	PreCG-R	5.3%	1.5%	1.3%	1.8%	0.6%	0.8%
	PreCG-L	9.2%	4.3%	2.8%	8.0%	4.5%	2.2%
	SFGdor-R	22.2%	12.7%	13.0%	6.0%	2.9%	5.0%
	SFGdor-L	24.0%	25.4%	20.7%	12.6%	10.5%	6.9%
	SMA-R	11.1%	27.5%	31.4%	16.3%	27.0%	40.2%
	SMA-L	10.5%	21.1%	25.2%	23.5%	38.0%	32.2%
	PoCG-R	2.1%	0.3%	0.2%	1.4%	0.2%	0.2%
	PoCG-L	3.4%	0.6%	0.4%	6.1%	1.3%	0.5%
	SPG-L	1.3%	0.0%	0.0%	1.6%	0.1%	0.0%
	PCL-R	6.6%	4.8%	3.1%	9.2%	8.8%	8.0%
	PCL-L	2.0%	1.1%	0.9%	8.9%	5.1%	2.6%
Fpz	SFGdor-R	9.9%	5.9%	5.8%	3.7%	2.1%	3.6%
	SFGdor-L	12.0%	9.2%	2.4%	6.6%	5.7%	1.7%
	ORBsup-R	6.7%	6.7%	11.2%	3.4%	3.5%	5.8%
	ORBsup-L	10.8%	15.6%	11.9%	13.3%	11.1%	7.1%
	MFG-R	1.1%	0.2%	0.4%	0.4%	0.1%	0.2%
	MFG-L	1.8%	0.3%	0.1%	1.0%	0.2%	0.1%
	ORBmid-R	2.2%	0.8%	1.8%	0.9%	0.3%	0.8%
	ORBmid-L	3.9%	2.1%	2.0%	3.0%	1.6%	1.0%
	SFGmed-R	15.4%	12.1%	8.3%	19.4%	13.1%	15.7%
	SFGmed-L	14.5%	13.5%	8.0%	19.9%	24.9%	12.2%
	ORBmed-R	10.5%	18.1%	22.1%	10.3%	14.9%	24.8%
	ORBmed-L	9.1%	13.5%	22.4%	12.3%	17.2%	19.8%
	REC-R	1.3%	1.5%	2.9%	3.2%	3.8%	5.5%

Table S6-2 Normalized PPL of corresponding brain regions ($L_{norm,M}$) for the circumferential and vertical SD pairs set at 10/10 fiducial points at 30-mm SD distance from 0-yo, 1-yo, and 2-yo.

SD distance = 30 mm		Circumferential SD pair			Vertical SD pair		
10/10 Points	AAL regions	0 year	1 year	2 year	0 year	1 year	2 year
AFz	SFGdor-R	21.9%	11.5%	18.1%	7.6%	3.0%	7.1%
	SFGdor-L	20.5%	24.9%	14.1%	11.0%	9.5%	5.4%
	MFG-R	3.0%	0.4%	1.0%	1.1%	0.1%	0.4%
	MFG-L	7.7%	4.6%	1.4%	2.5%	1.0%	0.6%
	SFGmed-R	25.2%	33.3%	36.3%	38.6%	35.8%	50.9%
	SFGmed-L	18.7%	24.6%	28.2%	34.2%	48.2%	33.2%
Fz	SFGdor-R	17.7%	12.7%	18.6%	6.6%	3.6%	9.0%
	SFGdor-L	35.2%	33.2%	17.8%	10.0%	9.1%	5.8%
	MFG-R	2.4%	0.3%	1.1%	1.0%	0.1%	0.7%
	MFG-L	6.4%	1.8%	1.3%	2.1%	0.6%	0.5%
	SMA-R	2.0%	0.3%	0.1%	2.8%	0.4%	0.1%
	SMA-L	1.6%	0.4%	0.1%	9.3%	0.4%	0.1%
	SFGmed-R	17.9%	26.1%	33.3%	29.2%	38.1%	52.8%
	SFGmed-L	16.5%	25.2%	27.9%	38.6%	47.3%	31.0%
FCz	PreCG-R	6.8%	0.0%	0.0%	0.4%	0.0%	0.0%
	PreCG-L	1.2%	0.0%	0.0%	1.1%	0.0%	0.0%
	SFGdor-R	21.9%	11.4%	15.3%	8.9%	3.1%	6.7%
	SFGdor-L	26.7%	25.0%	14.3%	13.6%	8.7%	5.0%
	MFG-R	3.0%	0.7%	1.6%	1.3%	0.2%	0.8%
	MFG-L	2.6%	1.2%	0.7%	1.2%	0.4%	0.3%
	SMA-R	12.3%	15.6%	13.0%	18.7%	17.6%	23.4%
	SMA-L	11.6%	18.6%	10.4%	23.1%	31.3%	15.8%
	SFGmed-R	5.9%	14.7%	21.3%	14.2%	15.8%	27.2%
	SFGmed-L	7.0%	12.8%	23.3%	15.7%	22.6%	20.8%

Table S6-3 Normalized PPL of corresponding brain regions ($L_{norm,M}$) for the circumferential and vertical SD pairs set at 10/10 fiducial points at 30-mm SD distance from 0-yo, 1-yo, and 2-yo.

SD distance = 30 mm		Circumferential SD pair			Vertical SD pair		
10/10 Points	AAL regions	0 year	1 year	2 year	0 year	1 year	2 year
CPz	PreCG-R	2.5%	0.5%	0.6%	1.4%	0.3%	0.5%
	PreCG-L	7.0%	2.8%	4.2%	7.6%	4.1%	3.2%
	SFGdor-R	1.2%	0.2%	0.2%	1.6%	0.2%	0.3%
	SFGdor-L	1.2%	0.2%	0.4%	3.0%	0.6%	0.7%
	SMA-R	1.2%	0.5%	0.8%	3.2%	1.6%	2.4%
	SMA-L	1.5%	0.9%	1.3%	5.3%	4.6%	4.2%
	PoCG-R	15.3%	5.6%	5.8%	3.0%	1.1%	1.8%
	PoCG-L	24.6%	29.6%	26.0%	14.5%	15.3%	11.1%
	SPG-R	4.9%	3.6%	2.2%	1.9%	1.1%	1.1%
	SPG-L	9.4%	8.6%	4.5%	14.7%	7.6%	4.4%
	PCUN-R	11.3%	18.7%	16.1%	13.5%	16.6%	18.8%
	PCUN-L	3.5%	7.1%	5.0%	10.9%	15.9%	12.1%
	PCL-R	10.7%	13.8%	21.2%	10.6%	16.1%	24.2%
	PCL-L	5.5%	7.9%	11.6%	8.5%	14.9%	15.2%
Pz	PoCG-R	1.3%	0.1%	0.2%	0.7%	0.1%	0.1%
	PoCG-L	3.8%	1.0%	0.9%	7.2%	2.3%	1.4%
	SPG-R	16.0%	5.1%	6.5%	3.0%	1.3%	1.9%
	SPG-L	40.3%	41.5%	28.6%	32.1%	32.2%	15.3%
	PCUN-R	24.8%	34.3%	41.7%	25.4%	27.0%	44.5%
	PCUN-L	9.8%	17.1%	21.2%	24.4%	35.2%	35.2%

Table S6-4 Normalized PPL of corresponding brain regions ($L_{norm,M}$) for the circumferential and vertical SD pairs set at 10/10 fiducial points at 30-mm SD distance from 0-yo, 1-yo, and 2-yo.

SD distance = 30 mm		Circumferential SD pair			Vertical SD pair		
10/10 Points	AAL regions	0 year	1 year	2 year	0 year	1 year	2 year
POz	CUN-R	7.9%	6.2%	8.0%	17.3%	12.5%	15.5%
	CUN-L	9.2%	16.1%	13.9%	15.3%	24.0%	15.2%
	SOG-R	17.8%	12.8%	16.9%	6.2%	5.3%	7.6%
	SOG-L	12.9%	8.7%	4.3%	8.9%	4.9%	1.9%
	MOG-L	2.9%	0.6%	0.4%	1.8%	0.4%	0.2%
	SPG-R	3.6%	6.4%	5.8%	1.5%	1.7%	2.1%
	SPG-L	25.8%	27.5%	24.2%	19.6%	19.3%	14.8%
	ANG-L	3.5%	0.7%	0.5%	1.1%	0.3%	0.1%
	PCUN-R	10.0%	14.3%	18.2%	14.9%	16.6%	26.7%
	PCUN-L	4.6%	6.2%	7.1%	12.6%	14.9%	15.6%
Oz	CAL-R	2.9%	2.2%	2.9%	9.6%	6.5%	9.0%
	CUN-R	20.6%	26.3%	37.0%	20.8%	29.4%	46.6%
	CUN-L	10.8%	12.8%	14.9%	21.3%	29.5%	22.1%
	SOG-R	15.9%	12.0%	15.3%	4.3%	4.7%	6.7%
	SOG-L	30.4%	37.4%	25.2%	27.0%	23.8%	10.9%
	MOG-R	1.4%	0.4%	0.9%	0.5%	0.3%	0.5%
	MOG-L	15.1%	7.6%	2.3%	6.3%	2.5%	0.8%
T3	STG-L	3.5%	9.2%	6.6%	15.0%	32.1%	25.8%
	TPOsup-L	3.6%	1.6%	1.5%	3.3%	1.5%	1.4%
	MTG-L	41.6%	78.7%	77.3%	41.5%	53.1%	57.2%
	TPOmid-L	8.3%	2.9%	3.1%	3.7%	0.9%	1.0%
	ITG-L	41.8%	7.4%	11.3%	34.6%	11.7%	13.9%

Table S6-5 Normalized PPL of corresponding brain regions ($L_{norm,M}$) for the circumferential and vertical SD pairs set at 10/10 fiducial points at 30-mm SD distance from 0-yo, 1-yo, and 2-yo.

SD distance = 30 mm		Circumferential SD pair			Vertical SD pair		
10/10 Points	AAL regions	0 year	1 year	2 year	0 year	1 year	2 year
C5	PreCG-L	3.6%	7.4%	5.7%	4.8%	4.3%	4.1%
	IFGoperc-L	3.8%	1.3%	1.3%	1.2%	0.4%	0.5%
	IFGtriang-L	1.9%	0.2%	0.3%	0.6%	0.1%	0.1%
	ROL-L	7.5%	15.1%	14.1%	4.1%	5.4%	3.6%
	PoCG-L	12.6%	29.0%	27.3%	42.2%	41.4%	42.8%
	SMG-L	7.5%	13.0%	10.2%	5.1%	7.8%	9.8%
	STG-L	51.4%	32.4%	38.2%	26.9%	37.5%	35.2%
	TPOsup-L	3.7%	0.7%	1.2%	2.0%	0.5%	0.4%
	MTG-L	7.1%	0.9%	1.5%	12.1%	2.5%	3.4%
C3	PreCG-L	22.5%	34.4%	34.6%	20.5%	27.8%	26.7%
	MFG-L	8.1%	9.5%	7.5%	8.7%	8.5%	13.6%
	IFGoperc-L	2.3%	0.6%	0.6%	0.6%	0.2%	0.2%
	PoCG-L	32.8%	38.7%	38.8%	46.7%	54.4%	44.7%
	IPL-L	1.9%	1.0%	1.2%	0.6%	0.2%	0.4%
	SMG-L	31.0%	15.4%	17.0%	20.1%	8.6%	14.0%
C1	PreCG-L	33.9%	39.0%	39.9%	31.1%	42.0%	40.2%
	SFGdor-L	20.0%	24.4%	21.8%	26.0%	35.5%	32.0%
	MFG-L	24.4%	27.4%	29.6%	17.8%	11.6%	18.3%
	SMA-L	1.4%	1.2%	0.7%	2.9%	3.2%	1.4%
	PoCG-L	17.4%	7.5%	7.4%	17.0%	7.1%	7.4%
C2	PreCG-R	32.6%	45.7%	40.4%	32.5%	46.3%	42.7%
	SFGdor-R	16.8%	13.3%	21.8%	28.0%	27.4%	31.6%
	MFG-R	21.9%	22.8%	27.1%	7.0%	6.5%	13.7%
	SMA-R	2.4%	1.1%	2.0%	6.2%	3.4%	4.5%
	PoCG-R	21.3%	15.7%	7.3%	19.9%	14.9%	6.2%
	SPG-R	1.0%	0.3%	0.1%	0.5%	0.1%	0.1%
	PCL-R	1.9%	0.8%	1.0%	2.6%	1.1%	0.8%

Table S6-6 Normalized PPL of corresponding brain regions ($L_{norm,M}$) for the circumferential and vertical SD pairs set at 10/10 fiducial points at 30-mm SD distance from 0-yo, 1-yo, and 2-yo.

SD distance = 30 mm		Circumferential SD pair			Vertical SD pair		
10/10 Points	AAL regions	0 year	1 year	2 year	0 year	1 year	2 year
C4	PreCG-R	22.7%	27.8%	38.4%	23.5%	22.8%	36.5%
	MFG-R	5.9%	2.4%	4.8%	3.4%	1.5%	3.7%
	PoCG-R	31.4%	44.4%	42.7%	41.4%	60.5%	48.2%
	IPL-R	22.4%	18.7%	9.3%	6.8%	5.0%	3.6%
	SMG-R	15.2%	6.5%	4.2%	21.9%	9.9%	7.6%
C6	PreCG-R	1.8%	1.5%	3.6%	4.4%	1.2%	4.6%
	IFGoperc-R	3.9%	0.4%	2.0%	1.5%	0.1%	0.7%
	IFGtriang-R	1.7%	0.1%	0.3%	1.0%	0.0%	0.2%
	ROL-R	6.1%	6.7%	5.2%	3.0%	1.5%	2.4%
	PoCG-R	19.4%	37.8%	44.2%	35.4%	42.6%	48.8%
	SMG-R	9.1%	12.9%	16.8%	6.4%	9.4%	7.5%
	STG-R	33.6%	35.1%	24.1%	17.3%	27.9%	26.7%
	TPOsup-R	1.3%	0.1%	0.1%	0.8%	0.0%	0.1%
	MTG-R	21.5%	5.1%	3.2%	28.3%	16.9%	8.5%
T4	STG-R	2.2%	2.2%	4.6%	6.0%	7.0%	9.4%
	TPOsup-R	1.7%	0.3%	0.9%	1.7%	0.2%	0.5%
	MTG-R	56.2%	74.6%	81.9%	53.3%	69.5%	68.2%
	TPOmid-R	2.0%	0.2%	0.3%	1.4%	0.1%	0.2%
	ITG-R	36.6%	22.4%	11.7%	35.2%	22.7%	20.5%
FT7	IFGoperc-L	1.5%	1.6%	1.3%	5.4%	4.8%	3.1%
	IFGtriang-L	4.8%	2.8%	2.9%	5.6%	2.9%	2.8%
	ORBinf-L	18.5%	11.3%	10.0%	6.6%	2.8%	2.8%
	ROL-L	0.9%	1.5%	0.7%	2.7%	6.7%	1.9%
	STG-L	7.1%	14.7%	10.1%	5.2%	10.1%	7.1%
	TPOsup-L	23.1%	33.9%	33.4%	33.9%	36.6%	36.9%
	MTG-L	25.6%	21.1%	26.7%	11.0%	14.7%	20.2%
	TPOmid-L	11.9%	11.3%	13.5%	21.0%	18.2%	21.9%
	ITG-L	4.4%	1.1%	1.1%	5.8%	2.0%	2.9%

Table S6-7 Normalized PPL of corresponding brain regions ($L_{norm,M}$) for the circumferential and vertical SD pairs set at 10/10 fiducial points at 30-mm SD distance from 0-yo, 1-yo, and 2-yo.

SD distance = 30 mm		Circumferential SD pair			Vertical SD pair		
10/10 Points	AAL regions	0 year	1 year	2 year	0 year	1 year	2 year
F7	MFG-L	3.8%	1.4%	0.9%	4.4%	1.1%	1.1%
	ORBmid-L	17.7%	5.0%	4.5%	6.7%	1.2%	1.5%
	IFGoperc-L	1.5%	1.1%	0.6%	1.0%	1.3%	0.5%
	IFGtriang-L	14.7%	14.4%	10.2%	35.8%	39.1%	35.1%
	ORBinf-L	41.8%	60.8%	59.9%	42.6%	47.2%	50.9%
	TPOsup-L	15.3%	15.1%	20.8%	6.4%	8.4%	8.9%
	TPOmid-L	2.1%	1.3%	2.3%	1.5%	1.0%	1.5%
AF7	SFGdor-L	4.7%	1.3%	1.2%	4.0%	0.7%	1.1%
	ORBsup-L	4.6%	2.7%	3.3%	2.2%	0.8%	1.5%
	MFG-L	16.5%	13.1%	7.8%	34.5%	28.9%	27.0%
	ORBmid-L	38.0%	46.3%	50.8%	39.8%	41.1%	48.7%
	IFGtriang-L	10.5%	6.3%	4.3%	5.9%	7.7%	5.2%
	ORBinf-L	23.6%	30.1%	31.8%	12.5%	20.6%	16.3%
Fp1	SFGdor-L	16.6%	16.3%	8.5%	27.6%	29.4%	24.3%
	ORBsup-L	13.7%	25.2%	25.5%	16.5%	24.5%	29.0%
	MFG-L	15.4%	12.5%	5.2%	13.3%	11.9%	6.2%
	ORBmid-L	26.5%	34.1%	39.1%	26.1%	27.5%	28.3%
	ORBinf-L	1.7%	0.6%	0.6%	1.1%	0.3%	0.3%
	SFGmed-R	3.5%	0.3%	0.5%	1.7%	0.2%	0.4%
	SFGmed-L	10.7%	4.8%	4.3%	6.9%	2.9%	4.2%
	ORBmed-R	2.3%	0.4%	1.4%	1.1%	0.2%	0.7%
	ORBmed-L	7.1%	5.5%	14.0%	3.9%	2.8%	5.9%

Table S6-8 Normalized PPL of corresponding brain regions ($L_{norm,M}$) for the circumferential and vertical SD pairs set at 10/10 fiducial points at 30-mm SD distance from 0-yo, 1-yo, and 2-yo.

SD distance = 30 mm		Circumferential SD pair			Vertical SD pair		
10/10 Points	AAL regions	0 year	1 year	2 year	0 year	1 year	2 year
Fp2	SFGdor-R	19.9%	19.0%	14.1%	33.2%	36.7%	28.3%
	ORBsup-R	10.5%	19.2%	22.1%	14.4%	23.6%	22.2%
	ORBsup-L	1.1%	0.1%	0.2%	0.6%	0.1%	0.1%
	MFG-R	16.5%	10.3%	8.8%	13.1%	7.0%	14.4%
	ORBmid-R	17.2%	31.1%	34.9%	14.9%	16.4%	23.8%
	ORBinf-R	2.1%	0.5%	1.4%	1.3%	0.2%	0.7%
	SFGmed-R	13.9%	6.0%	3.7%	11.1%	6.3%	3.2%
	SFGmed-L	4.1%	0.4%	0.4%	2.1%	0.4%	0.3%
	ORBmed-R	8.8%	11.9%	11.5%	5.6%	7.3%	4.9%
	ORBmed-L	2.9%	0.6%	1.1%	1.3%	0.4%	0.6%
	REC-R	0.9%	0.7%	1.4%	1.2%	1.4%	1.4%
AF8	SFGdor-R	9.2%	2.9%	2.2%	6.2%	1.3%	1.4%
	ORBsup-R	4.8%	2.4%	2.8%	2.7%	0.9%	1.2%
	MFG-R	20.2%	17.7%	11.5%	38.1%	27.8%	30.1%
	ORBmid-R	28.7%	47.6%	49.2%	30.6%	45.3%	41.8%
	IFGtriang-R	14.0%	9.9%	9.6%	7.4%	8.0%	10.6%
	ORBinf-R	20.2%	19.1%	23.7%	13.2%	16.3%	14.5%
F8	MFG-R	5.8%	0.8%	1.3%	5.4%	0.4%	1.3%
	ORBmid-R	14.8%	4.4%	4.9%	5.8%	0.6%	2.0%
	IFGoperc-R	2.3%	1.2%	1.3%	1.5%	2.0%	1.0%
	IFGtriang-R	19.2%	18.1%	23.8%	34.9%	36.4%	46.0%
	ORBinf-R	40.5%	54.0%	44.6%	42.5%	44.6%	33.7%
	STG-R	1.8%	1.5%	0.9%	0.6%	0.7%	0.4%
	TPOsup-R	10.6%	16.1%	19.5%	6.1%	12.2%	12.5%
	MTG-R	1.4%	1.7%	1.5%	0.6%	0.8%	0.7%
	TPOmid-R	1.0%	1.3%	1.5%	1.1%	1.5%	1.8%

Table S6-9 Normalized PPL of corresponding brain regions ($L_{norm,M}$) for the circumferential and vertical SD pairs set at 10/10 fiducial points at 30-mm SD distance from 0-yo, 1-yo, and 2-yo.

SD distance = 30 mm		Circumferential SD pair			Vertical SD pair		
10/10 Points	AAL regions	0 year	1 year	2 year	0 year	1 year	2 year
FT8	IFGoperc-R	2.0%	0.8%	1.7%	6.7%	2.5%	4.3%
	IFGtriang-R	5.8%	1.5%	3.7%	6.6%	2.0%	3.4%
	ORBinf-R	21.1%	4.3%	5.7%	7.5%	1.7%	2.1%
	ROL-R	1.7%	1.2%	1.7%	4.0%	5.8%	4.8%
	STG-R	8.1%	10.2%	10.4%	8.9%	20.0%	14.4%
	TPOsup-R	17.3%	20.7%	25.9%	22.5%	17.3%	24.2%
	MTG-R	33.9%	54.2%	44.6%	24.1%	41.2%	38.0%
	TPOmid-R	4.6%	4.4%	4.3%	11.3%	4.8%	6.1%
	ITG-R	3.4%	2.2%	1.4%	5.9%	3.4%	1.9%
TP7	STG-L	6.1%	7.5%	4.3%	25.4%	21.7%	10.2%
	MTG-L	54.2%	82.7%	81.2%	43.8%	55.7%	61.0%
	ITG-L	39.0%	9.6%	14.4%	29.7%	22.3%	28.5%
T5	MOG-L	4.1%	1.5%	1.7%	0.4%	0.9%	0.7%
	IOG-L	1.7%	0.3%	0.6%	0.6%	0.3%	0.5%
	STG-L	3.1%	3.0%	1.7%	13.4%	11.6%	4.0%
	MTG-L	67.9%	86.1%	83.8%	58.1%	68.7%	70.8%
	ITG-L	22.5%	8.1%	11.7%	25.2%	14.4%	22.5%
PO7	MOG-L	41.0%	48.2%	53.5%	29.7%	50.5%	57.7%
	IOG-L	1.7%	0.7%	1.2%	14.3%	2.1%	3.9%
	ANG-L	2.7%	4.7%	1.3%	12.1%	14.5%	4.9%
	MTG-L	51.0%	45.1%	43.0%	35.9%	31.7%	32.4%
	ITG-L	2.0%	0.8%	0.7%	6.6%	0.9%	0.7%
O1	CUN-R	2.0%	0.4%	1.3%	0.7%	0.2%	0.6%
	CUN-L	4.0%	1.4%	2.4%	2.2%	1.2%	1.5%
	SOG-L	21.2%	26.4%	27.8%	20.3%	17.7%	20.7%
	MOG-L	64.9%	69.0%	66.6%	63.9%	76.5%	74.3%
	ANG-L	1.8%	1.4%	0.5%	3.3%	2.4%	1.2%
	MTG-L	3.8%	0.7%	0.4%	0.2%	0.3%	0.2%

Table S6-10 Normalized PPL of corresponding brain regions ($L_{norm,M}$) for the circumferential and vertical SD pairs set at 10/10 fiducial points at 30-mm SD distance from 0-yo, 1-yo, and 2-yo.

SD distance = 30 mm		Circumferential SD pair			Vertical SD pair		
10/10 Points	AAL regions	0 year	1 year	2 year	0 year	1 year	2 year
O2	CAL-R	3.9%	1.2%	0.4%	5.9%	2.4%	0.6%
	CUN-R	17.4%	19.9%	10.6%	6.5%	9.3%	5.1%
	CUN-L	2.4%	1.4%	0.6%	0.9%	0.8%	0.4%
	SOG-R	29.7%	47.7%	43.8%	41.2%	58.4%	48.7%
	MOG-R	43.6%	28.4%	43.5%	40.9%	27.4%	43.8%
PO8	SOG-R	6.1%	6.0%	1.9%	1.4%	2.2%	1.0%
	MOG-R	71.8%	81.9%	77.1%	82.1%	84.7%	81.6%
	IOG-R	3.0%	1.2%	0.6%	4.2%	1.7%	0.8%
	ANG-R	4.3%	5.0%	6.3%	8.8%	8.4%	11.0%
	MTG-R	13.5%	5.3%	13.7%	1.9%	2.0%	5.1%
T6	MOG-R	23.0%	23.3%	14.7%	8.2%	16.0%	10.8%
	IOG-R	6.7%	4.8%	2.1%	23.5%	15.8%	8.0%
	ANG-R	2.2%	4.7%	4.0%	9.6%	10.4%	9.8%
	STG-R	1.7%	1.6%	2.9%	2.7%	1.0%	2.3%
	MTG-R	53.7%	61.4%	72.8%	35.9%	50.5%	61.0%
	ITG-R	11.9%	3.3%	2.5%	15.3%	4.5%	5.0%
TP8	STG-R	2.5%	3.0%	6.4%	7.2%	12.0%	12.8%
	MTG-R	64.5%	82.1%	86.3%	53.3%	66.4%	73.9%
	ITG-R	31.3%	13.6%	6.2%	37.6%	20.1%	11.9%
FC5	PreCG-L	7.7%	13.6%	12.3%	17.0%	17.8%	12.8%
	MFG-L	3.7%	1.2%	1.1%	3.0%	2.0%	1.4%
	IFGoperc-L	10.3%	17.2%	18.3%	24.8%	38.1%	35.1%
	IFGtriang-L	37.1%	37.6%	36.4%	22.0%	20.2%	26.2%
	ORBinf-L	4.7%	0.8%	0.9%	4.1%	1.5%	1.7%
	ROL-L	9.1%	14.6%	15.0%	5.3%	9.1%	7.9%
	PoCG-L	13.4%	10.5%	8.6%	4.8%	2.4%	2.0%
	STG-L	6.5%	2.0%	3.0%	3.2%	1.4%	1.8%
	TPOsup-L	5.5%	2.3%	4.0%	12.9%	7.1%	10.6%

Table S6-11 Normalized PPL of corresponding brain regions ($L_{norm,M}$) for the circumferential and vertical SD pairs set at 10/10 fiducial points at 30-mm SD distance from 0-yo, 1-yo, and 2-yo.

SD distance = 30 mm		Circumferential SD pair			Vertical SD pair		
10/10 Points	AAL regions	0 year	1 year	2 year	0 year	1 year	2 year
FC3	PreCG-L	25.8%	26.8%	23.6%	12.1%	12.1%	8.5%
	MFG-L	52.5%	60.7%	59.9%	53.3%	56.0%	54.1%
	IFGoperc-L	7.5%	7.1%	9.4%	13.1%	15.6%	17.6%
	IFGtriang-L	6.6%	4.1%	5.1%	17.6%	15.3%	18.6%
	PoCG-L	6.2%	0.6%	1.4%	1.8%	0.4%	0.5%
FC1	PreCG-L	4.6%	1.1%	0.7%	4.9%	0.3%	0.4%
	SFGdor-L	30.5%	46.2%	43.0%	32.3%	47.0%	42.3%
	MFG-L	53.9%	48.4%	49.4%	53.5%	47.4%	51.0%
	SMA-L	2.4%	1.7%	1.5%	4.7%	3.7%	3.3%
	SFGmed-L	5.9%	2.3%	4.8%	2.1%	1.2%	2.5%
FC2	PreCG-R	9.1%	1.1%	1.1%	2.8%	0.5%	0.6%
	SFGdor-R	29.3%	41.1%	32.0%	30.1%	34.8%	30.5%
	MFG-R	40.8%	48.3%	60.3%	47.7%	54.9%	63.4%
	SMA-R	6.0%	2.6%	1.5%	11.0%	7.3%	2.9%
	SMA-L	1.1%	0.2%	0.2%	1.5%	0.2%	0.2%
	SFGmed-R	7.9%	6.4%	4.5%	2.8%	2.1%	2.2%
	SFGmed-L	1.3%	0.2%	0.3%	0.8%	0.1%	0.2%
	PoCG-R	3.3%	0.0%	0.0%	0.3%	0.0%	0.0%
FC4	PreCG-R	23.1%	29.0%	21.9%	18.7%	19.5%	11.3%
	SFGdor-R	1.7%	0.2%	0.5%	1.5%	0.2%	0.4%
	MFG-R	57.8%	61.3%	69.2%	54.2%	64.1%	66.7%
	IFGoperc-R	3.3%	2.6%	2.7%	7.7%	5.3%	6.1%
	IFGtriang-R	5.2%	4.3%	4.4%	12.7%	9.6%	14.6%
	PoCG-R	7.7%	2.6%	1.3%	3.9%	1.3%	0.8%

Table S6-12 Normalized PPL of corresponding brain regions ($L_{norm,M}$) for the circumferential and vertical SD pairs set at 10/10 fiducial points at 30-mm SD distance from 0-yo, 1-yo, and 2-yo.

SD distance = 30 mm		Circumferential SD pair			Vertical SD pair		
10/10 Points	AAL regions	0 year	1 year	2 year	0 year	1 year	2 year
FC6	PreCG-R	5.6%	9.4%	8.8%	16.4%	24.7%	12.4%
	MFG-R	5.1%	1.6%	2.4%	5.9%	2.6%	3.8%
	IFGoperc-R	11.3%	14.3%	15.8%	17.6%	17.9%	25.9%
	IFGtriang-R	34.5%	31.5%	44.9%	20.6%	13.6%	35.7%
	ORBinf-R	2.5%	0.3%	0.3%	2.6%	0.4%	0.5%
	ROL-R	5.7%	7.7%	6.0%	5.7%	11.7%	7.0%
	PoCG-R	20.8%	29.5%	16.8%	11.1%	14.4%	6.8%
	STG-R	7.8%	4.1%	3.1%	7.9%	8.8%	3.7%
	TPOsup-R	2.7%	1.0%	1.3%	7.1%	4.6%	3.7%
	MTG-R	2.5%	0.5%	0.4%	3.8%	1.2%	0.5%
F5	SFGdor-L	1.1%	0.1%	0.2%	0.6%	0.0%	0.1%
	MFG-L	29.1%	33.2%	33.2%	36.9%	27.0%	27.3%
	ORBmid-L	4.8%	1.3%	1.7%	5.8%	1.3%	2.0%
	IFGoperc-L	5.1%	3.1%	1.4%	2.0%	1.1%	0.7%
	IFGtriang-L	48.0%	57.8%	58.0%	38.1%	56.6%	52.3%
	ORBinf-L	8.1%	3.8%	4.8%	15.0%	13.5%	17.1%
	TPOsup-L	1.4%	0.3%	0.3%	0.7%	0.2%	0.3%
F3	SFGdor-L	6.5%	1.9%	3.5%	5.4%	2.3%	2.5%
	MFG-L	66.4%	85.4%	85.2%	81.9%	91.9%	90.4%
	IFGoperc-L	3.5%	0.7%	0.6%	0.8%	0.2%	0.3%
	IFGtriang-L	20.7%	11.5%	10.1%	8.4%	5.1%	6.3%
F1	SFGdor-L	21.1%	40.5%	37.3%	40.3%	46.9%	47.8%
	MFG-L	54.6%	36.8%	39.5%	38.7%	45.7%	42.1%
	SFGmed-R	5.6%	1.5%	2.7%	4.0%	0.6%	1.3%
	SFGmed-L	16.6%	20.9%	20.1%	14.5%	6.6%	8.5%

Table S6-13 Normalized PPL of corresponding brain regions ($L_{norm,M}$) for the circumferential and vertical SD pairs set at 10/10 fiducial points at 30-mm SD distance from 0-yo, 1-yo, and 2-yo.

SD distance = 30 mm		Circumferential SD pair			Vertical SD pair		
10/10 Points	AAL regions	0 year	1 year	2 year	0 year	1 year	2 year
F2	SFGdor-R	25.2%	44.0%	44.8%	49.1%	61.2%	54.4%
	SFGdor-L	1.6%	0.1%	0.2%	0.8%	0.1%	0.1%
	MFG-R	34.2%	27.6%	33.0%	27.4%	24.3%	35.8%
	SFGmed-R	27.1%	26.2%	20.2%	16.7%	13.3%	8.8%
	SFGmed-L	9.7%	1.9%	1.7%	3.4%	1.1%	0.8%
F4	SFGdor-R	13.7%	8.0%	5.6%	9.7%	5.0%	3.8%
	MFG-R	63.3%	84.5%	84.0%	77.5%	87.7%	86.2%
	IFGoperc-R	2.8%	0.4%	0.4%	0.5%	0.1%	0.1%
	IFGtriang-R	17.0%	6.6%	9.6%	9.2%	6.8%	9.5%
	SFGmed-R	1.4%	0.3%	0.3%	1.2%	0.2%	0.2%
F6	SFGdor-R	1.9%	0.1%	0.2%	1.1%	0.1%	0.1%
	MFG-R	40.2%	24.8%	28.7%	40.2%	21.1%	22.0%
	ORBmid-R	3.3%	1.3%	2.1%	5.5%	2.2%	2.1%
	IFGoperc-R	6.3%	4.0%	1.3%	1.9%	1.1%	0.6%
	IFGtriang-R	40.7%	66.4%	65.4%	36.8%	64.9%	70.3%
	ORBinf-R	4.4%	2.2%	1.5%	12.5%	9.9%	4.2%
AF3	SFGdor-L	25.6%	35.5%	37.2%	29.2%	29.7%	36.2%
	ORBsup-L	1.5%	1.2%	1.6%	3.6%	3.3%	5.8%
	MFG-L	49.5%	55.3%	47.5%	48.9%	59.4%	45.5%
	ORBmid-L	2.9%	1.8%	2.5%	9.2%	4.9%	7.5%
	IFGtriang-L	1.7%	0.4%	0.4%	0.8%	0.2%	0.2%
	SFGmed-R	3.3%	0.2%	0.6%	1.3%	0.2%	0.4%
	SFGmed-L	13.7%	5.3%	9.6%	5.3%	2.1%	3.9%

Table S6-14 Normalized PPL of corresponding brain regions ($L_{norm,M}$) for the circumferential and vertical SD pairs set at 10/10 fiducial points at 30-mm SD distance from 0-yo, 1-yo, and 2-yo.

SD distance = 30 mm		Circumferential SD pair			Vertical SD pair		
10/10 Points	AAL regions	0 year	1 year	2 year	0 year	1 year	2 year
AF4	SFGdor-R	29.6%	41.3%	37.1%	42.3%	45.9%	36.0%
	ORBsup-R	1.2%	0.5%	0.8%	2.9%	1.6%	2.7%
	MFG-R	39.4%	43.5%	51.7%	34.8%	44.2%	51.2%
	ORBmid-R	2.2%	0.8%	1.6%	5.9%	2.9%	5.6%
	IFGtriang-R	2.6%	0.5%	1.0%	1.0%	0.2%	0.4%
	SFGmed-R	19.8%	12.5%	7.0%	9.1%	4.5%	3.3%
	SFGmed-L	2.7%	0.5%	0.4%	1.4%	0.2%	0.2%
CP5	PoCG-L	8.1%	2.3%	1.8%	3.0%	1.1%	1.0%
	SMG-L	25.8%	46.0%	39.8%	45.1%	49.7%	41.7%
	ANG-L	6.0%	8.5%	5.5%	0.5%	1.1%	1.5%
	STG-L	48.4%	38.5%	47.0%	27.1%	34.6%	39.8%
	MTG-L	10.4%	3.8%	5.1%	23.4%	12.9%	15.4%
CP3	PreCG-L	2.2%	0.8%	1.0%	7.5%	1.0%	1.1%
	PoCG-L	33.2%	30.5%	15.3%	22.8%	23.7%	18.6%
	SPG-L	2.5%	2.6%	3.1%	1.6%	2.2%	2.5%
	IPL-L	32.6%	45.6%	51.2%	19.5%	37.1%	45.3%
	SMG-L	26.7%	19.8%	27.7%	43.8%	34.4%	30.1%
	ANG-L	2.0%	0.5%	1.3%	2.8%	1.3%	2.1%
CP1	PreCG-L	15.9%	9.8%	11.1%	23.9%	18.0%	17.3%
	SFGdor-L	1.3%	0.3%	0.5%	2.2%	0.8%	0.8%
	PoCG-L	42.6%	53.3%	51.7%	29.5%	44.0%	46.3%
	SPG-L	32.5%	32.7%	32.3%	21.5%	29.9%	27.4%
	IPL-L	4.2%	2.8%	3.2%	18.3%	5.8%	6.8%

Table S6-15 Normalized PPL of corresponding brain regions ($L_{norm,M}$) for the circumferential and vertical SD pairs set at 10/10 fiducial points at 30-mm SD distance from 0-yo, 1-yo, and 2-yo.

SD distance = 30 mm		Circumferential SD pair			Vertical SD pair		
10/10 Points	AAL regions	0 year	1 year	2 year	0 year	1 year	2 year
CP2	PreCG-R	14.3%	5.8%	7.5%	13.3%	6.6%	12.8%
	SFGdor-R	2.0%	0.3%	0.5%	3.0%	0.6%	1.2%
	PoCG-R	38.2%	48.9%	50.5%	33.0%	42.1%	47.1%
	SPG-R	21.8%	32.2%	31.0%	24.2%	34.2%	25.1%
	IPL-R	2.6%	2.3%	3.0%	8.4%	4.8%	5.3%
	PCUN-R	14.1%	7.8%	4.5%	4.2%	3.6%	2.1%
	PCL-R	3.8%	2.1%	2.5%	9.8%	7.4%	5.7%
CP4	PreCG-R	3.7%	0.4%	1.5%	3.6%	0.5%	1.5%
	PoCG-R	32.6%	23.9%	27.2%	28.1%	28.5%	34.1%
	SPG-R	4.9%	3.0%	1.6%	2.4%	2.5%	1.3%
	IPL-R	46.6%	67.6%	66.1%	45.0%	63.8%	58.5%
	SMG-R	5.5%	1.4%	2.1%	14.8%	1.9%	3.3%
	ANG-R	5.8%	3.7%	1.4%	5.1%	2.6%	1.2%
CP6	PoCG-R	5.9%	1.8%	4.2%	3.1%	0.6%	2.0%
	IPL-R	4.6%	8.8%	8.6%	12.7%	24.4%	12.6%
	SMG-R	34.9%	51.4%	64.9%	33.2%	39.8%	55.5%
	ANG-R	13.7%	10.4%	4.9%	1.7%	3.3%	2.0%
	STG-R	21.6%	21.9%	14.3%	14.0%	21.2%	21.4%
	MTG-R	18.5%	5.5%	3.0%	34.0%	10.6%	6.4%
P5	MOG-L	9.5%	3.1%	3.8%	1.9%	2.1%	3.2%
	IPL-L	1.5%	4.8%	3.8%	15.1%	21.0%	14.3%
	SMG-L	10.0%	11.9%	6.7%	8.1%	4.3%	2.8%
	ANG-L	25.7%	55.9%	53.4%	27.2%	40.5%	47.0%
	STG-L	24.4%	12.6%	13.8%	7.6%	5.2%	2.9%
	MTG-L	28.7%	11.5%	18.3%	39.6%	26.8%	29.9%

Table S6-16 Normalized PPL of corresponding brain regions ($L_{norm,M}$) for the circumferential and vertical SD pairs set at 10/10 fiducial points at 30-mm SD distance from 0-yo, 1-yo, and 2-yo.

SD distance = 30 mm		Circumferential SD pair			Vertical SD pair		
10/10 Points	AAL regions	0 year	1 year	2 year	0 year	1 year	2 year
P3	PoCG-L	1.1%	0.5%	0.3%	1.3%	0.4%	0.4%
	SPG-L	10.4%	10.6%	8.4%	10.9%	13.5%	9.0%
	IPL-L	41.9%	51.8%	42.2%	25.3%	27.4%	32.7%
	SMG-L	8.4%	1.6%	0.8%	1.5%	0.5%	0.3%
	ANG-L	36.3%	35.0%	47.7%	53.2%	56.9%	56.9%
P1	PoCG-L	5.3%	1.5%	1.2%	5.3%	2.3%	1.5%
	SPG-L	63.1%	82.0%	78.7%	63.1%	80.0%	80.1%
	IPL-L	14.4%	6.9%	8.6%	4.2%	3.3%	3.5%
	ANG-L	8.6%	6.0%	7.7%	20.9%	12.5%	12.0%
	PCUN-R	2.0%	0.6%	0.9%	0.9%	0.3%	0.6%
	PCUN-L	4.5%	2.6%	2.7%	1.8%	1.0%	1.7%
P2	SOG-R	1.1%	0.4%	0.1%	5.3%	1.2%	0.4%
	PoCG-R	4.7%	0.6%	1.4%	5.5%	0.6%	1.2%
	SPG-R	48.2%	61.0%	63.9%	46.6%	67.3%	70.1%
	SPG-L	2.1%	0.5%	0.2%	1.3%	0.2%	0.2%
	IPL-R	7.7%	2.5%	3.8%	7.1%	3.6%	5.8%
	ANG-R	4.6%	2.0%	1.9%	3.2%	1.4%	2.7%
	PCUN-R	25.6%	30.7%	27.1%	25.4%	24.2%	18.6%
	PCUN-L	3.6%	2.1%	1.2%	2.1%	1.0%	0.8%
P4	SOG-R	2.6%	0.5%	0.2%	0.9%	0.3%	0.2%
	MOG-R	3.5%	0.8%	0.9%	19.3%	3.6%	2.4%
	PoCG-R	1.4%	0.4%	0.7%	1.3%	0.3%	0.8%
	SPG-R	15.9%	29.2%	16.9%	17.1%	26.9%	20.2%
	IPL-R	39.1%	31.7%	40.4%	14.9%	16.9%	28.5%
	ANG-R	35.3%	36.6%	40.3%	44.9%	51.4%	47.5%
	PCUN-R	1.1%	0.7%	0.4%	0.7%	0.3%	0.3%

Table S6-17 Normalized PPL of corresponding brain regions ($L_{norm,M}$) for the circumferential and vertical SD pairs set at 10/10 fiducial points at 30-mm SD distance from 0-yo, 1-yo, and 2-yo.

SD distance = 30 mm		Circumferential SD pair			Vertical SD pair		
10/10 Points	AAL regions	0 year	1 year	2 year	0 year	1 year	2 year
P6	MOG-R	26.8%	14.8%	6.8%	10.9%	8.4%	4.0%
	IPL-R	4.4%	6.5%	8.8%	14.7%	9.9%	13.9%
	SMG-R	14.6%	9.9%	12.7%	4.5%	2.0%	4.9%
	ANG-R	34.0%	61.5%	66.5%	50.7%	70.2%	65.2%
	STG-R	4.9%	0.8%	0.6%	0.9%	0.3%	0.4%
	MTG-R	14.4%	6.1%	4.3%	16.8%	8.9%	11.4%
PO3	CUN-L	3.2%	2.6%	2.5%	1.3%	0.9%	1.0%
	SOG-L	10.3%	22.4%	19.7%	11.1%	12.3%	13.0%
	MOG-L	22.3%	16.3%	21.1%	41.0%	31.2%	36.3%
	SPG-L	8.5%	9.8%	8.4%	16.5%	15.5%	11.9%
	ANG-L	52.6%	48.2%	47.4%	27.5%	39.2%	37.0%
PO4	CUN-R	3.5%	3.1%	1.5%	3.3%	1.8%	1.1%
	SOG-R	19.4%	36.5%	32.5%	37.7%	35.1%	25.7%
	MOG-R	36.6%	23.9%	24.7%	23.6%	25.0%	31.5%
	SPG-R	5.0%	8.1%	8.3%	14.8%	19.5%	13.3%
	IPL-R	12.1%	20.5%	23.8%	11.8%	14.5%	23.7%
	ANG-R	18.9%	5.0%	7.1%	3.1%	1.8%	3.0%
	PCUN-R	2.6%	1.9%	1.6%	3.8%	1.7%	1.5%